Kevin R. Keene

Function and structure of the eye muscles in myasthenia gravis

Novel methods to aid in diagnosis
and understanding of pathophysiology

Function and structure of
the eye muscles in myasthenia gravis

Novel methods to aid in diagnosis and understanding of pathophysiology

Proefschrift

ter verkrijging van
de graad van doctor aan de Universiteit Leiden,
op gezag van rector magnificus prof.dr.ir. H. Bijl,
volgens besluit van het college voor promoties
te verdedigen op donderdag 21 september 2023
klokke 16:15 uur

door

Kevin Rogi Keene

geboren te Delft
in 1992

Promotoren
Prof. Dr. J.J.G.M Verschuuren
Dr. H.E. Kan

Copromotor
Dr. J.W.M. Beenakker

Promotiecommissie
Dr. B.M. Verbist
Dr. Ir. M Froeling, UMC Utrecht
Prof. Dr. P.A. van Doorn, Erasmus MC
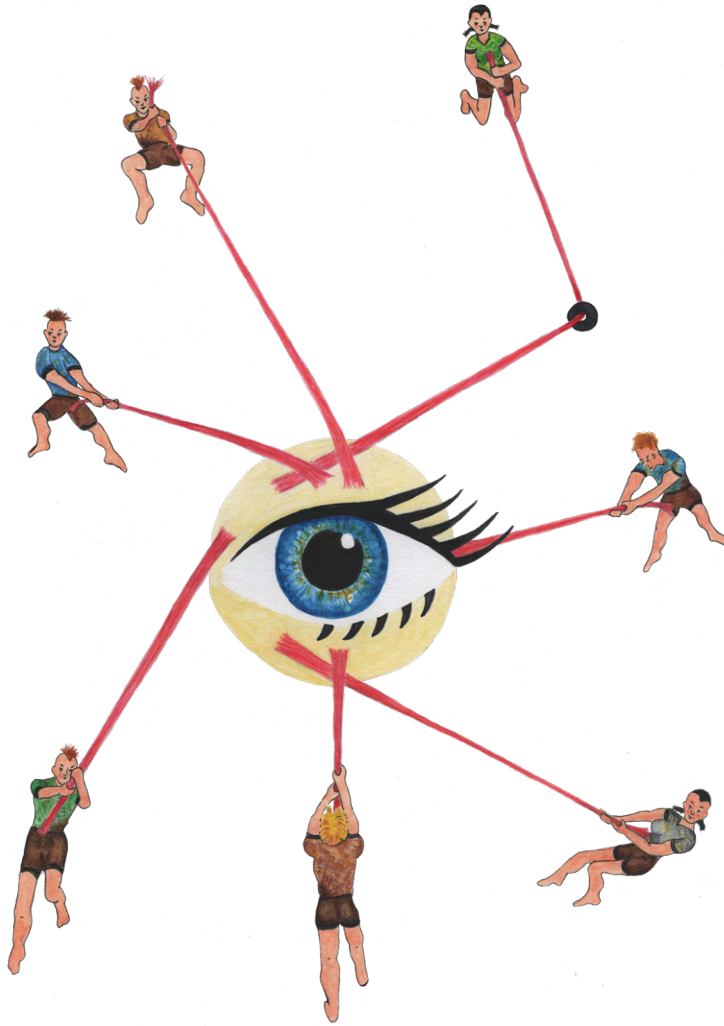Prof. Dr. G.P.M. Luyten

TABLE OF CONTENTS

1

General introduction

Myasthenia gravis (MG) is a muscle disease characterized by fluctuating and fatigable muscle weakness. Ocular and bulbar involvement is most common, where ocular symptoms, like double vision (diplopia) and drooping eye lids (ptosis), are experienced during the course of the disease.[1] In the generalized subtype of the disease all skeletal muscles can be involved including neck, arms, legs and respiratory muscles.

In this introductory chapter, MG will first be explained in more detail. Then, the challenges in diagnosis, therapy and outcome measure development of the clinical phenotype ocular MG are introduced, followed by three advanced methods that are studied to aid in these challenges: neurophysiological assessments, orthoptic measures and MR-imaging. The chapter ends with the overall aim of the thesis.

PART I – MYASTHENIA GRAVIS

Background and clinical course

MG is caused by auto-antibodies targeting proteins at the neuromuscular junction, including the acetylcholine receptor (AChR), muscle-specific tyrosine kinase (MuSK) or LRP4.[2,3] These antibodies can block neuromuscular signaling directly, block formation of a healthy neuromuscular structure and/or lead to the destruction of muscle membranes at the neuromuscular junction via complement activation (figure 1).

The prevalence of the disease is between 1 and 3.5 per 10.000 people.[4] The age of onset has a peak at an early age around 30 years and at a later age of around 50 years. The early peak is mainly caused by an early onset in young females, as is also common for other auto-immune diseases.[5] MG can or cannot be associated with a thymoma, a tumor of the thymus. In patients with thymoma either MG-related proteins are expressed, causing an auto-immune response, or dysregulation of the thymus results in the survival of auto-immune T-cells. No cure is available for MG, however with immunosuppressive treatments, thymectomy and medicine directly improving neuromuscular transmission muscle weakness and fatigue can be improved in many patients.[6,7]

In 10-15% of MG patients refractory symptoms occur, or the side effects of treatment do not outweigh the treatment effects.[8] The refractory symptoms can include ocular refractory ophthalmoplegia.[9] In the past few years, new medicine targeting complement, the FcRn receptor, or B-cell antigens have been developed, which is promising for these patient groups.[7]

Diagnosis

Diagnosis of MG consists of several steps (Figure 2). The first step involves serum analysis, where the auto-antibodies against AChR, MuSK or LRP4 can be detected. The presence of these antibodies form a definitive diagnosis of MG. If no antibodies are found, diagnosis can
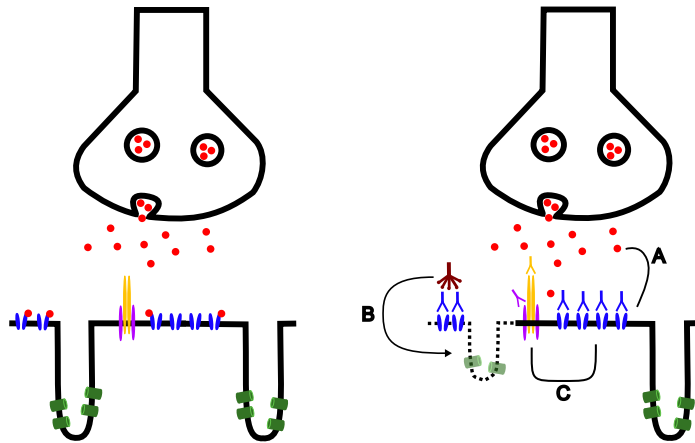
Figure 1. *Schematic of the neuromuscular junction. Left: The situation in a healthy control, where upon release of acetylcholine (AChR, in red) into the synaptic cleft, the AChR binds to the AChR-receptor (in blue) causing sodium influx eventually leading to activation of the voltage-gated sodium channels (in green) causing a fiber contraction. In purple and yellow the MuSK/LRP4 complex is shown which is responsible for AChR-receptor clustering.*
On the right the different disease mechanisms are shown in MG: ***A****. AChR-antibodies (blue) block the AChR receptors, and thereby neuromuscular signaling directly.* ***B.*** *Via complement activation (brown) and membrane-attack-complexes AChR-antibodies can lead to destruction of neuromuscular folds.* ***C.*** *MuSK (purple) and LRP4 (yellow) antibodies lead to neuromuscular failure due to blockage of healthy AChR clustering.*

be made definitive with additional electrophysiological tests. When a decrement is observed with repetitive nerve stimulation [RNS] or jitter is observed on single-fiber EMG (SF-EMG) the diagnosis is also definite. If these tests fail, diagnosis can be made probable with clinical improvement during additional clinical tests like the acetylcholinesterase inhibitor trial (see diagnostic flowchart in figure 2) or the ice-pack test. [2,3,10] If no definitive diagnosis can be made with serum testing and neurophysiological testing, but there is a clinical improvement after administration of a acetylcholinesterase inhibitor or there is a very clear ocular subtype with asymmetry and fluctuations in diplopia and ptosis, a probable diagnosis of seronegative MG can be made.

MG subtypes
MG patients are often divided into subgroups based on their clinical phenotype.[4] Ocular MG patients have sole involvement of the eye muscles with diplopia and drooping eye lids.[11] Bulbar MG patients have sole involvement of the muscles of the mouth and throat, affecting speech and swallowing. In generalized MG other muscles are also involved, like neck, arm, legs and respiratory muscles. There is an association between clinical phenotype and the

different antibodies. In AChR antibody positive MG the disease often starts ocular. MuSK antibody positive MG patients tend to have a more bulbar phenotype. Many patients start with either an ocular or bulbar phenotype and progress to a more generalized phenotype. In 85% of patients generalization occurs during the course of their disease. However, some patients remain purely ocular or bulbar. For example, in 90% of patients who have had the ocular form for more than 2 years no generalization will occur.[11]

The purely ocular subtype of MG is known to have specific challenges. In purely ocular MG half of patients are seronegative, while in a cross-section of all MG patients only 5% is seronegative.[12] Also, other diagnostic tests fail due to anatomical constraints in testing the eye muscles. Ocular MG is currently often excluded from clinical trials into the development of new therapies, because improvement of ocular symptoms is harder to measure than improvement of generalized muscle weakness. Additionally, the ocular symptoms can be refractory to therapy, leaving patients with invalidating ocular symptoms. Due to the number of challenges in ocular MG, this thesis will focus on this subtype.
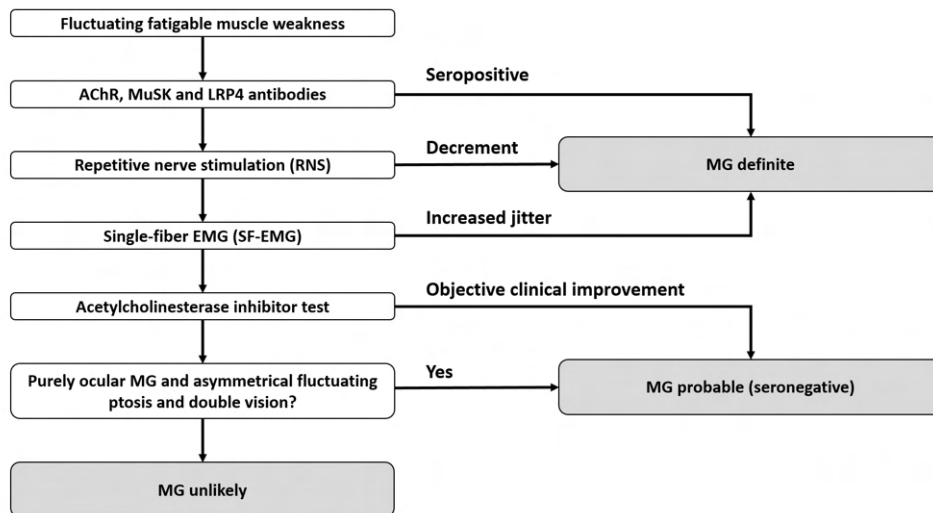
Figure 2. *Diagnostic algorithm for myasthenia gravis. Clinical pattern evaluation, antibody testing and neurophysiological testing are central elements in the diagnostic workup. Adapted from Gilhus NE et al. Myasthenia gravis. Nat Rev Dis Prim. 2019;5(1):30.*

PART II – CHALLENGES IN OCULAR MG

1

To understand the difficulties of diagnosing ocular MG and the challenges in studying ocular function and pathology, understanding of the ocular anatomy is important. The extra-ocular muscles, or the eye muscles, located behind the eye in the bony orbit, move the eye in all directions of gaze. The lateral rectus muscle abducts the eye and the medial rectus muscle adducts the eye. When the eye is in abduction the superior rectus muscle moves the eye up and the inferior rectus muscle moves the eye down. When the eye is in adduction the inferior oblique muscle moves the eye up and the superior oblique muscle moves the eye down (figure 3). When any of these muscles is weak it can result in double vision as experienced by the patient. The levator palpebrae superioris muscle, which is located above the superior rectus muscle, is responsible for lifting the upper eye lid.

Levator Palpebrae Superioris m.

Superior Rectus m.

Superior Oblique m.

Lateral Rectus m.

Medial Rectus m.

Inferior Rectus m.   **Inferior Oblique m.**
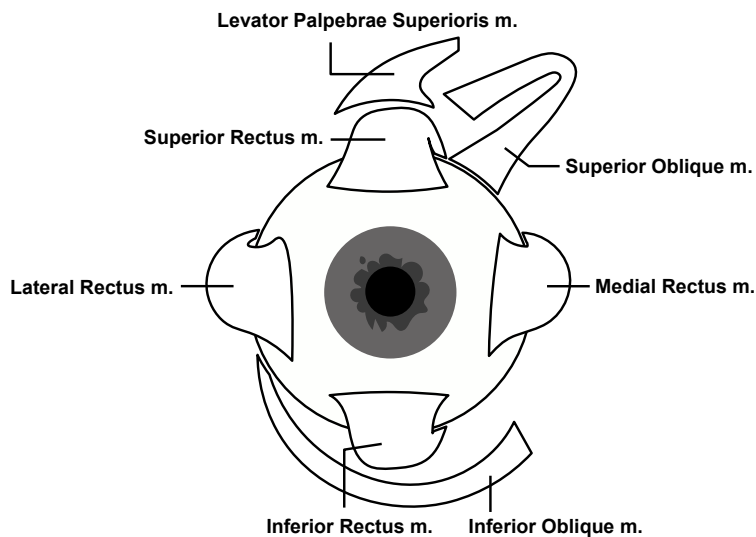
Figure 3. *Anatomy of the right eye with the six eye muscles and the levator palpebrae superioris muscle. The four recti muscles, the lateral, medial, superior and inferior rectus, and the two oblique muscles, the inferior and the superior oblique, move the eye in all directions. The levator palpebrae superior muscles is responsible for lifting the upper eyelid.*

Diagnostic challenge in seronegative myasthenia gravis

There is a diagnostic challenge in seronegative MG patients. Around 50% of ocular MG patients are seronegative. Moreover, the sensitivity of RNS is low in this ocular subgroup of MG. In figure 4 the amount of undiagnosed patients in the world are depicted after RNS for

the generalized and ocular subgroups. While SF-EMG has a higher sensitivity, it requires a specifically trained neurophysiologist to perform the measurement and is thus operator-dependent. In addition, these neurophysiological tests of the eye muscles are not directly possible due to anatomical constraints; the eye muscles and their innervating nerves are located behind the eye in the bony orbit. The ice-pack test and the acetylcholinesterase inhibitor test, however useful, are not fully objective and require symptoms to be present at that current moment. Therefore, additional diagnostics are needed for patients with seronegative disease, who are still regularly misdiagnosed or diagnosed after a considerable delay.[4]
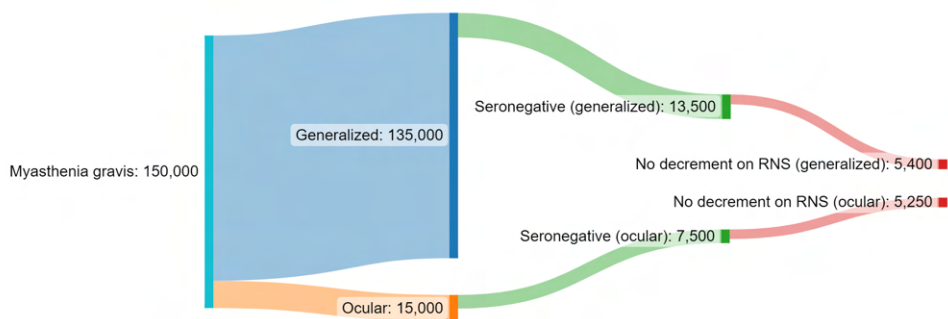
Figure 4. *Diagram depicting the amount of ocular MG patients in the world that remain undiagnosed in generalized MG as compared to ocular MG after antibody testing and repetitive nerve stimulation. 10% of MG patients remain purely ocular, of which 50% of patients are seronegative.*

Therapeutic challenge in refractory ocular myasthenia gravis

There is a therapeutic challenge in the MG patients who struggle with refractory disease, including those with refractory ophthalmoplegia.[9] Little is known about the pathophysiology of refractory ocular ophthalmoplegia in MG. From some case reports [13–16] and a case control study[17] into untreated ocular MG patients, atrophy and fat replacement of the eye muscles have been observed. Fat replacement is known to occur when skeletal muscles are damaged. Also in MuSK and AChR MG, muscle volume decrease and fat replacement of other muscles, like the bulbar muscles responsible for chewing, swallowing and speech, are observed.[18–21] Atrophy and damage of muscles could be an explanation why refractory disease can develop in MG, because severely atrophic and damaged muscles might not respond to therapy. As such, studying to what extent atrophy occurs in the eye muscles, as well as the influence of treatment on this, could aid in pathophysiological understanding of refractory ophthalmoplegia.

1

Lack of outcome measures in ocular myasthenia gravis

Several outcome measures are used to follow the severity of MG-related muscle weakness over time: Patient reported outcome measures like the *MG activities of daily living* (MG-ADL)[22] and quantitative muscle tests evaluating the severity of MG-related muscle weakness like the *quantitative myasthenia gravis score* (QMG).[23,24] For ocular MG patients, however, outcome measures specific for the ocular symptoms are not yet developed or used in the clinic. In recent clinical trials on new treatments[7], the ocular subtype of MG was usually excluded, probably also because the degree of ocular weakness has been difficult to quantify so far.[25,26] Patient reported outcome measures for ocular MG, like the *ocular myasthenia gravis rating scale* (OMGRate)[27] are being developed and evaluated, however more objective scales for the severity of ocular MG, like the QMG is for generalized MG, are missing.

PART III – POTENTIAL AIDS IN DIAGNOSTIC, THERAPEUTIC AND OUTCOME MEASURE CHALLENGES IN OCULAR MG

To overcome the challenges outlined above, methods are needed that can directly measure structure or function of the extra-ocular muscles. Three of these are outlined below: a new neurophysiological test using repetitive ocular vestibular evoked myogenic potentials (RoVEMP), orthoptic measurements and quantitative MRI. The RoVEMP test and orthoptic tests measure eye muscle function, and MRI is used to study eye muscle structure. If there are distinct differences in structure and function between diseases and between MG and healthy controls these methods could be used to aid in diagnosis. Structural and functional changes during the disease course could help in the pathophysiological understanding of refractory ophthalmoplegia, for example if the dysfunctional muscles are severely atrophic. And both distinct structural and functional measures that change during the disease course could function as outcome measures for clinical trials.

Repetitive ocular vestibular myogenic potentials

RNS of peripheral nerves is used to measure the pathologic decremental response of compound muscle action potentials (CMAPs) in MG. Due to depletion of acetylcholine at the neuromuscular junction after repetitive stimulation and partial neuromuscular blockage in MG, the excitation threshold of a part of the fibers is not reached resulting in a decrement in CMAPs.[28] As discussed above, RNS of the eye muscles is not directly possible due to anatomical constraints. However, via stimulation of the vestibular organ, ocular vestibular evoked myogenic potentials (oVEMP) can be elicited. The oVEMP reflex is generated by stimulation of the vestibular organ via vibration applied to the skull or sound to the ear.[29] Using electrodes under the eye, this reflex can be measured for the inferior oblique muscle,

which is located close to the electrodes in up-gaze.[30] Repetitive stimulation (RoVEMP) is in this way considered as a variant of RNS for the eye muscles and indeed a decrement is observed in MG patients (figure 5). [31,32] The diagnostic use of the RoVEMP test is established on a group level. However due to technical difficulties, like a low signal-to-noise ratio and blinking artefacts, the usefulness of the RoVEMP test for an individual patient and for follow-up is unknown. The test-retest reliability should be studied first. I hypothesize that with a good test-retest reliability the RoVEMP test could be useful in diagnostics, as an outcome measure and could help in understanding neuromuscular failure in the eye muscles.
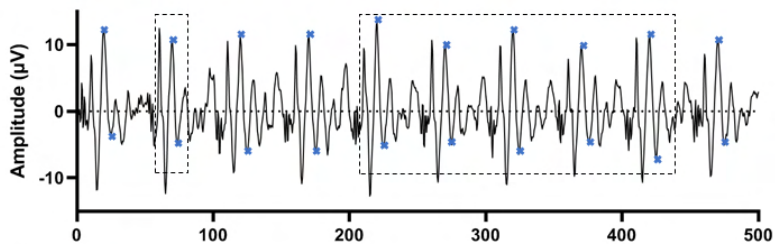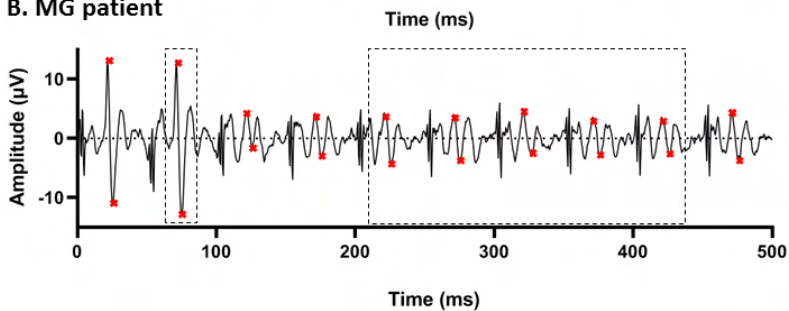
Figure 5. *Example RoVEMP signal in a myasthenia gravis (MG) patient (B) and a neuromuscular control. The signal from the MG patient clearly shows a decremental response after repetitive stimulation. From De Meel et al. Repetitive ocular vestibular evoked myogenic potentials in myasthenia gravis. Neurology. 2020;94(16):E1693-E1701.*

Orthoptic measurements

Orthoptists are the experts in diagnosing and treating defects in eye movement and problems with how the eyes work together. Several orthoptic tests enable measurements of the maximal movement of the eyes and relative deviations between the gazes of the eyes in all directions. These tests can objectively measure eye muscle function and the severity of double vision. A synoptophore can for example be used to measure the maximal movement

of the eye, or duction angles, in all eight gaze directions (up, down, abduction, adduction and the four diagonal gazes).[33,34] The Hess-chart is a test to measure the relative difference in gaze direction between two eyes. Using glasses with a red filter for one eye and a green filter for the other eye, and a screen with red LEDs and a green laser pointer, the difference in gaze direction between the eyes can be objectified.[35] (figure 6) These tests are currently not adapted for the measurement of MG-related fatigability of eye muscles. Since orthoptic measures are direct measures of eye muscle function, I hypothesize that these test when adapted for MG are promising in diagnostics, as an outcome measure and can help to understand the pathophysiology of diplopia in MG.

Synoptophore
Measuring duction angles

Hess chart
Measuring ocular deviations
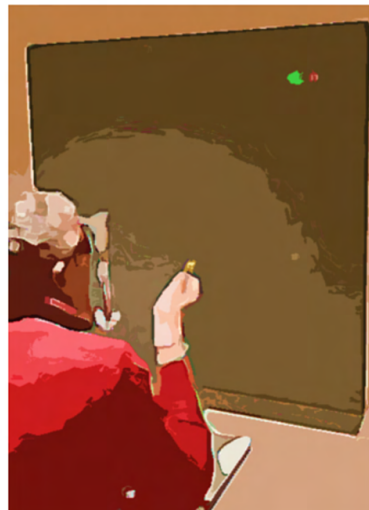
Figure 6. Example orthoptic measurements. On the left a synoptophore that is used for duction angle measurements. Duction angles are measured per eye individually and are a quantification of the angle an eye can move into all 8 primary directions of gaze. On the right a Hess chart that is used to measure the deviation between two eyes by using glasses with a red/green filter, red dots on a screen and a green laser pointer. Adapted from Keene KR et al. Diagnosing myasthenia gravis using orthoptic measurements: Assessing extra-ocular muscle fatigability.

Quantitative MRI in neuromuscular disease

Magnetic resonance imaging (MRI) is a medical imaging technique that uses a strong magnetic field and radio waves to visualize tissues in the body. Quantitative MRI can then assess certain tissue properties. In research into neuromuscular disease, quantitative MRI

is widely used as a biomarker for disease progression and disease activity.[36] Physical disability gets worse (disease progression) when disease activity causes more and more damage to muscle fibers. For example in dystrophic muscular disease, like Duchenne muscular dystrophy, Becker muscular dystrophy and facioscapulohumeral muscular dystrophy, muscles are progressive replaced by fat and fibrosis due to muscle damage. The fat fraction of these muscles as measured with MRI correlates with strength measures in many diseases[37], and can even predict clinical milestones in Duchenne muscular dystrophy[38]. Fat fraction is therefore a marker of disease progression and is used as surrogate outcome measure in clinical trials developing new therapies.[39] Using MR, the fat fraction of a muscle can be quantified and mapped using chemical shift based water fat separation (the Dixon method[40]). The Dixon method uses the difference in precession speed of water and fat to produce separate water and fat fraction maps (figure 7). A proton density weighted fat fraction (PDFF) can be calculated using these maps by dividing the fat signal by the water plus fat signal after correction for specific tissue properties.[37]
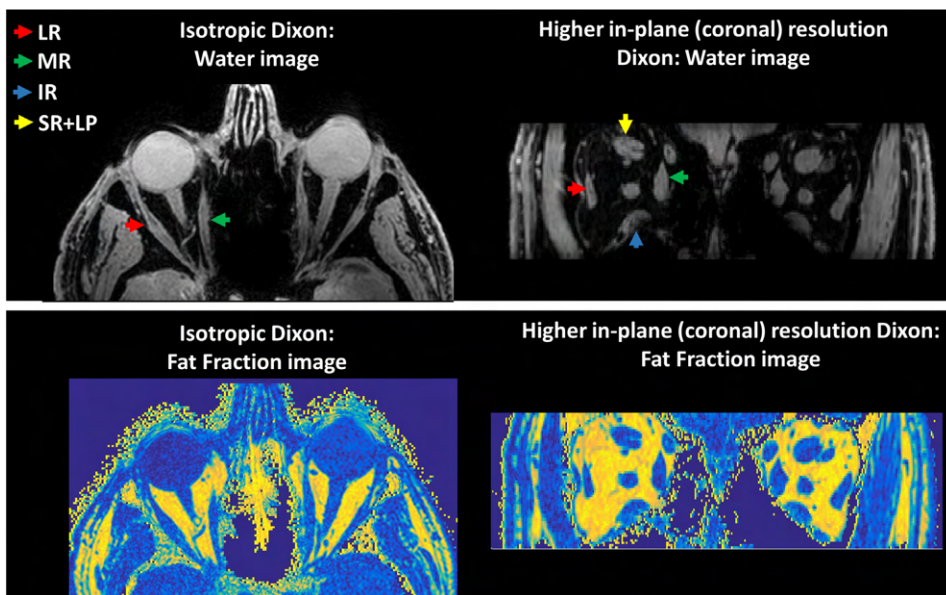
Figure 7. *Examples of water images on top and fat fraction maps below as measured with a chemical shift based water fat separation gradient echo MRI-scan. The colored arrows point out the lateral rectus muscle (LR; red), the medial rectus muscle (MR; green), the inferior rectus muscle (IR; blue) and the superior rectus and levator palpebrae muscle complex (SR+LP; yellow). Adapted from Keene KR et al. The feasibility of quantitative MRI of extra-ocular muscles in myasthenia gravis and Graves' orbitopathy. NMR Biomed 2021;34:e4407.*

The T2 relaxation time of the muscle is proposed as a measure of inflammation and edema reflecting disease activity.[41] Muscle cells mainly consist of water and the T2 of the muscle is around 30 ms. As more free water (e.g. edema) is present between and around the muscle cells the T2 of the tissue increases. Therefore, it is a very sensitive marker of inflammation, however it lacks specificity because it also increases in the presence of membrane leakiness and necrosis.[42] Measuring the T2 of only this water or muscle compartment is challenging, because in neuromuscular disease inside the voxels a combination of fat and water tissue is present. The muscle can be partly replaced by fat due to the disease process. In the presence of this fat, the signal inside a voxel originates from both the water from the muscle cells and the fat. Because fat also has a longer T2 relaxation time than muscle, this biases the T2 measurements towards a longer T2. The signal that is originating from the intramuscular fat should be accounted for in the used models by separating the signal in its two-components: the water signals and the fat signal.[43]

Quantitative MRI of the eye muscles
Applying quantitative MRI of the eye muscles is particularly challenging as compared to the skeletal muscles. Given the large amount of movement of the eye muscles, MR-measurements and MR-images are very prone to movement artefacts. The eye muscles are also very small with diameters of approximately half a centimeter and a length of approximately four centimeter. Therefore a high resolution is needed to image and measure the eye muscles without contamination from the surrounding orbital fat. In MRI the higher the resolution and the smaller the voxels, the lower the signal to noise ratio. Also due to the close proximity of air from the sinuses and bone from the orbit, the inhomogeneity of the main magnetic field (B0) is a challenge to overcome for quantitative measurements in this anatomical area.[44,45]. Recent studies have shown that the increased signal to noise ratio in an MRI with a magnetic field strength of 7 Tesla, combined with a cued instructed blinking to reduce eye-motion artefacts and localized shimming to minimize B0 artefacts, makes it possible to do high resolution images of the eyes (figure 7).[45,46] Since these challenges are overcome, I aimed to combine high resolution orbital MRI and quantitative MRI of muscles to study the structure of the eye muscles of MG patients as compared to healthy controls and other ocular diseases. These structural differences could aid patients in diagnostics, as outcome measure in clinical trials and to understand why ocular symptoms are resistant to therapy in some MG patients.

PART IV - AIMS AND OUTLINE OF THIS THESIS

I aimed to develop novel methods to improve the clinical care of ocular MG patients. First, I aimed to aid in the difficult diagnosis of ocular seronegative MG using the RoVEMP test, orthoptic measurements and quantitative MRI as diagnostic tools. Moreover, I aimed to gain a better understanding of EOM involvement in MG to better understand the pathogenesis of refractory ophthalmoplegia in MG. Lastly, I aimed to directly measure eye muscle function and structure in ocular MG to use as an outcome measure in clinical trials (figure 8).

An extensive literature review was performed into clinical and imaging clues to the diagnosis and follow-up of all diseases with ptosis and ophthalmoparesis (**chapter 2**). With the mentioned techniques I measured the EOM as directly as possible in MG patients. I examined the test-retest reliability of the RoVEMP test, a test that directly measures CMAP decrement of the EOM (**chapter 3**). I examined the EOM functionally by assessing maximal duction angles and deviations as proxies for muscles strength (**chapter 4**). Lastly, I examined structural changes of the EOM using quantitative MRI (**chapter 7**) after developing a method to qualitatively measure muscle inflammation (**chapter 5**) and after assessing the feasibility of doing quantitative MRI of the EOM on a 7 Tesla MR-scanner (**chapter 6**).

1

Figure 8. Summary of the three clinical challenges in ocular myasthenia gravis, the three introduced advanced methods that might aid these challenges and the hypotheses.

Methods

Ocular myasthenia gravis	**RoVEMP test** Neurophysiological measure of eye muscle fatigability	**Orthoptic measures** Functional measures of eye muscle weakness and fatigability	**Quantitative MRI** Structural quantitative measures of eye muscles
Diagnostic Half of patients is seronegative; need for diagnostic tests	Is the test-retest reliability sufficient for diagnosis?	Can orthoptic measures be adapted to measure MG-related fatigability to aid diagnostics?	Are there differences in eye muscle volume, T2 and fat fraction between MG, healthy controls and other diseases?
Understanding refractory ophthalmoplegia Needed for developing effective therapies	Can neuromuscular transmission failure be measured in the eye muscles?	Do eye muscles have a fatigable muscle weakness as is present in skeletal muscles?	Are refractory ocular symptoms in MG caused by eye muscle atrophy and fat replacement?
Ocular outcome measures Need for objective outcome measures of eye muscle weakness	Does decrement correlate with severity of ocular symptoms?	Can orthoptic measures aid as an objective outcome measure for eye muscle involvement in ocular MG?	Can volume, fat fraction and T2 of the eye muscles serve as an outcome measure in clinical trials?

(Challenges)

1. CJ Gorter MRI Center, Department of Radiology, Leiden University Medical Center, Leiden, Netherlands
2. Department of Neurology, Leiden University Medical Center, Leiden, Netherlands
3. Department of Ophthalmology, Leiden University Medical Center, Leiden, Netherlands
4. Duchenne Center Netherlands
5. Department of Radiology, Leiden University Medical Center, Leiden, Netherlands
6. Department of Radiation Oncology, Leiden University Medical Center, Leiden, Netherlands
7. Orbital Center, Department of Ophthalmology, Amsterdam University Medical Centers, Amsterdam, The Netherlands

Clinical and imaging clues to the diagnosis and follow-up of ptosis and ophthalmoparesis

Kevin R. Keene[1,2] | Hermien E. Kan[1,4] | Stijn van Meeren[3,7] | Berit M. Verbist[5]
Martijn R. Tannemaat[2] | Jan-Willem M. Beenakker[1,3,6] | Jan J.G.M Verschuuren[2,4]

ABSTRACT

Background

Ophthalmoparesis and ptosis can be caused by a wide range of rare or more prevalent diseases, several of which can be successfully treated. In this review, we provide clues to aid in the diagnosis of these diseases, based on the clinical symptoms, the involvement pattern and imaging features of extra-ocular muscles (EOM). Dysfunction of EOM including the levator palpebrae can be due to muscle weakness, anatomical restrictions or pathology affecting the innervation.

Methods

A comprehensive literature review was performed to find clinical and imaging clues for the diagnosis and follow-up of ptosis and ophthalmoparesis. We used five patterns as a framework for differential diagnostic reasoning and for pattern recognition in symptomatology, EOM involvement and imaging results of individual patients.

Results

The five patterns were characterized by the presence of combination of ptosis, ophthalmoparesis, diplopia, pain, proptosis, nystagmus, extra-orbital symptoms, symmetry or fluctuations in symptoms. Each pattern was linked to anatomical locations and either hereditary or acquired diseases. Hereditary muscle diseases often lead to ophthalmoparesis without diplopia as a predominant feature, while in acquired eye muscle diseases ophthalmoparesis is often asymmetrical and can be accompanied by proptosis and pain. Fluctuation is a hallmark of an acquired synaptic disease like myasthenia gravis. Nystagmus is indicative of a central nervous system lesion. Secondly, specific EOM involvement patterns can also provide valuable diagnostic clues. In hereditary muscle diseases like chronic progressive external ophthalmoplegia (CPEO) and oculo-pharyngeal muscular dystrophy (OPMD) the superior rectus is often involved. In neuropathic disease, the pattern of involvement of the EOM can be linked to specific cranial nerves. In myasthenia gravis this pattern is variable within patients over time. Lastly, orbital imaging can aid in the diagnosis. Fat replacement of the EOM is commonly observed in hereditary myopathic diseases, such as CPEO. In contrast, inflammation and volume increases are often observed in acquired muscle diseases such as Graves' orbitopathy.

Conclusions

In diseases with ophthalmoparesis and ptosis specific patterns of clinical symptoms, the EOM involvement pattern and orbital imaging provide valuable information for diagnosis and could prove valuable in the follow-up of disease progression and the understanding of disease pathophysiology.

2

INTRODUCTION

Ophthalmoparesis is dysfunction of the extra-ocular muscles (EOM), usually caused by muscle weakness, anatomical restrictions or pathology affecting their innervation. Three pairs of antagonizing EOMs move the eye in all directions: horizontally (medial rectus (MR) and lateral rectus (LR)) and vertically (superior rectus (SR), inferior rectus (IR), superior oblique (SO) and inferior oblique (IO)). Ptosis refers to the drooping of the upper eyelid and can be a disabling or disfiguring symptom. Ptosis is often caused by weakness of the levator palpebrae superioris muscle (LPS) which is responsible for elevating the upper eyelid, with help from the superior tarsal muscle (Muller's muscle). Eye lid retraction, often accompanied by bulging of the eye called proptosis, is generally caused by an increased orbital volume. In this review, we aimed to explore whether the symptomatology, the involvement pattern of EOM, and imaging can aid in diagnosis, follow-up and understanding of diseases with ophthalmoparesis and ptosis.

Causes of ophthalmoparesis and ptosis can be broadly divided into diseases affecting four anatomical locations: brain, nerve, synapse or muscle. These diseases can be either acquired or hereditary. Examples of *brain diseases* that present with ophthalmoparesis are Wernicke's encephalopathy and progressive supranuclear palsy. *Nerve dysfunction*, as seen in congenital fibrosis of the extra-ocular muscles (CFEOM)[47] or acquired nerve disorders, like Miller-Fisher syndrome[48] or Tolosa-hunt syndrome[49], can cause ophthalmoparesis and ptosis following the innervation pattern of the affected cranial nerves. The group of *synaptic diseases* include congenital myasthenic syndromes[50] and acquired synaptic disease such as myasthenia gravis, which is caused by auto-antibodies against neuromuscular junction-proteins.[2] Finally, the group of *muscle diseases* comprises disorders that directly affect the EOM. In acquired muscle disease, ophthalmoparesis and ptosis are often due to inflammation or enlargement of the EOM, orbital fat or other orbital structures. An example of acquired muscle disease is Graves' orbitopathy, in which Thyroid Stimulating Hormone Receptor (TSHR)-antibodies cause orbital inflammation[51]. Examples of hereditary muscle diseases that present with ophthalmoparesis are chronic progressive external ophthalmoplegia (CPEO)[52], caused by mitochondrial dysfunction and oculo-pharyngeal muscular dystrophy (OPMD), with pharyngeal and ocular muscle weakness caused by a mutation in the PABPN1 gene.[53]

To facilitate diagnostic reasoning, we used five main clinical patterns of symptoms that correspond to specific anatomical locations and disease characteristics pointing towards a hereditary or acquired cause of the disease (figure 1). We used these five patterns as a starting point for pattern recognition in symptomatology, EOM involvement and imaging results of individual patients. They do not provide a stringent classification because the
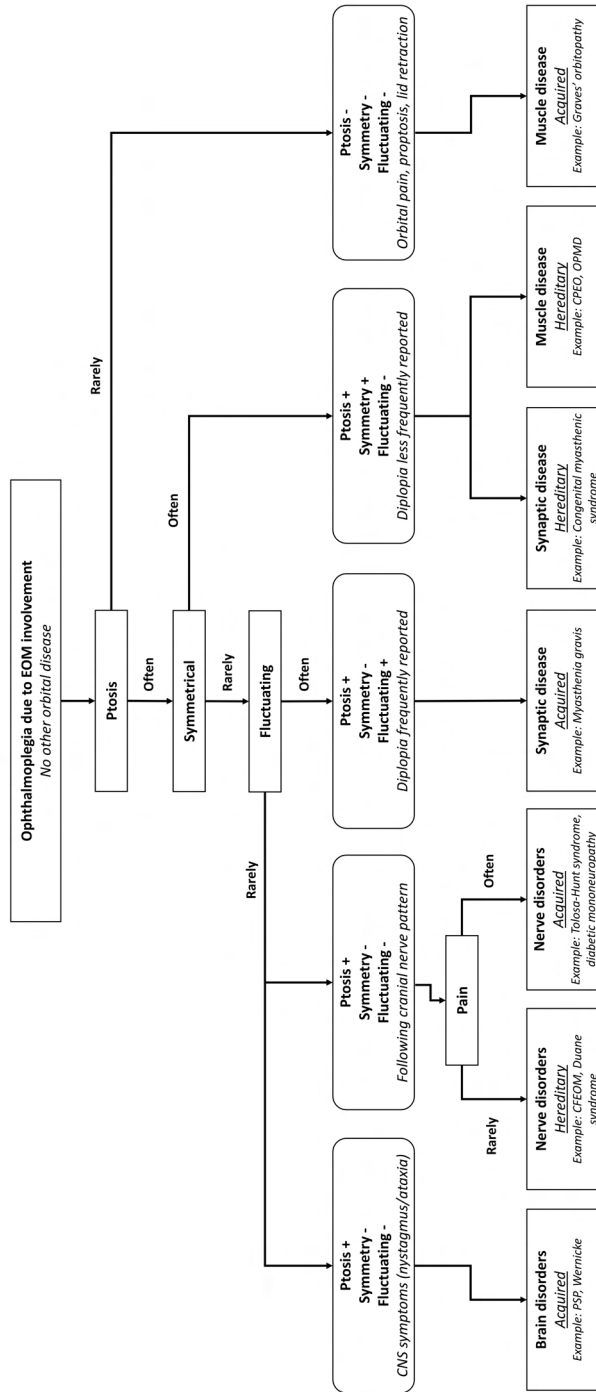
Figure 1. *Five patterns characterized by the presence of combination of ptosis, ophthalmoparesis, diplopia, pain, proptosis, nystagmus, extra-orbital symptoms, symmetry or fluctuations in symptoms. Each pattern was linked to anatomical locations and either hereditary or acquired diseases, as a starting point for clinical evaluation rather than providing a stringent, mutually exclusive classification.*

patterns are not completely mutually exclusive and exceptions do occur. Per pattern, we describe the severity of ptosis and ophthalmoparesis, the presence of diplopia, the symmetry, the presence of fluctuations and accompanying symptoms like pain and CNS symptoms. Per disease we describe the involvement pattern of individual EOM. Lastly, for imaging, we describe identification of causes of ophthalmoparesis and ptosis by identifying primary tumours, metastasis, infection or inflammation and changes due to dysinnervation. In addition, we describe how imaging can identify the involved EOM in specific diseases and help understand the pathophysiology of ophthalmoparesis and ptosis in specific diseases. Disorders of brain and nerve and orbital diseases causing secondary muscle dysfunction (e.g. tumours and infections) are beyond the scope of this paper, but are for a large part reviewed in a recent paper.[54]

Five patterns of clinical presentation of ophthalmoparesis and ptosis

Diseases with ophthalmoparesis or ptosis can be classified using different patterns of signs and symptoms (Figure 1 and Table 1). Diplopia is a patient-reported symptom, while ophthalmoparesis can be assessed with physical examination and quantified using orthoptic measures like ductions as measured with a synoptophore, Hess-chart or with the Goldmann perimeter.[55] We defined ptosis as a decreased distance between the borders of the eyelids due to drooping of the upper eyelid. Several reports provide criteria for ptosis using defined physical landmarks like the border of the eyelids and express their distance in millimetres.[54] This implies that the upper eyelid is lower than its normal anatomical position, typically 1–2 mm below the superior corneoscleral limbus.[56] Similarly, proptosis on MRI or CT is defined as a distance > 23 mm from the anterior surface of the globe to the interzygomatic line[57] or an asymmetry > 2 mm as measured with an exopthalmometer.[58] These strict definitions are not consistently used in the literature that we collected on the many different diseases. Therefore, we accepted the definition that was used in the selected papers.

Diplopia is less frequently seen in hereditary neuromuscular disease with ophthalmoparesis (e.g. in at least half of CPEO patients[59]), probably due to its slow progression, symmetrical involvement and facultative suppression.[52] Ptosis generally occurs symmetrically in these disorders. The co-occurrence of ptosis and ophthalmoparesis is commonly seen in hereditary neuromuscular disease and in synaptic disease, whereas ptosis is rarely present in acquired myopathic disease, commonly associated with pain, proptosis and/or swelling of eyelids and conjunctiva due to EOM enlargement and inflammation.

Table 1. *Differential diagnosis ophthalmoparesis and/or ptosis. Symptomatology is described as the presence of ptosis, ophthalmoparesis, diplopia, asymmetrical symptoms, pain, fluctuating symptoms and the presence of other non-ocular symptoms. The frequently involved EOM are mentioned for each disease (* a more specific description of the EOM involvement pattern can be found in supplementary table 1). The neuromuscular diseases are categorized in acquired and hereditary, and then clustered by the localization of the pathology.*

Hereditary disorders	Ptosis	Ophthal-moparesis	Diplopia	Asymmetry	Pain
Nerve					
CFEOM[47]	Yes	Yes	No	No	No
Duane syndrome[54,62]	Yes	Yes	No	No	No
Blepharophimosis syndrome (BPES)[54,62]	Yes	No	No	No	No
Marcus-Gunn syndrome [54,62]	Yes	No	No	No	No
Synapse					
<u>Presynaptic </u>Congenital Myasthenic Syndromes[12]: Congenital Lambert–Eaton-like, Choline acetyltransferase deficiency, Reduced quantal release, Paucity of synaptic vesicles and reduced quantal release	Yes	Rare	No	No	No
<u>Synaptic</u> Congenital Myasthenic Syndromes[12]: Endplate AChE deficiency, CMS with LAMB2 mutation	Yes	Yes	No	No	No
<u>Post-synaptic</u> Congenital Myasthenic Syndromes[12]: Slow Channel syndrome, AChR Deficiency, Fast channel syndrome, Rapsyn deficiency, Plectin deficiency, Dok-7 myasthenia	Yes	Yes	Rare	No	No
Muscle					
Progressive External Ophthalmoplegia [52]	Yes	Yes	Half of patients[59]	No	No
Pompe disease[83]	Yes	No	No	Yes	No
OPMD[53]	Yes	Yes	Rare[131]	No	No
Myotonic dystrophy type 1[80,81]	Yes	Rare[82,94]	No	No	No
Centronuclear myopathy[79,109]	Yes	Yes	No	No	No

Acquired disorders	Ptosis	Ophthal-moparesis	Diplopia	Asymmetry	Pain
Brain					
Progressive Supranuclear Palsy	No	Yes	No	No	No
Internuclear ophthalmoparesis (MS / stroke)	No	Yes	Yes	No	No
Wernicke Encephalopathy	Rare	Yes	Yes	No	No
Brain stem tumour[133]	Yes	Yes	Yes	Yes	No
Nerve					
Miller-Fisher syndrome[114]	Yes	Yes	Yes	No	No
Recurrent painful ophthalmoplegic neuropathy	Yes	Yes	Yes	Yes	Yes
Horner syndrome	Yes	No	No	Yes	No
Tolosa–Hunt syndrome[136]	Yes	Yes	Yes	Yes	Yes
Diabetic mononeuropathy[63]	Rare	Yes	Yes	Yes	No

Fluctuating	Most frequently involved EOM*	Other symptoms
No	LPS, SR (depends on affected nerves)[47,60,61,96]	No
No	LPS, LR, MR (aberrant innervation)	No
No	LPS	Horizontal narrowing of the eyelids, epicanthus inversus, lacrimal duct abnormalities
No	LPS	Upper eye lid retraction when chewing or laughing.
No		Other muscles
No	LPS, LR, SR, IO[50]	Other muscles
No	LPS, LR, SR, IO[50]	Other muscles
No	LPS, SR[52]	Other muscles and organs (heart)
No	LPS[83]	Other muscles
No	LPS, SR, LR [53]	Pharyngeal and leg muscles
No	LPS (cases of LR and MR).[94]	Other muscles
No	LPS, SR, LR[79,109]	Other muscles

Fluctuating	Most frequently involved EOM*	Other symptoms
No	SR, IO, IR, SO[132]	Parkinsonism, balance, dementia, bulbar symptoms
No	MR	Other CNS symptoms and nystagmus
No	LR[115]	Encephalopathy and ataxia. Predominantly nystagmus.
No	Location dependent.	Other cranial nerves and lateralized CNS symptoms
No	LR > LPS, SR, IR, MR[114]	Vestibular and facial
No	LPS, SR, IR, MR, IO (N. III)[134]	Attacks of headache
No	No EOM (superior tarsal muscle)[135]	Anhidrosis and myosis
No	LPS, SR, IR, MR, IO (N. III) or LR (N. VI)[49]	No
No	LPS, SR, IR, MR, IO (N. III) or LR (N. VI)[63]	Transient palsy. Presence of diabetes.

Table 1. *Continued*

Acquired disorders	Ptosis	Ophthal-moparesis	Diplopia	Asymmetry	Pain
Synapse					
Autoimmune LEMS[12,113,137]	*Yes*	*Rare[138]*	*Yes*	*Yes*	*No*
Autoimmune myasthenia gravis[12]	*Yes*	*Yes*	*Yes*	*Yes*	*No*
Botulism[139,140]	*Yes*	*Yes*	*Yes*	*No*	*No*
Acetylcholinesterase intoxication[141]	*Yes*	*Yes*	*Yes*	*No*	*No*
Muscle					
Orbital lymphoma	*Rare*	*Yes*	*Yes*	*Yes*	*Rare*
Idiopathic Orbital myositis[68]	*Rare*	*Yes*	*Yes*	*Yes*	*Yes*
IGG4-related disease of the orbit[66,67]	*Rare*	*Yes*	*Yes*	*Yes*	*Yes*
Thyroid orbitopathy / Graves' disease[143,144]	*No*	*Yes*	*Yes*	*Yes*	*Yes*
Systemic auto-inflammatory diseases[66,76]	*No*	*Rare*	*Rare*	*Yes*	*Yes*
Rare presentation of Amyloidosis[70]	*No*	*Rare*	*Rare*	*Yes*	*Rare*

LPS: Levator Palpebrae Superior, SR: Superior rectus muscle, IR: Inferior rectus muscle, LR: Lateral rectus muscle, MR: Medical rectus muscle, IO: Inferior oblique muscle, SO: Superior oblique muscle.

In the first pattern, constant ophthalmoparesis with diplopia is present with or without ptosis, and accompanied by central nervous system (CNS)-abnormalities such as upper gaze paralysis, nystagmus or other neurological extra-ocular manifestations. This pattern is characteristic of **acquired brain disease,** in which diplopia and ophthalmoparesis co-occur with evident CNS-abnormalities and the presence of nystagmus. The presence of nystagmus is evident in internuclear ophthalmoparesis caused by MS or stroke: when one eye adducts, nystagmus of the contralateral eye is observed. Examples of CNS-abnormalities accompanying the ocular symptoms are parkinsonism, dementia and swallowing problems (or dysphagia) in progressive supranuclear palsy and the triad of ataxia, ocular symptoms and an altered mental state in Wernicke encephalopathy. Moreover, nystagmus is also commonly present in Wernicke encephalopathy.

The second pattern consists of constant ophthalmoplegia or ptosis, and is often asymmetrical or painful. This pattern points towards **nerve disorders, either acquired or hereditary**. A patient with this pattern typically has constant painless ophthalmoplegia or ptosis that can be attributed to the innervation pattern of a specific cranial nerve. For example in CFEOM, the muscles that lack cranial nerve innervation become fibrotic. In CFEOM type I there is agenesis of the superior division of N. III[47,60] and in CFEOM type II, there is agenesis of the entire N III and N IV.[47,61] In other congenital ptosis syndromes, atrophy of the EOM are often secondary to abnormal innervation and development: in Duane syndrome the N. VI is absent and the LR is innervated by a branch of the N. III, Marcus-Gunn syndrome is caused by an

	Fluctuating	Most frequently involved EOM*	Other symptoms
	Yes	LPS [113]	Other muscles and autonomic
	Yes	LPS, IO, SR > LR, MR [110–112]	Other muscles (bulbar, neck)
	No	LPS[140]	Other muscles
	No	Unknown	Other muscles
	No	Location dependent. [142]	Depends on localization
	No	LR, SR, MR, IR [87,105]	Chemosis, Proptosis. Involvement of lacrimal gland and orbital fat.
	No	LR[89] > IR, SR [87,108]	Proptosis. Involvement of lacrimal gland, orbital fat and nerves.
	No	IR, MR, SR[87,105]	Eyelid retraction, proptosis and thyroid involvement.
	No	-	Involvement of other organs
	No	LR, MR[70]	Other organs

2

anomalous connection of motor fibres from the N. V to the n III. and blepharophimosis syndrome (BPES) with narrowing of the eyelids.[54,62] In acquired nerve diseases, the symptomatology is often asymmetrical since the nerve is affected unilaterally, e.g. in Horner syndrome, where only the superior tarsal muscle is affected, or diabetic mononeuropathy (often N. III[63]) . If the cause is within the cavernous sinus (e.g. Tolosa-Hunt syndrome), multiple ipsilateral cranial nerves can be affected (N. III in 80% of cases, N. VI in 70% of cases and N. IV in 30% of cases[49]). An exception to this pattern is Miller-Fisher syndrome, which often has a symmetrical bilateral involvement of several cranial nerves.

In the third pattern, patients present with fluctuating ophthalmoparesis with diplopia and asymmetrical ptosis, which is indicative of an **acquired synaptic disease** like myasthenia gravis[11]. In this pattern, muscle weakness fluctuates over larger periods of time and within one day, with symptoms becoming worse during the day and improving after a period of rest. In myasthenia gravis, the EOM are involved in about 80% of patients, but other muscles are often involved like the bulbar, neck and limb muscles.[1]

The fourth pattern is characterized by constant ophthalmoparesis with diplopia, but ptosis is not usual. These symptoms are most commonly asymmetrical and painful, but again without clear fluctuation. This is typical for **acquired muscle disease**. This pattern most often points to inflammatory disease: Graves' orbitopathy, IgG-4 related orbital disease (IgG4-ROD), idiopathic orbital inflammation and idiopathic orbital myositis.[64–68]. Patients experience

asymmetrical retrobulbar pain with accompanying ophthalmoparesis and sometimes proptosis. The differential diagnosis of painful ophthalmoparesis included the inflammatory diseases mentioned, but is very wide. It also includes vascular diseases such as aneurysms and dissections, neoplastic diseases such as lymphoma and metastases, infectious diseases including tuberculosis and extended bacterial infections and other inflammatory diseases like Tolosa-hunt syndrome (for a wider differential see Montagnese et al and Gladstone et al.).[68,69] Rarely, systemic auto-inflammatory diseases may present with a painful ophthalmoplegia, including amyloidosis[70], systemic lupus erythematosus [71,72], sarcoidosis[73] and Crohn's disease[74–76]. Therefore, a systemic diagnostic evaluation in inflammatory orbital diseases is important, as a systemic disease should be thoroughly excluded before labelling the disease idiopathic.[77] In these diseases ptosis is rarely observed or masked by proptosis, however due to bulging of one eye and contralateral lid retraction, the presence of ptosis is sometimes reported. This is referred to as pseudoptosis.

Lastly, the fifth pattern consists of ophthalmoparesis and ptosis, but without diplopia as a predominant feature. The pattern of symptoms indicates a **hereditary muscle disease.** OPMD and CPEO are hereditary muscle diseases that are directly associated with ophthalmoparesis and ptosis.[12,52,53,61,78]In general, diplopia is less frequently reported in these diseases.[52] In addition, there is no clear asymmetry, pain or fluctuation. The lack of diplopia in the presence of clear ophthalmoparesis points toward a hereditary muscle disease, because the brain can adapt to the slowly developing ophthalmoparesis, a phenomenon called facultative suppression. However, throughout their disease at least half of for example CPEO patients do experience diplopia at some time in the disease course.[59] . In centronuclear myopathy[79] and myotonic dystrophy type 1[80–82], ptosis and ophthalmoparesis occur regularly. In later stages of Pompe's disease, ptosis[83] may occur. In many other hereditary muscle diseases, including Duchenne muscular dystrophy[84], the eye muscles are remarkably spared. Congenital myasthenic syndrome, although a synaptic disease, also presents with ophthalmoplegia, often without diplopia, and symmetrical ptosis. The postsynaptic types of congenital myasthenic Syndrome (Slow Channel syndrome, AChR Deficiency, Fast channel syndrome, Rapsyn deficiency, Plectin deficiency) present more frequently with ocular symptoms than synaptic and presynaptic congenital myasthenic syndromes. [12]For clinical reasoning it is important to note that some congenital myasthenic syndromes can have an onset in early or even late adulthood, especially congenital myasthenic syndrome associated with rapsyn[85], agrin, plectin, ALG14, and GMPPB gene mutations.[86]

2

Imaging of extra-ocular muscles

Magnetic Resonance Imaging is the primary tool for the assessment of ophthalmoparesis. It provides detailed information on orbital soft tissues, cranial nerves and the posterior cranial fossa. Besides anatomic sequences (T1 weighted [T1w] and T2 weighted [T2w] images) functional sequences such as diffusion weighted imaging (DWI), reflecting the Brownian motion of water molecules and thereby sensitivity to tissue architecture. Also contrast-enhanced perfusion may be added to characterize lesions.[87,88] Compute tomography (CTCT) scans also demonstrate orbital pathology, in particular of bony origin. In MRI, there is a difference between quantitative and qualitative scans.[36] Quantitative scans allow for the numeric measurements of T1 and T2 (multi-echo spin-echo) relaxation times and for example chemical shift based water-fat separation scans allow for the quantification of fat fractions in tissue. Qualitative anatomical sequences can be used to identify a focal mass or changes in volume and cross-sectional area of the EOM, reflecting EOM enlargement due to hypertrophy or inflammation or atrophy. Changes in signal intensities on qualitative T1w, T2w or DWI images, and enhancement and contrast scans can all indicate different types of tissue alterations. For instance, oedema and/or inflammation will cause an increase in the T2 relaxation time of water, and thereby signal intensity increase on T2w images, which can be observed on fat-suppressed images. Fat replacement, i.e. the replacement of muscle tissue with fat, will be hyperintense on both T1w and T2w images[37] due to the shorter T1 relaxation and longer T2 relaxation time of fat. On fat-suppressed images, this will be shown as signal loss .[36] Fibrotic tissue has a very short T1 and T2 relaxation time, and hence is hardly visible on T1w and T2w images. The location and number of involved EOM may be suggestive of a specific disease (e.g. in IgG4 related orbitopathy usually bilateral involvement with a predilection for the lateral rectus muscle[89] is seen, while IOM is typically unilateral and mostly affects the medial rectus muscle). Supportive findings such as involvement of the lacrimal glands, increased orbital fat and vascular engorgement aid in the differential diagnosis but fall outside the scope of this paper.

For all diseases, we included MRI and CT studies in this review in which the EOM were studied or mentioned. Such studies were not available for all mentioned diseases; No MRI or CT studies describing the EOM were reported in Pompe's disease, in OPMD, Lambert-Eaton myasthenic syndrome (LEMS) and congenital myasthenic syndromes. For some diseases, we found only a small number of case reports; One case report describing a patient with myotonic dystrophy, in which no changes in the EOM were reported[82], and a small number of case reports of EOM involvement for systemic auto-inflammatory disease.[71,72,74–76] (Table 2)

Table 2. Reported imaging findings in the extra-ocular muscles for orbital disease with ophthalmoparesis and ptosis interpreted as histopathological changes: fat increases, inflammation, enlargement and atrophy. The neuromuscular diseases are categorized in acquired, synaptic and hereditary.

Disease	Volume changes on anatomical sequences	T2 weighted (T2w) imaging with fat suppression	T1 weighted imaging (T1w)/ T2 weighted (T2w) imaging without fat suppression / chemical shift based water-fat separation (Dixon)	Other findings
	Atrophy / Swelling	*Inflammation*	*Fat increase*	
Acquired disease				
Idiopathic Orbital myositis	*EOM enlargement with tendon involvement.* [68,87]	*Increased signal on T2w imaging of the affected EOM.* [64,100,101]		*Surrounding T2 increases due to cellulitis.* [100]
IGG4-related disease of the orbit	*EOM enlargement with tendon sparing (fusiform enlargement), mostly LR.* [89]	*Decreased signal on T2w imaging of the affected EOM.* [100]		*Lacrimal gland and infra-orbital nerve enlargement.* [89] *Optic nerve enlargement.* [68]
Thyroid orbitopathy / Graves' orbitopathy	*Fusiform enlargement of all EOM, often with tendon sparing, most pronounced in IR, MR and SR.* [51,90] *Increases in volume most pronounced in active stage; volume decreases in chronic but may still be enlarged.* [91]	*Increased signal in the acute inflammatory phase* [51,102]	*T1 hyperintense signal, mainly in chronic patients.* [14,51,93,105]	*Increased orbital fat volume. Enlarged lacrimal glands . Vascular engorgement.*
Systemic auto-inflammatory diseases	*Sarcoidosis: Bilateral EOM enlargement.* [88,145] *Crohn's disease: Enlargement of the SR and LPS.* [74] *Enlargement of the LR.* [76] *Enlargement of the IR.* [75] *Often with tendon involvement.*	*T2w hypo- or hyperintensity of affected EOM.* [74–76]		*Sarcoidosis: enlarged lacrimal gland, thickening and enhancement optic nerve*
Amyloidosis	*Enlargement of the LR muscle with tendon sparing in amyloidosis.* [70]	*No hyperintensity on T2w-STIR.* [70]		*An area without contrast enhancement, as compared to the rest of the EOM, is observed.* [70]
Orbital lymphoma	*Muscle enlargement or focal mass.* [146]	*Focal hyper- or isointense (as compared to the EOM) mass.* [146,147]	*Focal hypo- or isointense (as compared to the EOM) mass.* [146]	*Diffusion restriction: low ADC value.* [72,144]
Synaptic disease				
Autoimmune LEMS	*Not reported.*	*Not reported.*	*Not reported.*	

2

Autoimmune myasthenia gravis	Decreases in volume in chronically untreated/treatment resistant patients[13,17,97] and in Muscle-specific tyrosine kinase (MUSK) positive patients.[98] No changes or small increases in volume in chronically treated and recent myasthenia gravis patients.[14,99]	No hyperintensity on T2w scan in 20 myasthenia gravis patients.[104]	Increases in fat fraction in the EOM in myasthenia gravis on Dixon scans.[99] Central hypo-intensity on T2w scans with fat suppression.[104]	
Congenital Myasthenic Syndrome	Not reported.	Not reported.	Not reported.	
Hereditary disease				
Chronic Progressive External Ophthalmoplegia (CPEO)	Decrease in volume in all EOM, most pronounced in SR/LPS.[14] Decrease in cross-sectional area in all EOMS (43%).[93]	Two patients with STIR hyperintensities.[93]	T1 hyperintense signal that is hypointense on STIR.[14,93] Prolonged (global) T2 relaxation time.[93]	
Pompe disease	Not reported.	Not reported.	Not reported.	Not reported.
OPMD	Not reported.	Not reported.	Not reported.	Not reported.
Myotonic dystrophy	Case report: No changes in EOM.[82]	Case report: No changes in EOM.[82]	Case report: No changes in EOM.[82]	
CFEOM	Severe atrophy of LPS and SR in CFEOM type 1.[95] Atrophy of all EOM, especially also SO and LR is relatively spared in CFEOM type 2.[61,96]		Bright signal regions and longitudinal fissures in LR and MR in CFEOM type 2 on T1w imaging.[95]	Absence of superior division of N. III in CFEOM type 1.[60,95] Absence of N. III and N. IV in CFEOM type 2.[61]
Congenital ptosis syndromes (e.g. Duane syndrome and BPES)	Atrophy/hypoplasia of the SO in Duane syndrome.[148] Atrophy of the LPS in BPES[149]	Not reported	Increases in T2 showing fatty patches in the LPS.[149]	Aberrant innervation of LR by branch of N. III and absence of N. VI in Duane syndrome.[150]

MRI and volume of the extra-ocular muscles

In acquired muscle disease of the orbit, EOM enlargement in different extend with or without tendon involvement is a frequent observation. In idiopathic orbital myositis, EOM volume is increased with involvement of the tendons, presenting as tendon thickening. In contrast, Graves' orbitopathy [51,90] and IgG4-related orbital disease[89] (in 96% of patients) cause EOM enlargement of on average twice the size[68,91] with tendon sparing, known as fusiform enlargement. This specific pattern of enlargement can therefore be useful in differential diagnostics. An example of EOM enlargement in Graves' orbitopathy can be found in figure 2. In systemic diseases with EOM involvement, like Crohn's disease, sarcoidosis, systemic lupus erythematosus and amyloidosis, EOM volumes are increased as qualitatively described in several case reports.[70,72–75,92] In Graves' orbitopathy EOM volume usually decreases in the inactive stage of the disease (e.g. for the SR: 1.1 cm^3 in chronic inactive compared to 1.3 cm^3 in chronic active), but is still more than double compared to healthy EOM (0.6 cm^3).[91] EOM atrophy is a common finding in hereditary neuromuscular disease. In CPEO, the mean cross-sectional area of all EOM was 43% lower than for controls.[93] An example of atrophy in CPEO can be seen in figure 2. The most pronounced reduction is in the SR and the LPS muscle, which is consistent with the clinical presentation with ptosis and gaze limitations in elevation.[14] One case report reported normal volumes of the EOM in a patient with ophthalmoparesis associated with myotonic dystrophy.[94] In CFEOM, many imaging studies have shown that the denervated EOM are atrophic. In CFEOM type 1, caused by agenesis of the upper branch of the oculomotor nerve, there is atrophy of the LPS and the SR in all subjects, with an average volume reduction of 60% in the SR. [95] In CFEOM type 2, with more global dysgenesis of the oculomotor nerve, the SO and LR are relatively spared and the other EOM are severely atrophic. [61,96] In myasthenia gravis, an acquired synaptic disease, case reports describe qualitatively decreases in volumes in chronically untreated or treatment-resistant patients [13,97] and in muscle-specific tyrosine kinase (MUSK) positive myasthenia gravis patients.[98] However, normal volumes or slight increased volumes (0.8±0.2 cm^3 in MG and 0.6 ± 0.2 cm^3 in healthy controls, all recti EOM averaged) were observed in recently diagnosed and chronic myasthenia gravis patients.[14,99]

MRI and inflammation

When inflammation of orbital fat or muscle is the cause of ophthalmoparesis and ptosis, the inflammatory process is often shown as hyperintense on T2w MRI images due to the presence of oedema. The EOMs have an increased signal on T2w imaging with fat suppression in idiopathic orbital myositis [64,100,101], in active Graves' orbitopathy [51,102] and in systemic auto-inflammatory diseases like Crohn's disease, sarcoidosis and Systemic lupus erythematosus. [74–76,103] IgG4-ROD[100] demonstrates relatively low signal intensity on T2w -MR images because of its increased cellularity and amount of fibrosis. In hereditary muscle and synaptic disease,
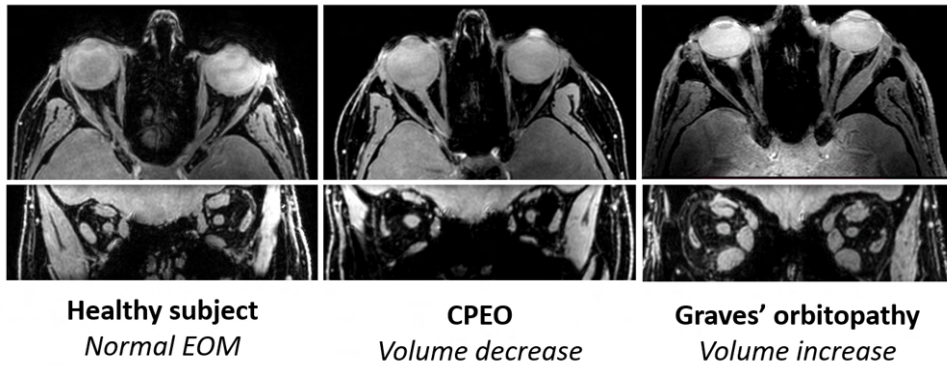
Healthy subject
Normal EOM

CPEO
Volume decrease

Graves' orbitopathy
Volume increase

Figure 2. *MRI scans of the orbit. Chemical shift based water-fat separation (using the Dixon technique) was used and the water image is shown; on top the transverse image and on bottom the coronal image. Volume decrease, indicative of atrophy, of the EOM is clearly demonstrated in CPEO and enlargement of the EOM in Graves' orbitopathy.*

however, evidence of inflammation is sparse. In two patients with CPEO, hyperintensities were observed on a T2w scan with fat suppression.[93] No hyperintensities were present on T2w scans in 20 myasthenia gravis patients.[104]

MRI and fat replacement of muscles

In the chronic stages of Graves' orbitopathy, an increase in fat in the EOM is observed on MRI, which is the result of adipogenesis by fibroblasts and fibrocytes. [90,105,106] In CPEO, an increase in signal intensity on a T1w scan has been described within EOM[14], as well as a quantitative increase in T2 relaxation time[93]; both indicative of fat replacement in the EOM. Signal loss on fat-suppressed images confirmed the presence of fat in this study. An example of fat replacement of the EOM as quantitatively measured with chemical shift based water-fat separation imaging (using the Dixon technique) in an OPMD patient can be seen in figure 3. The fat fraction of the EOM increases to up to 10% in myasthenia gravis patients on chemical shift based water-fat separation scans. [99] In addition, central hypo-intensities were observed on T2w scans with fat suppression in myasthenia gravis.[104] In myasthenia gravis, fat replacement appears to be less frequently reported in literature than in CPEO. In CFEOM type II, T1w imaging shows bright signal regions and longitudinal fissures in the LR and the MR, also indicative of fat replacement.[95]

Correlating quantitative MRI parameters with disease activity and disease severity

Only in a small number of the reviewed imaging studies, quantitative MRI parameters were correlated with disease activity or disease stage. In CPEO the range of eye movement was

correlated with the global T2 relaxation time of the EOM, a parameter mainly reflecting fat replacement: patients with a smaller range of motion had more fat replacement. [93] In Graves' orbitopathy, EOM volume as measured with MRI and ultrasound is strongly correlated with disease activity. Mild and pronounced active stages of disease (stages G1 and G2) show progressively larger EOM volumes (e.g. for the SR: 1.1 cm^3 in chronic inactive compared to 1.3 cm^3 in chronic active) than normal subjects. Hereafter, volumes decreases in later stages with longstanding active disease (stage G3) and chronic stages without active disease (stage G4) but remain about 10 percent higher than in normal subjects.[91] In another study into the natural course of Graves' orbitopathy with a follow-up of at least four years, also a slight increase of orbital fat volume from 15 to 16.8 ml, a decrease in muscle volume of 1 ml (decrease of ~20% on a muscle of 4.5 ml), and visible intramuscular fat was observed.[107] In case reports of the EOM in myasthenia gravis patients, long untreated and chronic myasthenia gravis patients appear to have EOM atrophy and fat replacement as qualitatively described.[13,97] On the contrary, a slight increase in EOM volume of 0.2 cm^3 was observed in chronically treated and recent myasthenia gravis patients, also suggesting differences between different disease stages. [14,99]

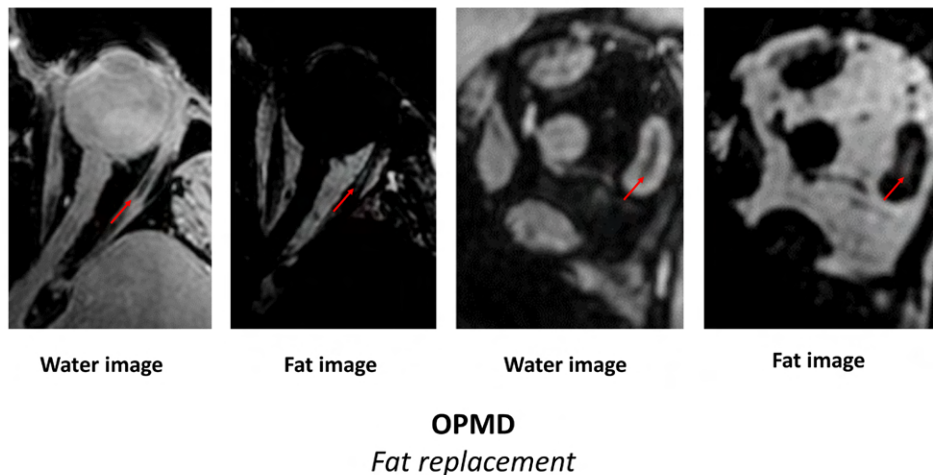**Figure 3.** *MRI scans of the orbit. Chemical shift based water-fat separation (using the Dixon technique) was used and the transverse water image (first), transverse fat image (second), the coronal water image (third) and the coronal fat image (fourth) are shown. This MRI scan demonstrates fat replacement of the EOM in a patient with OPMD. The fat replacement is predominantly observed in the lateral rectus muscles (red arrows).*

Clinical and radiological clues from the different combinations of extra-ocular muscle weakness

To accurately assess the involvement pattern of individual EOM in orbital disease, both imaging studies and orthoptic studies were reviewed (supplementary table 1 and figure 4). For the three most commonly acquired orbital diseases the involvement pattern is well described in literature. In Graves' orbitopathy, the IR, MR and SR are most predominantly asymmetrically involved with remarkable sparing of the LR and the oblique muscles. In idiopathic orbital myositis, involvement is unilateral and the LR is not spared.[87,105] In IgG4-ROD the LR is most often involved bilaterally[89], with the IR and SR affected subsequently.[108] Auto-inflammatory diseases with orbital involvement have a variety of involvement patterns, for example as extensively described in case reports for Crohn's disease with MR and oblique muscles relatively spared.[74–76] In a case report of systemic lupus erythematosus the MR and IR were involved[71] and in another case report the LR was solely involved.[72] In amyloidosis, the horizontal rectus muscles seem most predominantly affected.[70]

In hereditary muscle disease with orbital muscle involvement the LPS is most frequently affected. In CPEO, elevation limitation due to weakness of the SR is the second most present ocular symptom.[52] In OPMD the SR is the most affected muscle, followed by the LR.[53] In Pompe's disease[83], centronuclear myopathy[79] and myotonic dystrophy[80,81] the LPS is often the only affected ocular muscle, but case reports have described horizontal ophthalmoparesis with weakness of the MR and LR in myotonic dystrophy[82,94] and elevation and abduction limitations in centronuclear myopathy[109].

In synaptic disorders the individual variation of EOM involvement is high, with ptosis being more common than ophthalmoparesis. In literature, the ocular involvement pattern in myasthenia gravis differs, however elevation is most often found to be limited (IO > SR), followed by horizontal limitations (LR > MR). [110–112] In LEMS the LPS is frequently weak, causing ptosis in up to 54% of patients. EOM weakness does not occur frequently in LEMS, but 30% of patients have ocular motility abnormalities.[113] The pattern of congenital myasthenia gravis is similar to auto-immune myasthenia gravis with almost no limitations in depression, however horizontal eye movements (LR > MR) are more frequently limited than elevation.[50] In disorders where nerve pathology and lack of innervation cause muscle dysfunction, the involvement pattern is confined to the innervation area of one or more cranial nerves. In CFEOM the agenesis of (a branch) of the oculomotor nerve, or less common the abducens nerve, causes atrophy of the innervated muscles. Similarly, diabetic mononeuropathy also affects the oculomotor nerve and the abducens nerve.[63] In Tolosa-hunt syndrome the oculomotor nerve is affected in 80% of individuals, followed by the abducens nerve in 70% and the trochlear nerve in 30%[49]. In Miller-Fisher syndrome dysfunction of the LR, due to
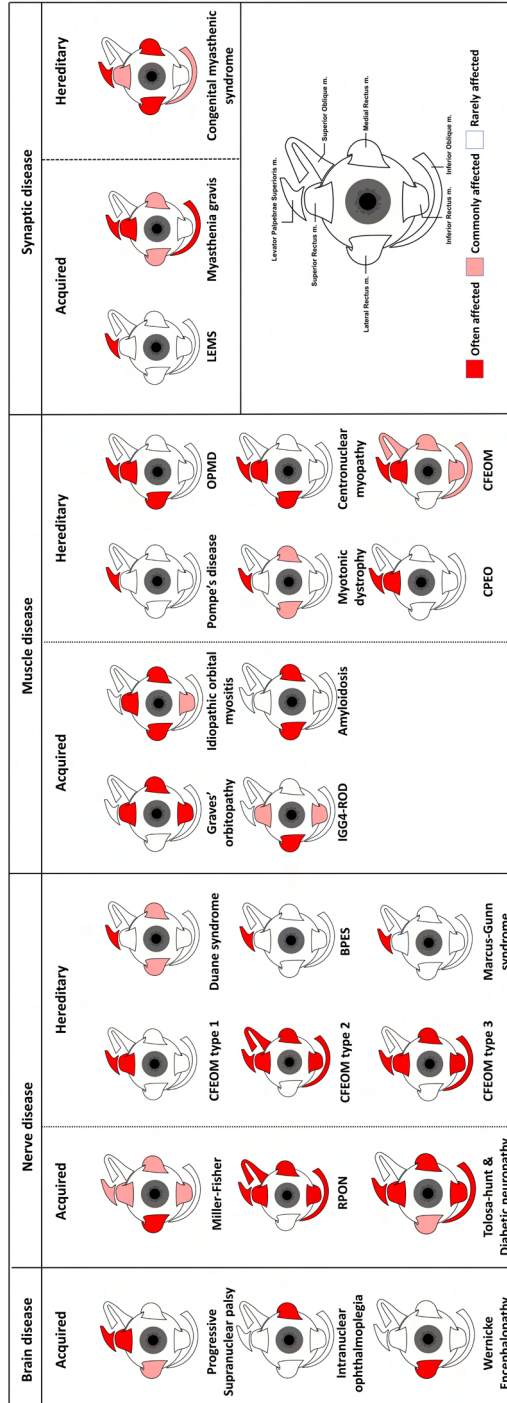
Figure 4. *Involvement pattern of the six extra-ocular muscles and the levator palpebrae superioris muscle for brain diseases, nerve diseases, muscle diseases and synaptic disease split into either acquired or hereditary. An example of the right eye is shown.*

involvement of the abducens nerve, is most commonly involved and the last to recover.[114] Interestingly in Miller-Fisher syndrome the ophthalmoparesis is mostly symmetrical.[114]

In brain disease with ophthalmoparesis, ptosis is unusual except for brain stem pathology such as brain stem tumors. Brain stem tumors are known to mimic other diseases, for example myasthenia gravis, and symptoms are dependent on tumor localization. In Wernicke's encephalopathy limitations in abduction due to palsies of the LR are most common.[115] Progressive supranuclear palsy is a disease that can mimic dementia and Parkinson's, and ophthalmoparesis is always in the vertical direction. Internuclear ophthalmoparesis is a rare gaze abnormality characterized by impaired adduction of the affected eye, with nystagmus of the abducted contralateral eye.

DISCUSSION

This review combines clinical symptoms and EOM involvement pattern on imaging to provide clues for diagnosis of diseases with ophthalmoparesis and ptosis, including acquired and hereditary diseases with pathology located in the brain, nerve, synapse or muscle.

Some general conclusions can be made, based on the combination of clinical symptoms, and the involvement pattern and imaging features of the different EOMs. Firstly, in brain disease some specific EOM weakness patterns, often accompanied by nystagmus, point towards a specific disease, with for example vertical gaze limitation in progressive supranuclear palsy and abduction limitation in Wernicke's encephalopathy. Secondly, nerve diseases follow the specific cranial nerve innervation pattern and in hereditary muscle diseases, the LPS and the SR are more frequently involved than the other EOM and the IR is usually spared. Thirdly, in synaptic diseases in general, the involvement pattern is highly variable per patient and over time, but the LPS and SR are most often involved, followed by the LR and MR; the IR is often spared. LEMS is an exception: ophthalmoparesis is rare and ptosis is more frequently observed. In acquired muscle diseases, the presence of pain and proptosis is often evident. The involvement pattern can be very specific per disease, for example in Graves' orbitopathy the progressive involvement of the EOM generally follows a specific order: IR>MR>SR>LR>SO. In general, the LPS and the oblique muscles are spared and the IR is involved, in contrast with hereditary diseases.

Imaging studies of the EOM in hereditary and acquired neural and synaptic diseases describe atrophy and an increase in fat in the EOM, indicating that denervated EOM have a tendency towards atrophy accompanied by fat replacement of muscle fibres. In hereditary muscle diseases such as CPEO, fat replacement is also observed, which is also indicative of

progressive muscle wasting.[14] Consequently, in myasthenia gravis, a synaptic disease, small increases in fat fraction are observed in patients with longstanding chronic or untreated disease and they show a small decrease in EOM volume[17] but more recent findings rather point to a small and variable increase in muscle volume[99]. In acquired orbital diseases, inflammation seen as hyperintensity on T2w scans with fat suppression is observed in active stages of disease, accompanied by increases in muscle volume. In the chronic stages of Graves' orbitopathy, an increase in fat in the EOM is observed due to adipogenesis by orbital fibroblasts and fibrocytes.[106]

Not in all neuromuscular diseases the EOMs are affected. This could provide valuable clues in the pathophysiology of EOM involvement and in disease pathophysiology in general, since the EOM differ anatomically and physiologically from skeletal muscles. They have distinct fibre type composition[116], multiple innervation[117], smaller motor units[118], higher levels of utrophin expression[119], a distinct contraction-excitation coupling[120], have an increased capability of regeneration and preferentially use glucose-based aerobic metabolic pathways.[84] The latter means that EOM are packed with mitochondria, explaining the predominant ocular phenotype in mitochondrial diseases such as CPEO. In other primary muscle diseases, such as Duchenne muscular dystrophy, the EOMs are remarkably spared, which has been hypothesized to be mainly due to the increased regenerative capacity of the EOM and higher levels of utrophin expression.[121] The LPS is relatively spared in acquired orbital disease with an inflammatory origin and is frequently affected in hereditary neuromuscular disease. This may be explained by differences between the EOM and the LPS. The LPS carries thicker muscle fibers[122] and has a higher arteriole-nerve distance.[123]

Fat increase in the EOM does occur in OPMD, indicative that muscle damage of the EOM also causes the replacement of muscle tissue by fat in dystrophic disease with EOM involvement. Fat increase in the EOM also occurs in synaptic neuromuscular disorders. This may indicate that (relative) muscle denervation of the EOM causes the replacement of muscle tissue with fat. This phenomenon has been described previously in denervating disease with skeletal muscle involvement.[124] In addition, there is evidence from histological studies of the EOM in myasthenia gravis that atrophy and fat replacement occur.[125] In chronic stages of acquired orbital muscle disease with an inflammatory origin, such as Graves' orbitopathy, there is evidence of adipogenesis by fibroblasts in a later stage of the disease.[14,51,93,105,106] Therefore, since intramuscular fat increase seems to correlate with the disease stage to some extent, it may be a valuable biomarker in the follow-up of disease progression.

In neuromuscular disease with known EOM involvement, MRI of the EOM is rarely performed compared to MRI of skeletal muscles. For OPMD, Pompe disease and congenital myasthenic

syndromes imaging of the EOM has not been described and in other diseases, like myotonic dystrophy, only a few case reports have been published. There are challenges when performing orbital MRI since the eyes are prone to motion and close to air-bone-tissue interfaces causing artefacts. However, scans can be optimized for these challenges.[44] Scan time can be reduced and cued blinking could be used[99] to prevent movement artefacts and for example spin-echo sequences are less sensitive to field inhomogeneities as compared to gradient-echo sequences.[126] Currently, it is recommended to include T1w sequences, T2w sequences with and without fat suppression, T1w scans with contrast and DWI. [87] Given the small size of the orbital structures, sequences with an in plane resolution of at least 0.8 mm and slices of 3 mm are generally sufficient to detect clinically relevant EOM swelling and atrophy in our experience, although reports show that an isotropic resolution below 0.6 mm are also clinically feasible.[127] These can be obtained with a brain MRI setup on 3T. To more directly assess the EOM pathophysiology in the context of research, we recommend to include scans with water-fat separation to study fat fraction increases of the EOM. T2w imaging with fat suppression is recommended to differentiate intra-muscular fat from inflammation/oedema, as is commonly performed in skeletal muscle imaging studies.[128] Many orbital inflammatory disease are now labelled as idiopathic and a systemic diagnostic evaluation might be needed to identify underlying and associated disease as proposed by McNab[77]. We believe that imaging can play an important role in this respect.

Additionally, quantitative MRI could be a valuable addition in the follow-up of disease progression and in the correlation of MRI to disease activity and disease progression, as is known in the field of neuromuscular diseases like Duchenne and Becker muscular dystrophy. In general, for these muscle diseases the recommended technique to quantify fat fraction is chemical shift based water-fat separation.[37] The feasibility of performing such scans of the EOM has been previously shown. [99] To quantify inflammation, T2 relaxation time maps of the water component could be acquired as is done in skeletal muscle.[36] Applying these quantitative techniques to study fat replacement and T2 relaxation time changes in the EOM could prove valuable in disease with EOM involvement. Finally, EOM volume can be quantified using anatomical scans such as T1w, T2 or Dixon. Clinical diagnostic evaluation of scans is conventionally performed by comparing the cross-sectional area of the EOM, which is generally sufficient to detect EOM swelling or atrophy. In the context of research however, we believe volume to be a more robust measure than cross-sectional area, because the entire EOM is included and the measurement is more independent of variations in EOM shape or position. Also, we observe a high variation in EOM volume in healthy controls (e.g. for the medial rectus 569±129 mm^3)[129], therefore including a healthy control group for reference in studies is recommended. To determine the source of this variation, future studies should focus on and the influence of orbital volume, age and race on EOM volume. In conclusion, in

diseases with ophthalmoparesis and ptosis specific patterns of clinical symptoms, the EOM involvement pattern and orbital imaging provide valuable information for diagnosis. Additionally, orbital imaging could prove valuable in the follow-up of disease progression and the understanding of disease pathophysiology.

SUPPLEMENTAL

Supplementary table 1. *Involved EOM in different orbital disease with ophthalmoparesis and ptosis. The neuromuscular diseases are categorized in acquired, synaptic and hereditary.*

Disease		Predominantly involved EOM
Hereditary disease		
Nerve		
CFEOMs	Type 1	LPS, SR due to a lack of superior division of N. III.[47,60]
	Type 2	LPS, SR, IR, MR, IO, SO all due to lack of N III and N IV. LR spared.[47,61]
	Type 3	LPS, SR, IR, MR, IO, due to more variable N. III involvement. [47,96]
Synapse		
Congenital Myasthenic Syndrome		Frequently: LPS, LR, SR/IO Commonly: MR, IR/SO High individual variation[50]
Muscle		
Chronic Progressive External Ophthalmoparesis (CPEO)		*Frequently: LPS, SR[52]*
Pompe disease		*Commonly: LPS[83]*
OPMD		*Frequently: LPS, SR, LR [53]*
Myotonic dystrophy		*Frequently: LPS most often case reports of LR and MR.[94]*
Centronuclear myopathy		*Frequently: LPS, SR, LR[79,109]*
Acquired disease		
Brain		
Progressive Supranuclear Palsy		Frequently: SR/IO[132] Less common: LR
Internuclear ophthalmoparesis (MS / stroke)		Adduction limitation (MR) with contralateral nystagmus.
Wernicke Encephalopathy		Frequently: LR[115] Nystagmus is the most observed neuro-ophthalmic finding.
Brain stem tumour		Depends on localisation of the tumour.
Nerve		
Miller-Fisher syndrome		Frequently (100%): LR[114] Common (48-60%): SR, IR, MR, LPS[114] Never isolated LR palsy
Recurrent painful ophthalmoplegic neuropathy		Frequently: LPS, SR, IR, MR, IO due to involvement of N. III[134] More rare: LR due to involvement of N. VI and SO due to involvement of N. IV
Horner		NO EOM involvement. Superior tarsal muscle, an accessory muscle that maintains elevation of the upper eyelid.[135]
Tolosa–Hunt syndrome		Frequently (80%): LPS, SR, IR, MR, IO due to involvement of N. III[49] Common (70%): LR due to involvement of N. VI[49] Rare (30%): SO due to involvement of N. IV[49]
Diabetic neuropathy		Frequently: LPS, SR, IR, MR, IO due to involvement of N. III or LR due to involvement of N. VI[63]
Synapse		
Autoimmune LEMS		Frequently: LPS No common pattern in the EOM, however 30% of patients have ocular motility abnormalities. [113]

Supplementary table 1. Continued

Disease	Predominantly involved EOM
Autoimmune myasthenia gravis	Frequently: LPS, IO, SR Commonly: LR, MR Rarely: SO, IR High individual variation. [110–112]
Botulism	Ptosis (LPS) in 37% and extraocular muscle palsies in 25%.[140]
Acetylcholinesterase intoxication	Unknown.
Muscle	
Idiopathic orbital myositis	*Frequently: LR, SR, MR, IR* *Involvement of tendon and often unilateral [87,105]*
IgG-4 related orbital disease	*Frequently: IR[108]* *Commonly: SR, LR* *With tendon sparing and often bilateral[87]*
Thyroid orbitopathy / Graves' orbitopathy	*Frequently: IR, MR, SR[105]* *Rarely: SO inflammation is frequently missed[151]* *With tendon sparing and often bilateral[87,105]*
Amyloidosis	*Several case reports with predominantly LR and MR, rarely IR.[70]*
Orbital Lymphoma	*Only one muscle affected, no specific EOM. [142]*

2

1. Leiden University Medical Center, Department of Neurology and Clinical Neurophysiology, The Netherlands
2. Albert Schweitzer Hospital, Department of Neurology and Clinical Neurophysiology, The Netherlands
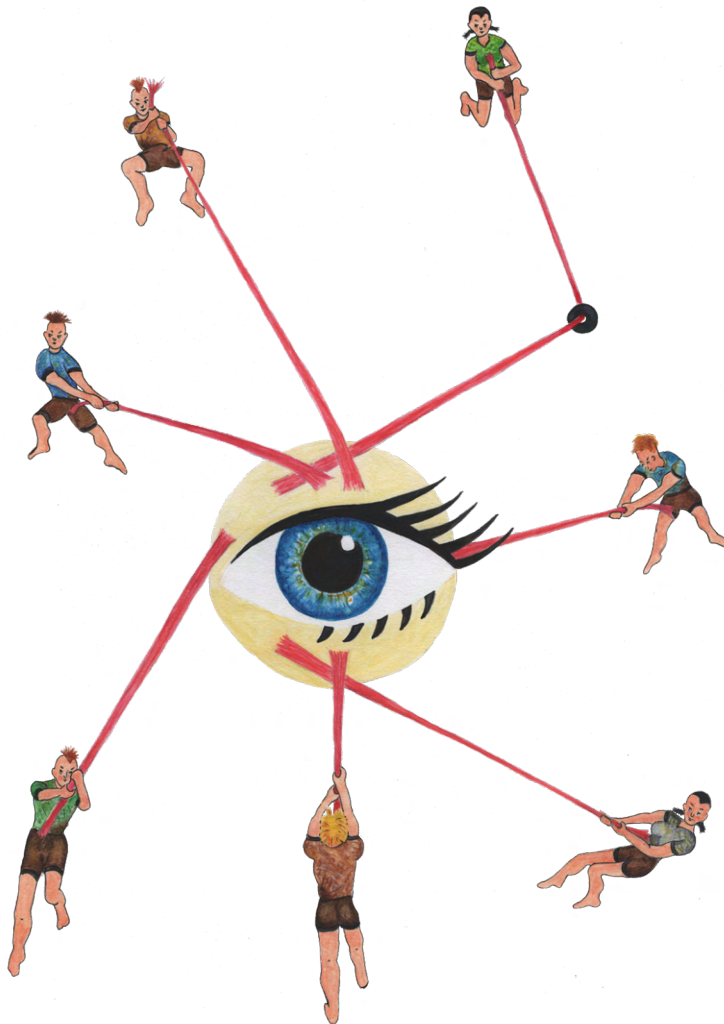
Test-retest reliability of repetitive ocular vestibular evoked myogenic potentials in myasthenia gravis and healthy controls

Kevin R. Keene[1] | Julia Bongers[1] | Robert H. P. de Meel[1]
Jeroen Venhovens[2] | Jan J. G. M. Verschuuren[1] | Martijn R. Tannemaat[1]

ABSTRACT

Introduction
Repetitive ocular vestibular evoked myogenic potentials (ROVEMP) are a novel diagnostic test to quantify neuromuscular transmission deficits in extraocular muscles (EOMs) in myasthenia gravis (MG). We aimed to investigate the test-retest reliability of the ROVEMP and the effect of amplitude and age.

Methods
We performed the ROVEMP test twice in 19 patients with MG (52.7±19.8 years) and 15 healthy controls (46.5±16 years). The Bland-Altman level of agreement was determined. The relationship between test-retest reliability and signal quality, participant age and signal amplitude was studied.

Results
Limits of agreement were [-179.9, 139.3] in MG and [-56.9, 89.5] in healthy controls. Difference between measurements correlated with signal amplitude (r=-0.50, p<0.001). Combining the primary cohort with previously published data from 114 subjects, we found a significant negative correlation between age and reference amplitude (r=-0.163, p=0.045).

Discussion
This study shows that in our hands, the test-retest reliability of the ROVEMP is not optimal. Measurements with higher reference amplitude had a better quality, higher reproducibility and increased diagnostic yield. We caution against the use of ROVEMP measurements of lower amplitude in clinical practice. In addition, given the correlation between age and amplitude, age matching of healthy controls and patients is essential in future studies.

INTRODUCTION

Myasthenia gravis (MG) is an autoimmune disorder affecting neuromuscular transmission, characterized by fluctuating muscle weakness involving variable combinations of ocular, bulbar, limb, and respiratory muscles.[5] At the onset of the disease, 85% of all patients present with pure ocular symptoms.[1,78] Early and accurate diagnosis in ocular MG (OMG) is challenging.[78,143,152] MG is diagnosed by a combination of typical clinical findings of fatigable muscle weakness and ancillary tests including antibody assays, repetitive nerve stimulation (RNS), single-fiber electromyography (SF-EMG) and edrophonium or neostigmine tests. Unfortunately, in patients with pure ocular symptoms, some of these tests, such as antibody tests and RNS have a low sensitivity[153], whereas others, including edrophonium and SF-EMG, are often unavailable outside specialized centers.[11] Moreover, the edrophonium test has safety concerns and has been primarily studied for ptosis rather than for diplopia in ocular patients.

A growing body of literature suggests that it is possible to quantify neuromuscular transmission deficits in the extraocular muscles (EOMs) using repetitive ocular vestibular evoked myogenic potentials (ROVEMP).[31,32] The oVEMP reflex is generated by stimulation of the otolith end-organs in response to bone-conducted vibration applied to the skull or air-conducted sound to the ear[29]. The excitatory myogenic response of the EOMs can be measured with electrodes underneath both eyes. [30,154] Valko et al. showed that by applying a train of ten repetitive oVEMPs, the amplitude of the evoked potential decreases gradually in MG patients, analogous to the decrement observed with RNS [31]. We have previously confirmed this finding in a larger cohort and confirmed the diagnostic yield of this test when patients with other neuromuscular diseases and Graves' orbitopathy were taken as a control group.[32]

Although the ROVEMP appears to be a promising novel diagnostic test in MG, its test-retest reliability has not been studied yet. In previous work, methodologic challenges that influence the signal were addressed: the signal must be averaged thirty[31] or forty[32] times due to low signal to noise ratio and excessive eye blinking artefacts led to the exclusion of five participants in the work of De Meel et al.[32] and four participants in the work of Valko et al.[31] These technical challenges could be a source of variation, potentially impairing the clinical utility of this test in individual patients. Therefore, we aimed to investigate the test-retest reliability of the ROVEMP test in MG patients and healthy controls. In addition, we aimed to identify areas amenable to technical refinement by studying the effect of amplitude, electrode resistance and age on test-retest reliability.

METHODS

The study was designed as a prospective case-control study, primarily aimed at quantifying the test-retest reliability of the ROVEMP test in MG patients and healthy controls in the primary cohort. Previously published data from 114 subjects[32] was added to increase the power to study the correlation between amplitude and age and the influence of amplitude selection on the diagnostic yield.

Study participants

This study was conducted at the outpatient clinic of Leiden University Medical Center between August and November 2020. The Medical Ethical Review Committee of Leiden University Medical Center approved the protocol (NL65522.058.18 - P18.091). We obtained written informed consent from all participants. MG patients were recruited from the Neurology outpatient clinic and healthy controls via posters and flyers in the hospital. In 19 MG patients and 15 healthy controls the ROVEMP test was performed twice by the same examiner, with approximately 3 hours between measurements.

The diagnosis of MG was based on typical clinical features, in combination with the presence of serum autoantibodies to the acetylcholine receptor (AChR) or a decrement >10% during RNS. To limit the effect of potential diagnostic uncertainty, seronegative ocular patients without a decrement >10% during RNS were not included. For all participants, we recorded age and sex. For MG patients, we recorded the presence of ptosis, diplopia and AChR antibodies, presence and size of the decrement found during RNS, Quantitative Myasthenia Gravis score (QMG) and Myasthenia Gravis Activities of Daily Living Profile (MG-ADL). For further analysis of correlations between age, amplitude and diagnostic yield we combined data from the participants and measurements of the current cohort with those of De Meel et al.[32]

ROVEMP test procedure

The procedures were the same as described previously.[32] Participants were positioned in supine position with their head on a pillow. The skin was cleaned with abrasive gel to improve skin conductance. Active electrodes (black squares in figure 1) were placed under each eye while the patient held maximal up-gaze to record myogenic activity from the inferior oblique muscles.[155] Reference electrodes (red squares in figure 1) were placed two centimeters below the active electrodes. The ground electrode was placed on the forehead (figure 1). If necessary, the resistance of all electrodes was optimized by repeated application of abrasive gel until an impedance level below 10 kOhm was recorded.
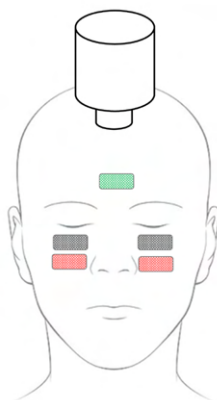
Figure 1. *Experimental set-up. The stimulus was a bone-conducted skull vibration delivered with a hand-held 'mini-shaker' positioned over the hairline. Active (black) and reference (red) electrodes measure the surface EMG signal from the inferior oblique muscles; ground electrode (green).*

The stimulus was a bone-conducted skull vibration delivered with a hand-held 'mini-shaker' positioned at the hairline (minishaker 4810; amplifier 2706, Bruel and Kjaer, Naerum, Denmark). Forty trains of 10 stimuli were administered at a rate of 20 Hz [156]. The trains were separated by 5 seconds during which participants were asked to close their eyes. The signals were sampled with a rate of 2000 per second and saved with Nim Eclipse software and a Nim Eclipse recording device (Medtronic Xomed, Inc, Jacksonville, FL). To reduce blinking artefacts, five "practice trains" were administered at the start of the measurement to allow patients to get used to the vibration. Participants were asked to try to suppress blinking during the test. Patients with MG using pyridostigmine were asked to refrain from taking pyridostigmine before the ROVEMP test. To determine reproducibility, the second ROVEMP test was performed approximately 3 hours after the first test by the same examiner.

ROVEMP data post-processing
Data analysis was performed using an in-house developed MatLab script (MathWorks, Natick, MA, USA), similar to previously described.[32] All signals were filtered using a 50Hz notch filter. Single measurement were analyzed for outliers using a median absolute deviation algorithm (MAD) and rejected if the MAD deviated two standard deviations from the mean of all MADs. Furthermore, an individual measurement was excluded by visual inspection if the signal showed clear noise artefacts. The remaining recorded signals were averaged and filtered using a 4th-order Butterworth 20Hz-high-pass filter to reduce baseline flutter. From the average signal, all peaks and troughs were automatically detected and the relevant oVEMP peaks (N1 and N2, figure 2A) and troughs (P1 and P2, see figure 2A) were selected by the

investigator. A peak or trough was automatically detected if there was a minimal increase or decrease of 0.8µV. The N2P2 amplitude was calculated for each oVEMP potential in the train of ten stimuli. For readability, the second N2P2 amplitude will be referred to as the reference amplitude throughout the manuscript. Decrement was calculated by dividing the reference amplitude of the ROVEMP signal (figure 2A) by the mean of the fifth to the ninth N2P2 amplitude (figure 2B).[31,32]
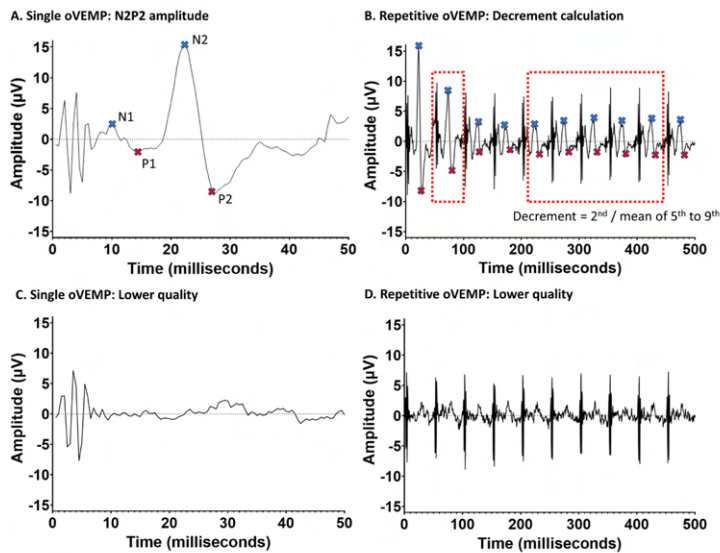

Figure 2. A. *A high quality single oVEMP signal, the N1, P1, N2 and P2 are depicted in the figure. The N2P2 amplitude is used as an outcome measure and in decrement calculations.* **B.** *Example of a repetitive oVEMP train from an MG patient with a clear decremental oVEMP response. Decrement is calculated by dividing the second N2P2-aplitude by the mean of the 5th to 9th amplitude.* **C.** *An example of a lower quality individual oVEMP with a lower amplitude.* **D.** *An example of a lower quality repetitive oVEMP train.*

To assess whether the subjective quality of the measurement was related to objective reproducibility and measures such as signal amplitude, three observers (KK, JB and MT) assessed the quality of each single ROVEMP as follows: The quality of a ROVEMP was considered to be high when ten clear multiphasic waves were observable. ROVEMP measurements with no clear multiphasic waves or a considerable amount of noise were classified as low quality. Example of a higher quality measurement can be seen in figure 2A and 2B and an example of a lower quality measurement can be seen in figure 2C and 2D. Discrepancies between the assessments of different investigators were resolved by majority vote.

Statistical analysis

Statistical analysis was performed using SPSS version 24 (IBM Corp, Armonk, NY). Values of p < 0.05 were considered statistically significant. Of the two decrements found in both eyes of the participant, the highest decrement was used for further analysis. The test-retest reliability of the decrement was assessed using Bland-Altman limits of agreement and an intraclass correlation coefficient (ICC) was calculated. To assess the difference in the reference amplitude between either higher quality or lower quality measurements, as well as MG patients and healthy controls, a two-way ANOVA was used. To correlate the reference amplitude with reproducibility we used the Spearman's rank coefficient and used test-retest difference as a surrogate marker for test-retest reliability. To assess whether age affected the reference amplitude, the raw data of de Meel et al.[32] was added and a Spearman correlation test was performed. To investigate the effect of the amplitude of the ROVEMP signal on diagnostic yield, receiver operating characteristics (ROC) curve analysis was performed before and after selection of measurements with a reference amplitude of at least 9 µV. For subjects with more than one ROVEMP test, we used the amplitude of the first measurement.

RESULTS

Participants

We included 19 patients with MG, and 15 healthy controls in the primary cohort. The mean age and percentage of men were comparable among patients with MG (52.7 ± 19.8 years; 37 %), and healthy controls (46.5 ± 16 years; 47%). Demographic and clinical baseline characteristics of all participants are shown in table 1. The cohort of De Meel et al., used to enrich our amplitude analysis to form a combined cohort, consisted of 92 MG patients (57 ± 18 years old; 48% male) and 22 healthy controls (51 ± 14 years; 46% male).

Test-retest reliability

The limits of agreement of MG patients were [-179.9, 139.3] and the limits of agreement of healthy controls were [-56.9, 89.5] in the primary cohort (Bland-Altman in figure 3). MG patients had a negative bias of -18.8%, whereas healthy controls showed a small positive bias of 3.1%. The intraclass correlation coefficient (ICC) for the intra-rater reliability was poor: -0.08 (-.40 – 0.26) for MG patients and 0.03 (0.33 – 0.39) for healthy controls.

Reference amplitude

Simple main effects analysis showed that measurements classified as "high quality" had a significantly higher reference amplitude (i.e. the second N2P2 amplitude, used in decrement

3

calculations), (9.58 ± 6.03 µV) than measurements of lower quality (5.51 ± 4.71 µV, p < 0.001). In addition, controls had a significantly higher reference amplitude (9.49 ± 6.47 µV) than MG patients (5.47 ± 4.15 µV, p = 0.001) in the primary cohort. A two-way ANOVA revealed a significant interaction effect between group and quality score on the reference amplitude, meaning that the influence of amplitude on quality of the measurement is different for MG patients and healthy controls. (p = 0.015)

A significant negative correlation was observed between the difference in decrement of the first and second measurement, used here as a proxy for reproducibility, and the reference amplitude (r = -0.50, p < 0.001, figure 4), suggesting that reproducibility was correlated with the amplitude of the signal.

Table 1. *Baseline characteristics of myasthenia gravis patients and healthy controls.*

Characteristic	Group; mean (SD)	
	MG (N=19)	Control (N = 15)
Age, years	52.7 (19.8)	46.5 (16)
Sex (% male)	37	47
Ptosis (yes)	8	-
Diplopia (yes)	5	-
AChR+ (positive)	17	-
Decrement >10 % RNS	7	-
QMG	12.9 (6.2)	-
MG-ADL	7.2 (3.6)	-

QMG: Quantitative Myasthenia Gravis score. MG-ADL: Myasthenia Gravis Activities of Daily Living score.
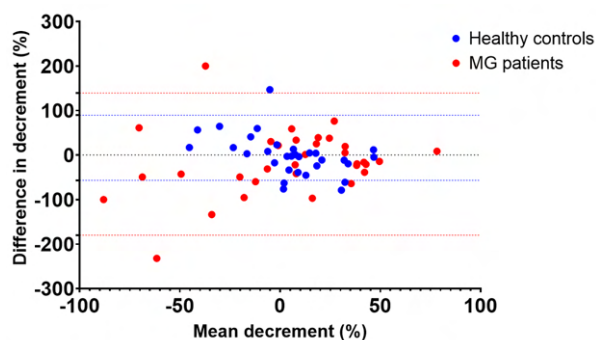

Figure 3. *Bland-Altman plot for the test and retest reliability separated for healthy controls (in blue) and myasthenia gravis patients (in red) per eye. The limits of agreement of MG patients were [-179.9, 139.3] and the limits of agreement of healthy controls were [-56.9, 89.5].*
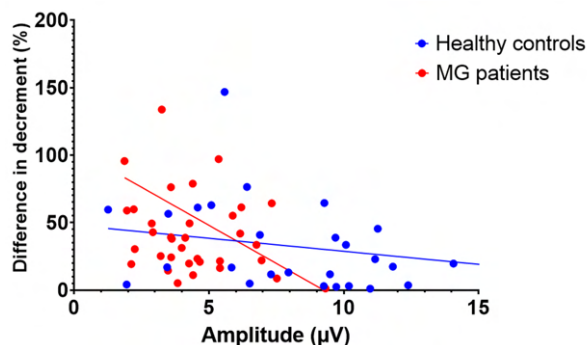
Figure 4. *Correlations between the difference in decrement between the test and retest measurement, as a proxy for reproducibility, and the reference N2P2 amplitude. Subjects with higher amplitudes appear to have a higher test-retest reliability, as the difference in decrement is significantly lower. Correlations and individual values are shown for healthy controls (blue) and myasthenia gravis patients (in red).*

Influence of electrode resistance

In the primary cohort, the mean measured electrode resistance was 5.26 ± 1.7 kOhm. The resistance did not differ between the higher quality (5.36 ± 1.96 kOhm) and lower quality (5.63 ± 1.53 kOhm) measurements (p = 0.40). Moreover, there was no correlation between electrode resistance and the reference amplitude (r= 0.05, p = 0.55).

Influence of age

Patients with high quality measurements were younger, as demonstrated by the significant difference in age for high quality (40.3 ± 15.6 years) and lower quality (58.9 ± 15.1 years) measurements (p < 0.001). In the primary cohort we found a significant correlation between age and amplitude in the first measurements (r = -0.282, p = 0.024), which was mainly caused by the healthy controls (r=-0.437, p=0.16) and not by the MG patients (r=-0.033, p=0.852). When we combined data from the 34 subjects studied in this work with previously published data from 114 subjects [32], we also found a significant negative correlation between age and the reference amplitude in the combined cohort (r = -0.163, p = 0.045) (figure 5). This correlation was driven by healthy controls, in whom we observed a significant negative correlation between age and reference amplitude (r = -0.42, p = 0.009). In contrast, for MG patients, no significant correlation was found (r= -0.11, p = 0.240).

Diagnostic yield and reference amplitude

ROC analysis based on the combined cohort of 147 subjects (37 healthy controls and 111 MG patients) showed an area under the curve of 0.69 (sensitivity of 68% and specificity of 71% at a cut-off of 16% decrement). Diagnostic yield improved substantially when only

measurements with a reference amplitude of at least 9mV were included (16 healthy controls and 46 MG patients): AUC was 0.80 and both sensitivity and specificity increased to 81% at a cut-off value of 11.26% (figure 6). Additionally, ROC analysis on participants below the age of 55 (the mean of the combined cohort) showed an AUC of 0.73 as compared to an AUC of 0.54 for participants above the age of 55, confirming the influence of age on diagnostic yield.
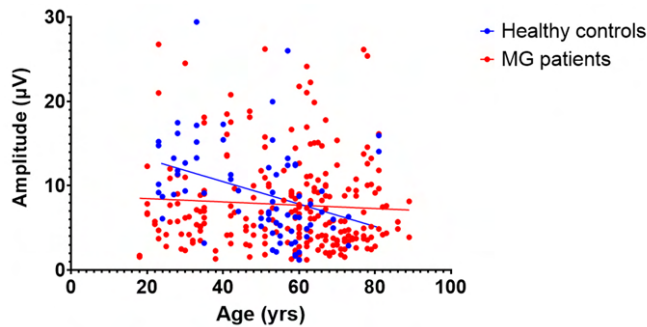
Figure 5. *For healthy controls (blue) and MG patients (red) the correlation between age and reference amplitude is shown. Healthy controls showed a significant negative correlation between age and reference amplitude (r = -.42, p = .009). However, for MG patients, no significant correlation was found (r= -.11, p = .240).*

Figure 6. *Receiver operating characteristics (ROC) analysis showing the effect of selecting only measurements with high amplitudes on diagnostic yield. A. Entire cohort: optimal cut-off value > 15.81%, sensitivity 68%, specificity 71% and area under the curve (AUC) 0.69. B. After selecting of cases with a reference N2P2 amplitude of at least 9 μV. Optimal cut-off value > 11.26%: sensitivity 81%, specificity 81% and AUC 0.80.*

DISCUSSION

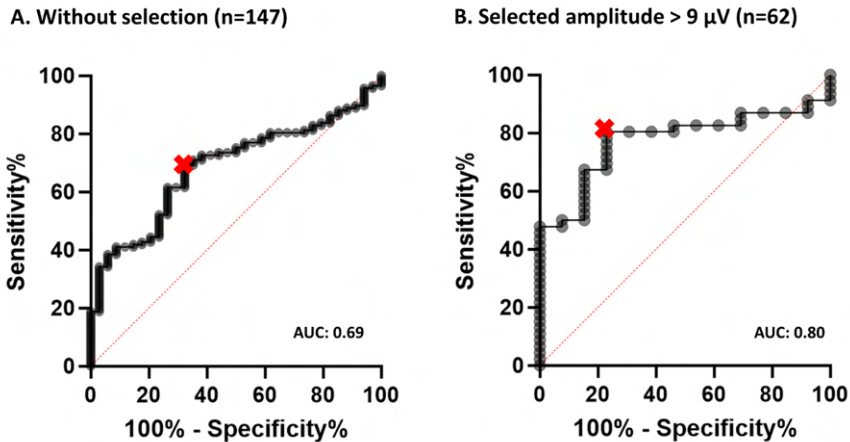We aimed to study the test-retest reliability of the ROVEMP test for diagnosing myasthenia gravis and identify areas amenable to technical refinement. For MG patients, Bland-Altman analysis showed limits of agreement from -179.9% to 139.3%. In healthy controls, the limits of agreement were smaller (-56.9% to 89.5%). In the context of previously proposed cut-off values of 9% and 15% [31,32] for MG diagnosis, the test-retest reliability of the ROVEMP is suboptimal.

Several observations indicate that the reproducibility of the ROVEMP is related to its signal to noise ratio (SNR), and that the amplitude of the signal (expressed here as the amplitude of the reference N2P2) is the limiting factor for many measurements. The N2P2 amplitude was significantly correlated with the absolute difference between two repeated tests and the diagnostic yield improved when only measurements with a reference amplitude of at least 9μV were included. In addition, measurements judged to be of low quality by qualitative visual assessment had significantly lower amplitudes than measurements of high quality. Unfortunately, the amplitude of the signal appears to be affected by disease, as MG patients had a significantly lower second N2P2 amplitude than healthy controls, and age, with higher amplitudes in younger participants. Surprisingly, the measured electrode resistance did not correlate with the amplitude of the signal, suggesting that technical optimization by reducing electrode resistance is not a viable method to improve SNR. Not all variability in amplitude between subjects can be explained by these factors; the cause is currently unclear.

We hypothesize that the lower amplitudes observed in MG patients are related to the disease, analogous to the previously described finding that compound muscle action potential (CMAP) amplitudes are lower in MG patients with severe disease.[28,157] Moreover, the amplitude of the reference amplitude declined significantly with age in healthy controls. This corresponds to previous research showing lower N1P1 oVEMP amplitudes in older adults[29] and lower CMAP amplitudes in a healthy older adults. [158] Unfortunately, these findings might reduce the clinical utility of the ROVEMP. The average age at onset of MG is 44 years[159] and since the subjective quality of the ROVEMP signal and objective measures such as the N2P2 amplitude decline with age, the quality of a measurement must be taken into account for older patients in clinical practice, as diagnostic yield appears to be low in subjects over 55 years of age. In previous studies, more young healthy controls were included compared to the patient groups: in the work of Valko et al. the mean age was 47 years for healthy controls, and 58 years for patients[31] and in the work of de Meel et al., the standard deviation of the age was higher in the healthy control group.[32] Moreover, the number of ocular MG patients was slightly higher in these studies compared to the current work. Both the difference in age and phenotype

may help explain the higher AUC found in these studies, respectively 0.80 and 0.78, compared to the AUC of 0.69 in the current work. In addition, in the work of Valko et al., 4 subjects (7% of the total population) were excluded from further analysis due to excessive blinking artifacts. Similarly, the results of 5 subjects were excluded by de Meel et al. due to excessive artefacts. The exclusion of these measurements in both studies may have skewed the results towards a higher diagnostic yield compared to the current study. In future diagnostic studies, age matching between healthy subjects and MG patients must be performed to avoid bias as a result of age effects on the ROVEMP signal. Additionally, future studies including a younger cohort of healthy controls and MG patients prospectively could potentially show a higher diagnostic yield, because young subjects are likely to have higher amplitudes and more reliable tests.

Limitations of this study include the single center of inclusion and the single observer performing the tests and retests. However, it is likely that reproducibility would have decreased further when data from different centers would have been combined. Our main conclusions would therefore probably not be affected.

Measurements were selected using the arbitrary cutoff of 9µV. Although this threshold was chosen somewhat arbitrarily, it confirmed the negative effect of the signal amplitude on clinical utility of the ROVEMP by comparing the diagnostic yield of the entire cohort to a selection of cases with a higher reference amplitude, or a lower age, and showing that the AUC, sensitivity and specificity were all higher when cases with a low amplitude were excluded.
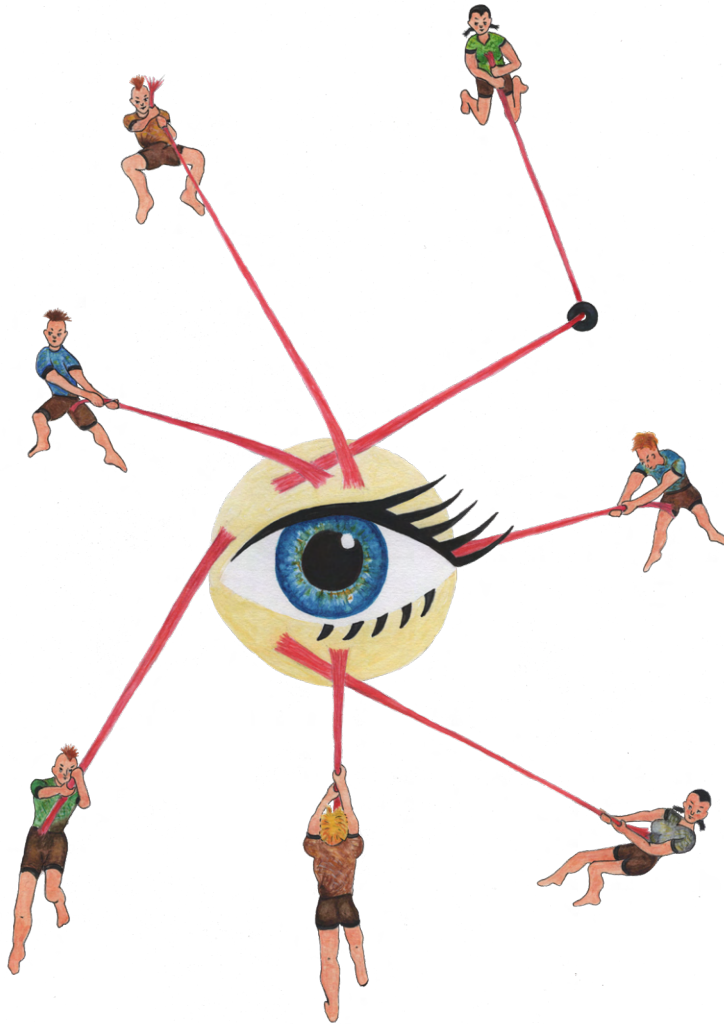
Despite its low reproducibility, our results confirm that the ROVEMP appears to be able to detect a decrement in patients with MG, suggesting that it is able to quantify neuromuscular transmission deficits in the EOMs. This is highly promising, as there is no alternative neurophysiological method to study the EOMs, which are the most commonly affected muscles in MG.

However, we caution against the use of ROVEMP measurements of lower amplitude in clinical practice. In diagnostically challenging patients, a ROVEMP test result with a high amplitude and clear decrement could be of clinical value in addition to standard diagnostic tests. Unfortunately, this approach limits the use of this test in a substantial number of patients, as only 42% of all subjects in our investigations had a reference amplitude of at least 9µV. Particularly in older patients, it is likely that the ROVEMP will not yield an unequivocal result. Based on our current findings, we believe that the ROVEMP test is especially suitable to detect changes at group level (e.g. in the context of studies on therapeutic interventions).

CONCLUSIONS

This study shows that the test-retest reliability of the ROVEMP is not optimal. Measurements with a higher reference amplitude had a better quality, higher reproducibility and an increased diagnostic yield. Therefore, we caution against the use of ROVEMP measurements of lower amplitude in clinical practice. We recommend further studies aimed at optimization of the SNR to increase diagnostic yield and reliability of the ROVEMP, perhaps by improving stimulus parameters[156] or reducing blink artefacts. In addition, given the correlation between age and amplitude, age matching of healthy controls and patients is essential in future studies.

3

1. CJ Gorter MRI Center, Department of Radiology, Leiden University Medical Center, Leiden, Netherlands
2. Department of Neurology, Leiden University Medical Center, Leiden, Netherlands
3. Department of Ophthalmology, Leiden University Medical Center, Leiden, Netherlands
4. Department of Radiation Oncology, Leiden University Medical Center, Leiden, Netherlands

Diagnosing myasthenia gravis using orthoptic measurements:
Assessing extra-ocular muscle fatiguability

Kevin R. Keene[1,2] | Johan M. de Nie[3] | Mechteld J. Brink [3] | Irene C. Notting[3]
Jan J.G.M Verschuuren[2] | Hermien E. Kan[1]
Jan-Willem M. Beenakker[1,3,4] * | Martijn R. Tannemaat[2] *

These authors contributed equally to this work.

ABSTRACT

Introduction

Diagnosing ocular myasthenia gravis (MG) can be challenging because serum antibodies are often not detected. We aimed to explore whether determining extra ocular muscle (EOM) weakness using orthoptic measures, including an adapted Hess chart examination, can aid in diagnosing MG.

Methods

We conducted a prospective study among patients with acetylcholine receptor antibody positive MG (20 recently diagnosed, 19 chronic) and 14 seronegative MG patients. We compared orthoptic measures to 19 healthy and 18 disease controls with Graves orbitopathy, chronic progressive external ophthalmoplegia or oculo-pharyngeal muscular dystrophy. Maximal eye duction angles were measured using a synoptophore. Gaze deviations between eyes were measured using standard Hess chart examination with addition of one minute persistent gaze to assess MG-associated fatiguability. Receiver operating characteristics curve analysis was performed.

Results

For duction angles, the area under the curve(AUC) was 0.73 comparing MG to healthy, and 0.69 comparing to patient controls. For the outer field of the Hess chart, the AUC was 0.89 comparing to healthy and 0.54 to patient controls. For drift, the AUC was 0.93 comparing to healthy and 0.93 to patient controls. The sensitivity and specificity of the presence of drift was 81% and 100%.

Discussion

Orthoptic measurements can be used to diagnose MG by quantifying EOM weakness and fatiguability. Drift during persistent gaze on a Hess chart is specific for MG, and could be used for diagnostic purposes. The Hess chart examination is widely available, inexpensive and fast. Moreover, orthoptic measurements may be a clinically relevant outcome measure for clinical trials.

INTRODUCTION

Myasthenia gravis (MG) is an auto-immune disease with auto-antibodies targeting proteins at the neuromuscular junction, including the acetylcholine receptor (AChR).[2,160] Fatigable and fluctuating muscle weakness is the hallmark of MG.[21] In 85% of MG patients, the first symptoms are ocular, and consist of diplopia and ptosis. Ten to fifteen percent of MG patients have only ocular symptoms.[161] In 50% of ocular patients no detectable antibodies are found in serum.[162] In this subgroup, labelled seronegative MG (SNMG), diagnosis is challenging.[160] Distinguishing ocular MG from mimics, such as Graves orbitopathy (GO), chronic progressive external ophthalmoplegia (CPEO) and ocular pharyngeal muscular dystrophy (OPMD) can be challenging given the similarity in ocular symptoms[163] and the inaccessibility of extra-ocular muscles (EOM)s for needle EMG. Therefore, there is a need for accurate, non-invasive diagnostics for ocular SNMG.[4]

Three pairs of EOMs move the eye in all directions: horizontally (medial rectus (MR) and lateral rectus (LR)), vertically when the eye is in abduction (superior rectus (SR), inferior rectus (IR)) and vertically in adduction (superior oblique (SO) and inferior oblique (IO)). The oblique muscles are also responsible for torsional movement of the eye with contraction of the SO, causing incyclotorsion, and the IO, causing excyclotorsion. In MG, diplopia is caused by fatigable weakness of these EOMs. This fatiguability of the EOMs has been studied qualitatively in previous work by using patient reported diplopia during persistent gaze.[164] Additionally, testing fatiguability in sustaining gaze at the bedside is part of the standard examination procedure in ocular MG, with the advantage that the levator palpebrae superioris can also be tested by assessing ptosis during sustained up gaze.[165] Using orthoptic tests, the absolute movement limitation of each eye can be quantified with the synoptophore and deviations between two eyes with the Hess chart. In ophthalmology, these quantitative orthoptic measurements are routinely performed, e.g. during planning of strabismus correction surgery.[35,166,167]

Orthoptic measures have been tested before as an additional diagnostic tool in a small group of ocular MG patients by adding the Hess chart as an objective measure before and after the edrophonium test.[168] However, the standard Hess chart does not take muscle fatiguability into account and evaluating the diagnostic value of orthoptic measures in a well-defined cohort of MG patients could be of interest. Therefore, we aimed to explore whether orthoptic measurements can aid in diagnosis, and whether adding one minute of persistent gaze to the Hess chart makes it possible to detect MG-related fatiguability.

METHODS

Participants
We included a convenience sample of MG, GO, CPEO and OPMD patients from the Neurology Department and the Ophthalmology Department of the LUMC, Radboud University and the Rotterdam Eye Hospital. Healthy controls were recruited using posters and by asking relatives of the included MG patients.

MG patients were divided in three groups: chronic, recently diagnosed and seronegative. The diagnosis of AChR MG was based on clinically confirmed fluctuating muscle weakness in combination with the presence of serum autoantibodies to AChR in the chronic and recently diagnosed MG patient groups. Seronegative myasthenia gravis (SNMG) was defined as clinically confirmed fluctuating muscle weakness in combination with abnormal decrement during RNS, increased jitter during single fiber EMG testing or a positive response to an acetylcholinesterase inhibitor without the presence of AChR or muscle-specific kinase (MuSK) serum autoantibodies.[4] Recently diagnosed MG patients fulfilled two criteria: 1)The diagnosis was established less than a year ago and 2)They had never been treated with immunosuppressants; Chronic MG was defined as all patients who received the diagnosis more than a year ago. In the seronegative MG group no selection was made for disease duration or immunosuppressant status. We also included three disease mimic groups: Graves orbitopathy, CPEO and OPMD, and a group of healthy age and sex-matched controls. The diagnosis of Graves orbitopathy was defined as the presence of TSH-receptor serum autoantibodies with the presence of ocular symptoms.[169] The diagnosis of CPEO was confirmed with a limb muscle biopsy in all patients[170] and the diagnosis of OPMD was confirmed with molecular genetic testing of the PABPN1 gene.[171] Healthy controls with a history of strabismus were excluded, as were patients with simultaneous diagnosis of MG and Graves orbitopathy.

For the MG patients a quantitative myasthenia gravis (QMG) score [23,24] and a myasthenia gravis activities of daily living (MG-ADL) scale[22] were recorded.

Standard protocol approvals, registrations, and patient consents
The Medical Ethics Review Committee of the Leiden University Medical Center approved the study and its use of human subjects under reference number P19.028. All patients and healthy controls provided informed, written consent prior to study participation.

Measuring duction angles using the synoptophore
Duction angles were defined as the range of motion of the eye in degrees in all directions. In this study, unilateral duction angles in all eight cardinal positions of gaze were determined

under standardized conditions using the synoptophore (Clement Clarke International, 2002, Edinburgh way, Harlow, Essex, CM20 2TT. England) (figure 1A).[33] The patient was instructed to follow a fixation target in all directions. The arm of the synoptophore was moved from zero degrees towards the final position of gaze, whilst the patient maintained fixation. When it became apparent for the single observer that the eyes had stopped following the fixation target, a duction measurement was recorded in degrees. Vertical duction angles were measured up to +/- 30° during elevation and depression and horizontal duction angles were measured during adduction and abduction up to +/- 40°. The vertical ductions in the four corners were measured in either 25° adduction or abduction.
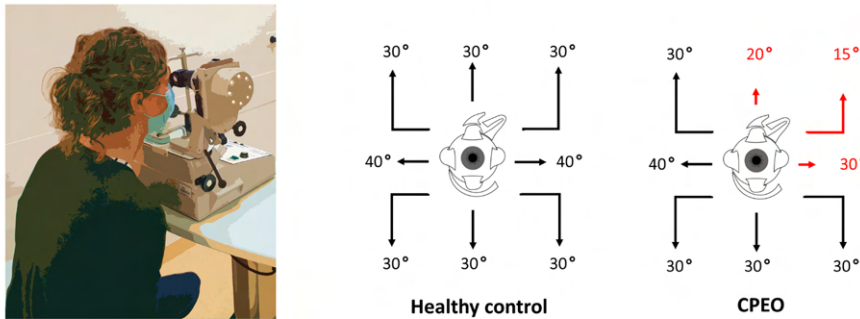
Hess chart

The Hess chart is a routinely used test in for example the planning of corrective strabismus surgery. The aim of the Hess chart is to determine the deviation between two eyes when fixing on one point by using the difference in foveal projection of the eyes.[35] Cyclotorsion of the eyes cannot be measured with the Hess chart. In this study, the eyes were tested sequentially, starting with the left eye. The patient wore glasses with a green filter in front of the tested eye and a red filter in front of the reference eye. The patient was instructed to place a green light from a laser pointer (only visible to the tested eye) for each of the points on the red light (only visible to the reference eye) as illuminated on the Hess screen by the observer (Clement Clarke International, V6908000, Edinburgh way, Harlow, Essex, CM20 2TT. England). The location of the green light from the laser was manually annotated by a single examiner on a Hess chart. This location was estimated with a precision of a single degree using the five degree grid lines on the chart.[172] The central point and all eight inner field points were measured first in a consistent order (vertical order: central, top and bottom, horizontal order per vertical line: middle, left and right). Subsequently, the outer field points were all measured in the same order and the conventional Hess chart examination was extended with one minute of persistent gaze to determine fatiguability for these outer field points in the same run. The first positions after fixation and the maximal deviations during this one-minute period were charted by the researcher. (figure 1B). When a patient was unable to maintain one minute of persistent gaze, the maximum deviation was noted. When the green light was out of scope of the Hess screen (i.e. on the wall behind the screen) a measurement was considered *out of range*. No other orthoptic eye movement examinations were performed in this patient cohort.

Translating the Hess chart measures to weakness of individual EOM

In general, deviations on the Hess chart cannot be directly linked to an individual EOM, as the movement of both eyes are correlated and therefore under-action in one direction could be caused by over-action of the antagonizing EOM of the other eye. However, considering that the disease mechanism is muscle weakness in MG, CPEO and OPMD, it is very unlikely

that the affected EOM itself gives rise to an over-action on the Hess chart in its own direction. As a result, in these patients under-acting directions can be directly linked to the weakness of an individual EOM (figure 2) and over-actions, including out of range measurements, can be excluded as these are the result of an under-acting muscle of the contra-lateral eye. For GO, this interpretation cannot be made, as over-actions are often the result of swelling and stiffening of the EOM.[173,174] Therefore, the translation to the involvement pattern of individual EOM was not made for GO patients.

Figure 1A. *In all eight cardinal positions of gaze, unilateral duction angles were measured using the synoptophore, as depicted in the photograph on the left. An example of a healthy participant with no duction limitations is shown in the middle. On the right, a CPEO patient with limited ductions in elevation and adduction.* **Figure 1B.** *On the left a photograph of the Hess screen test is shown. The patient wears red-green glasses and is asked to point at the red light with a green laser pen. The deviations in the inner field, the outer field and after one minute of persistent gaze are charted by the researcher. Typical example of a measurement from a healthy control and an MG patient are shown.*
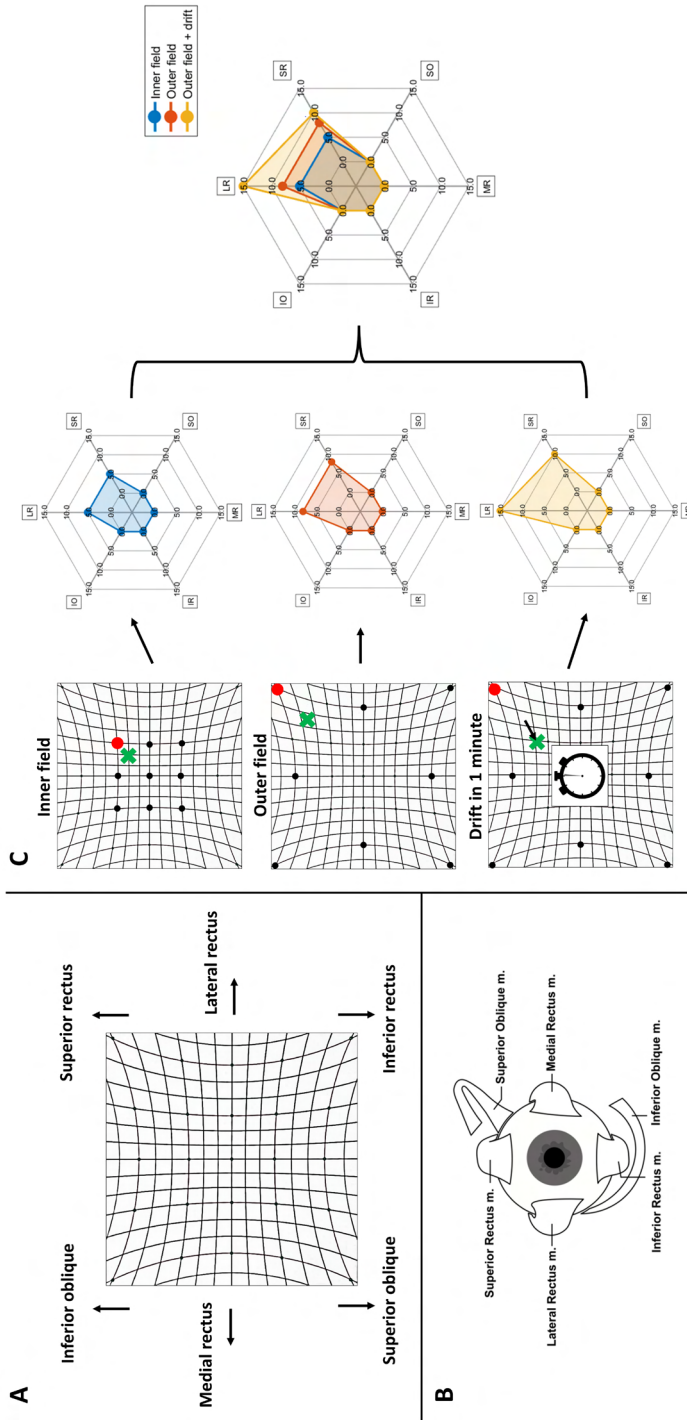
Figure 2A. *The under-action on the Hess chart was attributed to weakness of the individual EOM by using the directions shown next to the chart.* **Figure 2B.** *Anatomical representation of the right eye with the four recti eye muscles and the two oblique eye muscles.* **Figure 2C.** *The deviations in degrees for the individual EOM were plotted in a spider plot for the inner field, the outer field and drift during one minute of persistent gaze in the outer field.*

Sum-scores for the duction angle limitations and the Hess chart deviations

To quantify the total muscle weakness for the inner field, the outer field and drift, the degrees of deviation for all six muscles were summated to calculate sum-scores.[175] A sum-score of more than six degrees for the outer field was considered to be clinically relevant, as this was the average of the healthy controls plus two standard deviations.

Statistical Analysis

Hess chart deviations, duction angles as measured with the synoptophore and continuous baseline characteristics were compared between all groups using one-way ANOVA with Dunnett's multiple comparisons test for post-hoc comparisons. Post-hoc comparison was performed with healthy controls as a reference group. Categorical baseline characteristics were compared using Pearson's chi-squared test. To determine the diagnostic yield of the duction angles as measured with the synoptophore, and the inner field, outer field and drift as measured with the Hess chart, we created receiver operating characteristics (ROC) curves and reported the area under the curve (AUC) with 95%-confidence intervals (CI) and p-values. All data is presented as number of patients (percent) for categorical variables and as mean ± SD for continuous variables. Statistical analysis was performed with SPSS version 23 (IBM Corp, Armonk, NY) and p values below 0.05 were considered significant.

Data availability

Anonymized data presented in this article will be made available at the request of a qualified investigator. Requests should be made to M.R. Tannemaat (m.r.tannemaat@lumc.nl). Raw Hess charts and spider plots depicting the affected EOM per individual participant have been added as supplementary data.

RESULTS

Participant characteristics

We included 16 healthy controls, 20 recently diagnosed MG patients, 19 chronic MG patients, 14 SNMG patients, 6 CPEO patients, 6 OPMD patients and 6 GO patients. Demographic and clinical baseline characteristics of all participants are shown in table 1. No significant differences were found between sex and age between all groups. No significant differences were found between MG phenotype (ocular or generalized), MG-ADL and QMG between recently, diagnosed, chronic and seronegative MG. There was an obvious difference in disease duration between recently diagnosed and chronic MG patients. The ocular MG patients and the generalized MG patients did not significantly differ in age (60.4±10.9 vs. 52.2±19.7). Sex was significantly different between ocular and generalised MG patients (78% male vs. 35% male, p<0.001).

Table 1. *Baseline characteristics and sum-scores of 87 participants included in this study: 16 healthy controls, 20 recently diagnosed myasthenia gravis (MG) patients, 19 chronic MG patients, 14 seronegative MG (SNMG) patients, 6 chronic progressive external ophthalmoplegia (CPEO) patients, 6 oculo-pharyngeal muscular dystrophy (OPMD) patients and 6 Graves orbitopathy (GO) patients. Data are presented as number of patients (%) for categorical variables and as mean ± SD for continuous variables.*

	MG Recently diagnosed n=20	MG Chronic n=19	MG Seronegative n=14	CPEO n=6	OPMD n=6	GO n=6	Healthy controls n=16	p-value
Age (yrs)	59±19	51±16	57±9	49±14	62±10	44±12	54±13	0.243
Sex								0.754
Female	7 (35%)	9 (47%)	7 (50%)	3 (50%)	4 (67%)	4 (67%)	9 (56%)	
Male	13 (65%)	10 (53%)	7 (50%)	3 (50%)	2 (33%)	2 (33%)	7 (44%)	
Phenotype								0.105
Ocular	12 (60%)	6 (32%)	9 (64%)	-	-	-	-	
Generalized	8 (40%)	13 (68%)	5 (36%)	-	-	-	-	
Disease duration (months)	4.0±2.2	75.6±87.9	25.6±60.5*	-	-	22.8±35.9	-	<0.0001
MG-ADL	5.8±3.3	5.5±4.2	5.0±2.7	-	-	-	-	0.791
QMG	9.2±6.0	9.8±7.7	8.3±4.6	-	-	-	-	0.812
Sum-scores								
Duction angle limitations	10±15	23±47	22±30	121±61	40±44	7±15	0±0	<0.0001
Inner field deviations	13±12	16±15	15±15	23±25	3±1	17±24	2±3	0.021
Outer field deviations	16±12	11±13	23±19	19±19	11±9	25±20	2±2	<0.0001
Drift in one minute	13±8	12±7	12±10	0±0	0±0	1±2	0±0	<0.0001

* Four of the seronegative MG patients had chronic disease with a time since diagnosis of over one year.

4

Duction angles as measures with the synoptophore

Duction angles, as measured with the synoptophore, are depicted in figure 3 for all eight cardinal directions per eye, with the fraction of patients' eyes per group that did not have any limited ductions in green. None of the healthy controls had duction limitations. In the combined MG group, limitations in elevation were most prevalent (36% patients affected of which 58% both eyes were affected, with a mean of 15 degrees limitation), compared to horizontal abduction (19% of patients affected of which 50% both eyes affected, with a mean of 16 degrees limitation) and adduction (19% of patients affected of which 20% both eyes affected, with a mean of 19 degrees limitation). In addition, a limitation in depression was observed in only one MG patient unilaterally (figure 3).

Deviations and drift on Hess chart

Qualitatively, large differences were already apparent in the pattern on the Hess charts between different groups. Hess charts obtained from recently diagnosed MG patients, chronic MG patients, CPEO patients and healthy controls are shown in figure 4 (for the Hess charts of all groups see supplementary figure 1 and for the Hess charts of individual patients see the supplementary PowerPoint file). All patient groups showed more deviations in both inner and outer fields than healthy controls, especially vertically. An exodeviation below 5 degrees was seen in many healthy controls, which is a known phenomenon with binocular testing, commonly referred to as divergence bias.[167] In addition, drift (as depicted in red in figure 4) was much more prevalent in the MG groups, compared to both other patient groups and healthy controls.
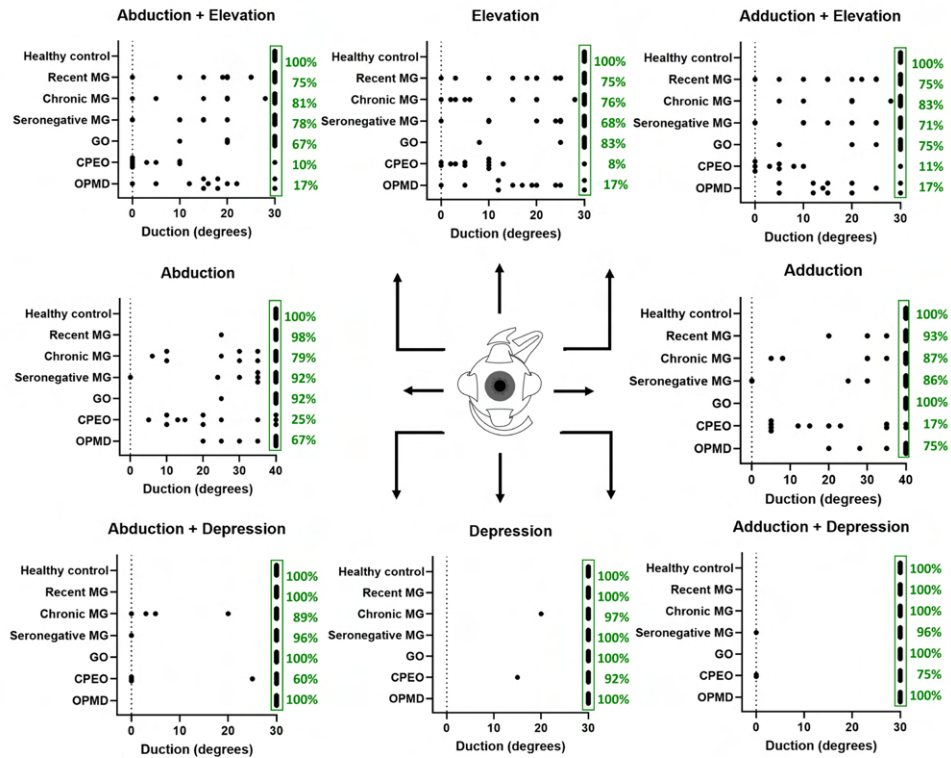

Figure 3. *Duction angles as measured with the synoptophore for all eight cardinal directions per eye. In green, the fraction of patients' eyes per group that did not have any limited ductions. Depression limitations are clearly less prevalent than elevation and horizontal limitations for all patient groups. No limited ductions were found in healthy controls.*
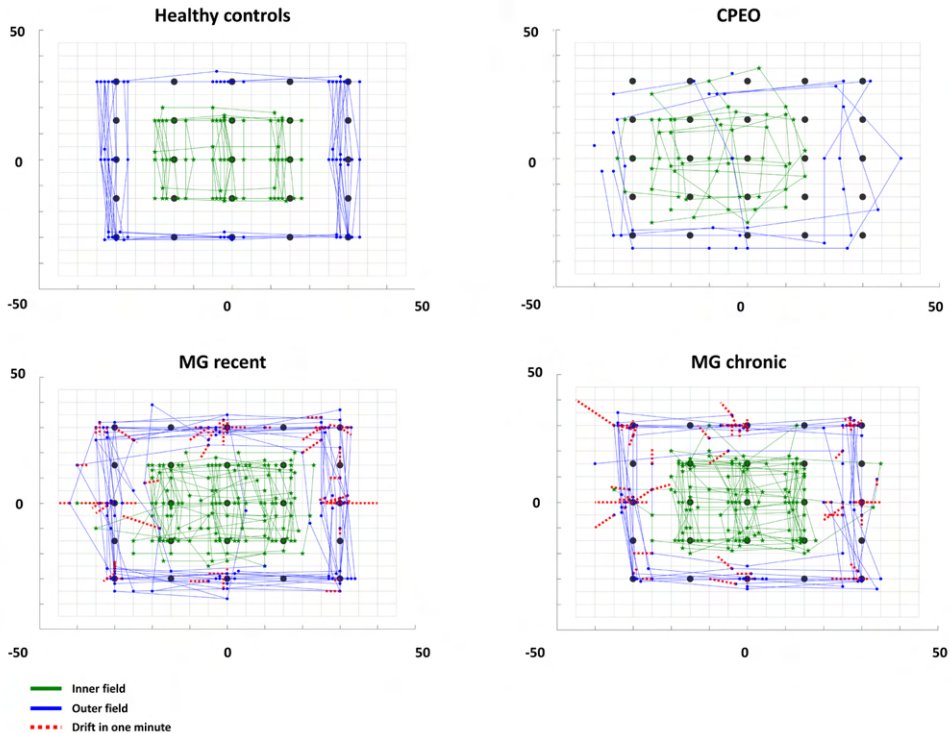
Figure 4. *Hess charts corresponding to the left eyes of all healthy controls, CPEO patients, recently diagnosed MG patients and chronic MG patients. Individual patients are superimposed. Measurements of the inner field are green and measurements of the outer field are blue and connected. Drift after one minute is plotted using red dashed lines.*

Sum-scores for duction angle limitations, deviations and drift

The sum-scores for the duction angle limitations as measured with the synoptophore and the deviations as measured with the Hess chart are depicted in figure 5. Sum-scores for duction angle limitations were significantly different (0 degrees for healthy controls, 10 degrees for recent MG, 23 degrees for chronic MG, 22 degrees for seronegative MG, 7 degrees for GO, 121 degrees for CPEO and 40 degrees for OPMD, $p<0.0001$); post-hoc analysis showed CPEO was different from healthy controls ($p<0.0001$). For the inner field of the Hess chart, significant differences were found between groups (2 degrees for healthy controls, 13 degrees for recent MG, 16 degrees for chronic MG, 15 degrees for seronegative MG, 17 degrees for GO, 23 degrees for CPEO and 3 degrees for OPMD, $p = 0.02$), and post-hoc analysis showed chronic MG ($p=0.03$) and CPEO ($p=0.02$) patients were different from healthy controls. For the outer field, significant differences were found between groups (2 degrees for healthy controls, 16 degrees for recent MG, 11 degrees for chronic MG, 23 degrees for seronegative

MG, 25 degrees for GO, 19 degrees for CPEO and 11 degrees for OPMD, p < 0.0001), and post-hoc analysis showed recent MG (p=0.02), seronegative MG (p=0.0007) and GO (p=0.004) were different from healthy controls. Drift sum-scores were significantly different between all groups (0 degrees for healthy controls, 13 degrees for recent MG, 12 degrees for chronic MG, 12 degrees for seronegative MG, 1 degree for GO, 0 degrees for CPEO and 0 degrees for OPMD, p < 0.0001), and post-hoc analysis showed that all three MG groups (p<0.0001) were different from healthy controls. The duction angle limitation sum-scores were not significantly different between ocular (9±22 degrees) and generalized (21±42 degrees) subgroups of MG. For the Hess chart, comparing ocular and generalised MG, the inner field (19 vs. 16 degrees), outer field (20 vs. 15 degrees) and drift sum-score (14 vs. 10 degrees) did also not differ significantly.
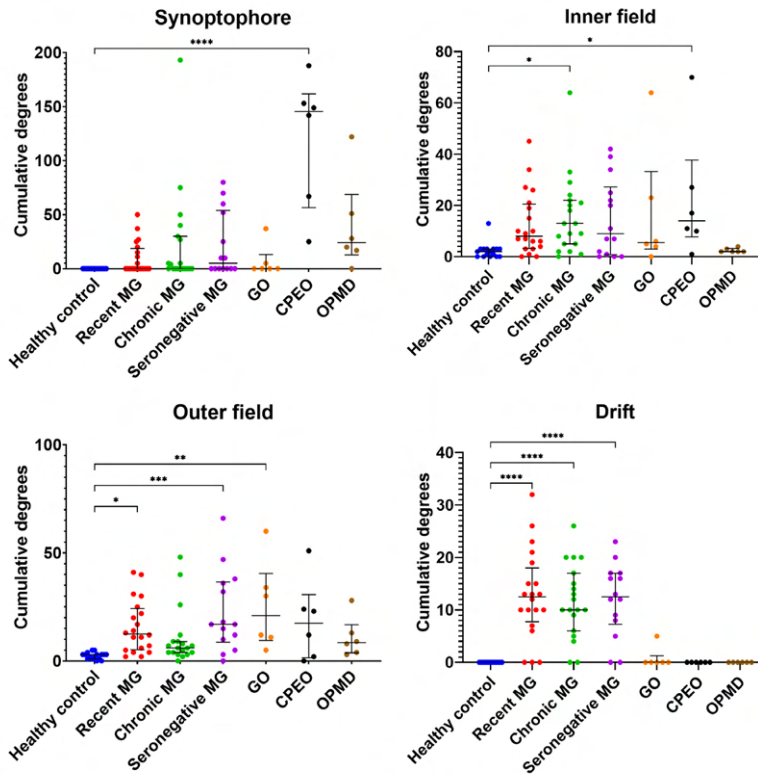
Figure 5. *Sum-scores for limitations in duction angles of both eyes as measured with the synoptophore, and the relative deviations between eyes on the Hess chart for the inner field, outer field and the drift during one minute persistent gaze are depicted per group. Significant post-hoc group differences are marked with asterisks. Most limited ductions were observed in the CPEO patients, in contrast with the Hess chart deviations given the symmetry of EOM involvement in CPEO. With the exception of one GO patient, the drift phenomenon occurred exclusively in MG patients.*

Figure 6. *Receiver operating characteristics (ROC) curves for the duction angles as measured with the synoptophore, and the inner field, outer fiel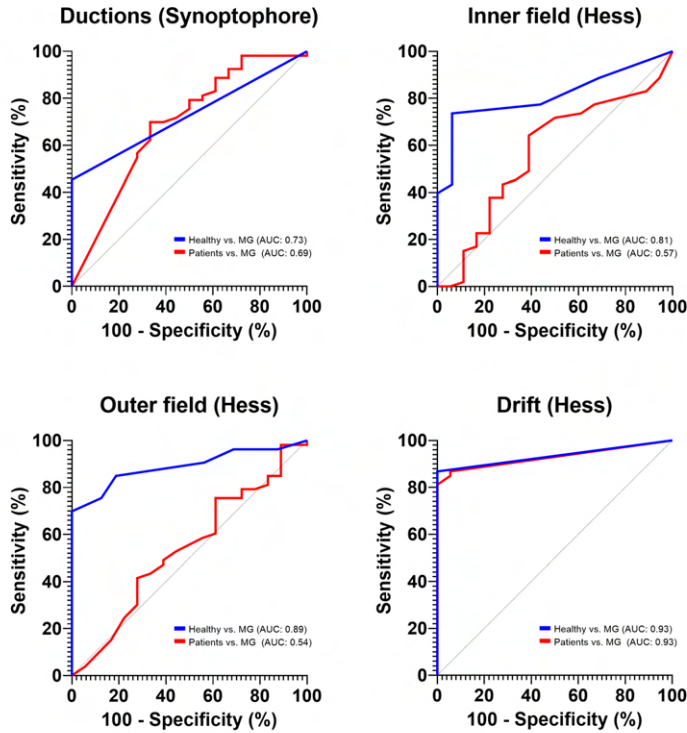d and the drift on the Hess chart. The ROC curve comparing MG patients and healthy controls is depicted in blue and the ROC curve for MG patients and other patient groups is depicted in red. The AUC of MG versus the other patient groups is highest for the drift on the Hess chart, with a specificity of 100% and a sensitivity of 81% at a sum-score threshold of six degrees.*

Hess deviations in MG patients without duction limitations

Of the 24 MG patients who had limited ductions, the average sum-score for the Hess chart inner field and outer field was 21.8±15.1 and 22.4±17.8 degrees respectively. Of the 29 MG patients who did not have any limited duction, the average sum-score for the Hess chart inner field and outer field was 8.2±9.6 and 10.3±9.2 degrees respectively. Twelve of these patients (41%) had an outer field sum-score above six degrees and therefore had clinically relevant Hess chart deviations without duction limitations.

Diagnostic value of orthoptic measures

ROC curves were calculated for the duction angles as measured with the synoptophore, and the inner field, outer field and the drift on the Hess chart by comparing the MG patients with healthy controls and with GO, CPEO and OPMD patients combined ('patient controls') and

are shown in figure 6. For duction angles, AUC was 0.73 (CI: 0.61 to 0.85, p=0.006) for MG compared to the healthy controls and 0.69 (CI: 0.54 to 0.84, p=0.016) for MG compared to patient controls. For the inner field of the Hess chart, the AUC was 0.81 (CI: 0.71 to 0.91, p=0.0002) compared to healthy controls and 0.57 (CI: 0.41 to 0.73, not significant) compared to patient controls. For the outer field, the AUC was 0.89 (CI: 0.81 to 0.96, p<0.0001) compared to healthy controls and 0.54 (CI: 0.38 to 0.70, not significant) compared to patient controls. For drift, the AUC was 0.93 (CI: 0.88 to 0.99, p<0.0001) compared to healthy controls and 0.93 (CI: 0.87 to 0.99, p<0.0001) compared to patient controls. The AUC was similar for ocular versus generalized MG (both 0.94). The highest diagnostic yield in MG patients compared to the other patient groups was achieved for the drift sum-score, with a sensitivity of 81% and specificity of 100%, using a threshold of six degrees.

Extra-ocular muscle involvement pattern
Horizontal movement and up-gaze was most deviant, with at least one LR and an MR deviating more than five degrees in 43% and 57% of MG patients, and at least one SR and an IO deviating more than five degrees in respectively 45% and 40% of MG patients. Downgaze deviated less frequently more than five degrees, with an IR and an SO being involved in 28% and 23% of MG patients. Only one healthy control showed a deviation for the MR muscle of five degrees or higher.

DISCUSSION

In this work, we studied whether our extended orthoptic tests could aid in the diagnosis of MG. We applied the Hess chart in a novel way, by assessing drift on the Hess chart as a direct measure of EOM fatiguability. The presence of drift during one minute of persistent gaze had a sensitivity of 81% and a specificity of 100%, compared to our patient control groups. This test could therefore constitute a promising, highly specific diagnostic test for MG, as it is relatively easy to implement in routine clinical testing, affordable and widely available.

Ocular seronegative MG is challenging to diagnose, resulting in misdiagnoses and treatment delays.[4] The diagnosis of ocular MG can be made probable by bedside testing for fatiguability and fluctuations in ocular symptoms. These tests include ptosis assessment during persistent up gaze, observations of rapid initial saccades[176] or Cogan's twitch, repeated observations to assess fluctuations and an examination before and after the administration of an acetylcholinesterase inhibitor. Additionally, quantitative and objective tests to diagnose ocular MG exist. Currently, these patients are diagnosed with single-fiber electromyography and repetitive nerve stimulation, but both these tests have limitations.[160] The diagnostic yield of

single-fiber electromyography appears to vary, with sensitivities ranging from 0.62 to 0.99 and specificities ranging from 0.66 to 0.98 in different studies.[177] Repetitive nerve stimulation is very specific but not very sensitive in ocular MG.[177] Given the anatomical difficulty of electrophysiological testing of the eye muscles directly, more objective measures of EOM fatiguability are lacking.[178] Other new diagnostic tests have recently been developed for the diagnosis of ocular MG, such as repetitive ocular vestibular evoked potentials[179,180] or videonystagmography[181], but these tests require specialized equipment. Our extended orthoptic tests are objective, specific and sensitive to the fatiguability of the EOM in MG, and therefore constitute an easily implementable diagnostic alternative.

The use of orthoptic tests enabled us to objectively quantify the overall pattern of involved EOMs in our patient groups. Despite fluctuations in weakness and involvement pattern, some EOMs appear to be more frequently involved in MG than others. In previous studies on the involvement pattern of EOM in MG, the SR, the IO and the MR have been reported to be more frequently involved than the IR, SO and the LR, without any consistent pattern.[164,182–185] We confirm these findings with similar frequencies of involved EOM, although variability between patients remains high. In CPEO and OPMD, the SR appears to be the most predominantly involved muscle, in line with results from previous studies.[131,186,187]

Interestingly, a remarkably high percentage (41%) of MG patients without a measurable ophthalmoparesis had Hess chart deviations. The limitations in ductions are measured monocularly using the synoptophore and translate directly to the degree of ophthalmoparesis. This might be partially explained by measurement limitations of the synoptophore, which are 30 degrees vertically and 40 degrees horizontally. The difference between the limitation of the synoptophore and the maximal gaze in healthy volunteers is most pronounced in depression, where volunteers showed an average of 55 degrees maximal gaze.[188] We hypothesize that absolute limitations in ductions only occur in cases in which EOM weakness is so severe that movement of the eye is restricted in certain directions. In contrast, Hess chart-derived deviations are based on a relative mismatch in gazing direction between both eyes. The Hess chart thus detects minor strength differences between the EOMs of both eyes, which are assumed to receive the same input following Hering's law of equal innervation[189]. Our data suggest that such subtle differences in contraction force are more prevalent in MG than severe EOM weakness causing absolute duction limitations.

In addition to diagnosis, orthoptic measures could also benefit future clinical trials by quantifying the effect of novel treatments on EOM weakness in MG patients. Twenty percent of MG patients develop a treatment-resistant ophthalmoplegia during their disease course and therapeutic strategies are lacking in this patient group, because a limited number of

clinical trials have been performed for the treatment of ocular MG.[190] In recent clinical trials on new treatments targeting complement, the FcRn receptor and B-cells[7], purely ocular subtypes of MG were usually excluded, probably because the degree of ocular weakness has been difficult to quantify so far.[25,191] More clinical research is therefore needed on the therapeutic management of ocular MG[192,193], and our data show that the extended orthoptic tests can be a sensitive and specific outcome measure to quantify the severity of EOM involvement in future clinical trials.

In future research, we suggest to perform the Hess chart measurements repeatedly with an interval of several weeks or months. This will likely provide insight on the fluctuation of the individual EOM involvement, as changes in affected EOM have been shown to be highly typical in MG.[194] Therefore, we would also like to emphasize the value of structural documentation of findings during bedside eye movement examination; the presence of ptosis and serial orthoptic testing and assess fluctuations in these findings. Additionally, it could further increase the diagnostic yield for the few patients that did not show drift on the Hess chart, as fluctuations are not likely in other causes of diplopia. Additionally, combining eye tracking methods using, for example video goggles[195] and the Hess chart to further quantify the drift phenomenon in MG patients over time could aid in an even more objective evaluation.

The main limitation of this study is that the included cohorts were not prospectively and consecutively recruited. Moreover, the examiner was not blinded to the diagnosis which may have biased the Hess chart and synoptophore measurements. However, drift was so apparent (see supplementary videos) that we do not expect this to have influenced our main results. In addition, the test does not require any qualitative interpretation and therefore the quantitative measures are not likely to be influenced by knowledge of the diagnosis.

In conclusion, orthoptic measurements are valuable in identifying EOM fatiguability in MG. As drift was only present in MG, measuring persistent gaze using a Hess chart holds promise as a highly specific, non-invasive and easy to perform diagnostic test for MG. In addition, orthoptic measurements can be used to identify the severity of involvement of individual EOMs in MG, which may be a promising and clinically relevant outcome measure for clinical trials including ocular MG patients.

Acknowledgements
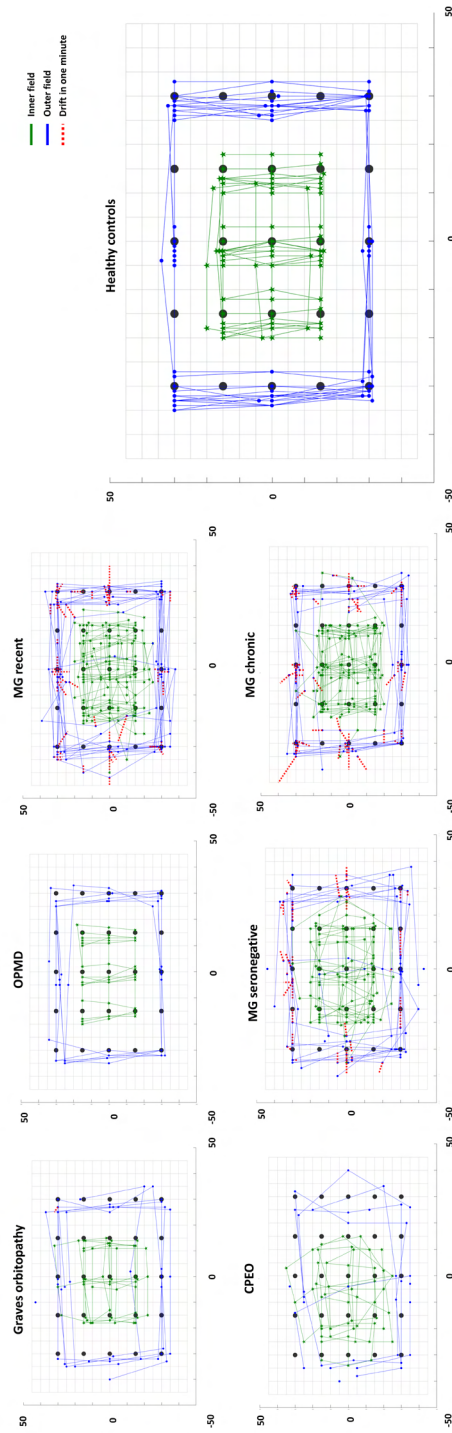
Supplementary figure 1. *The raw Hess charts belonging to the left eyes of all included health controls, MG subgroups, CPEO patients and OPMD patients. Individual patients are plotted on top of each other. Measurements of the inner field are plotted in green and measurements of the outer field are plotted in blue and connected. The drift after one minute is depicted with a red dashed line.*

1. C.J. Gorter center for high field MRI, Department of Radiology, Leiden University Medical Center, Leiden, the Netherlands
2. Department of Neurology, Leiden University Medical Center, Leiden, the Netherlands
3. Amsterdam University Medical Center, Amsterdam, the Netherlands
4. Duchenne Center Netherlands, the Netherlands
5. Department of Ophthalmology, Leiden University Medical Center, Leiden, the Netherlands
6. Department of Neurology, UMC Utrecht Brain Center, University Medical Center Utrecht, Utrecht University, the Netherlands
7. Department of Radiology, University Medical Center Utrecht, Utrecht, the Netherlands

T2 relaxation time mapping in healthy and diseased skeletal muscle using extended phase graph algorithms

Kevin R. Keene[1,2] | Jan-Willem Beenakker[1,5] | Melissa T. Hooijmans[3]
Karin J. Naarding[2,4] | Erik H. Niks[2,4] | Louise A.M Otto[6] | W. Ludo van der Pol[6]
Martijn R. Tannemaat[2] | Hermien E. Kan[1,4] | Martijn Froeling[7]

ABSTRACT

Purpose
Multi-echo spin-echo (MSE) transverse relaxometry mapping using multi-component models is used to study disease activity in neuromuscular disease (NMD) by assessing the T2 of the myocytic component ($T2_{water}$). Current extended phase graph (EPG) algorithms are not optimized for fat fractions above 50% and the effects of inaccuracies in the $T2_{fat}$ calibration remain unexplored. Hence, we aimed to improve the performance of EPG fitting methods over a large range of fat fractions, by including the slice selection flip angle profile, a through-plane chemical shift displacement correction, and optimized calibration of $T2_{fat}$.

Methods
Simulation experiments were used to study the influence of the slice flip angle profile with chemical shift and $T2_{fat}$ estimations. Next, in vivo data from four NMD cohorts were studied for different $T2_{fat}$ calibration methods and $T2_{water}$ estimations.

Results
Excluding slice flip angle profiles or chemical shift displacement resulted in a bias in $T2_{water}$ up to 10 ms. Furthermore, a wrongly calibrated $T2_{fat}$ caused a bias of up to 4 ms in $T2_{water}$. For the in vivo data, one-component calibration led to a lower $T2_{fat}$ compared to a two-component method, and $T2_{water}$ decreased with increasing fat fractions.

Conclusion
In vivo data showed a decline in $T2_{water}$ for increasing fat fractions, which has important implications for clinical studies, especially in multi-center settings. We recommend using an EPG based model for fitting $T2_{water}$ from MSE sequences with two-component $T2_{fat}$ calibration. Moreover, we recommend including the slice flip angle profile in the model with correction for through-plane chemical shift displacements.

INTRODUCTION

Quantitative MRI shows promising results as a biomarker in the follow-up of disease progression in neuromuscular diseases (NMD).[36] In these diseases, inflammation and progressive fat replacement of muscle tissue are major histological hallmarks. While imaging of the fat fraction using MRI or MR-spectroscopy (MRS) is used to assess disease progression, transverse relaxometry mapping or T2 relaxation time mapping has been applied as an MRI marker for disease activity.[124,196,197]

Quantitative measurements of T2 relaxation time are commonly performed using T2prep sequences[198], multi-acquisition single TE SE sequences, IDEAL-CPMG[199], MR spectroscopy[200] or multi-spin-echo (MSE) sequences[201]. Acquisition times for multi-acquisition sequences are longer[202] (typical acquisition time 10 min) compared to MSE sequences (typical acquisition time: 3 min) and more sensitive to motion artefacts, while MR spectroscopy can only give information for a single muscle. Therefore, MSE is commonly used, as it allows for fast scans with a large field-of-view.[201] To measure the T2 relaxation time from a MSE sequence, a mono-exponential decay can be fitted to the signal intensity as a function of echo time. However, this combined T2 relaxation time, also defined as the 'global T2 relaxation time'[203], represents the combined relaxation of all different components, including the T2 relaxation time of water and fat. In the presence of fat replacement, which is often the case in NMD, this combined T2 is primarily affected by the fat signal, which has a relatively long T2 relaxation time, masking the more subtle changes in T2 due to the other changes in muscle tissue.[41] Therefore, in NMD it is preferred to separate the signal into different components for water ($T2_{water}$) and fat ($T2_{fat}$), where the T2 of the myocytic component ($T2_{water}$) has been proposed as a more accurate biomarker for disease activity.[203]

Assessment of $T2_{water}$ using MSE has been performed using various approaches including fat suppression and modeling. Fat suppression has the advantage that it is available on all scanners, however, it is sensitive to field inhomogeneities and is often unable to suppress the entire fat spectrum[204,205] As an alternative, different modelling approaches have been proposed to separate the contribution of the water and fat signal. Originally, bi-exponential[206] or tri-exponential[207,208] methods were introduced to separate both contributions to the signal at the successive echo times. However, these models assume a perfect mono-exponential decay for the components, which is generally not observed in vivo. One important deviation from this perfect mono-exponential decay are stimulated echoes that result in a oscillation of the measured signal.[209,210] This oscillation results in an overestimation of the T2, when estimated using an exponential model. As a result, the accuracy and reproducibility of these exponential models are limited.[41]

5

To overcome these limitations, which are primarily caused by deviations from the assumed Hahn echo sequence due to for example a lower B1, fitting using extended phase graphs (EPG)[211] has been proposed. The EPG concept is a tool for describing the magnetization response in multi-pulse MR sequences, using a Fourier based magnetization description. Similar to exponential models a two component EPG model can be used to account for the fat signal, which has been shown to yield $T2_{water}$ values in the range of the gold standard MRS, and which were largely independent of fat fractions up to 50% in several NMDs.[212,213] However, there are still several aspects that are not taken into account in the currently used EPG analyses.

Firstly, current analyses do not report $T2_{water}$ values above a fat fraction of about 50%[41], while in muscular dystrophies fat fractions above 50% are not an exception[197], thereby limiting the applicability of the method. Secondly, the effect of inaccuracies in the estimation of T2 fat remain unexplored. Determination of the $T2_{fat}$ from MSE sequences is challenging as the spectral components of fat each have different T2 relaxation times which, due to J-coupling, also depends on the echo-spacing.[43,214,215] The current EPG implementations calibrate T2 relaxation time of the fat component using subcutaneous fat[208], thereby assuming that the $T2_{fat}$ in muscle is similar to subcutaneous fat. However, subcutaneous fat contains on average only 90% fat and 10% water[216], rather than 100% fat. Thirdly, the spatial variation of the flip angle across the slice is not taken into account.[41]. Due to the limited duration of the RF-pulses, the excitation and refocusing pulses do not provide a homogeneous flip angle across the excited slice. This is especially the case in T2-mapping using MSE, as short RF-pulses are applied to facilitate short echo spacings.[209,210] Fourthly and finally, the chemical shift displacement between water and fat in the slice direction has to be taken into account. When the slice selection gradient of the excitation pulse is different from the slice selection gradient of the refocusing pulse, the flip angle profiles are not aligned for the protons in fat. Therefore, the fat protons experience a different refocusing than the water protons, resulting in different strength of the stimulated echoes of the fat signal.

In the present work, we aim to improve the performance of EPG fitting methods to determine $T2_{water}$ in muscles of different NMDs with a large range of fat fractions by studying the effect of the incorporation of the flip angle profile with a chemical shift displacement in the slice direction and the assumptions for the calibration of the $T2_{fat}$. We present the importance of including slice flip angle profiles with a chemical shift displacement in the slice direction and correct calibration methods for the T2 of the fat component. Furthermore, we show the performance of the model in four clinical cohorts, which show a gradual decline in $T2_{water}$ for increasing fat fractions.

METHODS

A signal model based on extended phase graphs, including a slice flip angle profile with a chemical shift between water and fat, was used to fit the MSE signal. The fit was performed using a dictionary fitting method as proposed by Marty et al.[41] The performance of this model was studied in simulation experiments. The influence of the slice flip angle profile with the chemical shift and the influence of the assumed $T2_{fat}$ were studied in simulation 1 and 2 respectively. Using in vivo data from four patient cohorts, we performed two additional experiments. In experiment 1 the performance of different calibration methods for the $T2_{fat}$ was examined and in experiment 2 the model was applied to the data, to study the performance and the outcome parameters. All analyses were performed in Matlab (MATLAB 2016a, The Mathworks of Natick, Massachusetts, USA).

EPG-model

The model used for the MSE signal simulation comprises a water and a fat signal simulated with extended phase graphs[211], including the T1, the T2 and the B1. The slice flip angle profiles of the RF-pulses were calculated using Bloch equations at 30 samples along the slice flip angle profile (3x slice thickness).[209,210] Slice angle profiles for a B1 of 70%, 100% and 130% are shown in figure 1A, respectively for the water signal, the fat signal and the combined signal.

Since the slice selection gradients can differ between the excitation and refocusing pulses, the slice flip angle profiles are not aligned for the protons in fat (figure 1). This chemical shift artefact was incorporated in the model for the fat signal, by shifting the fat signal in the slice direction according to:

$$\Delta L = \frac{1}{\gamma * G} * \Delta f * B0$$

with ΔL the shift in location in meters, γ the Larmor frequency in hertz/Tesla, G the gradient strength in Tesla/meter, Δf the chemical shift between water and fat in hertz/Tesla and B0 the field-strength of the scanner in Tesla.

Fitting of MSE signal

The measured signal vector S with size N_{echo} (the number of echo's) can be approximated using a bi-component EPG model where the modeled signal vector $\hat{S}$ can be defined as

$$\hat{S} = w \, S_{water} + f \, S_{fat} = [S_{water} \quad S_{fat}] \begin{bmatrix} w \\ f \end{bmatrix}$$

83
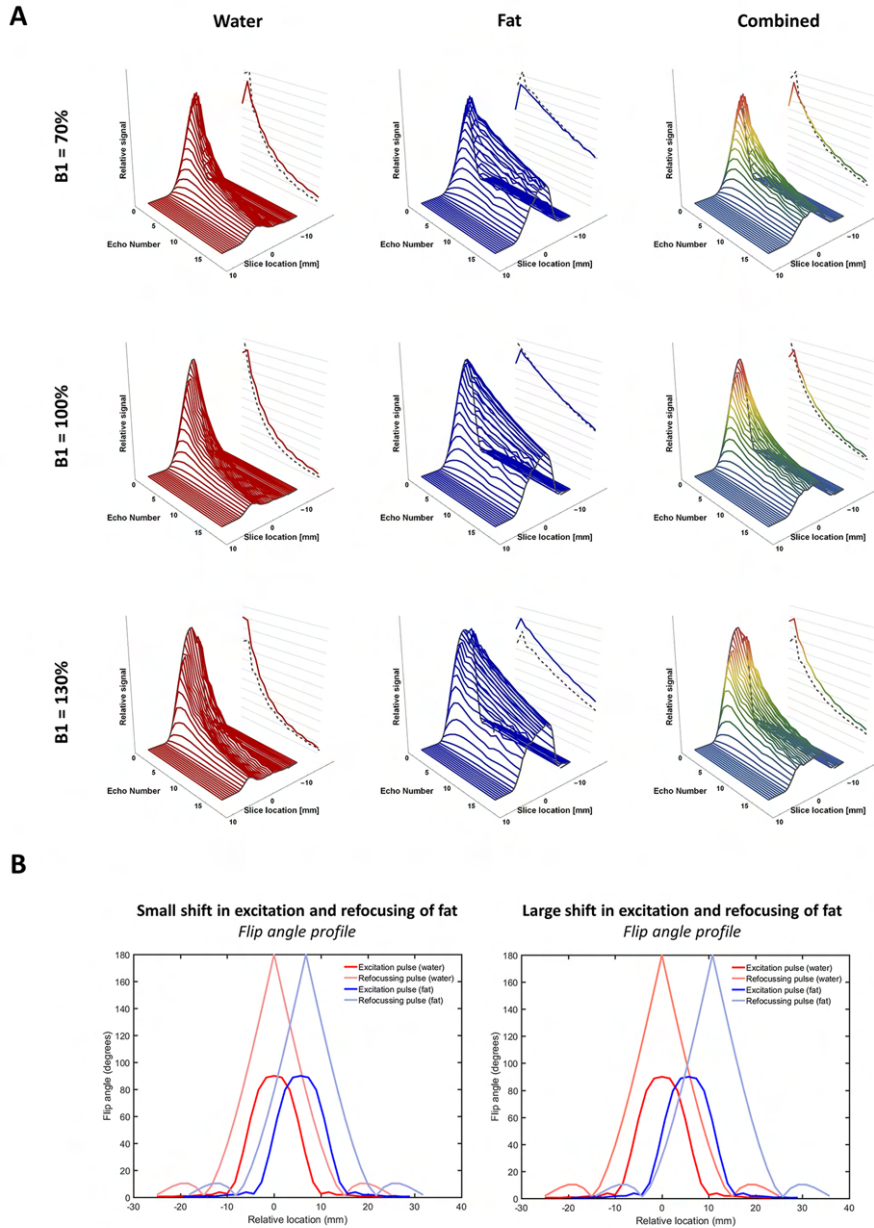
Figure 1: A: *Signal profiles for a B1 of 70%, 100% and 130%, from left to right. Noticeable is the asymmetry around a B1 of 100%. The right dotted line in each signal profile represents the signal in the center of the slice, and the right colored line depicts the final signal after averaging all signal contributions. **B**: Example flip angle profile of the pulses throughout the slice. On the left an example of a flip angle profile with a minor shift (1.1 mm) between the excitation and refocusing pulse as experienced by the fat is shown and on the right an example of a major shift (5.1 mm).*

With w and f the water and fat signal amplitudes. The signal at each echo of the water and fat component are S_{water} and S_{fat}, respectively, and are defined as

$$S_{water} = \sum_{m=1}^{M} EPG\left(T1_{wat}, T2_{wat}, B1, \Delta TE, N_{echo}, \alpha_{ex}^m, \alpha_{ref}^m\right)$$

$$S_{fat} = \sum_{m=1}^{M} EPG\left(T1_{fat}, T2_{fat}, B1, \Delta TE, N_{echo}, \alpha_{ex}^m, \alpha_{ref}^m\right)$$

With a_{ex} and a_{ref} the flip angle profiles along the slice direction of the excitation and refocusing pulses, respectively, and M the number of samples along the slice profile.

The signal was fitted using a dictionary-based method. The pre-calculated dictionary contains a range of values for T2$_{fat}$, T2$_{water}$ and B1. The T2 parameters ranged between boundaries based on literature values (T2$_{fat}$: 120-200 ms with 2 ms steps and T2$_{water}$: 10 ms-60 ms with 1ms steps) and the B1 value ranged between 50%-140% (with 2% steps), since the incorporation of the flip angle profile breaks the B1 symmetry around 100% for the excitation pulse (see fig 1A).[210] The th dictionary EPG signals d_{water}^i and d_{fat}^i with $T2_{wat}^i$ and $B1^i$ are defined as

$$d_{water}^i = \sum_{m=1}^{M} EPG\left(T1_{wat}, T2_{wat}^i, B1^i, \Delta TE, N_{echo}, \alpha_{ex}^m, \alpha_{ref}^m\right)$$

$$d_{fat}^i = \sum_{m=1}^{M} EPG\left(T1_{fat}, T2_{fat}, B1^i, \Delta TE, N_{echo}, \alpha_{ex}^m, \alpha_{ref}^m\right)$$

For each dictionary value of $T2_{wat}^i$ and $B1^i$ the water and fat amplitudes w^i and f^i, and the modelled signal $\hat{S}^i$ at the ith dictionary index are estimated using a matrix formulation of the multiple regression model:

$$\begin{bmatrix} w^i \\ f^i \end{bmatrix} = \begin{bmatrix} d_{water}^i \\ d_{fat}^i \end{bmatrix}^{-1} S$$

$$\hat{S}^i = \begin{bmatrix} d_{water}^i & d_{fat}^i \end{bmatrix} \begin{bmatrix} w^i \\ f^i \end{bmatrix}$$

The optimal dictionary values $T_{2,wat}^i B_1^i$ and the corresponding amplitudes of the water and fat signal w^i and f^i are determined by minimizing the Euclidian norm

$$\operatorname{argmin} \left\| S - \hat{S}^i \right\|_2$$

5

To include a water fraction $g(0 \leq g \leq 1)$ with $T_{1,watfat}$ and $T_{2,watfat}$ in the dictionary fat signal, d^i_{fat} was defined as

$$d^i_{fat} = \sum_{m=1}^{M} (1-g) EPG\left(T1_{fat}, T2_{fat}, \boldsymbol{B1}^i, \Delta TE, N_{echo}, \boldsymbol{\alpha}^m_{ex}, \boldsymbol{\alpha}^m_{ref}\right)$$
$$+ g\, EPG\left(T1_{watfat}, T2_{watfat}, \boldsymbol{B1}^i, \Delta TE, N_{echo}, \boldsymbol{\alpha}^m_{ex}, \boldsymbol{\alpha}^m_{ref}\right)$$

Simulation experiments

To assess the incorporation of the slice flip angle profile, the chemical shift of the slice profile between water and fat, and the effect of the assumed $T2_{fat}$, the MSE signal evolution was simulated using EPG assuming a known slice flip angle profile (figure 1). In the simulations the $T2_{water}$ was fixed at 30 ms, B1 and fat fractions were randomized between the possible boundaries (B1: 50%-140% and the fat fraction: 0%-100%) and the $T2_{fat}$ was modelled with gaussian distribution (mean of 150 ms and standard deviation 10 ms). The $T1_{water}$ and $T1_{fat}$ were fixed on 1400 ms and 365 ms respectively. Two simulation experiments as described below were performed, one to investigate the effect of slice flip angle profiles, and one to investigate the effect of using wrongly calibrated $T2_{fat}$.

Simulation 1 − The effect of the slice flip angle profile
We conducted two simulations to study the effect of incorporating the flip angle profile and the chemical shift of the slice profile between water and fat signals on the estimated $T2_{water}$. In **simulation 1A,** the data was simulated assuming the full slice flip angle profile and fitting was done with and without assuming the full slice flip angle profile. Next in **simulation 1B,** data was simulated assuming using the full slice flip angle profile with a large and a small chemical shift between water and fat slice profiles. The simulated data was fitted with and without accounting for the chemical shift. The used slice flip angle profiles for the small and large chemical shift are shown in figure 1.

Simulation 2 −The effect of $T2_{fat}$
To study the effect of wrongly calibrated $T2_{fat}$ on the estimated $T2_{water}$, we conducted a simulation in which a full slice flip angle profile and chemical shift was incorporated. In **simulation 2,** data was simulated with $T2_{fat}$ = 150 ± 10 ms. Next the data was fitted with a correct, an overestimated and an underestimated $T2_{fat}$ of 150 ms, 180 ms and 120 ms, respectively.

In vivo experiments
Study populations and MR scans
To study the effect of T2 calibration methods in vivo, we used data from four different clinical

cohorts that contained MSE data of both patients and healthy controls. The four cohorts contained data from 92 patients and 56 healthy controls. These datasets were acquired in the context of four clinical studies and will be used for methodological purposes in the current work.[217–220] The Medical Ethics Review Committee of the Leiden University Medical Center (LUMC) and the University Medical Center Utrecht (UMCU) approved the studies and all patients or parents provided written informed consent prior to study participation.

All patients were scanned on a 3T Philips MRI system. The first cohort (**cohort 1**) comprised of 18 non-ambulant patients with Duchenne muscular dystrophy (DMD) (17.1±5.1 years, range 9-24 year) and 11 age matched healthy controls (14.7±4.0 years, range 10-25 year), from the LUMC[220]. In this cohort upper-arm scans had been acquired. The second cohort (**cohort 2)** comprised of 22 patients with DMD (9.3±3.1 years, range 5-16 year, 16 ambulant and 6 non-ambulant) and 12 age matched healthy controls (9.7±2.9 years, range 5-14 years), from the LUMC.[219] The third cohort (**cohort 3**) comprised of 23 patients with Becker muscular dystrophy (BMD) (42.7±13.6 years, range 18-67 year, all ambulant) and 13 age matched healthy controls (43.0±13.7 years, range 21-63 year), also from the LUMC[217]. In both cohort 2 and cohort 3 lower-leg scans had been acquired. The fourth and final cohort (**cohort 4**) comprised of 29 patients with spinal muscular atrophy (SMA) (29.6±18.0 years, range 17-71 years, 48% male, 14 patients had SMA type 2 and 15 patients had SMA type 3) and 20 age matched healthy controls (37.9±12.8 years, range 17-71 years, 40% male), from the UMCU[218]. In this cohort upper-leg scans had been acquired. In each data set, regions of interest were manually drawn on 5 slices that consisted of the entire cross-sectional muscle compartment without the bone and subcutaneous fat (figure 2). The sequence parameters for each cohort are depicted in table 1.

With the data of these cohorts we performed two experiments as described below. The first experiment aimed to compare three different $T2_{fat}$ calibration methods using voxels from the subcutaneous fat. The second experiment evaluated the effect of these fat calibration methods on the $T2_{water}$ estimation.

Calibration of $T2_{fat}$

The $T2_{fat}$ was calibrated on subcutaneous fat using a fat mask based on the last echo in the echo sequence.[208] The mask was determined by thresholding the last echo in the MSE sequence with the mean signal intensity (figure 2). The signal was fitted for each voxel using the library method described above, fixing the $T2_{water}$ and the water/fat quantities as described below. The $T2_{fat}$ was obtained by averaging all fitted voxel in the fat mask.
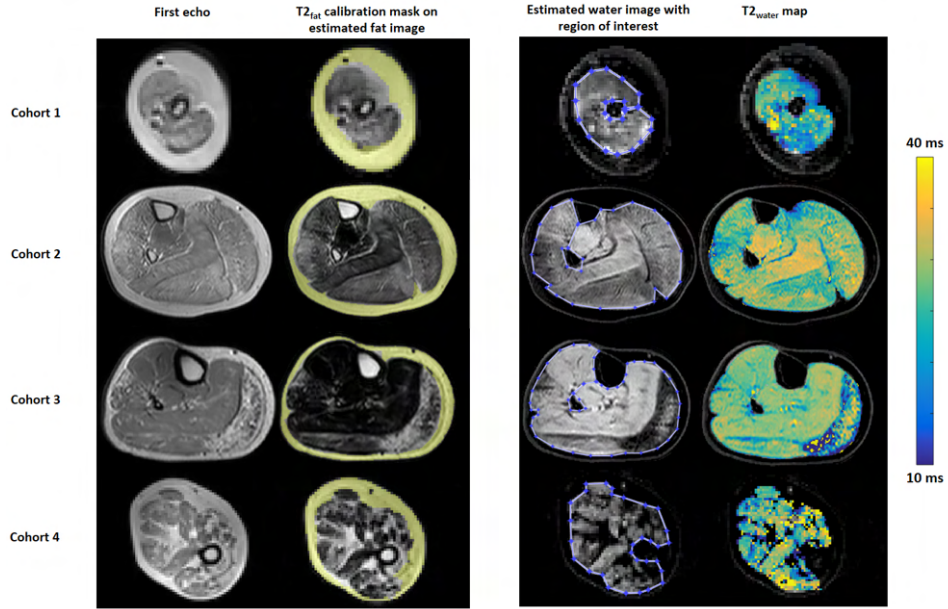
5

Figure 2. *Example raw data and maps from one patient in all four cohorts. From left to right the signal for the first echo, the estimated fat map with the T2$_{fat}$ calibration mask, the estimated water map with the region of interest and the T2$_{water}$ map are depicted.*

Experiment 1 − in vivo calibration of T2$_{fat}$

The T2$_{fat}$ of the subcutaneous fat was estimated using three different methods. The first, **method A,** assumed one fat component with a 100% fat fraction. The second, **method B**, estimated T2$_{fat}$ using a fixed fat fraction of 90% (based on literature values[221]) and a water component of 10%, where both relaxation times are fitted in the model. In the third and last method, **method C**, calibration was done using a fixed fat fraction of 90% and a fixed T2$_{water}$ in the fat of 20 ms, to stabilize the fit with low water signal.

Experiment 2 − In vivo T2 estimation

To study the performance of the different methods of calibration, we compared the outcome parameter T2$_{water}$ for 5 slices of the patient cohorts using **method A, B and C** as described above. In summary, with **method A** the T2$_{fat}$ is calibrated assuming one fat component (fat fraction 100%), with **method B** the calibration is performed using a fixed fat fraction of 90% and a 10% water-fraction with a fitted T2$_{water}$ and with **method C** the calibration is done using a fixed fat fraction of 90% and a 10% water-fraction with T2$_{water}$ of 20 ms. In the last two methods fitting is performed with the calibrated T2$_{fat}$ that also includes a 10% water

Table 1. *Acquisition and pulse parameters for the four cohorts. Cohort 1 included Duchenne's muscular dystrophy (DMD) patients with healthy controls (HC), cohort 2 included DMD patients with healthy controls, cohort 3 included Becker muscular dystrophy (BMD) patients with healthy controls and cohort 4 included spinal muscular atrophy (SMA) patients and healthy controls.*

	Cohort 1 DMD: n=18 HC: n=11	Cohort 2 DMD: n=22 HC: n=12	Cohort 3 BMD: n=23 HC: n=13	Cohort 4 SMA: n=29 HC: n=20
Anatomical location	Upper arm	Lower leg	Lower leg	Upper leg
Sequence parameters				
First echo time	8.0 ms	8.0 ms	8.0 ms	7.6 ms
Time between echoes	8.0 ms	8.0 ms	8.0 ms	7.6 ms
Number of echoes	17	17	17	17
Repetition time	3000 ms	3000 ms	3000 ms	4598 ms
Slice thickness	10 mm	10 mm	10 mm	6 mm
Slice gap	20 mm	20 mm	20 mm	0 mm
Slices	5	5	5	13
Resolution	2.0 mm x 2.0 mm	1.6 mm x 1.6 mm	1.6 mm x 1.6 mm	3.0 mm x 3.0 mm
ΔChemical shift*	0.1 mm	1.1 mm	1.1 mm	0.9 mm
Excitation pulse				
Bandwidth	1000 Hz	1000 Hz	1000 Hz	768 Hz
Gradient strength	1.78 mT/m	1.78 mT/m	1.78 mT/m	2.28 mT/m
Refocusing pulse				
Bandwidth	632 Hz	632 Hz	632 Hz	486 Hz
Gradient strength	1.80 mT/m	1.48 mT/m	1.48 mT/m	1.90 mT/m

* Chemical shift displacement difference in slice direction between excitation and refocusing pulse for fat.

5

component with respectively the calibrated T2$_{water}$ and a T2$_{water}$ of 20 ms. Example T2$_{water}$ maps are shown in figure 2.

Statistics

For the simulation experiments, the relation between simulated fat fractions and fitted T2$_{water}$ values and fitted fat fractions was obtained using LOWESS-regression. For analysis a linear regression analysis was performed, and the slope and intercept were reported. The voxels that were fitted with boundary values (T2$_{water}$ shorter than 10 ms and longer than 60ms) were excluded from statistical analysis and depicted in red in the figures. For the calibration experiment (**experiment 1**), smoothed histograms were generated for all calibrated values. Average T2$_{water}$ values between different calibration methods were compared using paired T-tests. T2$_{fat}$ values within the different calibrations were compared using a Kruskal-Wallis test with post-hoc comparison using Bonferroni correction. For the in vivo fitting experiment (**experiment 2**) LOWESS regression was used to assess the relation between T2$_{water}$ and fat fractions.

Data availability

The used Matlab scripts and one example dataset presented in this article will be made available at the request of a qualified investigator. Requests should be made to K. R. Keene (k.r.keene@lumc.nl). A Mathematica version of the fitting algorithm is available at Github (https://github.com/mfroeling/QMRITools).

RESULTS

Simulation 1: The effect of the slice flip angle profile

In **simulation 1A,** data was simulated assuming the slice flip angle profile and fitted with and without taking the flip angle profile into account. The results of the fit are depicted in figure 3. Without incorporation of the flip angle profile, the results show an overestimation of $T2_{water}$, with a median of 40 ms (5th-95th percentile: 34-57 ms), and with many voxels on the dictionary boundaries (30%). The results also show an underestimation of the fitted fat fraction for the entire range of values (intercept: -2.26%, slope: 0.87). However, fitting with incorporation of the flip angle profile resulted in a median $T2_{water}$ of 30 ms (5th-95th percentile: 26 - 35 ms), and only 1.5% of fits were on dictionary boundaries. The correlation between the simulated and fitted fat fraction show an intercept of 0.3% and a slope of 0.99.

In **simulation 1B,** data was simulated assuming a small and a large chemical shift between water and fat, and fitting with and without assuming the chemical shift (figure 2B). The results for the fits simulated and fitted with the small and large chemical shift are comparable ($T2_{water}$: median: 30 ms [5th-95th percentile: 26 – 35 ms], on dictionary boundaries: 1.5%; fat fraction: intercept: 0.3%, slope: 0.99), and show no underestimation or overestimation of the $T2_{water}$ and the fat fraction (figure 4). However, when the chemical shift is not included in the analysis, $T2_{water}$ was overestimated with a median of 32ms (5th-95th percentile 28 – 51 ms) and 34ms (5th-95th percentile: 30 – 53 ms) for the small and large chemical shift respectively. The fat fraction is globally underestimated, and the fit is increasingly unstable for higher fat fractions (small shift: intercept: 0.72%, slope: 0.92; high shift: intercept: -1.28%, slope: 0.79).

Simulation experiment 2 – The influence of the T2fat

In **simulation 2A,** data was simulated with a known $T2_{fat}$ and fitted with an underestimated, correct and overestimated $T2_{fat}$ (figure 5). A baseline was established by fitting the values with an average $T2_{fat}$, with the median of the $T2_{water}$ at 30 ms (5th-95th percentile: 23 – 38 ms) with 4% of voxels on the dictionary boundaries and no apparent error in the fitted fat fraction (intercept: 0.6%, slope: 1.0). With an underestimation of the $T2_{fat}$, the $T2_{water}$ is underestimated and the fat fraction is overestimated, and the fit is more unstable ($T2_{water}$: median: 26ms (5th-
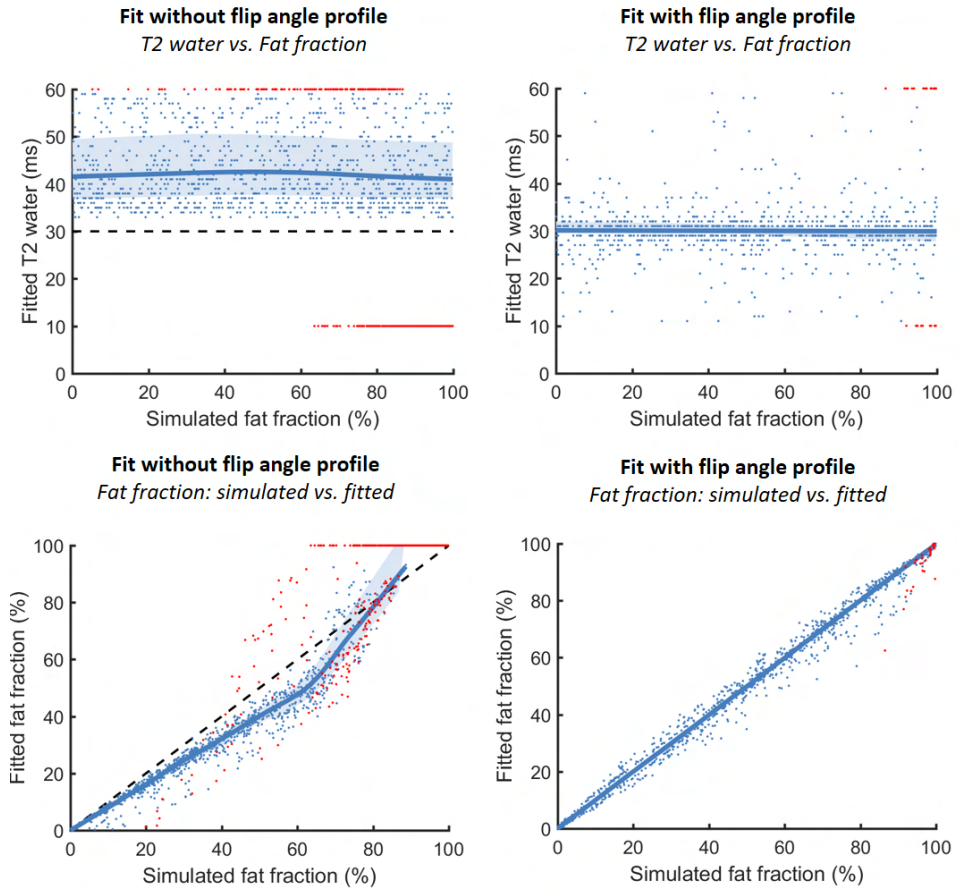
Figure 3. **Simulation 1A** shows the relationship between the simulated FF and the fitted T2$_{water}$ for simulation without incorporation of the flip angle profile (T2$_{water}$: median: 40 ms [34 ms – 57 ms], on dictionary boundaries:30%) and fitted with incorporating the flip angle profile (top row) (T2$_{water}$: median: 30ms [26 ms – 35 ms], on dictionary boundaries: 1.5%). In the bottom row, the relation between the simulated fat fraction and fitted fat fraction is shown without and with flip angle profile. The values that fitted on dictionary boundaries are depicted in red and the correctly fitted values are depicted in blue. A reference line is shown at a T2$_{water}$ of 30 ms and a unity line is shown for the fat fractions.

95th percentile: 14 – 30 ms), on dictionary boundaries: 26%; fat fraction: intercept: 2.71%, slope: 1.11). With an overestimation of the T2$_{fat}$, the T2$_{water}$ is overestimated and the fat fraction is underestimated (T2$_{water}$: median: 33 ms (5th-95th percentile: 30 – 51ms), on dictionary boundaries: 9%; fat fraction: intercept: 0.32%, slope: 0.84).

Experiment 1 – In vivo calibration of T2$_{fat}$

The T2$_{fat}$ values for the three described methods to calibrate the T2$_{fat}$ are depicted as smoothed histograms in figure 6, separated for all four clinical cohorts. In **method A,** where the calibration was done assuming one fat component (fat fraction 100%), a median T2$_{fat}$ of 137 ms, 132 ms, 131 ms, and 144 ms was found for cohort 1 to 4 respectively. The T2$_{fat}$ differed significantly between cohorts (p<0.001) except between cohort 2 and 3, which were acquired with the same sequence. Using **Method B,** the calibration was done using a fixed fat fraction of 90% and a fixed water component of 10%, of which both the relaxation times were fitted. This method results in a median T2$_{fat}$ of 149 ms, 141 ms, 140 ms and 158 ms, which again differed significantly (p<0.001) except between cohort 2 and 3. The water component had a median T2$_{water}$ around 27 ms, 24 ms, 24 ms and 22 ms for cohorts 1 to 4. The histogram for cohort 1 shows that a portion of the values are over 30 ms, possibly representing the T2$_{water}$ of muscle. In the last experiment (**method C**) the calibration was performed using a fixed fat fraction of 90% and a T2$_{water}$ component in the fat of 20ms. This method results in a median T2$_{fat}$ of 150 ms, 142 ms, 140 ms and 159 ms for cohorts 1 to 4 respectively, which is similar to the results of experiment 1B (also statistically different between all cohorts except cohort 2 and 3, p<0.001).

The one-component fitting model leads to a lower T2$_{fat}$ compared to the two-component fitting model. Notable is the difference of approximately 10ms in median T2$_{fat}$ between the cohorts for all methods, except for cohort 2 and 3 which have similar T2$_{fat}$ values. Comparing method B and C seem to result in similar T2$_{fat}$ values.

For cohort 1 there was a difference in T2$_{fat}$ for the two component calibrations between the healthy controls and patients, explaining the difference in the histograms with method B and C. In this cohort the average calibrated T2$_{fat}$ was 139 ms for healthy controls and 155 ms for the patients in cohort 1 (DMD arm scans), while for the other cohorts the histograms of the healthy controls and patient overlap, for example for cohort 3 (BMD leg scans) the average calibrated T2$_{fat}$ was 140 ms for both the healthy controls and BMD patients.
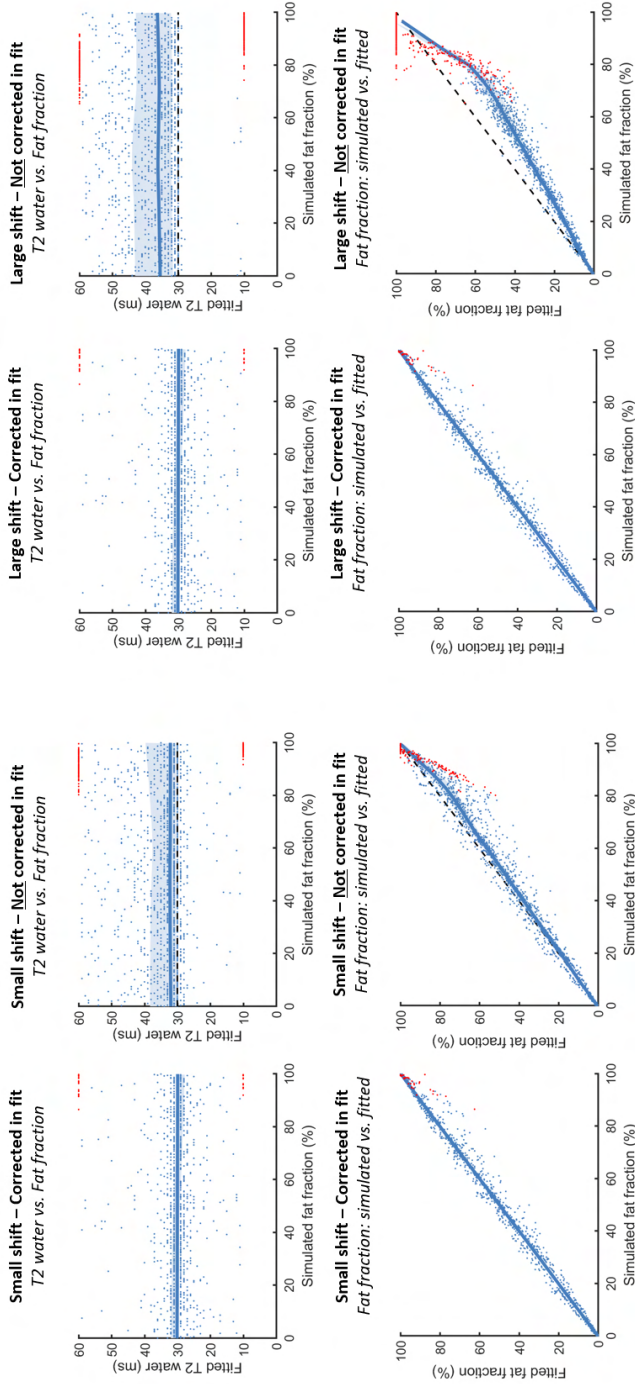
Figure 4. Simulation 2 *showing the effect of simulating data with a chemical shift in the location of the pulses and fitting it with or without incorporating the chemical shift of the slice. The four figures on top show the simulation with a small shift ($T2_{water}$: median: 32 ms (28 ms – 51 ms), on dictionary boundaries: 6.8%; fat fraction: intercept: 0.72%, slope: 0.92) and the four figures on bottom show the simulation with a large shift ($T2_{water}$: median: 34 ms (30 ms – 53 ms), on dictionary boundaries: 22%; fat fraction: intercept: -1.28%, slope: 0.79). The values that fitted on dictionary boundaries are depicted in red and the correctly fitted values are depicted in blue. A reference line is shown at a $T2_{water}$ of 30 ms and a unity line is shown for the fat fractions.*

5
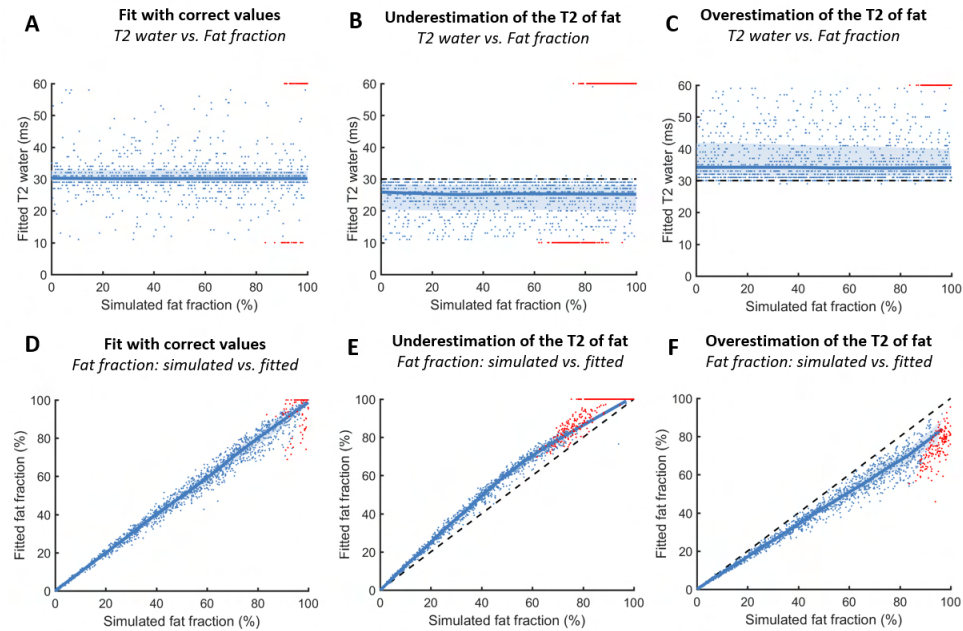
Figure 5. Simulation 2 *shows the effect of fitting simulated data with different assumed T2$_{fat}$ values. The top row shows the T2$_{water}$ for assuming the correct T2$_{fat}$ (T2$_{water}$: median: 30 ms [23 ms − 38 ms], on dictionary boundaries: 4%, fig. A), an underestimation of T2$_{fat}$ (T2$_{water}$: median: 26 ms [14 ms − 30 ms], on dictionary boundaries: 26%, fig. B) and an overestimation of T2$_{fat}$ (T2$_{water}$: median: 33 ms [30 ms − 51 ms], on dictionary boundaries: 9%, fig C.). Fig. D, E and F show the relationship between the simulated FF and fitted FF. The values that fitted on dictionary boundaries are depicted in red and the correctly fitted values are depicted in blue. A reference line is shown at a T2$_{water}$ of 30 ms and a unity line is shown for the fat fractions.*

Table 2. *The average T2$_{water}$ and fat fractions (+ standard deviations) for the four cohorts divided in healthy controls and patients. The results are shown for the one-component calibration (method A) and the two-component calibration (method C). Regions of interest included the entire muscle compartment without the bone and subcutaneous fat.*

Cohort		One-component calibration		Two-component calibration	
		Fat fraction	T2$_{water}$	Fat fraction	T2$_{water}$
1. DMD arm	Healthy controls	4.7 ± 1.7%	27.4 ± 1.0 ms	4.9 ± 1.7%	27.5 ± 1.0 ms
	DMD patients	55.8 ± 15.0%	19.6 ± 4.7 ms	62.0 ± 10.4%	24.0 ± 2.2 ms
2. DMD leg	Healthy controls	9.2 ± 3.7%	28.8 ± 0.6 ms	9.9 ± 3.0%	29.2 ± 0.6 ms
	DMD patients	39.0 ± 22.6%	25.5 ± 4.9 ms	41.4 ± 24.2%	28.8 ± 3.9 ms
3. BMD	Healthy controls	11.9 ± 2.5%	28.8 ± 0.7 ms	14.7 ± 9.1%	29.2 ± 0.7 ms
	BMD patients	29.1 ± 17.2%	27.0 ± 2.9 ms	30.1 ± 18.5%	27.8 ± 2.2 ms
4. SMA	Healthy controls	17.3 ± 7.2 %	28.5 ± 0.7 ms	18.1 ± 6.9%	29.2 ± 0.7 ms
	SMA patients	84.1 ± 19.4%	20.6 ± 4.2 ms	86.3 ± 24.7%	27.1 ± 3.4 ms

Experiment 2 – In vivo T2 estimation

The T2$_{water}$ values differed less than 1ms between method B and C for all patients (mean difference 0.7ms, p<0.001, paired t-test). Method B resulted in unphysiologically high T2$_{water}$ values of the fat component (above 35ms) in healthy controls, showing that this calibration method is less stable. Therefore method C was used to compare one-component versus two-component calibrations. The average T2$_{water}$ for healthy controls was comparable between these two methods of calibration. The T2$_{water}$ was 27.4 ms, 28.8 ms, 28.7 ms and 28.5 ms for the one-component calibration and 27.5 ms, 29.2 ms, 29.2 ms and 29.2 ms for the two-component calibration for cohort 1 until 4 respectively. For the patients, the T2$_{water}$ in the one-component calibration is lower (p<0.001, paired t-test) than the two-component calibration. The T2$_{water}$ was 19.6 ms, 25.5 ms, 26.6 ms and 20.6 ms for the one component calibration, and 24.0 ms, 28.8 ms, 27.7 ms and 27.1 ms for the two-component calibration, for cohort 1 to 4. The fat fractions were higher in patients than in healthy controls (table 2).

In figure 7 the relation between fat fraction and T2$_{water}$ is shown for each cohort and the three calibration methods. Using the one-component calibration method, with increasing fat fraction the T2$_{water}$ decreases for all cohorts. With the two-component calibrations, the negative correlation between T2$_{water}$ and fat fractions is reduced in cohorts 1 to 3 (DMD and BMD cohorts), especially in the fat fraction range < 50%, and absent in cohort 4 (SMA cohort).
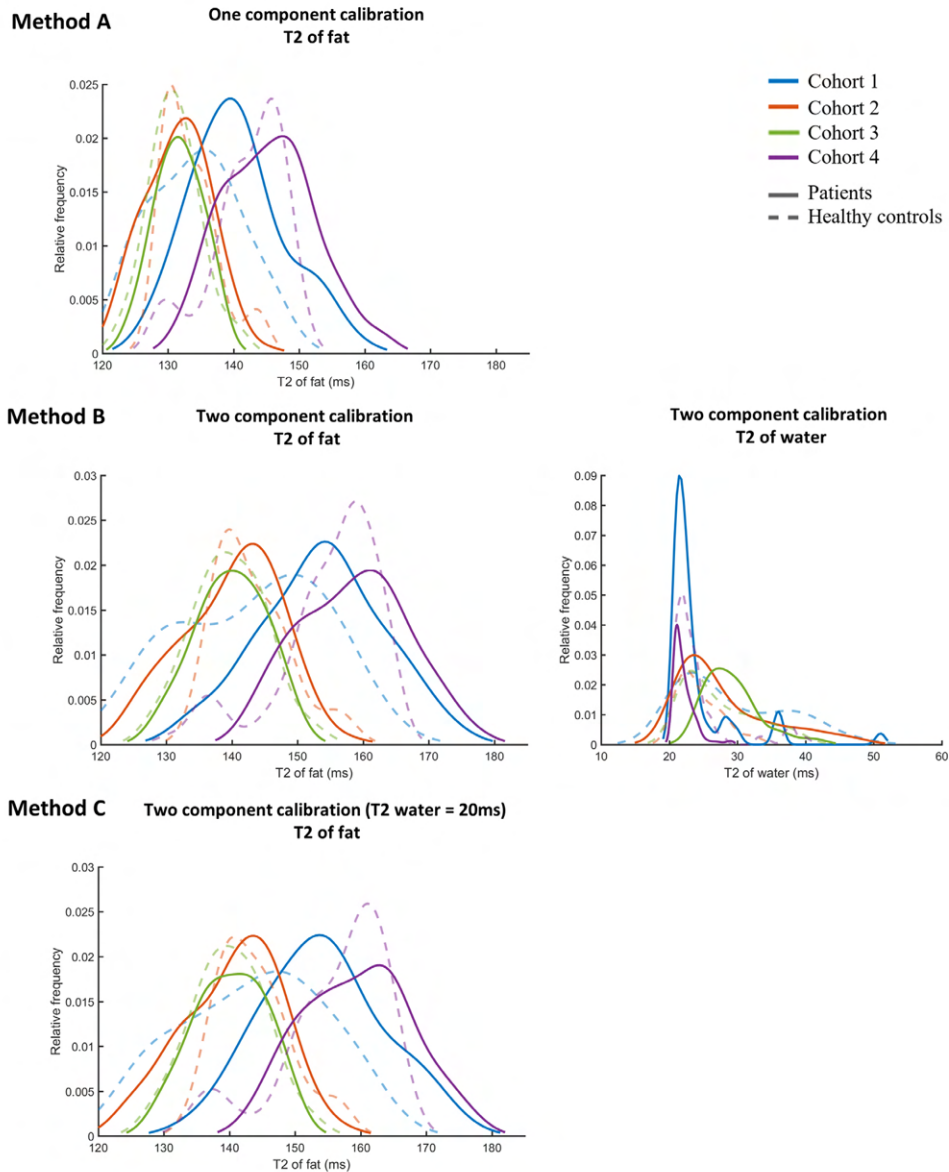
5

Figure 6. *Outcome of the calibration of the $T2_{fat}$ on subcutaneous fat for the methods A, B and C. The values for the patients in the cohorts are shown as a solid line and the values for the healthy controls are shown as a dashed line. Method A with one component calibration leads to a lower $T2_{fat}$ (137 ms, 132 ms, 131 ms, 144 ms, for cohort 1-4 respectively) than method B with two component calibration (149 ms, 141 ms, 140 ms, 158 ms, for cohort 1-4 respectively). The calibrated $T2_{fat}$ is comparable for method B without a fixed $T2_{water}$ and method C with a fixed $T2_{water}$ (150 ms, 142 ms, 140 ms, 159 ms, for cohort 1-4 respectively).*
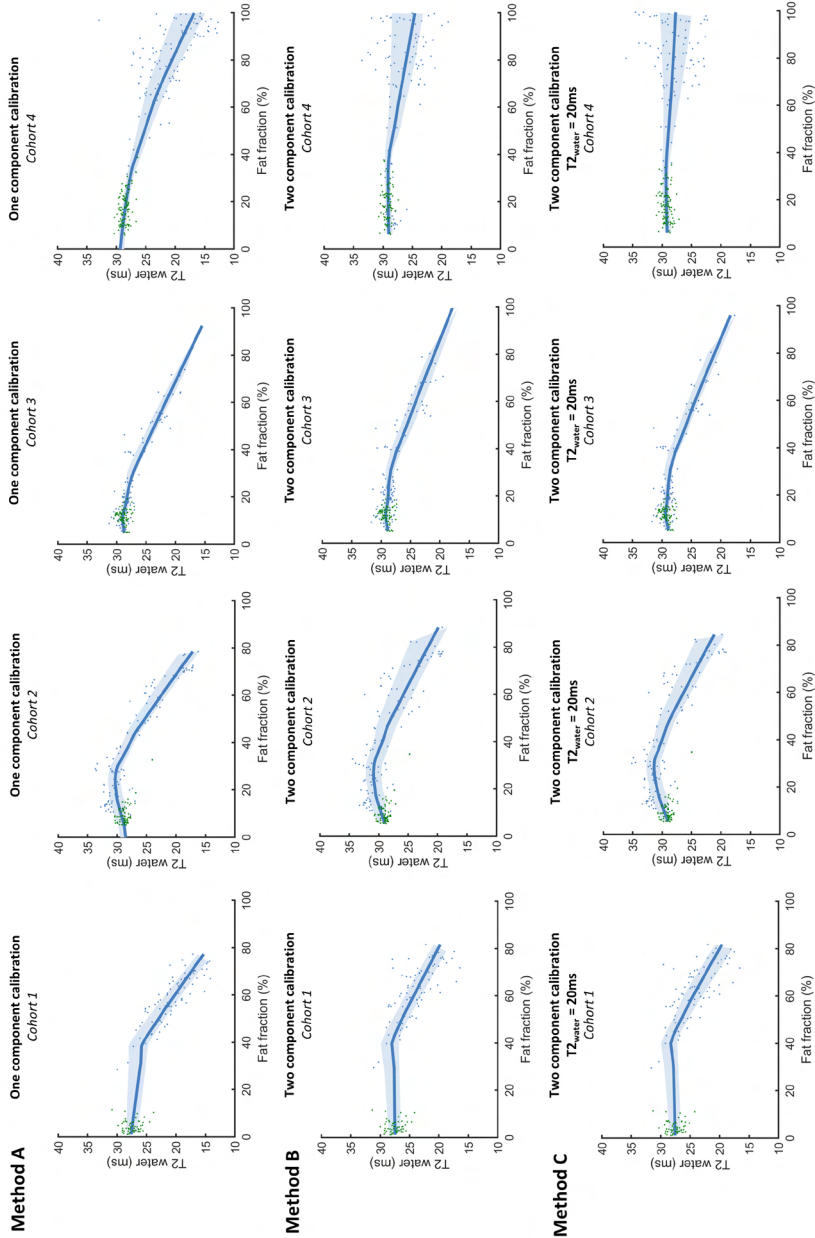
Figure 7. *The association between the fat fraction and the T2 of the water component in vivo in four cohorts (cohort 1-4 from left to right) for the two calibration methods A (top row), B (middle row) and C (bottom row). Healthy controls are depicted in green and patients in blue. Values are shown for each 5 slices per individual.*

DISCUSSION

Multi-echo spin-echo transverse relaxometry mapping using multi-component models are used to study disease activity in neuromuscular disease. Recently, an EPG model has been introduced to obtain separate T2 values for water and fat, accounting for B1 and stimulated echoes.[41] We improved this model and showed the importance of including slice flip angle profiles with a chemical shift displacement in the slice direction. Different calibration methods for the T2 of the fat component showed that the assumption of the T2 of the fat component has a large influence of the estimation of $T2_{water}$. Finally, we studied the performance of the model in four clinical cohorts, which showed a gradual decline in $T2_{water}$ for increasing fat fractions.

Our simulations showed that not including the flip angle slice profile introduced an overestimation of the $T2_{water}$ up to 10 ms and an underestimation of the fat fraction up to 20%. Accordingly, without accounting for the flip angle slice profile the calibrated $T2_{fat}$ is also overestimated. Including the flip angle profile also improved the stability of the fit in higher fat fractions, with fewer voxels reaching the dictionary boundaries. With better defined slice profiles, which can be obtained by increasing RF duration, this effect can likely be reduced. Additionally, simulations showed the importance of including the slice profile chemical shift in EPG simulations for the fat signal, when the gradient strength of the slice selection gradient differs for the excitation and refocusing pulse. The water fat shift in the slice-encoding direction is larger at high field, with thin slices and with large differences between the slice encoding gradients of the excitation and refocusing RF pulses. Including the flip angle profile and its chemical shift makes $T2_{water}$ values comparable between different sequences and different MRI systems, improving comparison between cohorts in literature and in multi-center trials. These simulations show that it is essential to be aware of the sequence used in clinical studies, especially in the context of multicenter studies where exact sequence parameters between MR systems and/or vendors are likely different.

The assumption of the T2 of the fat component has a large influence of the estimation of $T2_{water}$. Assuming one general $T2_{fat}$ without specific calibration is not recommended, since the T2 of the fat component can differ for different scanners and sequences due to J-coupling.[43] The $T2_{fat}$ can automatically be calibrated on the subcutaneous fat as a reference for fatty tissue. From in vivo studies[221] and Dixon scans of subcutaneous fat, we know that the fat fraction in subcutaneous fat is around 90%. Our simulations show that the $T2_{fat}$ is underestimated by approximately 10ms when using a one component model for fat calibration. Therefore, performing a two-component fit improves the accuracy of the estimated $T2_{fat}$ and therefore the accuracy of the estimated $T2_{water}$ and fat fraction.

In the in vivo data we studied, the calibrated $T2_{fat}$ differed between sequences, which could be explained by differences in scan and sequence parameters. The echo time, slice thickness and profiles all influence J-coupling of fat protons which might result in different apparent $T2_{fat}$ values. Additionally, between subjects within the same cohort there was a variation in the $T2_{fat}$, possibly reflecting differences in composition of subcutaneous fat between subjects and MRI acquisition parameters like B1. For cohort 1 with upper-arm scans of DMD patients and healthy controls, there was a difference in the calibrated $T2_{fat}$ between healthy controls and patients (figure 6). This can probably be attributed to partial volume effects, as the thickness of the subcutaneous fat is covered by a relatively sparse number of voxels in the arms due to the low resolution of these scans, and the subcutaneous fat in the arm only covered two to four voxels in most healthy controls. To allow accurate and robust calibration of $T2_{fat}$ it is essential that there are enough pure subcutaneous fat voxels, preferably equally distributed over slices and in regions with varying B1. As such, basing the calibration on a small manual region is not recommended.

The in vivo analyses of four cohorts, with healthy controls and patients with different neuromuscular diseases, was performed with two proposed calibration methods. Assuming the subcutaneous fat to be one component of only fat, we saw a gradual decline in the $T2_{water}$ with increasing fat fractions for all cohorts. Assuming subcutaneous fat to consist of 90% fat and 10% water, the decline in $T2_{water}$ for higher fat fractions decreased for DMD and BMD, and was even absent in the SMA cohort (cohort 4). The decrease of $T2_{water}$ with increase of fat fraction in our cohorts is consistent with the $T2_{water}$ measured with the gold standard spectroscopy in patients due to other neuromuscular disease with fatty replacement.[222] Spectroscopy based $T2_{water}$ measurements are typically performed using voxel localization containing both muscle and intramuscular fat. Therefore, similar to the model here, spectroscopy based $T2_{water}$ estimations are likely biased towards lower $T2_{water}$ as well, with increasing contributions of the water component of fat, which has a lower $T2_{water}$ compared to muscle.
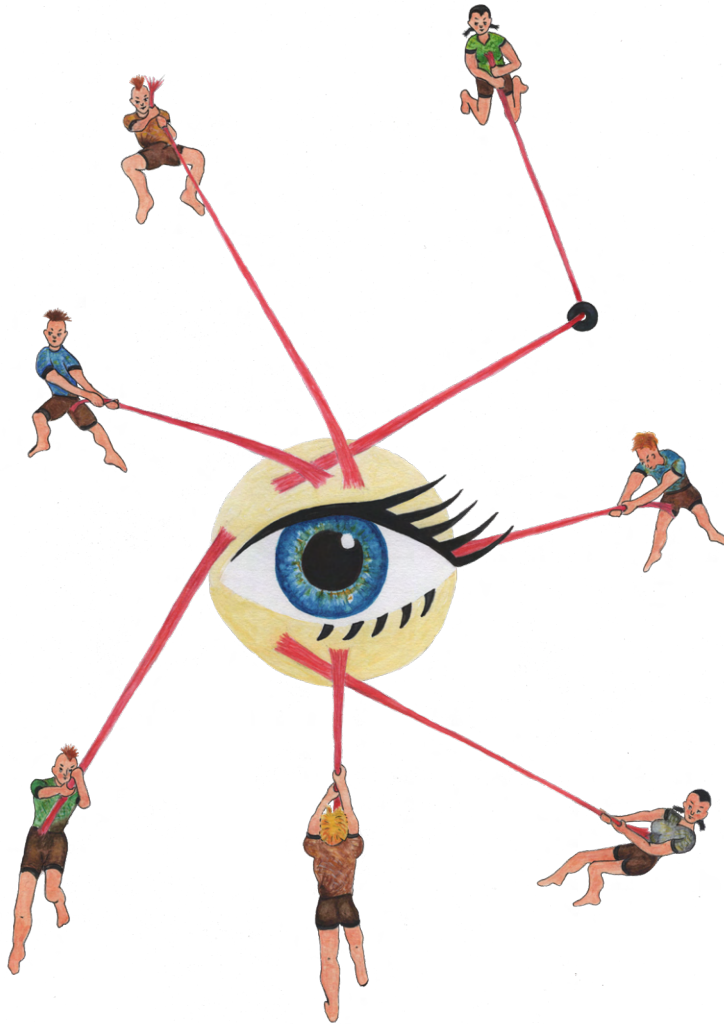
While the scope of this work was methodological optimization of multi-component MSE fitting, data from the two-component fitting method can be used to look at clinical differences (figure 7; method C). The dependence of $T2_{water}$ on the fat fraction was different in the SMA cohort compared to the DMD and BMD cohorts. This may be explained by differences in pathophysiology between SMA and dystrophinopathies (DMD/BMD). SMA is a disease characterized by muscle atrophy, presumably caused by the effects of denervation secondary to motor neuron degeneration, in addition to some fat replacement of muscle tissue.[223] In BMD and DMD pathophysiology is primarily characterized by replacement of muscle tissue by fat and endomysial fibrosis, of which the latter can reach up to 35% of muscle biopsy

areas in histological studies.[224] The $T2_{water}$ of fibrotic tissue is below 10 ms[39,225], possibly explaining the $T2_{water}$ decrease in severely affected DMD and BMD individuals with high amounts of fat replacement. Alternatively, susceptibility differences between muscle water and fat and have also been mentioned as explanations.[222] However, to fully explain this difference further work is needed.

There are some limitations of the used model. We assumed that the fat in tissue contributes to the signal as one mono-exponential component. However, fat contains several components with different relaxation times and J-coupling interactions.[43] These J-coupling effects influence the signal in a complex matter by stimulated echoes, possibly causing the relaxation to deviate from pure mono-exponential behavior. Furthermore, we assume a fixed water fraction in the fat calibration, and for fitting stability for this fraction we fixed the T2 relaxation of this water component to 20 ms. The assumption of a fixed $T2_{water}$ for the water component in fat resulted in the most stable fit for all investigated cohorts, even though the calibration method with a two-component calibration in fat shows a 0.7ms difference in $T2_{water}$. In addition, in our final recommended model (C) the assumptions of ~10% fat contribution and a water T2 in fat of ~20 ms are supported by previous work.[221,226] In future work in different cohorts, the $T2_{water}$ of the fat component could be included in the fit and the stability of that model could be studied. Additionally, for the calibration of $T2_{fat}$, we assume that the fatty replacement in muscle tissue has the same composition and relaxation parameters as subcutaneous fat. However, differences exist in the composition of different fat tissues.[216] More research is needed to quantify the composition of fat that infiltrates the muscle in neuromuscular diseases to mitigate potential biases due to these assumptions.

To conclude, we recommend using an EPG based model for fitting $T2_{water}$ from the MSE signal with calibration of $T2_{fat}$ assuming two components. Moreover, we recommend including the slice flip angle profile in the model which includes chemical shift displacements. In vivo data showed a gradual decline in $T2_{water}$ for increasing fat fractions, with important implications for clinical studies using $T2_{water}$ as an outcome parameter. Using these recommendations, $T2_{water}$ measurements will be more reliable and will allow for better comparison of values between centers and diseases.

5

1. CJ Gorter center for high field MRI, Department of Radiology, Leiden University Medical Center, Leiden, Netherlands
2. Department of Neurology, Leiden University Medical Center, Leiden, Netherlands
3. Department of Ophthalmology, Leiden University Medical Center, Leiden, Netherlands
4. Duchenne Center Netherlands

The feasibility of quantitative MRI of extra-ocular muscles in myasthenia gravis and Graves' orbitopathy

Kevin R. Keene[1,2] | Luc van Vught[1,3] | Nienke M. van de Velde[2] | Isabeau A. Ciggaar[1,3]
Irene C. Notting[3] | Stijn W. Genders[3] | Jan J.G.M Verschuuren[2,4] | Martijn R. Tannemaat[2]
Hermien E. Kan[1,4] | Jan-Willem M. Beenakker[1,3]

ABSTRACT

Introduction

While quantitative MRI could be instrumental in diagnosis and assessment of disease progression in orbital diseases involving the extra-ocular muscles (EOMs), acquisition can be challenging as EOM are small and prone to eye-motion artefacts. We explored the feasibility of assessing fat fractions (FF), muscle volumes and water T2 (T2$_{water}$) of EOM in healthy controls (HC), myasthenia gravis (MG) and Graves' orbitopathy (GO) patients.

Methods

FF, EOM volumes and T2$_{water}$ values were determined in twelve HC (age 22-65 years), eleven MG (28-71 years) and six GO patients (28-64 years) at 7Tesla using Dixon and multi-echo-spin-echo sequences. The EOM were semi-automatically 3D-segmented by two independent observers. MANOVA and t-tests were used to assess differences in FF, T2$_{water}$ and volume of EOM between groups ($p<0.05$). Bland-Altman limits of agreement (LoA) was used to asses reproducibility of segmentations and Dixon scans.

Results

The scans were well tolerated by all subjects. The bias in FF between the repeated Dixon scans was -0.7% (LoA: ±2.1%), for the different observers, the bias in FF was -0.3% (LoA: ±2.8%) and 0.03cm^3 (LoA: ± 0.36cm^3) for volume. Mean FF of EOM in MG (14.1±1.6%) was higher than in HC (10.4±2.5%). Mean muscle volume was higher in GO (1.2±0.4cm^3) and MG (0.8±0.2cm^3) compared to HC (0.6±0.2cm^3). The average T2$_{water}$ for all EOM was 24.6ms±4.0ms for HC, 24.0ms±4.7ms for MG patients and 27.4ms±4.2ms for the GO patient.

Discussion

Quantitative MRI at 7 Tesla is feasible for measuring FF and muscle volumes of EOM in HC, MG and GO patients. The measured T2$_{water}$ was on average comparable to skeletal muscle, although with higher variation between subjects. The increased FF in the EOM in MG patients suggests that EOM involvement in MG is accompanied by fat replacement. The unexpected EOM volume increase in MG may provide novel insights in underlying pathophysiological processes.

INTRODUCTION

In diseases that involve the extra-ocular muscles (EOM), local muscle weakness or muscle swelling results in complaints such as double vision and ptosis. The auto-immune disease myasthenia gravis (MG) is characterized by fatigable muscles. Auto-antibodies, targeting the acetylcholine receptor (AChR) or muscle specific tyrosine kinase (MuSK), disturb transmission at the neuromuscular junction. In 85% of patients, MG starts with diplopia and ptosis, which are both caused by EOM weakness.[1,227] Currently, MG is diagnosed by either the presence of autoantibodies in serum, or abnormal findings during neurophysiological testing.[5] However, in patients with pure ocular symptoms, the sensitivity of these tests is low (0.44 for testing antibodies, 0.34 for repetitive nerve stimulation and variable between 0.66 and 0.98 for single-fiber EMG).[10] As a result, the diagnosis remains a challenge and there is a need for more sensitive diagnostic tests.[2] Moreover, there is a need for prognostic markers to predict disease progression in ocular MG[228] and refractory MG[8].

Graves' orbitopathy (GO) is an orbital disease caused by auto-antibodies against thyroid proteins, including the thyroid-stimulating hormone receptor (TSH-R).[51,229,230] Due to inflammation and swelling of the EOM, symptoms of GO include upper eyelid retraction, proptosis and diplopia.[65] At a later stage of the disease, fibrosis appears in the EOM as a result of the longstanding inflammation. There is an unmet clinical need to categorize patients, since immunosuppressant medication and radiotherapy are only effective in the active stage of GO.[144]

Quantitative MRI can be used to assess disease progression and to study pathophysiology of skeletal muscle in neuromuscular disease, by assessing fat replacement, muscle size and T2 relaxation time changes.[36] Assessment of such structural changes in individual EOM by quantitative MRI may therefore also contribute to understanding the pathophysiology and pattern of muscle involvement of the EOM in orbital disease.[87,231] As such, it could contribute to identifying diagnostically challenging subgroups in GO and aid in the follow-up of therapeutic response in MG.

In the current work we explored the feasibility and value of quantitative MRI of the EOM in MG and GO patients and healthy controls. These specific patients groups were chosen because distinct structural changes are expected in both diseases and additional diagnostic tests could directly improve clinical care. In MG there is histological evidence for fat replacement, fibrosis and atrophy of the EOM[125], while in GO the EOM are known to be swollen and inflamed at an early stage, and fat-replaced and fibrotic at a later stage of the disease[232]. However, the EOM are challenging to assess with quantitative MRI. Since they are small, the

6

high resolution needed for MRI of these muscles results in a poor signal-to-noise ratio. In addition, MRI of the EOM is prone to eye-motion artefacts, which reduce the image quality. Moreover, the surrounding bone from the orbit and air from the nasal sinuses lead to an inhomogeneous B0 field. However, recent studies have shown that the increased signal to noise ratio at 7 Tesla, combined with a cued blinking paradigm to reduce eye-motion artefacts and localized shimming to minimize B0 artefacts, enable high resolution imaging of the eyes.[46] [45] Based on these protocols we therefore developed a dedicated protocol for anatomical and functional imaging of the EOM.

METHODS

Participants
All patients were recruited from the outpatient clinics of the neurology and the ophthalmology departments. The diagnosis of MG was confirmed by a neurologist, based on a combination of clinically confirmed fluctuating muscle weakness and the presence of AChR antibodies or abnormal decrement by repetitive nerve stimulation. The diagnosis of GO was confirmed by an ophthalmologist, based on the presence of the characteristic orbital abnormalities (eyelid retraction, redness/swelling of the eyelids/conjunctiva and enlarged EOM or orbital fat) and the presence of anti-TSH-R antibodies. For MG and GO patients, both acute (diagnosis less than 3 months ago) and chronic (diagnosis more than 1 year ago) stages of the disease were included, to assess a wide variety of structural changes to study the sensitivity of the dedicated MRI protocol. Healthy controls were recruited from the Radiology database for healthy controls.

The local medical ethics committee approved the study and all study participants gave written informed consent prior to MR-scanning.

MR examination
We performed chemical shift based water fat separation using the Dixon method to quantify fat replacement and muscle volume and Multi echo Spin-echo (MSE) to assess the T2 relaxation time of water ($T2_{water}$), as an indicator of disease activity[203]. All subjects were scanned in supine position on a 7T Philips Achieva MRI (Philips Healthcare, Best, The Netherlands) using a cued-blinking paradigm[3] with the upper 16 elements of a 32-channel head-coil (Nova Medical). Patients were asked to blink on visual cues provided on a screen; the MRI acquisition was halted during blinking. A 3-point multi-acquisition 3D Dixon scan was acquired (resolution: 0.8x0.8x0.8mm³, first time to echo (TE)/ΔTE/repetition time (TR)/flip-angle (FA)/scan time:2.4ms/0.33ms/10ms/3°/3:50min). The 3D volumetric Dixon scan

was planned with the frequency encoding in the left-right direction and was angulated in the coronal plane if needed, to include both orbits in the field of view. In a subset of seven MG patients and five healthy controls, a second Dixon scan was acquired (resolution: 0.7x1.0x0.7 mm³, first TE/ ΔTE/TR/FA/scan time:2.4ms/0.33ms/10ms/3°/3:50min) to study the value of a higher resolution in the coronal plane, while maintaining the same voxel-volume. These Dixon scans with a higher resolution in the coronal plane were used to study the reproducibility of the fat fraction (FF) measurement, by comparing them to the isotopic Dixon scan. In another subset of participants, containing five MG patients, one GO patient and seven healthy controls, a MSE scan was acquired per orbit (resolution: 1.2x1.2x3.0mm³, first TE/ΔTE/TR: 12ms/12ms/4000ms, 24 echo's, 3 slices per eye, scan time: 2:44min). This coronal scan was planned with one orbit ins the field of view perpendicular to the medial and lateral rectus muscle. The scan times were kept under four minutes, as previous experience shows this minimizes movement artefacts. Higher order shimming was performed for all scans, to minimize the susceptibility artefacts caused by the bony structures of the orbit and the nasal cavities.

Data analysis and segmentation

Dixon scans were reconstructed with seven-peak reconstruction using the manufacturer's software to yield water and fat images. No T2* correction was performed, given the short echo spacing of 0.33ms. To minimize eye movement artefacts, the scan time was minimized by using a relatively low TR of 10ms. A correction for the resulting T1-weighting in the water and fat images, was incorporated in the FF calculation, assuming T1 values of 1400ms (correction factor: 1.22) and 365ms (correction factor: 1.08) for water and fat respectively[233]:

$$\text{Fat fraction} = \frac{1.08 * \text{Fat}}{1.22 * \text{Water} + 1.08 * \text{Fat}}$$

Scans were excluded if there were obvious motion artifacts. For the Dixon scans, the four rectus EOM (lateral rectus muscle, medial rectus muscle, inferior rectus muscle and the superior rectus and levator palpebrae muscle complex) were semi-automatically 3D-segmented on the water image, using a seed-growing algorithm with a manually set threshold for each subject in ITK-SNAP[234] (Figure 1) by one observer (KK). After automatic segmentation, the regions of interest were manually corrected to remove blood vessels, regions of orbital fat and regions of other eye muscles. The superior rectus muscle was segmented together with the levator palpebrae muscle as one complex, as their proximity hindered accurate separation in some cases. The segmentation was eroded with one acquisition voxel to account for partial volume effects in the FF calculation. To assess the segmentation reproducibility, an independent physician (NvdV) repeated the segmentation process for the muscles of the right eye of all subjects. The average FFs of the EOM were

determined using an in-house developed Matlab script (Matlab 2016a, The Mathworks of Natick, Massachusetts, USA) by averaging the voxels in the regions of interest after exclusion of the eroded voxels and correction of the water-fat-shift between the fat and water image. The EOM volumes were determined by multiplying the number of voxels in the uneroded region of interest with the voxel volume. The used Matlab scripts and one example dataset presented in this article will be made available at the request of a qualified investigator. Requests should be made to K. R. Keene (k.r.keene@lumc.nl).

The MSE scans were analyzed using a two-component Extended Phase Graphs (EPG) model, consisting of a water and a fat component, as described before.[235] In this model the main scan parameters, such as flip angle and slice profile, were incorporated and the same fixed T1 for the water and fat compartment was used as described above for T1 correction of the Dixon scans. The difference in water-fat shift in the slice direction between the excitation and refocusing pulses, due to different slice selection gradients for both pulses, was also incorporated in the model. This is especially important at high field strengths, as the shift scales linearly with the magnetic field strength and is 1.2mm for the performed MSE scan. A dictionary matching algorithm was used to obtain the T2 of the water component, the B1 map and FF, for each voxel.[41,211] This dictionary was created using $T2_{water}$ values from 10ms to 60ms, $T2_{fat}$ values from 120ms to 200ms, FF values from 0% to 100% and B1 values from 50% to 140%. To obtain a $T2_{fat}$ value for the match, the $T2_{fat}$ is conventionally calibrated on the subcutaneous fat, assuming it consists only of fat tissue and it has a similar T2 as the
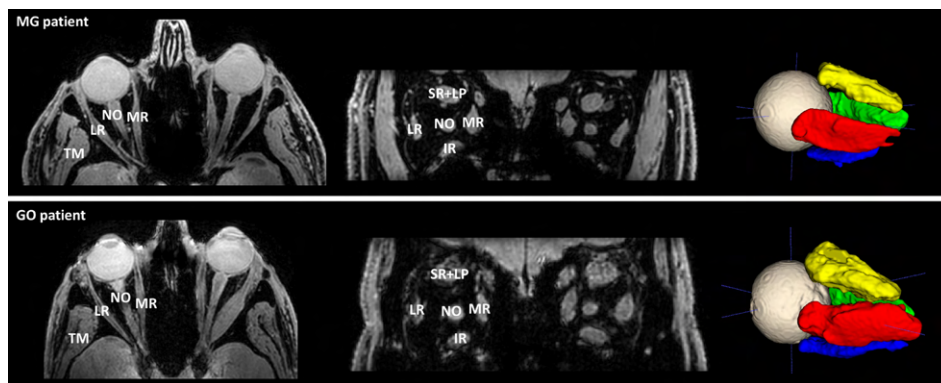

Figure 1. *Transverse slice and a coronal slice of the Dixon water image (left) depicting a myasthenia gravis (MG) patient (top) and Graves' orbitopathy (GO) patient (bottom), showing the lateral rectus muscle (LR), the medial rectus muscle (MR), the inferior rectus muscle (IR) and the superior rectus and levator palpebrae muscle complex (SR+LP). The temporalis muscle (TM) and the optic nerve (NO) are also labeled in the figures. On the right, the 3D regions of interest are shown after automatic segmentation using ITK-SNAP. Notice the enlarged extra-ocular muscles in the GO patient.*

fat replacement in skeletal muscles.[207] However, in this work the $T2_{fat}$ was calibrated on the orbital fat, since subcutaneous fat was not present in the field of view. For the MSE scans, the EOM were segmented by drawing regions of interest per slice using the FF map as an anatomical reference by one observer (KK).

Statistics

The Bland-Altman bias and limits of agreement between the FFs of the two Dixon scans were calculated for all participants together, and separately for the healthy controls and MG patients. The FFs and muscle volumes from the segmentation performed by the two independent observers were compared using Bland-Altman analysis. Mean FF and muscle volumes were compared using MANOVA with post-hoc tests with Bonferroni multiple-testing correction on the patient average and on the individual muscles after averaging the EOM of the left and right eye per patient. Mean $T2_{water}$ values were compared using a two-tailed t-test between healthy controls and MG patients, but not for the GO patient, since only one observation was present. The correlation between age and FF was tested using Pearson correlations for all three groups separately. The correlation between FF and volume was tested for healthy controls for all EOM. Significance level for all tests was set at 0.05.

RESULTS

Subject characteristics

Twelve healthy subjects (41.0±15.9 years, 42% male), eleven MG patients (52.5±15.9 years, 64% male) and six GO patients with active disease (47.7±14.0 years, 50% male, clinical activity score[236] ≥ 3) were included in this pilot study (table 1).

Data quality

All scans but one Dixon scan with higher resolution in the coronal plane from an MG patient were free from visible motion artefacts. This scan was excluded from the analysis. Reconstructed water, FF and $T2_{water}$ maps and the first and last echo of the MSE scan are shown in figure 2.

Agreement on semi-automatic segmentation

The EOM were semi-automatically segmented by two independent observers separately. Figure 3 shows Bland-Altman plots depicting the bias and limits of agreement between the two independent observers for FF (A) and volume (B). The mean bias and limits of agreement in FFs and volume were respectively -0.3% [95% confidence interval(95%CI): -3.1%; 2.6%] and 0.03cm³ [95%CI: -0.33cm³; 0.39cm³].

Table 1. *Baseline characteristics of the three groups*

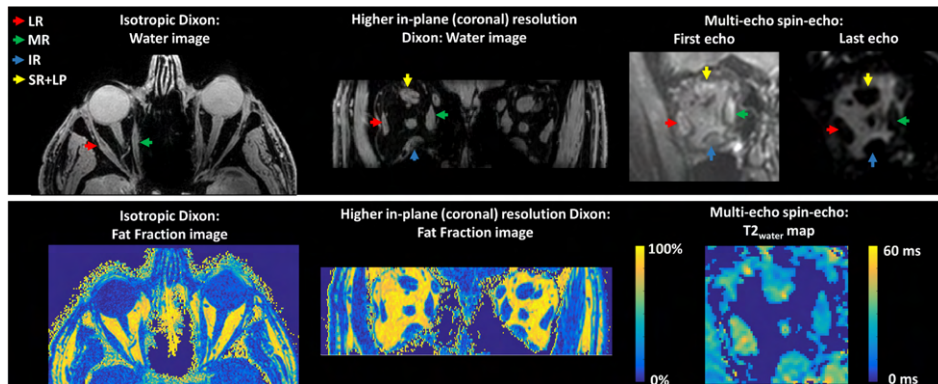|	Healthy controls N = 12	Myasthenia gravis N = 11	Graves' orbitopathy N = 6
Age, y	*41.0 ± 15.9*	*52.5 ± 15.9*	*46.7 ± 14.0*
Gender			
Male	*5 (42%)*	*7 (64%)*	*3 (50%)*
Female	*7 (58%)*	*4 (36%)*	*3 (50%)*
Disease onset			
< 3 months	*-*	*5 (45%)*	*3 (50%)*
> 1 year	*-*	*6 (55%)*	*3 (50%)*
Medication			
Pyridostigmine	*-*	*10 (91%)*	*-*
Prednisone	*-*	*6 (55%)*	*2 (33%)*
Other immunosuppressants	*-*	*1 (9%)*	*-*
MG phenotype			
Ocular	*-*	*7 (64%)*	*-*
Generalized	*-*	*4 (36%)*	*-*
Anti-TSH-R antibodies	*-*	*-*	*6 (100%)*
Anti-AChR antibodies	*-*	*10 (91%)*	*-*

Figure 2. *Examples of water images and fat fraction maps of the isotopic Dixon scan and the Dixon scan with a higher resolution in the coronal plane on the left. On the right the first echo, the last echo and the T2$_{water}$ map are shown for the multi-echo spin-echo scan. The colored arrows point out the lateral rectus muscle (LR; red), the medial rectus muscle (MR; green), the inferior rectus muscle (IR; blue) and the superior rectus and levator palpebrae muscle complex (SR+LP; yellow).*
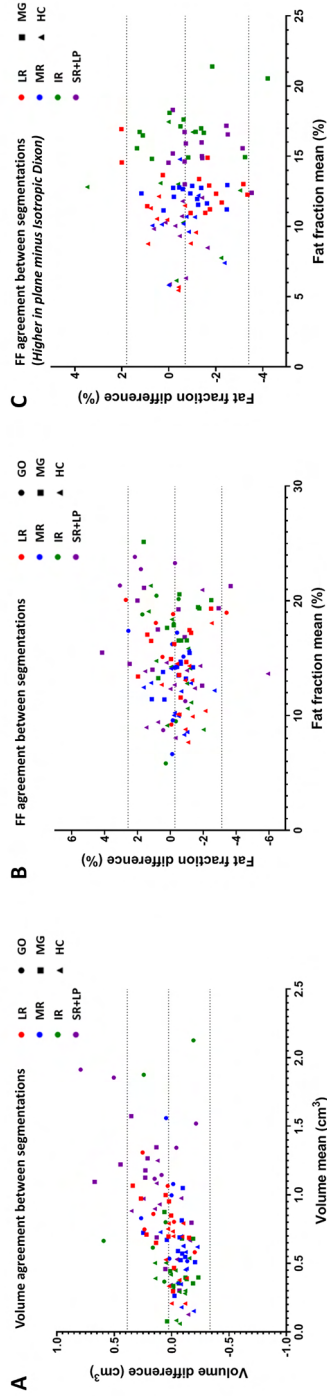
Figure 3. *Bland-Altman plots depicting the agreement between two independent observers who separately semi-automatically segmented the extra-ocular muscles of the right orbits. The four extra-ocular muscles are shown in separate colors: the lateral rectus (LR) muscle, the medial rectus muscle (MR), the inferior rectus muscle (LR) and the superior rectus and levator palpebrae muscle complex (SR+LP). Groups are shown in different shapes: Graves' ophthalmopathy patients (GO), myasthenia gravis patients (MG) and healthy controls (HC). Figure A shows the agreement in muscle volume (bias: 0.03cm³ [limits of agreement: -0.33cm³- 0.39cm³]). Figure B shows the agreement in fat fractions (bias: -0.3% [limits of agreement: -3.1% - 2.6%]). Figure C shown the agreement between the isotropic Dixon scan and the scan with a higher resolution in the coronal plane (bias: 0.7% [limits of agreement: -3.4%; 1.8%]).*

6

Reproducibility of fat fraction measurement by Dixon scans

In one patient the second Dixon scan was excluded from the analysis due to severe motion artefacts. On visual inspection, the isotropic Dixon scan was of higher quality compared to the Dixon scan with a higher resolution in the coronal plane. The gain of resolution in the coronal plane was accompanied with a loss of resolution in the transversal plane to maintain sufficient SNR and therefore unwanted partial volume effects were present. The Bland-Altman bias and limits of agreement between the two Dixon scans were -0.7% [95%CI: -3.4%; 1.8%] for all participants, with the Dixon scan with a higher resolution in the coronal plane giving on average lower FFs. In the MG patient group the bias and limits of agreement were -1.0% [95% CI: -3.7%; 1.7%], and in healthy controls the level of agreement was -0.4% [95% CI: -2.6%; 1.7%] (figure 3C).

Muscle volume

The mean muscle volumes of the four recti muscles were higher in GO patients ($1.2\pm0.4cm^3$) than in healthy controls ($0.6\pm0.2cm^3$; p<0.001) (figure 4). The mean EOM volume was also higher in MG patients ($0.8\pm0.2cm^3$) than in healthy controls (p=0.007). Assessing all four muscles separately, the volumes of all four rectus EOM differed significantly between GO patients and healthy controls (lateral rectus muscle: p=0.033, medial rectus muscle: p=0.001, inferior rectus muscle: p<0.001 and superior rectus and levator palpebrae muscle complex: p=0.001). No significant differences were observed comparing individual EOM between healthy controls and MG patients. A difference between GO and MG patients was present in the medial rectus muscle (p=0.035) and the inferior rectus muscle (p=0.001) (figure 5).

Fat fractions

The mean FFs of the EOM where higher in MG patients ($14.1\pm1.6\%$) compared to those of healthy controls ($10.4\pm2.5\%$; p=0.008) (figure 6) and similar between MG and GO patients ($13.9\pm4.4\%$). The variability in FFs appeared higher in GO patients than in MG patients and healthy controls. When analyzed individually, all four rectus EOM differed between MG patients and healthy controls (lateral rectus muscle: p=0.011, medial rectus muscle: p=0.048, inferior rectus muscle: p<0.033 and superior rectus and levator palpebrae muscle complex: p=0.003). A difference between healthy controls and GO patients was observed in the lateral rectus muscle (p=0.029) and the superior rectus and levator palpebrae muscle complex (p=0.003) (figure 7). For each group, Pearson correlations did not indicate a relation between the FF and age (r=0.006 and p=0.86 for healthy controls, r=-0.21 and p=0.69 for GO patients and r=0.31 and p=0.38 for MG patients). In healthy controls no dependence of FF on volume was observed (slope: $-2.1 \%/cm^3$ [95%CI: -4.3 to 0.1], r=0.19 and p=0.06).
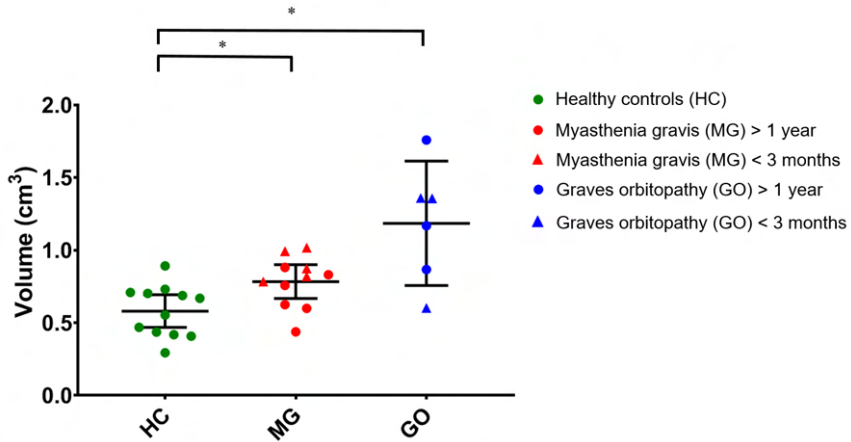
Figure 4. *Mean muscle volumes of the four recti muscles per subject. Data are shown as mean and standard deviation for healthy controls (green), myasthenia gravis (MG) (red) and Graves' orbitopathy (GO) patients (blue). The mean volume was 0.6±0.2cm³ in healthy controls, 0.8±0.2cm³ in MG patients and 1.2±0.4cm³ in GO patients. The MG and GO patients had a significantly higher muscle volume compared to muscle controls (p=0.007 and p<0.001 respectively). Statistical significance is indicated by asterisks.*
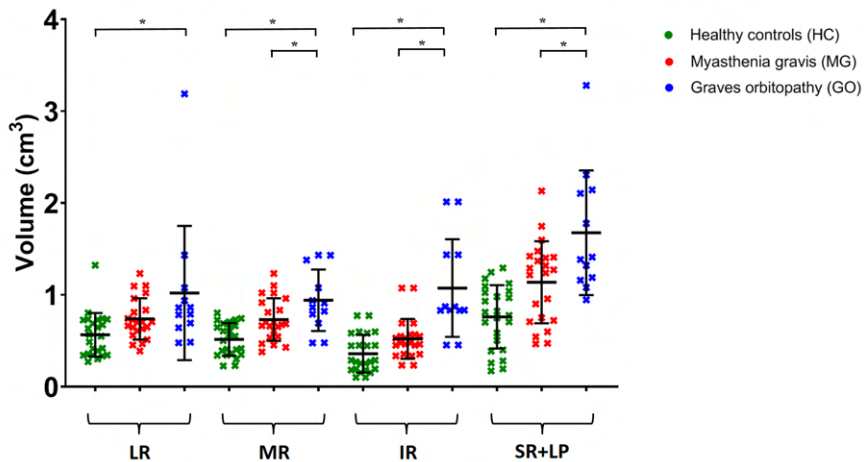

Figure 5. *Muscle volumes for individual extra-ocular muscles of both eyes are shown as mean and standard deviation for healthy controls (green), Myasthenia gravis (MG) (red) and Graves' orbitopathy (GO) patients (blue). All four rectus EOM differed significantly between GO patients and healthy controls (lateral rectus muscle (LR): p=0.033, medial rectus muscle (MR): p=0.001, inferior rectus muscle (IR): p<0.001 and superior rectus and levator palpebrae muscle complex (SR+LP): p=0.001, left and right averaged). The difference between GO and MG patients was present in the medial rectus muscle (p=0.035) and the inferior rectus muscle (p=0.001). Statistical significance is indicated by asterisks.*
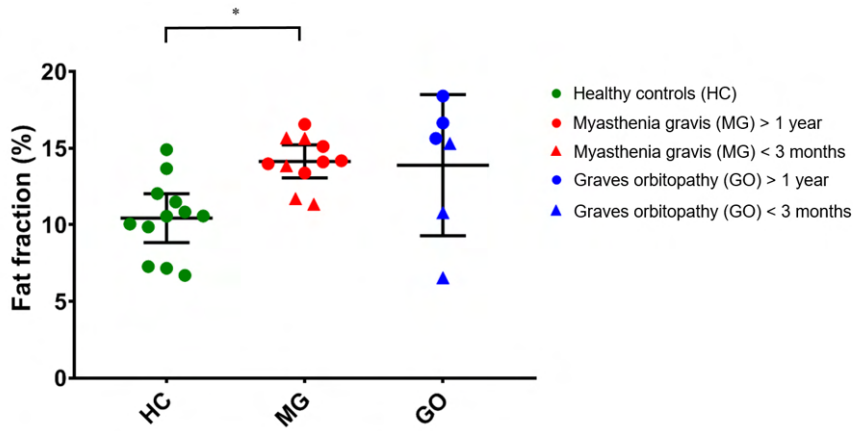
Figure 6. *Mean muscle fat fractions of the four recti muscles per subject, divided per group. Data are shown as mean and standard deviation for healthy controls (green), Myasthenia gravis (MG) (red) and Graves' orbitopathy (GO) patients (blue). The mean fat fraction was 10.4±2.5% in healthy controls, 14.1±1.6% in MG patients and 13.9±4.4% in GO patients. MG patients had a significantly higher fat fraction compared to controls (p = 0.008). Notable is the high variability between muscles in the GO patient group. Statistical significance is indicated by asterisks.*

Figure 7. *Fat fractions of individual extra-ocular muscle of both eyes are shown as mean and standard deviation for healthy controls (green), myasthenia gravis (MG) (red) and Graves' orbitopathy (GO) patients (blue). All four rectus EOM differed significantly between MG patients and healthy controls (lateral rectus muscle (LR): p=0.011, medial rectus muscle (MR): p=0.048, inferior rectus muscle (IR): p<0.033 and superior rectus and levator palpebrae muscle complex (SR+LP): p=0.003, left and right averaged). The difference between healthy controls and GO patients was present in the lateral rectus muscle (p=0.029) and the superior rectus muscle (p=0.003). Statistical significance is indicated by asterisks.*

Water T2

The average T2$_{water}$ for all EOM was 24.6±4.0ms for the healthy controls, 24.0±4.7ms for the MG patients and 27.4±4.2ms for the GO patient. No significant differences between healthy controls and MG patients were found. T2$_{water}$ values for individual EOM are depicted in figure 8.
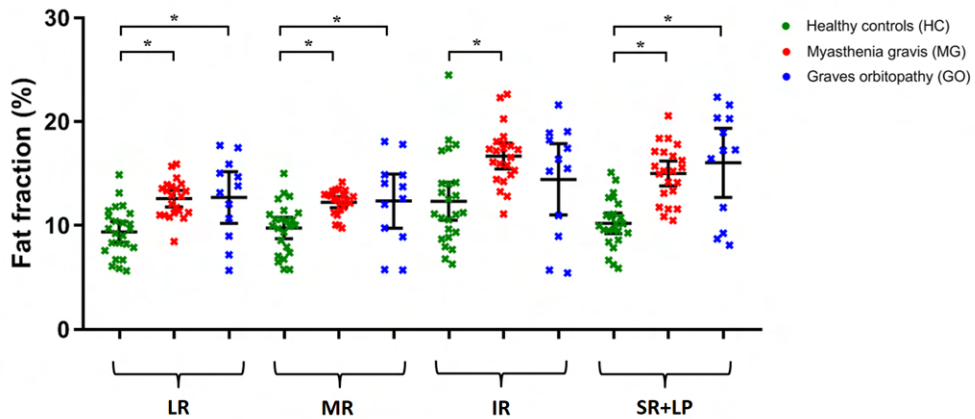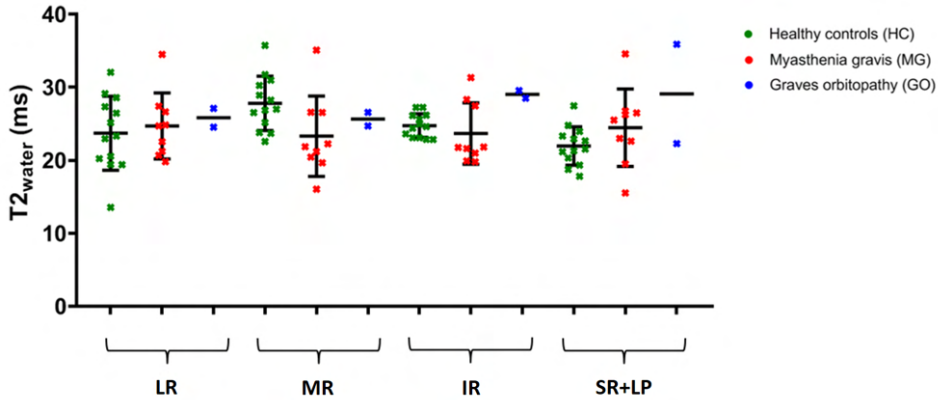

Figure 8. *T2$_{water}$ values of individual extra-ocular muscle of both eyes are shown as mean and standard deviation for healthy controls (green), Myasthenia gravis (MG) (red) and Graves' orbitopathy (GO) patients (blue). For one healthy control and one MG patient, only the EOM from one eye are included. The average T2$_{water}$ for all EOM was 24.6±4.0 ms for the healthy controls, 24.0±4.7 ms for the MG patients and 27.4±4.1 ms for the GO patient.*

DISCUSSION

The present work aimed to study the feasibility of quantitative MRI of EOM in diseases that affect the eye muscles. We showed that the EOM could be reproducibly semi-automatically segmented with a small inter-observer variation and that FFs could be reproducibly measured in healthy controls and MG and GO patients between different scans. With that, we were able to detect small differences in muscle volume and FF between healthy controls and two patient cohorts, as well as T2$_{water}$ values similar to spectroscopy measured values in skeletal muscles, but small differences cannot be excluded as the study was not powered to detect these.

All scans but one were free from visible motion artefacts, indicating that all subjects could adhere to the protocol. The mean bias in FF between the segmentations of two independent observers was low (0.3%) and the limits of agreement were below ±3% in FF, which is in the same range as previously reported values in segmentation of the vastus lateralis in patients with Duchenne muscular dystrophy (bias: 0.1%, limits of agreement: ±1.1%)[38], in healthy

controls and patients with diabetes type 2 in all leg muscle compartments (bias: -0.2, limits of agreement: ±2.6%)[237] and in patients with myotonic dystrophy type 1 in lower leg muscles (limits of agreement: ±2.5%)[238]. The scan-to-scan reproducibility between the two Dixon scans with different resolutions showed a low average bias in FF (-0.7%) and narrow limits of agreement (-3.4% to 1.8%), which is lower than the difference found between the patients and the controls (i.e ~4%), indicating the feasibility of assessing FFs using this method to detect affected muscles. For comparison, Dixon measurements in skeletal muscles have been reported to have a reproducibility (limits of agreements) of ±1% for water-fat phantoms[239], ±1.1% for thigh muscles in healthy controls[240] and ±2.5% for the leg muscles in patients with Duchenne muscular dystrophy.[200] These techniques could be used in future longitudinal studies to study the disease progression in conditions affecting the EOM and to relate time varying clinical observations such as painful eyes to the current condition of the EOM in terms of fat replacement and inflammation.

We found FFs of approximately 10% in the EOM, which is higher than the 2-5% commonly observed in skeletal muscles in healthy volunteers.[240–242] Although the high FF could be an intrinsic property of EOM, this could also be the result of noise bias. Earlier studies in skeletal muscles have shown that low SNR could result in an overestimation of the FF in the low FF ranges.[243] Although the strong contrast between the orbital fat and the muscles and globe, suggests more than sufficient SNR for anatomical evaluation of the images, some noise can be observed in the temporal muscle, a large skeletal muscle close to the orbit. In a representative healthy subject, this temporal muscle also showed a relatively high FF of 9.3% (data not shown). A Dixon-reconstruction of fourfold down-sampled source images of the same subject, which increased the SNR twofold, resulted in a reduction in FF from 9.3% to 5.1% was observed, showing that the used protocol is susceptible to noise bias in the low FF ranges. This could explain the relatively high FF observed in the EOM. We therefore recommend that future studies use a higher SNR for the Dixon acquisition, for example by using a higher flip angle or a two flip angle approach.[243] Additionally, the overestimation of the FF could have been caused by partial volume effects of the EOM with the surrounding orbital fat, due to the small size of these muscles (~ 1cm^3).

Muscle volumes were measured using 3D segmentation on the water image from the Dixon scans. The limits of agreement for the muscle volumes segmented by the two independent observers ranged between -0.33cm^3 and 0.39cm^3. These limits do not reach the 0.6cm^3 difference observed between GO patients and healthy controls, but are higher than the difference of 0.2cm^3 observed between the MG patients and healthy controls. On visual inspection (figure 3), the highest differences between observers were found in the superior rectus and levator palpebrae muscle complex, which is the hardest to delineate, because the

complex contains two separate muscles. An overall dependence of volume difference between observers on mean volume was observed (figure 3A), but there was virtually no mean bias (0.03cm³). Moreover, as no dependence of FF on the volume was present in healthy controls, the segmentation was not likely to have influenced the observed FF differences between groups.

Using MSE and EPG analysis, we found T2 values of the myocytic compartment ($T2_{water}$) for EOM to be comparable to the $T2_{water}$ in healthy skeletal muscle, as measured with MR spectroscopy.[39,222,244] The standard deviation of $T2_{water}$ between the EOM (4.0ms, 4.7ms and 4.2ms for respectively healthy controls, MG patients and GO patients) was higher than previously measured using an EPG model in leg muscles between subjects (1.4ms-2.1ms)[41,241]. This variation between $T2_{water}$ of muscles could be expected in the patients as different patients have a different pattern of muscle involvement. In GO, for example the inferior rectus muscle is usually affected earlier in the disease, followed later by the other EOM.[87] In the healthy controls, however, a smaller variation, comparable to other skeletal muscles, was expected. Two assumptions in the analysis may have contributed to this higher variation. Firstly, the calibration of the $T2_{fat}$ was performed on the orbital fat, under the assumption that its composition is similar to intra-muscular fat[216]. Orbital fat is, however, known to be involved in inflammatory conditions, such as GO.[245] This variation in orbital fat T2, which is not necessarily also present in the T2 of the intra-muscular fat, might result in an erroneous variation in intra-muscular $T2_{fat}$. Secondly, our model assumes that the ROI to calibrate the $T2_{fat}$ only contains orbital fat. However, in reality there is vascularization in the orbital fat which will result in a small, patient-specific, inaccuracy in the measured orbital $T2_{fat}$, which will subsequently influence the obtained $T2_{water}$. A high variation between individual EOM in patients is to be expected, as MG and GO are known to selectively affect specific EOM.[78,90] Due to the high variation, the power was limited to detect mean differences in $T2_{water}$ between groups. For future studies, we recommend establishing baseline values per EOM and use Z-scores to detect EOM with an abnormal $T2_{water}$.

Although the patient cohorts were small, clear differences were found between cohorts. The measured FFs of the EOM were higher in MG and GO patients compared to healthy controls and muscle volumes were higher in GO patients. Edematous EOM are a common finding in GO patients[65] and fat replacement of EOM has been described in late-stage GO patients[51]. The variability in muscle volume was high in GO patients, possibly due to the inclusion of patients with varying disease severity and the inflammation of only a portion of the EOM in individual patients.

6

The increase in FF in the EOM in MG has been described in histological studies[125], but the increase in muscle volume in the EOM of MG patients was unexpected. In MG, AChR or MuSK antibodies can result in structural damage of the muscle membrane at the neuromuscular synapse, which is usually located at the middle of the muscle fiber, but this is not a dystrophic process.[2] In dystrophic muscle diseases fat replacement of muscle tissue is commonly observed, and can almost completely replace normal muscle tissue.[37,246] In neuropathic diseases, like hereditary motor and sensory neuropathy (HMSN) or hereditary neuropathy with liability to pressure palsies, FFs have been observed up to 15% in calf muscle[124]. Which is a relatively small increase (up to 10%) in FF, comparable to the small increase in FF (up to 8%) that we observed in the EOM in MG. In a recent case report, histological findings in a seronegative MG patient also included adipocyte replacement of muscle fiber,[247] and fat replacement has been seen in bulbar muscles of MuSK positive MG patients.[18] Our results agree with these observations, and indicate that involvement of EOM in MG patients is accompanied by fat replacement. Interestingly, our results so far suggest that FFs of MG patients with a disease onset less than three months before the scan did not appear to differ from chronic MG patients.

Severe MG can induce chronic denervation and therefore might behave as a neuropathic condition. Muscular atrophy in skeletal muscle is observed in 10% of AChR+ MG patients with long-standing disease.[20] In MuSK+ MG patients early atrophy is seen in the bulbar muscles.[18,19,248] In other neurogenic muscle diseases, like HMSN, also a decrease in muscle volume has been observed.[124] However, in this work we observed an increase in EOM volume in MG patients, which is not consistent with the expected atrophy. This unexpected increase in muscle volume raises questions about its pathophysiology. Firstly, it is possible that inflammatory processes in the EOM result in swollen muscles. In MG, complement activation is observed, resulting in activation of the membrane attack complex and destruction of the neuromuscular endplate.[249] To what extent this inflammatory process affects the EOM is unknown. Secondly, (pseudo)hypertrophy may be an explanation of the increase in EOM volume, which had been observed in some muscular dystrophies.[250]

A limitation of this work was that the groups in this pilot study were not fully age matched, as the maximum age of healthy volunteers was limited to 65 years, based on the inclusion criteria of our IRB approval. This upper age limit did not apply to both patient groups. However, an earlier study showed that the EOM do not change in muscle thickness, size and fatty tissue volume between age groups.[251] In addition, when analysing all three groups in this study separately, we did not see any age effects on EOM FFs. Therefore, age does not appear to be a major confounder in our study. Secondly, due to the exploratory nature of this pilot study with ongoing sequence development, not all sequences were applied to all patients.

As a result, the second Dixon scan for reproducibility and the MSE sequence was only performed in a subgroup of patients, and the T2 relaxometry only to one GO patient. Lastly, this study was performed on a 7 Tesla MR-scanner to increase the SNR at the high resolution required for imaging the EOM.[46] However, downsides of scanning at 7 Tesla are the increase in susceptibility differences, B0 inhomogeneities and chemical shift artefacts. These challenges were successfully solved using higher order shimming and the in-plane chemical shift displacement was set at 1.0 acquisition pixels and corrected for in postprocessing. Future studies can determine if these same results can be achieved at clinical field strengths, such as 3 Tesla.

In conclusion, despite the challenges of size and movement, quantitative MRI is feasible for measuring FFs and muscle volumes of individual EOM in healthy controls, MG and GO patients at 7 Tesla. We measured water T2 relaxation times comparable to values measured in skeletal muscle, but found a high variability between individuals and between different EOM. Detection of group differences for this parameter will therefore only be possible when large differences between groups are present, only affected EOM are included in the analyses, or when using large sample sizes. We found an increase in EOM volume and FF in MG and GO patients. The unexpected increase in EOM volume in MG may provide novel insights in underlying pathophysiological processes. The diagnostic value of these findings and their value in the follow-up of disease progression should be the subject of future prospective studies.

6

1. CJ Gorter MRI center, Department of Radiology, Leiden University Medical Center, Leiden, Netherlands
2. Department of Neurology, Leiden University Medical Center, Leiden, Netherlands
3. Department of Ophthalmology, Leiden University Medical Center, Leiden, Netherlands
4. Department of Neurology, Radboud University Medical Center, Nijmegen, Netherlands
5. The Rotterdam Eye Hospital, Rotterdam, Netherlands
6. Department of Radiation Oncology, Leiden University Medical Center, Leiden, Netherlands
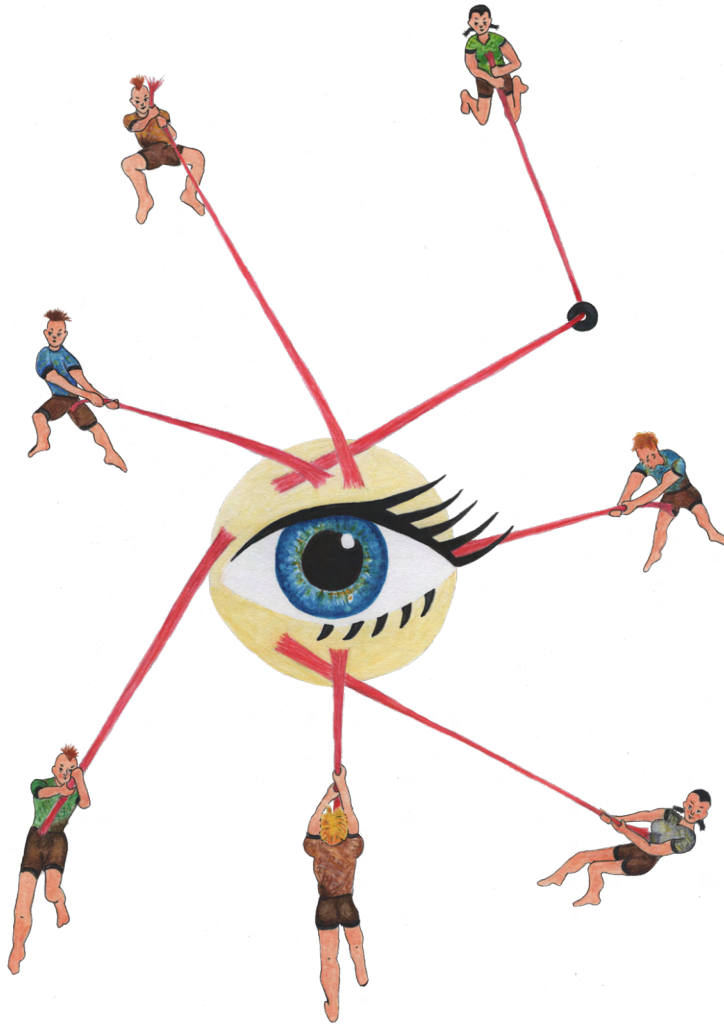
Eye muscle MRI in myasthenia gravis and other neuromuscular disorders

Kevin R. Keene [1,2] | Irene C. Notting[3] | Jan J.G.M Verschuuren[2]
Nicol Voermans[4] | Ronald O.B. de Keizer[5] | Jan-Willem M. Beenakker[1,3,6]
Martijn R.Tannemaat[2] | Hermien E. Kan[1]

ABSTRACT

Introduction
MRI of extra-ocular muscles (EOM) in patients with myasthenia gravis (MG) could aid in diagnosis and provide insights in therapy-resistant ophthalmoplegia. We used quantitative MRI to study the EOM in MG, healthy and disease controls, including Graves' ophthalmopathy (GO), oculopharyngeal muscular dystrophy (OPMD) and chronic progressive external ophthalmoplegia (CPEO).

Methods
Twenty recently diagnosed MG (59±19yrs), nineteen chronic MG (51±16yrs), fourteen seronegative MG (57±9yrs) and sixteen healthy controls (54±13yrs) were included. Six CPEO (49±14yrs), OPMD (62±10yrs) and GO patients (44±12yrs) served as disease controls. We quantified muscle fat fraction (FF), $T2_{water}$ and volume. Eye ductions and gaze deviations were assessed by synoptophore and Hess-charting.

Results
Chronic, but not recent onset, MG patients showed volume increases (e.g. superior rectus and levator palpebrae [SR+LPS] 985±155mm^3 compared to 884±269mm^3 for healthy controls, p<0.05). As expected, in CPEO volume was decreased (e.g. SR+LPS 602±193mm^3, p<0.0001), and in GO volume was increased (e.g. SR+LPS 1419±457mm^3, p<0.0001). FF was increased in chronic MG (e.g. medial rectus increased 0.017, p<0.05). In CPEO and OPMD the FF was more severely increased. The severity of ophthalmoplegia did not correlate with EOM volume in MG, but did in CPEO and OPMD. No differences in $T2_{water}$ were found.

Interpretation
We observed small increases in EOM volume and FF in chronic MG compared to healthy controls. Surprisingly, we found no atrophy in MG, even in patients with long-term ophthalmoplegia. This implies that even long-term ophthalmoplegia in MG does not lead to secondary structural myopathic changes precluding functional recovery.

INTRODUCTION

Myasthenia gravis (MG) is a muscle disease characterized by fluctuating and fatigable muscle weakness. MG is caused by auto-antibodies targeting proteins at the neuromuscular junction, including the acetylcholine receptor (AChR), muscle-specific tyrosine kinase (MuSK) or LRP4.[2,3] Most patients experience ocular symptoms like diplopia and ptosis during the course of their disease.[1,44] Both the diagnosis of ocular MG and the treatment of refractory ocular symptoms are major challenges in MG. In half of the ocular MG patients, no serum auto-antibodies against AChR, MuSK or LRP4 are found. Moreover, the sensitivity of repetitive nerve stimulation is low in ocular MG, and while single-fiber EMG has a higher sensitivity, it requires a specifically trained neurophysiologist to perform the measurement and is thus operator-dependent. [2,3,10] Ocular MG can therefore pose a significant diagnostic challenge.[4,252] Furthermore, in some MG patients a therapeutic resistant ophthalmoparesis develops and little is known about its pathophysiology.

MRI of the extra-ocular muscles (EOM) can be used to directly assess structural changes in the EOM, and can therefore be of significance both for diagnostics in seronegative MG and for understanding the pathophysiology of therapy-resistant ophthalmoplegic MG. In skeletal muscles, quantitative MRI is widely used to study fat replacement, muscle size and T2 relaxation time changes.[36] Recently, we showed that quantitative MRI of individual EOM (lateral rectus[LR], medial rectus[MR], inferior rectus[IR] and superior rectus[SR]) and the levator palpebrae superioris muscle (LPS) in a small group of MG patients was feasible. [99] Diagnostically, MRI of the EOM is rarely performed in MG and little is known how structural EOM changes in MG relate to changes observed in other ocular diseases. For example, in Graves' orbitopathy (GO), characteristic fusiform swelling of the EOM and adipogenesis in the EOM are observed on MRI, and volume correlates with disease stage. [91] Furthermore, in chronic progressive external ophthalmoplegia (CPEO) EOM are atrophic and EOM volume correlates with maximal range of eye movements.[93]

MRI could also aid in understanding therapy resistant ophthalmoplegia in MG. Several case reports[13–16] and a study with a larger cohort[17] suggest that untreated MG and MuSK MG patients can have EOM atrophy. Atrophy is therefore a proposed mechanism of refractory ophthalmoplegia in MG.[3,9,11,125] As such, studying to what extent atrophy occurs in the EOM, and what the influence of treatment is, could aid in pathophysiological understanding. Additionally, by correlating EOM function to structural changes with orthoptic tests, the influence of atrophy on function can directly be assessed. We have previously shown that orthoptic tests are sensitive to ' MG related EOM weakness.[253]

7

We hypothesize that in MG structural changes are present in the EOM. In the current study, we first aimed to identify structural EOM differences in a large group of MG patients using quantitative MRI parameters to aid in diagnostics. Secondly, we aimed to identify structural changes in EOM that could explain refractory ophthalmoplegia in ocular MG. To this end, untreated recently diagnosed, treated chronic and seronegative MG patients were included. Finally, we studied correlations between orthoptics and quantitative MRI parameters to determine whether structural changes were related to functional deficits.

METHODS

Participants

We included a convenience sample of MG, GO, CPEO and OPMD patients from the Neurology Department and the Ophthalmology Department of the LUMC, Radboud university and the Rotterdam Eye Hospital as described before. Given logistics and the COVID-19 pandemic including a consecutive sample of patients was not possible, however we asked patients as consecutively as possible. Age matched healthy controls were recruited using flyers and posters and by sending letters asking patients' relatives. Detailed data from the orthoptic tests have been reported separately.[253]

Three groups of autoimmune MG patients were included: recently diagnosed, chronic and seronegative. The diagnosis in chronic and recently diagnosed MG patients was based on the combination of typical muscle weakness and the presence of serum autoantibodies to AChR.[2–4] Seronegative myasthenia gravis (SNMG) was defined as clinically confirmed fluctuating muscle weakness in combination with abnormal decrement during repetitive nerve stimulation (RNS), increased jitter during single fiber EMG testing or a positive response to an acetylcholinesterase inhibitor, together with absence of AChR or muscle-specific kinase (MuSK) serum autoantibodies.[4] In recently diagnosed MG patients the diagnosis, as described above, was established less than a year ago and they were not treated with systemic immunosuppressants. Chronic MG patients received their diagnosis more than a year ago and no selection was made based on previous treatments. SNMG patients were selected regardless the disease duration or corticosteroid use in the past. We also included three other disease groups with EOM involvement: GO, CPEO and OPMD, and a group of healthy age and sex-matched controls. The diagnosis of GO was defined as the presence of TSH-receptor serum autoantibodies with presence of ocular symptoms.[144] The diagnosis of CPEO was confirmed by genetic testing or with skeletal muscle biopsy[52] and the diagnosis of OPMD was confirmed with genetic testing of the PABPN1 gene.[171] Participants with a history of strabismus were excluded. Patients with a simultaneous diagnosis of MG and GO were excluded. None of MG and none of GO patients had received orbital surgery or radiotherapy.

Two of the CPEO and one of the OPMD patients had surgery involving the levator palpebrae to correct their ptosis.

For the MG patients a quantitative myasthenia gravis (QMG) score [23,24] and a myasthenia gravis activities of daily living (MG-ADL) scale[22] were recorded.

Standard protocol approvals, registrations, and patient consents
The Medical Ethics Review Committee Leiden Den Haag Delft approved the study and its use of human subjects. All patients provided informed, written consent prior to study participation.

MR examination
All subjects were scanned in supine position on 7T Philips Achieva MRI (Philips Healthcare, Best, The Netherlands) with the upper 16 elements of a 32-channel head-coil (Nova Medical). Using cued-blinking[45] the MRI acquisitions were halted periodically, and patients were visually instructed to blink. Scan-times were kept short, under 4 minutes, to reduce movement artefacts.[126] We performed a chemical shift based water fat separation gradient echo scan (from now on referred to as Dixon scan) to quantify muscle fat fraction and muscle volume[99] and Multi echo Spin-echo (MSE) to assess the T2 relaxation time of water ($T2_{water}$), as an indicator of disease activity[41,235].

Volumes and fat fractions: Dixon scan
MR acquisition
A 3-point multi-acquisition 3D Dixon scan was acquired (resolution: $0.8x0.8x0.8mm^3$, first time to echo (TE)/ΔTE/repetition time (TR)/flip-angle (FA)/scan time:2.4ms/0.33ms/8ms/7°/3:50min). DREAM B1 maps were acquired for the last 5 participants (3 slices, $1.2x1.2x3.0mm^3$).[254]

Postprocessing
The real and imaginary echo data from the Dixon scan were used to reconstruct water and fat images using Iterative decomposition of water and fat (IDEAL) using an in-house developed Matlab script (Matlab 2016a, The Mathworks of Natick, Massachusetts, USA; https://git.lumc.nl/neuroscience/StandardizedDixonPipeline), without B0 field smoothing, T2* corrections or region growing algorithms.[37]

Segmentation
The EOM were semi-automatically segmented on the water image in 3D using the seed growing algorithm of ITK-SNAP[234], which is possible given the distinct contrast between the

EOM and the intra-orbital fat. After seed growing, possible intra-orbital arteries, veins and nerves were manually removed from the 3D volume of interest. The SR was segmented together with the levator palpebrae given the difficulty of segmenting them separately. This muscle complex is referred to as the *superior rectus plus levator palpebrae superioris* (SR+LPS). All segmentations were done by the same observer (KK).

Analysis

The water and fat images were used to calculate fat fraction maps. Corrections for T1 weighting were applied to the fat fractions per voxel for the Dixon scan using the Ernst angle equation using an effective flip angle and the repetition time of 8ms.[233] As the B1 varies spatially, an EOM-specific effective flip angle of the 7 degree pulse was calculated based on the B1 measurements obtained in 5 participants. To this end, all eight recti EOM were segmented manually on the middle slice of the B1 map and EOM specific values were calculated by averaging the voxels in the regions of interest.

$T2_{water}$: Multi-echo spin-echo (MSE) scans
MR acquisition

A MSE scan was acquired per orbit (resolution: $1.2 \times 1.2 \times 3.0mm^3$, first TE/$\Delta$TE/TR: 9ms/9ms/4000ms, 24 echo's, 3 slices per eye, scan time: 2:44min, slice selection gradient strength: excitation 3.15 mT/m and refocusing 3.78 mT/m). This scan was planned with one orbit in the field of view perpendicular to the MR and LR muscles. In the $T2_{water}$ analysis of skeletal muscle, the subcutaneous fat that is present in the field of view is conventionally used to calibrate the T2 of the fat compartment ($T2_{fat}$). However, no subcutaneous fat is present in the field of view in the acquired orbital scans. Therefore, for calibration of the $T2_{fat}$ an additional MSE neck scan was acquired and $T2_{fat}$ was calibrated on subcutaneous fat of the neck. In the last three echoes of both acquisitions, the RF-pulses were disabled.

Postprocessing

The MSE scans were analyzed using a two-component Extended Phase Graphs (EPG) model, consisting of a water and a fat component, as described before with corrections for the flip-angle slice profile[235]. The T2 of the fat compartment was calibrated on subcutaneous fat of the neck. The dictionary used for fitting contained $T2_{water}$ values from 10ms to 60ms, $T2_{fat}$ values from 120ms to 200ms and B1 values from 50% to 100%. Water, fat, fat fraction, $T2_{water}$ and residual maps were exported. An in-house developed Matlab script was used to perform this dictionary fitting(https://git.lumc.nl/neuroscience/multicomponent_t2_epg).

Segmentation

The EOM were segmented by drawing regions of interest polygons per slice using the water map as an anatomical reference by one observer (KK).

Analysis

The EOM specific T2$_{water}$ values were calculated by averaging the voxels in the regions of interest for all slices after erosion of one voxel.

Orthoptic measurements

Measurements

Duction angles were defined as the range of motion of the eye in degrees in all eight cardinal gaze directions (horizontal, vertical and diagonal). In this study, unilateral duction angles were determined using the synoptophore (Clement Clarke International, 2002, Edinburgh way, Harlow, Essex). Elevation/depression was measured up to +/- 30° and abduction/adduction was measured up to +/- 40°. Gaze deviations between eyes were measured using standard Hess-chart examination.[35] Both measurements were performed by a single not masked observer (KRK). To recapitulate, the synoptophore measures limited ductions for one eye at the time, while the Hess-chart examination is based on the testing of deviations between both eyes in different gaze directions. The orthoptic studies were performed contiguous with the MRI on the same day. Given logistic problems patients were asked but not obliged to refrain from pyridostigmine use. The patients who used pyridostigmine generally took it in the morning at home before travelling to the hospital, they were then scanned at noon and the orthoptic evaluation was contiguous at one o'clock. Therefore in most patients the pyridostigmine effect was worn out before testing. However we did not structurally record the times.

Analysis

The EOM of MG patients were divided in 'affected' and 'not affected' for both orthoptic tests: A group of EOM with and without any duction limitations and a group of EOM with or without deviations above 5 degrees on the Hess-chart. The cut-off point of 5 degrees is commonly used in orthoptic clinical practice. The duction limitation or Hess-chart deviation in the primary direction of action of specific EOM was used (e.g. abduction for the LR and adduction for the MR). Additionally, we defined the severity of ophthalmoplegia per patient as the sum of duction limitations in all directions for both angles. This sum-score was used to study correlations between EOM volume and the severity of ophthalmoplegia.

Statistical Analysis

EOM specific values were compared between disease groups and myasthenia groups using repeated measures ANOVA defining laterality (left and right eye) as a repeated measure to assess differences between all groups that could be used to aid in diagnostics. Post-hoc testing was performed using Dunnett's multiple comparisons test. For the second aim, correlation within and between quantitative MRI measures and the continuous variables age

7

and duction limitations were analyzed using Pearson correlations. For age and functional correlation the EOM measures were combined and volume was normalized to the mean of the healthy control per individual EOM, to correct for anatomical differences in size between different EOM (e.g., the SR+LPS is on average bigger than the LR). For volume, fat fraction and $T2_{water}$ the amount of patients with zero, one or more than one muscle higher or lower than 2 standard deviations (SD) above and below the mean of healthy controls were calculated. Statistical analysis was performed with SPSS version 23 (IBM Corp, Armonk, NY) and p values below 0.05 were considered significant.

Data availability
The authors confirm that the data supporting the findings of this study are available within the article and its supplementary material (supplementary table 1). This data is made available strictly for academic usage and not for commercial purposes.

RESULTS

Examples of axial and coronal orbital water images from Dixon scans are shown in figure 1A for a healthy control and in figure 1C for CPEO, GO, a recent MG and a chronic MG patient. An example of fat replacement in an OPMD patient is shown in figure 1B.

Participant characteristics
We included 16 healthy controls, 20 recently diagnosed MG patients, 19 chronic MG patients, 14 SNMG patients, 6 CPEO patients, 6 OPMD patients and 6 GO patients. MRI data could not be acquired in four participants due to claustrophobic symptoms before scanning and in two participants due to a faulty amplifier resulting in poor scan quality. These six patients (three seronegative MG, one recent MG, one chronic MG and one GO patient) were excluded from the analyses. In four MG patients no neck reference MSE scan was obtained due to time constraints, therefore these patients were excluded from the $T2_{water}$ analysis. Demographic and clinical baseline characteristics of all participants are shown in table 1. No significant differences were found between the baseline characteristics sex and age between all groups.

Muscle volumes differ between disease groups
Volume differences were observed between disease groups (table 2). No volume differences were observed between the combined MG patient cohort and healthy controls in all recti EOM. For example, the volume for the LR was 728.1 ± 116.8 mm³ in healthy controls and 751.2 ± 159.6 mm³ in MG (figure 2A) and the volume for the SR+LPS was 883.8 ± 268.5 mm³ in healthy controls and 984.7 ± 153.7 mm³ in MG (figure 3A). Differences were observed
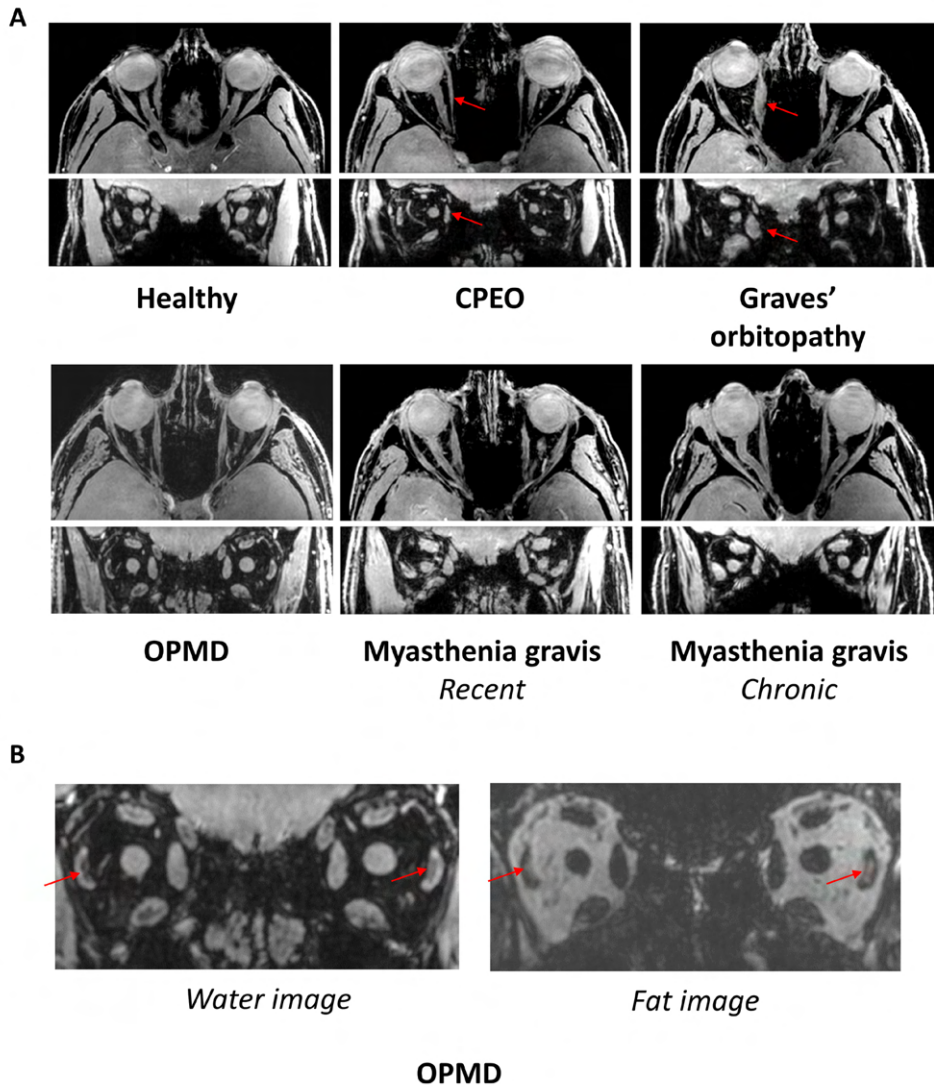
Figure 1. A. *MRI scans from the orbit showing the extra-ocular muscles in a healthy control, a chronic progressive external orbitopathy (CPEO) patient, a Graves' orbitopathy patient, an oculopharyngeal muscular dystrophy (OPMD) patient, a recent myasthenia gravis patient and a chronic myasthenia gravis patient. The axial and coronal water images are shown from a chemical shift based water-fat separation gradient echo scan, a technique to separately image and quantify water and fat. The red arrows indicate the atrophic medial rectus muscle in the CPEO patient and the swollen medial rectus muscle in the Graves' orbitopathy patient.* **B.** *Example of fat replacement of the lateral rectus muscles in an OPMD patient as depicted by the red arrows. On the left the coronal water image and on the right the coronal fat image are shown.*

Table 1. Baseline characteristics and sum-scores of 87 participants included in this study: 16 healthy controls, 20 recently diagnosed myasthenia gravis (MG) patients, 19 chronic MG patients, 14 seronegative MG (SNMG) patients, 6 chronic progressive external ophthalmoplegia (CPEO) patients, 6 oculopharyngeal muscular dystrophy (OPMD) patients and 6 Graves' orbitopathy (GO) patients. Data are presented as number of patients (%) for categorical variables and as mean ± SD for continuous variables. Synoptophore abnormalities is defined as having limited duction angles in any direction in one or both eyes. Hess-chart abnormalities is defined as having gaze deviations between the eyes above 5 degrees in any direction.

	MG Recently diagnosed	MG Chronic	MG Seronegative	CPEO	OPMD	GO	Healthy controls	p-value
	n=20	n=19	n=14	n=6	n=6	n=6	n=16	
Age (yrs)	59±19	51±16	57±9	49±14	62±10	44±12	54±13	0.243
Sex								0.754
Female	7 (35%)	9 (47%)	7 (50%)	3 (50%)	4 (67%)	4 (67%)	9 (56%)	
Male	13 (65%)	10 (53%)	7 (50%)	3 (50%)	2 (33%)	2 (33%)	7 (44%)	
Phenotype								0.105
Ocular	12 (60%)	6 (32%)	9 (64%)	-	-	-	-	
Generalized	8 (40%)	13 (68%)	5 (36%)	-	-	-	-	
Disease duration (months)	4.0±2.2	75.6±87.9	25.6±60.5	-	-	22.8±35.9*	-	<0.0001
MG-ADL	5.8±3.3	5.5±4.2	5.0±2.7	-	-	-	-	0.791
MG-ADL (ocular items)	2.8±1.1	1.7±0.8	2.9±1.2	-	-	-	-	0.165
QMG	9.2±6.0	9.8±7.7	8.3±4.6	-	-	-	-	0.812
QMG (ocular items)	2.2±0.7	1.2±0.7	2.5±1.0	-	-	-	-	0.365
Pyridostigmine on study day	25%	15%	14%	-	-	-	-	0.680
Hess-chart abnormalities	15	15	11	6	5	5	0	
Synoptophore abnormalities	9	10	7	6	5	1	0	
Ptosis at visit	10	5	5	5	5	0	0	

* Two Graves' orbitopathy patients were diagnosed > one year ago and four patients < one year ago.

between MG patients and CPEO (p<0.0001), OPMD (p<0.05) and GO (p<0.0001) patients in the SR+LPS (figure 3A). The LR volume was different between MG and CPEO (p<0.0001) and GO (p<0.05, figure 2A). The MR volume differed between MG and CPEO (<0.01) and the IR volume between MG and GO (p<0.0001). When looking at the subgroups of MG patients, volume was increased in chronic MG patients as compared to healthy controls in the SR+LPS (p<0.05 figure 4) and the IR (p<0.05). Volume was not different in recently diagnosed and seronegative MG patients for all EOM.
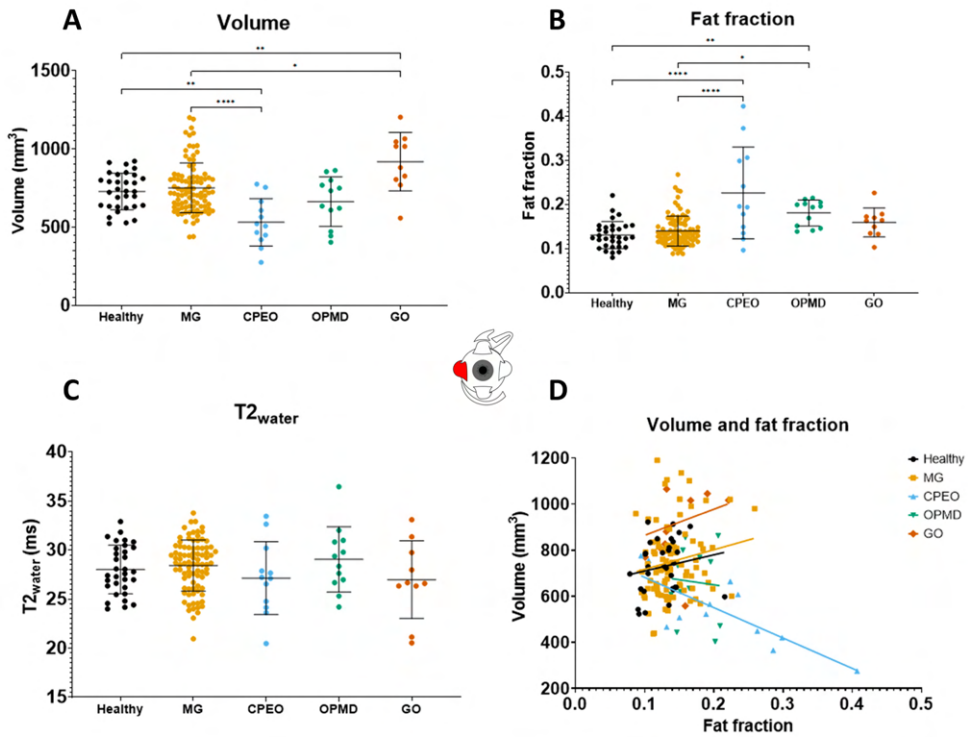

Figure 2. *Volume values, fat fraction values, T2$_{water}$ values and the correlation between fat fraction and volume of the **lateral rectus** as measured with quantitative MRI for the different groups: healthy controls, myasthenia gravis (MG), chronic progressive external ophthalmoplegia (CPEO), oculopharyngeal muscular dystrophy (OPMD) and Graves' orbitopathy. (GO).*
* is p ≤ 0.05; ** is p ≤ 0.01; *** is p ≤ 0.001; **** is p ≤ 0.0001

Fat fractions are higher in CPEO, OPMD and chronic MG

Fat fraction differences were observed between disease groups (table 2). No fat fraction differences were observed between the combined MG patient cohort and healthy controls. For example, the fat fraction of the LR was 0.131 ± 0.031 for healthy controls and 0.140 ± 0.034 for all MG groups combined (figure 2B) and for the SR+LPS the fat fraction was 0.142 ± 0.026 in healthy controls and 0.162 ± 0.049 in MG (figure 3B). Differences were observed between MG patients and CPEO for all EOM (figure 2B). Between MG and OPMD the fat fraction differed for the IR ($p<0.05$) and the SR+LPS ($p<0.05$). When looking at subgroups of MG patients, differences in fat fraction were observed between chronic MG patients and healthy controls in the MR (0.017 difference, $p<0.05$) and SR+LPS (0.028 difference, $p<0.05$), but not for recently diagnosed and seronegative MG patients.

Volume correlates with fat fraction in MG, CPEO and Graves' orbitopathy

In MG patients, volume and fat fraction correlated moderately in MR, IR and SR+LPS muscles (e.g. for SR+LPS $r=0.27$, $p<0.001$, figure 3D): bigger EOMs had higher fat fractions, with an average difference of 5% between a SR+LPS of 500 mm^3 and 1500 mm^3. In CPEO, a decrease in muscle volume was accompanied by an increase in fat fraction in the LR ($r=-0.79$, $p<0.01$, figure 2D) and the SR+LPS ($r=-0.61$, $p<0.05$, figure 3D). In OPMD, volume and fat fraction did not correlate and only the volume of the IR strongly correlated positively with fat fraction in GO ($r=0.81$, $p<0.01$).

Volume correlates with age in MG

Combining all EOM, we observed a negative correlation between age and normalized volume in MG patients ($r=-0.25$, $p<0.01$) but not in healthy controls ($r=-0.02$, n.s.). This difference might however be explained by the fact that a portion of the MG patient received immunosuppressant treatment including corticosteroids. Additionally a positive correlation between age and fat fraction was observed in healthy controls ($r=0.17$, $p<0.05$) and in MG patients ($r=0.28$, $p<0.0001$).

All patient groups show limited ductions and Hess-chart abnormalities

Limited ductions were observed in CPEO (6 out of 6) and OPMD (5 out of 6) patients (table 1). In 26 of 53 MG patients, limited duction were found, which was comparable in chronic MG (10 out of 19), recent MG (9 out of 20) and seronegative MG (7 out of 14). Hess-chart abnormalities were observed in almost all patient control groups (6/6 in CPEO, 5/6 in OPMD and 5/6 in GO). In MG 41 out of 53 patients had Hess-chart abnormalities, meaning that 80% of included MG patients had clinical or subclinical diplopia.

Table 2. The quantitative MRI parameters (volume, fat fraction and $T2_{water}$) for all individual extra-ocular muscles for the MG groups recently diagnosed, chronic and seronegative, for the disease controls chronic progressive external ophthalmoplegia (CPEO), oculopharyngeal muscular dystrophy (OPMD) and Graves' orbitopathy (GO), and the healthy controls. For volume, fat fraction and $T2_{water}$ the amount of patients with zero, one or more than one muscle higher or lower than 2 standard deviations (SD) above and below the mean of healthy controls are mentioned. Per quantitative MRI parameter an ANOVA was performed and for the group comparison a post-hoc testing was performed using Dunnett's multiple comparisons test to correct for multiple testing.

	MG Recently diagnosed n=19	MG Chronic n=18	MG Seronegative n=11	CPEO n=6	OPMD n=6	GO n=5	Healthy controls n=16	p-value with MG groups combined
Volume								
Lateral rectus (mm³)	753.5 ± 126.7	753.5 ± 187.6	685.0 ± 145.7	531.0 ± 116.8*	662.6 ± 158.5	918.6 ± 186.2*	728.1 ± 116.8	<0.0001
Medial rectus (mm³)	664.8 ± 117.6	691.5 ± 154.0	569.5 ± 101.5	497.1 ± 121.3*	618.0 ± 103.8	775.6 ± 188.5*	629.8 ± 142.2	0.0002
Inferior rectus (mm³)	517.3 ± 121.3	565.4 ± 156.8*	408.9 ± 124.4	432.4 ± 134.5	546.3 ± 164.9	857.1 ± 424.0*	480.4 ± 134.5	<0.0001
Superior rectus plus levator palpebrae (mm³)	953.1 ± 252.8	1028.0 ± 267.7*	972.4 ± 298.5	602.0 ± 192.9†	739.8 ± 199.8†	1419.0 ± 457.1*	883.8 ± 153.7	<0.0001
0 muscles out of 2 SD range (n [%])	13 (68%)	8 (44%)*	5 (46%)	2 (33%)*	3 (50%)	0 (0%)*	11 (69%)	<0.01
1 muscles out of 2 SD range (n [%])	2 (11%)	4 (22%)*	4 (36%)	0 (0%)*	2 (33%)	0 (0%)*	5 (31%)	
2+ muscles out of 2 SD range (n [%])	4 (21%)	6 (33%)*	2 (18%)	4 (67%)*	1 (17%)	5 (100%)*	0 (0%)	
Fat fraction								
Lateral rectus	0.142 ± 0.032	0.147 ± 0.040	0.114 ± 0.022	0.226 ± 0.104*	0.181 ± 0.029*	0.160 ± 0.033	0.131 ± 0.031	<0.0001
Medial rectus	0.135 ± 0.028	0.140 ± 0.030*	0.137 ± 0.026	0.202 ± 0.061*	0.163 ± 0.018*	0.142 ± 0.028	0.123 ± 0.019	0.0075
Inferior rectus	0.174 ± 0.052	0.187 ± 0.046	0.151 ± 0.042	0.223 ± 0.057*	0.194 ± 0.035	0.199 ± 0.077	0.169 ± 0.045	<0.0001
Superior rectus plus levator palpebrae	0.167 ± 0.050	0.170 ± 0.055*	0.140 ± 0.030	0.199 ± 0.077†	0.233 ± 0.028*†	0.194 ± 0.052*	0.142 ± 0.026	<0.0001
0 muscles out of 2 SD range (n [%])	10 (53%)	9 (50%)*	7 (64%)	2 (33%)*	1 (17%)*	2 (40%)	13 (81%)	<0.01
1 muscles out of 2 SD range (n [%])	5 (26%)	4 (22%)*	4 (36%)	0 (0%)*	0 (0%)*	2 (40%)	3 (19%)	
2+ muscles out of 2 SD range (n [%])	3 (16%)	5 (28%)*	0 (0%)	4 (67%)*	5 (83%)*	1 (20%)	0 (0%)	

Table 2. *Continued*

	MG Recently diagnosed n=19	MG Chronic n=18	MG Seronegative n=11	CPEO n=6	OPMD n=6	GO n=5	Healthy controls n=16	p-value with MG groups combined
T2_{water}								
Lateral rectus (ms)	28.4 ± 2.2	28.7 ± 2.5	28.0 ± 3.1	27.1 ± 3.7	29.1 ± 3.3	27.0 ± 4.0	28.0 ± 2.5	*n.s.*
Medial rectus (ms)	26.3 ± 2.9	28.3 ± 3.3	28.3 ± 3.3	28.5 ± 3.2	26.4 ± 1.8	26.6 ± 4.9	27.0 ± 2.6	*n.s.*
Inferior rectus (ms)	24.5 ± 3.6	25.8 ± 3.4	26.8 ± 3.9	24.7 ± 3.0	29.3 ± 2.7*	25.1 ± 6.2	24.3 ± 4.0	*0.0053*
Superior rectus plus levator palpebrae (ms)	27.7 ± 2.1	29.1 ± 2.5	29.5 ± 2.7	28.9 ± 3.2	28.0 ± 2.4	27.7 ± 3.4	28.7 ± 2.1	*n.s.*
0 muscles out of 2 SD range (n [%])	13 (68%)	12 (67%)	5 (46%)	1 (16.5%)	4 (67%)	1 (20%)	11 (69%)	*n.s.*
1 muscles out of 2 SD range (n [%])	6 (32%)	4 (22%)	4 (36%)	4 (67%)	2 (33%)	2 (40%)	5 (31%)	
2+ muscles out of 2 SD range (n [%])	0 (0%)	2 (11%)	2 (18%)	1 (16.5%)	0 (0%)	2 (40%)	0 (0%)	

* The bold values are significantly different from healthy controls after post-hoc testing.
† Two of the CPEO and one of the OPMD patients had surgery involving the levator palpebrae to correct for their ptosis and excluded from the mean
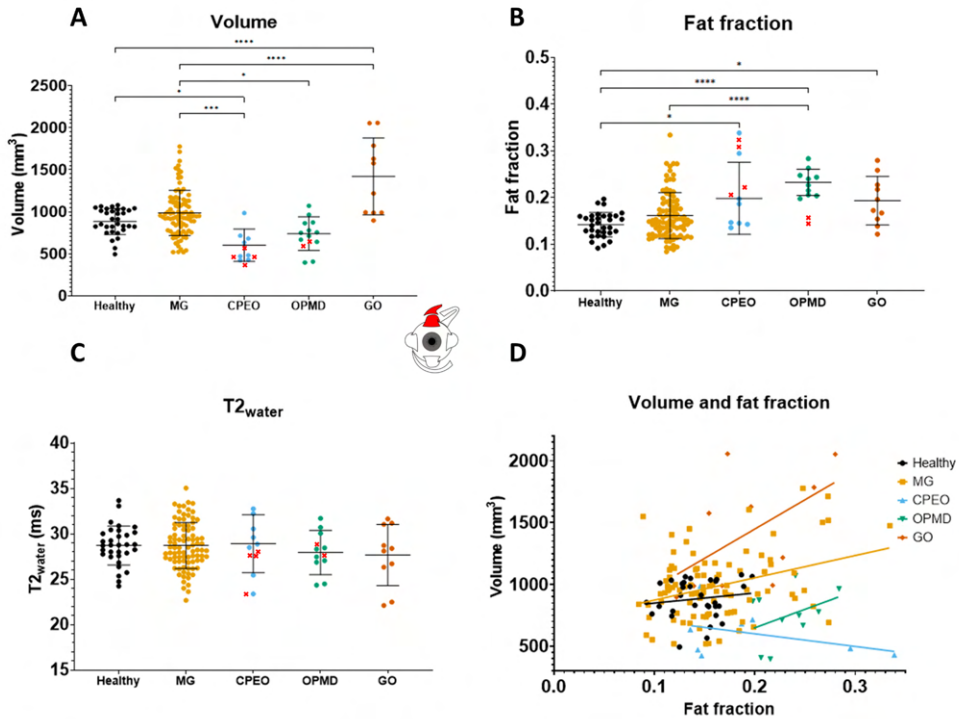
Figure 3. *Volume values, fat fraction values, T2$_{water}$ values and the correlation between fat fraction and volume of the* **superior rectus plus the levator palpebrae** *as measured with quantitative MRI for the different groups: healthy controls, myasthenia gravis (MG), chronic progressive external ophthalmoplegia (CPEO), oculopharyngeal muscular dystrophy (OPMD) and Graves' orbitopathy (GO). The values marked with a red cross in OPMD and CPEO are from patients who had eyelid corrective surgery involving the levator palpebrae and were excluded from the mean.*
* is p ≤ 0.05; ** is p ≤ 0.01; *** is p ≤ 0.001; **** is p ≤ 0.0001

qMRI parameters do not correlate with orthoptic measures in MG

In all MG patients, volumes and fat fractions of individual EOM were compared in patients with or without limited duction angles. Additionally, a similar comparison was made between patients with and without deviations on the outer field of the Hess-chart. EOM responsible for duction limitations did not have a significantly different normalized volume or fat fraction than EOM not responsible for duction limitations as shown in figure 5A and 5B. In addition, the normalized volume and fat fraction of the EOM that showed a deviation on the Hess-chart were comparable to the normalized volume and fat fraction of EOM that did not (figure 5C and 5D).
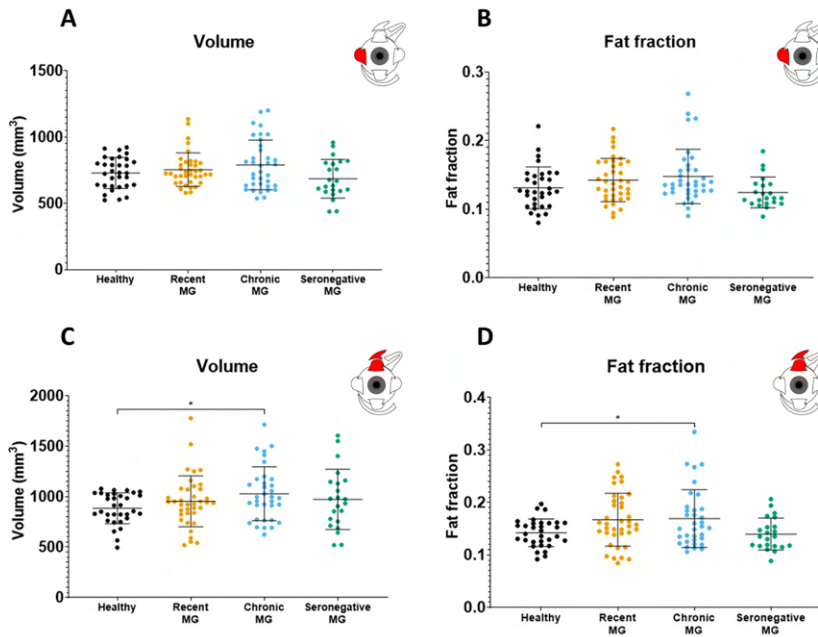
Figure 4. *Volume values and fat fraction values for **the lateral rectus and the superior rectus plus levator palpebrae** as measured with quantitative MRI for the different myasthenia gravis groups as compared to healthy controls: recently diagnosed myasthenia gravis, chronic myasthenia gravis and seronegative myasthenia gravis.*
* is p ≤ 0.05; ** is p ≤ 0.01; *** is p ≤ 0.001; **** is p ≤ 0.0001

The severity of ophthalmoplegia on a patient level was defined as the sum-score of limited ductions in all directions. This sum-score did not correlate with volume in MG for all EOM. In CPEO, a significant negative correlation between volume and this sum-score was observed in the LR (r=-0.79, p<0.01), MR (r=-0.75, p<0.01) and SR (r=-0.63, p<0.05). Additionally, in OPMD a significant negative correlation between volume and this sum-score was present in the MR (r=-0.71, p<0.05), LR (r=-0.76, p<0.01) and SR (r=-0.58, p<0.05). In GO a negative relationship was only significant in the LR (r=-0.65, p<0.05).

We compared the sum-score of duction limitations between different groups based on the number of muscles with volume and fat fraction below/over two standard deviations from the healthy controls (zero, one or more than one). For volume, MG patients had an average sum-score of 7.4 degrees when zero muscles were out of the 2SD range, 12.4 degrees when one muscle was out of range and 38 degrees when more than two muscles were out of range (p < 0.05).
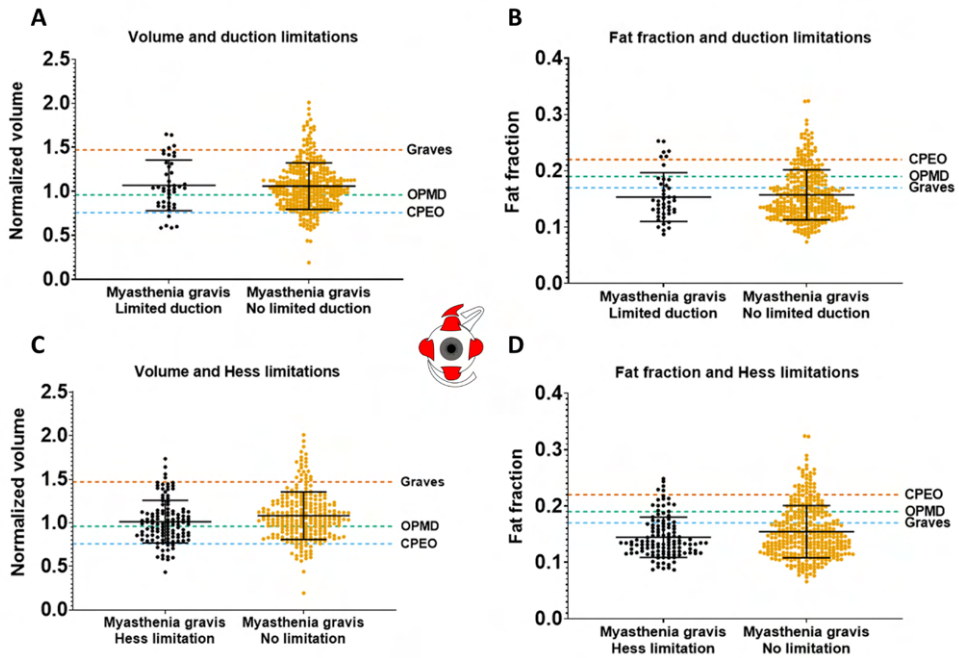
Figure 5. *Volume and fat fraction for individual extra-ocular muscles in muscles with or without limited function, as measured with synoptophore (duction angles) and the outer field of the Hess-chart in myasthenia gravis patients. The averages of CPEO, OPMD and Graves' orbitopathy patients are shown as dashed lines as a reference for higher/lower volume and fat fraction values. No significant differences were observed.*

7

T2$_{water}$ is comparable between MG and healthy controls

No significant differences in T2$_{water}$ for all individual EOM were found between MG patients and healthy controls and between MG groups (figure 2C, figure 3C and table 2). Only for the IR, significant differences were found between OPMD (29.3 ± 2.7 ms) and CPEO (24.7 ± 3.0 ms, $p < 0.05$), MG (25.6 ± 3.7 ms, $p < 0.05$) and healthy controls (24.3 ± 4.0 ms, $p < 0.01$). Relatively large standard deviations for T2$_{water}$ were observed for all groups including healthy controls (2.5 ms, 2.6 ms, 4.0 ms and 2.1 ms, respectively for LR, MR, IR and SR+LPS) for all EOM.

DISCUSSION

In this work we systematically evaluated quantitative MRI and orthoptic tests to measure both structure and function of the EOM in a large and well-defined cohort of MG patients, neuromuscular controls and healthy controls. We found no atrophy and limited fat replacement in MG, even in patients with residual ophthalmoplegia. Instead, volume and fat fraction of EOM were slightly increased in chronic MG patients, which raises pathophysiological questions. The observed differences in EOM volume and fat fraction in CPEO, OPMD and GO validate MRI as a sensitive technique to study EOM. MRI of the EOM is generally not helpful to differentiate recent onset, chronic or seronegative MG from healthy controls in individual patients. In individual cases MRI of the EOM could be supportive in differential diagnostics of MG as compared to CPEO, OPMD and Graves. Our observations suggest that in most MG patients with refractory EOM weakness, no structural anatomical changes are present in the EOM precluding functional recovery after optimal treatment.

Our results show that MRI is not of immediate benefit for distinction between MG and healthy subjects. Muscle volume and FF were not different between healthy controls and seronegative MG patients, the subgroup which often poses diagnostic challenges. However, in individual cases orbital MRI can be useful to distinguish MG from common MG mimics like GO[143], OPMD and CPEO. In the latter three disorders the pattern of EOM involvement may be a diagnostic imaging marker, as earlier proposed by Ferreira et al.[87] In CPEO, the SR+LPS was most fat replaced and decreased in volume followed by the MR and LR, with relative sparing of the IR, which is in line with literature, pathophysiology and the clinical involvement pattern.[14,93] In OPMD, the SR+LPS was also most fat replaced as expected[53,171], followed by the LR and IR with relative sparing of the MR. In GO, EOM volume increased up to 190% without significant fat fraction increases, in line with previously described MRI and ultrasound measures described.[91,105] Apparently, edematous swelling of EOM and adipogenesis result in increase in the amount of water and fat. [106] The involvement pattern was comparable to literature with predominant involvement of IR, SR+LPS and MR muscles. [87,91]

The unexpected absence of atrophy in MG is an important finding, as it excludes major structural changes in the muscles as a relevant factor in the pathophysiology of refractory ocular MG. In MG, EOM volumes and fat fractions were similar to healthy controls for most patients. In diseases with denervation like chronic fibrosis of the EOM (CFEOM)[47,95] atrophy is observed. Similarly, we expected a decrease in muscle volume in chronic MG, especially in treatment refractory patients, due to synaptic denervation caused by the antibody-mediated neuromuscular junction damage and as observed in several case reports[13–16]. Given the absence of atrophy, it appears that long lasting functional denervation does not lead to EOM

atrophy, in contrast to skeletal muscles. Possibly the unique innervation pattern with mono- and multisynaptic muscle fibers in the EOM can partly explain this.[255–257] One case report also found no histological abnormalities in the EOM of a severely affected MG patient.[258] Several other case reports[13–16] on refractory AChR MG reported atrophy and fat replacement. In another study including severely refractory and untreated ocular MG patients[17] atrophy and fat replacement was reported, with a decrease in mean EOM thickness of 0.3mm and fat replacement as scored qualitatively. However, in that study, cross-sectional area was measured instead of volume, which can be affected by gazing direction and measurement location. The difference between this untreated refractory cohort and the chronic MG patients in the present study might also be explained by treatment effect, as all chronic MG patients in our study were treated with immunosuppressant medication drugs. This suggests a beneficial effect of immune suppressant treatment to prevent EOM atrophy. Moreover, the absence of gross structural muscle changes suggests that receptor blockage or damage at the neuromuscular junction are the main causes of ophthalmoplegia. This might imply that new treatments directed at the neuromuscular junction might still be able to reverse this refractory weakness.

In chronic MG patients the average EOM volume was significantly increased by approximately 20%. One possible explanation is a hypertrophic muscular response, as observed in other chronic muscular diseases like Duchenne muscular dystrophy[259] and in Charcot-Marie-Tooth disease type 1A[260]. Complement-mediated inflammation at the neuromuscular junction could possibly cause edema of muscle fibers.[21] Additionally, the copresence of fat in enlarged muscles in chronic MG suggests the presence of muscle damage, which may be secondary to muscle inflammation. We note that the chronic MG patients were relatively affected with a high MG-ADL and QMG (table 1), this might be due to selection bias from being a tertiary referral center as an academic center and we included patients that came on the outpatient clinic with symptoms.

Although there were distinct differences in orthoptic measurements between patients and groups, in chronic MG patients with residual ophthalmoparesis the EOM were not atrophic. Additionally, there was no correlation between volume and fat fraction, and the orthoptic functional measures of individual EOM. On the other hand, in CPEO and OPMD a decrease in volume did correlate with orthoptic measures of EOM weakness. In these myopathic diseases, smaller EOM showed more limitations in eye movement. This has previously been reported for CPEO, where muscle size and T2 relaxometry correlated with range of eye movement.[93] The EOM of CPEO patients also show more volume decrease and FF increase than OPMD, which also fits with the clinical pattern with more presence of ophthalmoparesis in CPEO and more ptosis in OPMD. Altogether, this also shows that our methods were

7

sensitive enough to detect correlations between EOM function and quantitative MRI. We did not structurally document whether the patients had ocular symptoms in the past. Therefore some MG patients without ocular symptoms at the time of the study could have had ocular involvement in the past, which might have resulted in structural changes in the EOM at the time of the MRI.

We observed a large, ~3 ms, variation in $T2_{water}$ of the EOM in healthy controls, which is larger than the average 1 ms previously observed in skeletal muscles[41,235]. This might have masked the small expected increases in $T2_{water}$ of 3 to 5 ms associated with minor inflammation.[41] Validation of the methodology on the semispinalis capitis, a major cervical muscle, in the same healthy volunteers showed lower variation in $T2_{water}$ of 0.89ms (supplementary material "Assessment of large variation in $T2_{water}$"). We therefore performed a set of additional analyses on the potential origin of high variation observed in the EOM. These analyses included an assessment of the accuracy of EPG-based B1 determination and the influence of surrounding orbital fat that was superimposed on the MR-signal of the EOM. Similar to a recent 3T study on intra-ocular tumors[261], we observed a relatively low B1 in the EOM. Additionally, the T2 of the orbital fat appeared to be lower than the subcutaneous fat conventionally used as reference. However, correcting for these EOM-specific effects did not resolve the high variation in $T2_{water}$. As a result, the origin of the high $T2_{water}$ variation in the EOM remains unknown. It could, for example, have been a limitation of the two-component EPG model which does not incorporate a, currently unknown, EOM specific contribution to the MR-signal. Alternatively, the $T2_{water}$ of the EOM could indeed have had a relatively high variation between subjects, making it a less useful metric to assess subtle changes due to inflammation.

For a better understanding of the pathophysiology of EOM changes in MG, a next step would be to include a group of patients with MuSK MG and congenital myasthenia syndrome. In these subgroups, we hypothesize that the EOM are atrophic due to the long lasting deficits in neuromuscular junction transmission, as has been shown for skeletal muscles in certain subtypes of congenital myasthenic syndrome using MRI.[262] Knowing whether EOM atrophy is present in these subgroups might aid in understanding how MG pathology behaves differently in EOM as compared to skeletal muscles. Additionally, microscopic evaluation of damage at the neuromuscular junctions in the EOM of MG patients may shed light on the pathophysiology of refractory ophthalmoparesis in chronic MG patients.[9]

Funding and/or Conflicts of interests/Competing interests

7

8

Summary, general discussion and future
perspectives

The overall aim of the studies described in this thesis was to develop novel methods to improve the clinical care of ocular MG patients. In this thesis the eye muscles were directly studied in patients with myasthenia gravis (MG) using electrophysiology, orthoptics and quantitative MRI. The overall sub aims of this thesis were: **1.** To develop diagnostic tools to aid in the difficult diagnosis of ocular seronegative MG, **2.** To gain a better understanding of eye muscle involvement in MG to better understand the pathogenesis of refractory ophthalmoplegia in MG, and **3.** To develop tools to directly measure eye muscle function in ocular MG to use in clinical trials.

SUMMARY

In **chapter 2** an extensive literature review was performed into clinical and imaging clues to the diagnosis and follow-up of all diseases with ptosis and ophthalmoparesis. This review combined clinical symptoms, imaging and eye muscle involvement pattern to provide clues for diagnosis of diseases with ophthalmoparesis and ptosis, including acquired and hereditary diseases with pathology located in the brain, nerve, synapse and muscle. The clinical patterns were characterized by the combinations of the presence of ptosis, ophthalmoparesis, diplopia, pain, proptosis, nystagmus, extra-orbital symptoms, symmetry or symptom fluctuations. Additionally, imaging findings of the eye muscles in hereditary muscle, neural and synaptic diseases are atrophy and an increase in fat in the eye muscles. In acquired orbital diseases, inflammation seen as hyperintensity on T2w scans with fat suppression is observed in active stages of disease combined with increases in eye muscle volumes. In diseases with ophthalmoparesis and ptosis, specific patterns of clinical symptoms, the eye muscle involvement pattern and orbital imaging provide valuable information for diagnosis and for understanding of disease pathophysiology.

In **chapter 3** the test-retest reliability was assessed of an electrophysiological test directly measuring decrement in the eye muscles, the *repetitive ocular vestibular evoked myogenic potentials* (RoVEMP) test. The RoVEMP test is a novel diagnostic test to diagnose neuromuscular transmission deficits in the eye muscles in MG. The test-retest reliability of the RoVEMP test was assessed in 19 MG patients and 15 healthy controls. The study showed that in our hands the test-retest reliability of this test is not optimal, with Bland-Altman limits of agreement in decrement of -180% to 139% in MG patients. This reliability correlated significantly with the amplitude of the RoVEMP signal and the amplitude correlated negatively with age. Based on these findings, we believe that the ROVEMP test is especially suitable to detect changes at group level after careful age-matching and we caution against the use of RoVEMP measurements with lower amplitudes in clinical practice.

In **chapter 4** the EOM were functionally assessed with orthoptic tests, measuring maximal duction angles and deviations as proxies for eye muscle strength. We applied the Hess chart in a novel way, by assessing drift during persistent gaze on the Hess chart as a direct measure of eye muscle fatigability. A remarkably high percentage (41%) of MG patients without a measurable ophthalmoparesis had Hess chart deviations. This suggests that subtle differences in contraction force are more prevalent in MG than severe eye muscle weakness causing absolute duction limitations. We studied whether these extended orthoptic tests could aid in the diagnosis of MG. The presence of drift during one minute of persistent gaze had a sensitivity of 81% and a specificity of 100%, compared to our patient control groups. This test could therefore constitute a promising, highly specific diagnostic test for MG, as it is relatively easy to implement in the clinic, affordable and already widely available. In addition to diagnosis, orthoptic measures could also benefit future clinical trials by quantifying the effect of novel treatments on eye muscle weakness in MG patients.

In **chapter 5** and **chapter 6** studies are described into the methodology of quantitative MRI in skeletal muscle and in extra-ocular muscles. In **chapter 5** we developed an extended phase graphs (EPG) based method to measure the T2 of water as a measure of disease activity, for example muscle inflammation. The model assumed a two-component model with calibration of the T2 of fat on subcutaneous fat also including a water component. Additionally, the model includes the slice flip angle profile with corrections for chemical shift displacements. The method was optimized on skeletal muscle in cohorts of healthy controls, Duchenne muscular dystrophy, Becker muscular dystrophy and spinal muscular atrophy patients. In vivo data showed a gradual decline in the T2 of water for increasing fat fractions, with important implications for clinical studies using the T2 of water as an outcome parameter. Using our model, these T2 relaxometry measurements will be more reliable and will allow for better comparison of values between centers and diseases. In **chapter 6** a pilot study was performed to test whether doing quantitative MRI of the eye muscles is feasible using a 7-Tesla MR-scanner. In this pilot study we found an increase in eye muscle volume and FF in MG and Graves' orbitopathy patients. The increase in fat content in the eye muscles in MG has been described in histological studies before, but the increase in muscle volume in the eye muscles of MG patients was unexpected. We also measured water T2 relaxation times comparable to values measured in skeletal muscle, but found a high variability between individuals and between different EOM. We concluded that despite the challenges of size and movement of the eye muscles, quantitative MRI is feasible for measuring fat fraction and muscle volume of individual eye muscles in healthy controls, MG and Graves' orbitopathy patients at 7 Tesla.

8

In **chapter 7** a quantitative MRI study of the eye muscles is described in a large and well-defined cohort of MG patients, neuromuscular and healthy controls. We included recently diagnosed MG patients, chronic MG patients and seronegative MG patients and compared the eye muscle findings to healthy controls, CPEO, OPMD and Graves' orbitopathy patients. We found no atrophy and limited fat replacement in MG, even in patients with residual ophthalmoplegia. This suggests that the functional impairment of the eye muscles in chronic MG is not due to atrophic muscle fibers or other structural muscle damage on a macroscopic level. These observations suggest that in most MG patients with refractory eye muscle weakness, no structural anatomical changes are present in the eye muscles precluding functional recovery after optimal treatment. Instead of the expected atrophy, volume and fat fraction of the eye muscles were slightly increased in chronic MG patients, which raises pathophysiological questions. Unfortunately, measuring the T2 of water as an inflammatory marker at 7 Tesla turned out to be difficult, due to a high variation in measurements. Diagnostically, orbital MRI did not prove to be useful in differentiating healthy controls from MG patients in our study. Also in the seronegative MG subgroup, which is harder to diagnose, no significant changes of the eye muscles were present as compared to healthy controls. However, differences in eye muscle volume and fat fraction were observed in CPEO, OPMD and GO as compared to MG which could be supportive in differential diagnostics.

GENERAL DISCUSSION

In this thesis, three different methods were evaluated for directly measuring function or structure of the eye muscles to aid in ocular MG. All methods taught us something about the pathophysiology of eye muscle involvement in MG and about refractory ocular symptoms. The most promising finding was the lack of atrophy in the eye muscles of MG patients, because this could mean that refractory ophthalmoplegia in MG might still be susceptible to other therapeutical options. Additionally, using orthoptic measurements we found that contraction asymmetry is more important than absolute movement limitation of the eyes implying that there might be a role of the central nervous system in the cause of diplopia in MG. Orthoptic measures showed to be particularly useful for diagnosing MG and to quantify the severity of ocular symptoms in MG for clinical trials. MRI turned out to be less useful in diagnosis due to little eye muscle changes in MG, but MG-mimics like CPEO, OPMD and Graves' orbitopathy could be identified due to more severe structural changes like eye muscle swelling or atrophy. Lastly, orthoptic tests could also be relevant as an outcome measure in clinical trials in ocular MG. These tests quantify deviations between the eyes, the amount of ophthalmoparesis and can measure the presence of eye muscle fatigability. All mentioned findings, advantages and disadvantages of the three studied methods are summarized in figure 1 and discussed in more detail below.

Methods

Ocular myasthenia gravis	RoVEMP test *Neurophysiological measure of eye muscle fatigability*	Orthoptic measures *Functional measures of eye muscle weakness and fatigability*	Quantitative MRI *Structural quantitative measures of eye muscles*
Diagnostic *Half of patients is seronegative; need for diagnostic tests*	• Low test-retest reliability, not reliable for diagnosing individuals • Does have diagnostic yield on group level	• Specific and sensitive to MG related fatigability • Useful, cheap and easy diagnostic test in ocular MG	• Little differences between MG and healthy controls • Differences between MG and MG-mimics (e.g., Graves', CPEO)
Understanding refractory ophthalmoplegia *Needed for developing effective therapies*	• Proven neuromuscular failure in eye muscles	• Mismatch between duction limitations and Hess chart deviations • Fatigability of the eye muscles in MG	• No atrophy in MG, not even in refractory ocular patients • Little increase in eye muscle volume and fat fraction in chronic MG
Ocular outcome measures *Need for objective outcome measures of eye muscle weakness*	• Low test-retest reliability makes it less useful in follow-up • Potential as outcome measure before and after therapy in large cohorts	• Can quantify the severity of ophthalmoplegia and eye deviations • Sensitive to MG-related fatigability	• Only little eye muscle changes in MG, not useful for follow-up in clinical trials

Challenges

Figure 1. *Summary of the three clinical challenges in ocular myasthenia gravis, the three introduced advanced methods to aid in these challenges and the findings. Findings that are useful in diagnostics and as outcome measures are depicted in green and findings that are not or less useful in red.*

8

147

The first sub aim was to identify if the mentioned methods might aid in the diagnosis of ocular MG. Firstly, the RoVEMP test showed an average decrement in the eye muscles of MG on group level. However, we found a low test-retest reliability and the RoVEMP test as currently technically implemented is therefore not useful for diagnoses. This low reproducibility is mostly explained by the low signal-to-noise ratio of the measured muscle potential and the presence of blinking artifacts in many patients. Secondly, MRI showed only little differences in the eye muscles between MG and healthy controls, especially in the challenging seronegative patients. MRI is therefore not suitable to differentiate seronegative MG patients form healthy controls. However differences in eye muscle volume and fat fraction were observed in other neuromuscular and orbital diseases as compared to MG, which could be supportive in differential diagnostics in case of clinical doubt. Also in coexisting Graves' orbitopathy and ocular MG, which co-occur frequently, MRI could be supportive when eye muscles are severely swollen.[143] For example in a patient with positive antibodies and severely swollen eye muscles, the presence of both diagnoses is likely. Lastly and most promising, orthoptic tests with added persistent gaze are very specific and sensitive in diagnosing MG. Adding persistent gaze to the Hess chart makes this test very sensitive to MG-related fatigability. In 87% of MG patients a drift in time on the Hess chart was observed. In virtually no other neuromuscular disease controls and healthy controls this phenomenon was observed. Orthoptic tests that are sensitive to MG-related fatigability could therefore be a superior test in diagnosing MG in seronegative (ocular) patients. Comparing our methods, the orthoptic tests show the most promise, are most easily implementable, the fastest and most cost-efficient as compared to other diagnostic tests in MG. Therefore it would be recommended to add an orthoptic evaluation to the clinical workup of every ocular MG patient with the addition of measuring MG-related eye muscle fatigability. With extended research this might even reduce the amount of diagnostic tests needed in the clinical workup.

Measuring the eye muscles directly with three different methods, we learned more about the pathophysiology of ocular symptoms in MG. Using the RoVEMP test, we showed on a group level the presence of decrement of the eye muscles and therefore that neuromuscular transmission is impaired in the eye muscles, as it is in skeletal muscles.[32] It also showed that the myogenic potentials of the inferior oblique muscle are lower in MG than in healthy controls, probably due to fewer fibers being excited. Secondly, using the orthoptic Hess-chart we showed that also eye muscles show the characteristic fatigable weakness as known in the skeletal muscles in MG. MG patients showed less absolute limitations in eye movement as compared to relative deviations. This suggests that a subtle asymmetry in force between the eye muscles is more prevalent in MG than severe ophthalmoparesis. This might be caused by a difference in neuromuscular transmission failure between left and right assuming equal

innervation following Hering's law.[171] Interestingly, these results suggest a possible role for aberrant central nervous system eye muscle coordination in MG. This might indicate that the central nervous system is unable to adapt to the asymmetrical and fluctuating weakness of the eye muscles. Lastly, structural changes in the eye muscles were assessed using MRI. We expected atrophy of the eye muscles, especially in chronic therapy-resistant ocular MG. However, we found virtually no volume decreases in the eye muscles in MG and instead we found a small increase in muscle volume in chronic MG. This might be caused by compensatory muscle hypertrophy or by oedema due to inflammation at the neuromuscular junctions. In histological studies there is sparse evidence of inflammation and knowing whether inflammation is present could aid in the choice of therapy for an individual patient. For example new drugs targeting complement activation might be more effective in the presence of active inflammation. In literature there is evidence of atrophy of the eye muscles in untreated MG patients with MuSK and AChR antibodies. Our cohorts were however treated to the current standard of care, and did not how atrophy. This might stress the importance of timely intervention to preserve muscle. Additionally, the absence of macroscopic eye muscle damage in refractory ocular MG gives hope for the possibility of future therapeutical interventions in this subgroup.

To further speculate on what we learned about the pathophysiological mechanism; Using the RoVEMP test we proved the presence of neuromuscular transmission failure in the eye muscles in MG and that certain muscle fibers are blocked. We showed using adapted orthoptic tests that eye muscles show an increase in weakness during persistent gaze, which makes it probable that direct AChR-receptor blockage is increasing over time due to receptor downregulation and depletion of AChR. Using MRI we showed that chronic eye muscle dysfunction in MG does not lead to atrophy, at least not in patients who are treated. It seems that despite the relative denervation which is present due to the blockage of synaptic transmission, the trophic signaling between the nerve and the muscle fibers stay intact. The sustained trophic signaling would explain the lack of atrophy. It is possible that due to the known multiple innervation[117] of eye muscle fibers, not all synapses fail for one muscle fiber. Also in the distinct contraction-excitation coupling and calcium handling[120] there might be a clue why the eye muscles might be more resilient to atrophy. Currently it remains unknown whether there is inflammation present in the eye muscles in MG. One might speculate that the eye muscles are more prone to inflammation due to complement activation at the neuromuscular junction, because the eye muscles lack complement inhibitory proteins and significantly more neuromuscular junctions are present per relative muscle fiber. Inflammation might possible explain the small volume increases and fat replacement in chronic MG as observed on MR-images.

8

Given their specialized function and cooperation, large differences exist between the eye muscles and skeletal muscles. As mentioned before on a biophysiological level, but also on a functional and anatomical level. Functionally it should be taken into account that the eye muscles cooperate in a very complex way, via connective tissue pulleys[263] and their combined forces move the eye in all directions. This balance could be very delicate, but also resilient to weakness of one eye muscle. Weakness of one eye muscle might result in an imbalance causing double vision, but feedback loops involving the visual centers of the brain might correct for these imbalances. Therefore the direct translation of EOM weakness as measured with orthoptic tests, or structural changes in MRI, might not translate to symptoms of double vision as expected. The direction of the measured force by a skeletal muscle is easier to predict and well-studied. Anatomically, the eye muscles also have different layers: the orbital and the global layer. The orbital layer initiates eye movement and the global layer activates later is responsible for holding the gaze.[252,264] These layers are normally hard to tell apart using MRI, however in the lateral and medial rectus muscle on our high resolution 7 Tesla images we observed a stripe of fat or connective tissue in the middle which seems to separate these layers. Using high resolution MRI, possibly in different gazing directions, one could study which layer is more affected in MG by assessing deformation and volume changes. Additionally, our high resolution images might aid in the understanding of these layers in several other diseases with eye muscles involvement, and opens an interesting research field in for example strabismus surgery.

Lastly, the studied methods can serve as objective outcome measures in clinical trials for ocular symptoms of MG. Currently, ocular MG is often excluded from clinical trials,[190] also because the degree of ocular weakness has been difficult to quantify.[25,26] The ocular symptoms of MG do however cause significant disability and lower quality of life. Orthoptic measures directly measure the weakness of the eye muscles, therefore being a good objective marker to quantify ocular disease severity of the eye muscles in MG as compared to the QMG for generalized MG. With our addition to implement one minute persistent gaze in the Hess chart, this orthoptic test is also sensitive to MG-related fatigability. Given the small changes we observed in MG with our quantitative MRI parameters, MRI does currently not have a direct role as an outcome measure in clinical trials. Additionally, the RoVEMP test could have an added value in objectifying neuromuscular transmission failure on group levels in clinical trials, for example in drugs that are targeting the neuromuscular junction directly like acetylcholinesterase inhibitors.

FUTURE PERSPECTIVES

As MG patients with seronegative disease are still regularly misdiagnosed or diagnosed after a considerable delay, additional tests are needed. Combining these multiple diagnostic test to synergistically increase sensitivity and specificity could aid in solving this diagnostic challenge in seronegative MG. For the Hess chart, which has a high specificity and is therefore a promising diagnostic test, I believe the sensitivity could be even further improved by repeated measurements with a focus on variability over time. Both fatigability and fluctuations are hallmarks and specific to MG, therefore measuring fluctuation over time could increase the diagnostic yield even further. I would recommend to perform a prospective diagnostic study including serum auto-antibody testing, neurophysiological tests and orthoptic tests (with additional testing of fatigability and fluctuation). It would be recommended to include both generalized and ocular MG patients, but also patient controls with neuromuscular disease, orbital disease and e.g. strabismus patients, to widely assess and validate the additional diagnostic value of orthoptic tests in both groups. I hypothesize that the orthoptic tests might prove to be the superior diagnostic test in diagnosing seronegative ocular MG.

The RoVEMP test and MRI turned out to be of no use in the direct diagnoses of seronegative ocular MG. The test-retest reliability of our currently implemented RoVEMP test should be improved to increase its reliability to be reliable enough for individual patient diagnosis. The focus should be on technical improvements of the signal to noise ratio. I propose for example to increase the amplifier strength, to increase the sample frequency to sample the short peaks more dense and to develop methods to correct for blinking artefacts. Orbital MRI currently shows promise in differential diagnostics to other disease, but not to separate healthy controls and MG. So far, we have studied the eye muscles while stationary using MRI, however measuring the eye muscles during movement over time in 4D could be a diagnostically interesting step forward. The cooperation of the eye muscles might show a specific pattern in MG, which might aid in diagnosis or understanding of ocular MG. A high sample frequency is however needed, while preserving sufficient resolution, but recent studies have shown it is possible to get to a temporal resolution of up to 35 ms.[265] Additionally, given literature evidence of skeletal muscle atrophy in AChR and MuSK positive MG[18,248], I propose to study the skeletal muscles as well in MG patients. Skeletal muscle MRI could aid in the understanding of refractory symptoms in bulbar and generalized MG.

Currently, $T2_{water}$ measurements are validated in skeletal muscles and turned out to be difficult to measure in the orbital region. Therefore a logical next step would be to perform $T2_{water}$ measurements of the skeletal muscles in MG patients to study whether the inflammatory process driven by complement activation can be measured using MRI at all. If MRI would be

8

able to identify MG patients where complement activation is the predominant pathophysiological mechanism, this might aid in therapeutic choice. These patients might for example benefit more from complement inhibiting medicine. If $T2_{water}$ does indeed show an increase in skeletal muscles in MG, it is worth improving the $T2_{water}$ measurements of the eye muscles, by for example trying to measure at 3 Tesla with higher magnetic field homogeneity, getting rid of the chemical shift displacement in the slice direction or by increasing the B1 in the orbit. Next to $T2_{water}$, other quantitative MRI parameters reflecting muscle activation profiles or muscle energy metabolism are worth investigating as a diagnostic or prognostic biomarker in MG. For example motor unit MRI shows promising results in measuring the size, shape and position[266,267] of single motor units as well as the width and contraction time of muscle twitches.[268] A portion of the total amount of motor units are known to be blocked in MG and excitation times show different delays, a phenomenon known as jitter. Motor unit MRI could potentially measure the amount of blocked motor units and the excitation contraction delay per motor unit, and could therefore be an interesting diagnostic biomarker in MG patients.

We aimed to explain how the eye muscles change macroscopically in MG, especially in the presence of refractory ocular symptoms, but found no severe atrophy. A next step would be to study the EOM microscopically. Acquiring histological samples of the eye muscles of MG patients with different phenotypes, for example after strabismus surgery or post-mortem, could aid in understanding of refractory ocular symptoms and the presence of inflammation at the neuromuscular junction in MG. We hypothesize that in refractory ocular MG the damage at the neuromuscular junction, for example visible as a decrease in neuromuscular folding, could be different or to another extent than in skeletal muscles. The eye muscles differ from skeletal muscle in that they have distinct fiber type composition[116], multiple innervation[117], smaller motor units[118], increased level of complement activation, higher levels of utrophin expression[119], a distinct contraction-excitation coupling[120], have an increased capability of regeneration and preferentially use glucose-based aerobic metabolic pathways.[84] The neuromuscular junction of the eye muscles might be more prone to damage than skeletal muscles, due to more antibody exposure, more complement activations or the presence of more neuromuscular junctions per muscle volume. On the other hand, due to higher capability of regeneration[84] damage might be more reversible in the eye muscles than in skeletal muscle. Combinations of these properties also explain why the eye muscles are not involved in all neuromuscular disease, for example in Duchenne muscular dystrophy the utrophin expression makes up partly for the lack of dystrophin expression. To conclude, histological research of damage at the neuromuscular junction, complement activation and auto-antibody concentrations might explain why eye muscles are preferentially involved in MG and to explain the pathophysiology of treatment resistant ophthalmoparesis in MG. I propose to start by

comparing histological samples of the eye muscles between treatment responsive ocular MG patients and treatment resistant ocular MG patients (post-mortem or after strabismus surgery), and study if the refractory ophthalmoplegic patients do indeed have less neuromuscular folding and more complement activation.
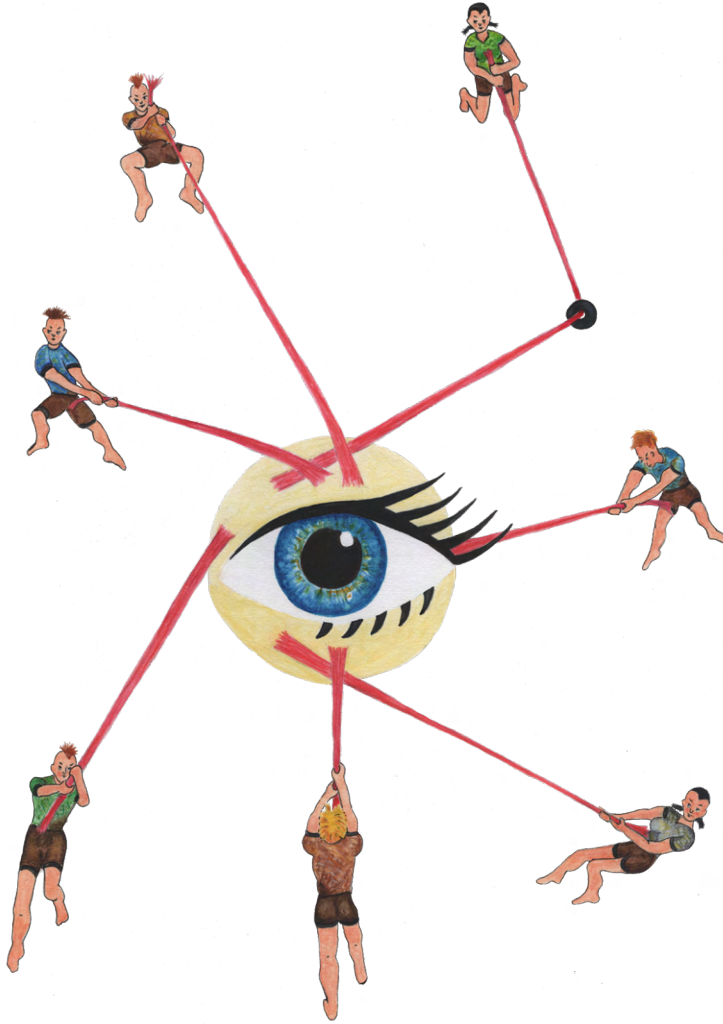
Ocular MG patients should be more regularly included in therapeutic trials, due to the severity of disability experienced by ocular MG patients and the lack of treatment options in refractory ocular MG. To facilitate the objective evaluation of MG related ocular symptoms in these trials, orthoptic tests should be included in these trials to follow the ocular symptoms over time and before/after treatment. Recently, patient reported outcome measures for ocular MG are being developed in addition to the currently used MG rating scales that focus more on generalized symptoms.[27] These patient reported outcome measures and our proposed orthoptic test should be evaluated over time in a larger cohort of (ocular) MG patients and their relation should be studied. If these patient reported outcome measures and the orthoptic tests show high correlations, they would be very useful in the follow-up of patients in clinical trials like the combination MG-ADL and QMG currently used for generalized MG. I also recommend to implement regular orthoptic measurements in the follow-up of ocular symptoms of MG in clinical care and study the natural course of these symptoms over time in a larger cohort.

To conclude, the most promising next research steps following from the findings in this thesis are 1. Diagnostically, orthoptic tests should be studied prospectively combined with existing diagnostic tests to have a combined higher diagnostic yield for ocular MG. Additionally, utilizing the two hallmarks of muscle weakness in MG, namely the fluctuations and fatigability, new diagnostic tests should be developed. Moreover, I propose to study the skeletal muscle in generalized MG using several quantitative MRI techniques. 2. Pathophysiologically, I propose a histological study of the eye muscles (post-mortem or after strabismus surgery) in ocular MG comparing treatment responsive and refractory patients, focusing on complement activation and destruction of neuromuscular junctions. 3. As an outcome measure in clinical trials, orthoptic measures should be included to quantify therapeutic improvement of ocular symptoms in MG.

8

9

References

1. Grob D, Brunner N, Namba T, Pagala M. Lifetime course of myasthenia gravis. *Muscle Nerve*. 2008;37(2):141-149. doi:10.1002/mus.20950

2. Gilhus NE, Tzartos S, Evoli A, Palace J, Burns TM, Verschuuren JJGM. Myasthenia gravis. *Nat Rev Dis Primers*. 2019;5(1):30. doi:10.1038/s41572-019-0079-y

3. Fortin E, Cestari DM, Weinberg DH. Ocular myasthenia gravis: An update on diagnosis and treatment. *Curr Opin Ophthalmol*. 2018;29(6):477-484. doi:10.1097/ICU.0000000000000526

4. Punga AR, Maddison P, Heckmann JM, Guptill JT, Evoli A. Epidemiology, diagnostics, and biomarkers of autoimmune neuromuscular junction disorders. *Lancet Neurol*. 2022;21(2):176-188. doi:10.1016/S1474-4422(21)00297-0

5. Gilhus NE, Verschuuren JJ. Myasthenia gravis: Subgroup classification and therapeutic strategies. *Lancet Neurol*. 2015;14(10):1023-1036. doi:10.1016/S1474-4422(15)00145-3

6. Huijbers MG, Marx A, Plomp JJ, Le Panse R, Phillips WD. Advances in the understanding of disease mechanisms of autoimmune neuromuscular junction disorders. *Lancet Neurol*. 2022;21(2):163-175. doi:10.1016/S1474-4422(21)00357-4

7. Verschuuren JJ, Palace J, Murai H, Tannemaat MR, Kaminski HJ, Bril V. Advances and ongoing research in the treatment of autoimmune neuromuscular junction disorders. *Lancet Neurol*. 2022;21(2):189-202. doi:10.1016/S1474-4422(21)00463-4/ATTACHMENT/30BA1066-C5F6-47B0-9DF6-0F4E2013D4C4/MMC1.PDF

8. Mantegazza R, Antozzi C. When myasthenia gravis is deemed refractory: Clinical signposts and treatment strategies. *Ther Adv Neurol Disord*. 2018;11. doi:10.1177/1756285617749134

9. Heckmann JM, Nel M. A unique subphenotype of myasthenia gravis. *Ann N Y Acad Sci*. 2018;1412(1):14-20. doi:10.1111/nyas.13471

10. Benatar M. A systematic review of diagnostic studies in myasthenia gravis. *Neuromuscular Disorders*. 2006;16(7):459-467. doi:10.1016/j.nmd.2006.05.006

11. Smith S V., Lee AG. Update on Ocular Myasthenia Gravis. *Neurol Clin*. 2017;35(1):115-123. doi:10.1016/j.ncl.2016.08.008

12. Verschuuren JJGM, Palace J, Erik Gilhus N. Clinical aspects of myasthenia explained. *Autoimmunity*. 2010;43(5-6):344-352. doi:10.3109/08916931003602130

13. Gratton SM, Herro A, Bermudez-Magner JA, Guy J. Atrophy and Fibrosis of Extra-Ocular Muscles in Anti-Acetylcholine Receptor Antibody Myasthenia Gravis. *Open J Ophthalmol*. 2014;04(04):117-119. doi:10.4236/ojoph.2014.44019

14. Ortube MC, Bhola R, Demer JL. Orbital Magnetic Resonance Imaging of Extraocular Muscles in Chronic Progressive External Ophthalmoplegia: Specific Diagnostic Findings. *Journal of AAPOS*. 2006;10(5):414-418. doi:10.1016/j.jaapos.2006.04.012

15. Pedapati R, Ravishankar U, Hazeena P, Shanmugam S, Chandrasekharan A, Venkatasubramanian S. Extraocular muscle atrophy in myasthenia gravis. *Ann Indian Acad Neurol*. 2022;25(3):483. doi:10.4103/AIAN.AIAN_1039_21

16. Pedapati R, Ravishankar U, Hazeena P, Shanmugam S, Chandrasekharan A, Venkatasubramanian S. Extraocular Muscle Atrophy in Myasthenia Gravis. *Ann Indian Acad Neurol*. 2022;0(0):0. doi:10.4103/aian.aian_1039_21

17. Velonakis G, Papadopoulos VE, Karavasilis E, Filippiadis DK, Zouvelou V. MRI evidence of extraocular muscle atrophy and fatty replacement in myasthenia gravis. *Neuroradiology*. 2021;63(9):1531-1538. doi:10.1007/S00234-021-02753-4/TABLES/3

18. Farrugia ME, Robson MD, Clover L, et al. MRI and clinical studies of facial and bulbar muscle involvement in MuSK antibody-associated myasthenia gravis. *Brain*. 2006;129(6):1481-1492. doi:10.1093/brain/awl095

19. Nikolić A V., Bačić GG, Daković M, et al. Myopathy, muscle atrophy and tongue lipid composition in MuSK myasthenia gravis. *Acta Neurol Belg*. 2015;115(3):361-365. doi:10.1007/s13760-014-0364-1

20. Oosterhuis H, Bethlem J. Neurogenic muscle involvement in myasthenia gravis. A clinical and histopathological study. *J Neurol Neurosurg Psychiatry*. 1973;36(2):244-254. doi:10.1136/jnnp.36.2.244

21. Vilquin JT, Bayer AC, Le Panse R, Berrih-Aknin S. The Muscle Is Not a Passive Target in Myasthenia Gravis. *Front Neurol*. 2019;10. doi:10.3389/fneur.2019.01343

22. Wolfe GI, Herbelin L, Nations SP, Foster B, Bryan WW, Barohn RJ. Myasthenia gravis activities of daily living profile. *Neurology*. 1999;52(7):1487-1489. doi:10.1212/wnl.52.7.1487

23. Jaretzki A, Barohn RJ, Ernstoff RM, et al. Myasthenia gravis: Recommendations for clinical research standards. *Neurology*. 2000;55(1):16-23. doi:10.1212/WNL.55.1.16

24. Howard JF, Freimer M, O'Brien F, Wang JJ, Collins SR, Kissel JT. QMG and MG-ADL correlations: Study of eculizumab treatment of myasthenia gravis. *Muscle Nerve*. 2017;56(2):328-330. doi:10.1002/MUS.25529

25. Howard JF, Utsugisawa K, Benatar M, et al. Safety and efficacy of eculizumab in anti-acetylcholine receptor antibody-positive refractory generalised myasthenia gravis (REGAIN): a phase 3, randomised, double-blind, placebo-controlled, multicentre study. *Lancet Neurol*. 2017;16(12):976-986. doi:10.1016/S1474-4422(17)30369-1

26. Howard JF, Bril V, Vu T, et al. Safety, efficacy, and tolerability of efgartigimod in patients with generalised myasthenia gravis (ADAPT): a multicentre, randomised, placebo-controlled, phase 3 trial. *Lancet Neurol*. 2021;20(7):526-536. doi:10.1016/S1474-4422(21)00159-9

27. Wong SH, Eggenberger E, Cornblath W, et al. Preliminary Findings of a Dedicated Ocular Myasthenia Gravis Rating Scale: The OMGRate. *Neuro-Ophthalmology*. 2020;44(3):148-156. doi:10.1080/01658107.2019.1660686

28. Oh SJ, Eslami N, Nishihira T, et al. Electrophysiological and clinical correlation in myasthenia gravis. *Ann Neurol*. 1982;12(4):348-354. doi:10.1002/ana.410120406

29. Piker EG, Jacobson GP, Burkard RF, McCaslin DL, Hood LJ. Effects of age on the tuning of the cVEMP and oVEMP. *Ear Hear*. 2013;34(6). doi:10.1097/AUD.0b013e31828fc9f2

30. Weber KP, Rosengren SM, Michels R, Sturm V, Straumann D, Landau K. Single motor unit activity in human extraocular muscles during the vestibulo-ocular reflex. *Journal of Physiology*. 2012;590(13):3091-3101. doi:10.1113/jphysiol.2011.226225

31. Valko Y, Rosengren SM, Jung HH, Straumann D, Landau K, Weber KP. Ocular vestibular evoked myogenic potentials as a test for myasthenia gravis. *Neurology*. 2016;86(7):660-668. doi:10.1212/WNL.0000000000002383

32. de Meel RHP, Keene KR, Wirth MA, et al. Repetitive ocular vestibular evoked myogenic potentials in myasthenia gravis. *Neurology*. 2020;94(16):E1693-E1701. doi:10.1212/WNL.0000000000009306

33. UK HS. SYNOPTOPHORE Information guide. https://www.haag-streit.com/fileadmin/Haag-Streit_UK/Downloads/CCO_downloads/Synoptophore_downloads/Synoptophore_Info_Guide.pdf

9

34. Guo J, Li X, Ma R, Qian J. Correlation between uniocular deviation and duction changes following different decompression surgeries in thyroid eye disease. *BMC Ophthalmol*. 2021;21(1). doi:10.1186/s12886-021-01892-9

35. Roper-Hall G. The Hess Screen Test. *American Orthoptic Journal*. 2006;56(1):166-174. doi:10.3368/aoj.56.1.166

36. Strijkers GJ, Araujo ECA, Azzabou N, et al. Exploration of new contrasts, targets, and MR imaging and spectroscopy techniques for neuromuscular disease-A workshop report of working group 3 of the biomedicine and molecular biosciences COST action BM1304 MYO-MRI. *J Neuromuscul Dis*. 2019;6(1):1-30. doi:10.3233/JND-180333

37. Burakiewicz J, Sinclair CDJ, Fischer D, Walter GA, Kan HE, Hollingsworth KG. Quantifying fat replacement of muscle by quantitative MRI in muscular dystrophy. *J Neurol*. 2017;264(10):2053-2067. doi:10.1007/s00415-017-8547-3

38. Naarding KJ, Reyngoudt H, Van Zwet EW, et al. MRI vastus lateralis fat fraction predicts loss of ambulation in Duchenne muscular dystrophy. *Neurology*. 2020;94(13):E1386-E1394. doi:10.1212/WNL.0000000000008939

39. Carlier PG, Marty B, Scheidegger O, et al. Skeletal Muscle Quantitative Nuclear Magnetic Resonance Imaging and Spectroscopy as an Outcome Measure for Clinical Trials. *J Neuromuscul Dis*. 2016;3(1):1-28. doi:10.3233/JND-160145

40. Dixon WT. Simple proton spectroscopic imaging. *Radiology*. 1984;153(1):189-194. doi:10.1148/radiology.153.1.6089263

41. Marty B, Baudin PY, Reyngoudt H, et al. Simultaneous muscle water T2 and fat fraction mapping using transverse relaxometry with stimulated echo compensation. *NMR Biomed*. 2016;29(4):431-443. doi:10.1002/nbm.3459

42. Tardif-de Géry S, Vilquin JT, Carlier P, et al. Muscular transverse relaxation time measurement by magnetic resonance imaging at 4 Tesla in normal and dystrophic dy/dy and dy(2j)/dy(2j) mice. *Neuromuscul Disord*. 2000;10(7):507-513. doi:10.1016/S0960-8966(00)00122-X

43. Hardy PA, Henkelman RM, Bishop JE, Poon ECS, Plewes DB. Why fat is bright in rare and fast spin-echo imaging. *Journal of Magnetic Resonance Imaging*. 1992;2(5):533-540. doi:10.1002/jmri.1880020511

44. Niendorf T, Beenakker JWM, Langner S, et al. Ophthalmic Magnetic Resonance Imaging: Where Are We (Heading To)? *Curr Eye Res*. 2021;46(9):1251-1270. doi:10.1080/02713683.2021.1874021

45. Beenakker JWM, van Rijn GA, Luyten GPM, Webb AG. High-resolution MRI of uveal melanoma using a microcoil phased array at 7 T. *NMR Biomed*. 2013;26(12):1864-1869. doi:10.1002/nbm.3041

46. Lindner T, Langner S, Graessl A, et al. High spatial resolution invivo magnetic resonance imaging of the human eye, orbit, nervus opticus and optic nerve sheath at 7.0 Tesla. *Exp Eye Res*. 2014;125:89-94. doi:10.1016/j.exer.2014.05.017

47. Heidary G, Engle EC, Hunter DG. Congenital fibrosis of the extraocular muscles. *Semin Ophthalmol*. 2008;23(1):3-8. doi:10.1080/08820530701745181

48. Al Othman B, Raabe J, Kini A, Lee AG. Update: The Miller Fisher variants of Guillain-Barré syndrome. *Curr Opin Ophthalmol*. 2019;30(6):462-466. doi:10.1097/ICU.0000000000000611

49. Filho ARG, Faccenda PG, Estacia CT, Correa BS, Curi I. Tolosa-Hunt Syndrome. *Rev Bras Oftalmol*. 2018;77(5):289-291. doi:10.5935/0034-7280.20180063

50. Mansukhani SA, Bothun ED, Diehl NN, Mohney BG. Incidence and Ocular Features of Pediatric Myasthenias. *Am J Ophthalmol*. 2019;200:242-249. doi:10.1016/j.ajo.2019.01.004

51. Parmar H, Ibrahim M. Extrathyroidal Manifestations of Thyroid Disease: Thyroid Ophthalmopathy. *Neuroimaging Clin N Am*. 2008;18(3):527-536. doi:10.1016/j.nic.2008.03.003

52. McClelland C, Manousakis G, Lee MS. Progressive External Ophthalmoplegia. *Curr Neurol Neurosci Rep*. 2016;16(6):1-10. doi:10.1007/s11910-016-0652-7

53. Renard D, Ferraro A, Lorenzini MC, et al. Orthoptic and video-oculographic analyses in oculopharyngeal muscular dystrophy. *Muscle Nerve*. 2015;52(4):554-558. doi:10.1002/mus.24600

54. Díaz-Manera J, Luna S, Roig C. Ocular ptosis: Differential diagnosis and treatment. *Curr Opin Neurol*. 2018;31(5):618-627. doi:10.1097/WCO.0000000000000600

55. Holmes JM, Leske DA, Kupersmith MJ. New methods for quantifying diplopia. *Ophthalmology*. 2005;112(11):2035-2039. doi:10.1016/j.ophtha.2005.06.013

56. Latting MW, Huggins AB, Marx DP, Giacometti JN. Clinical Evaluation of Blepharoptosis: Distinguishing Age-Related Ptosis from Masquerade Conditions. *Semin Plast Surg*. 2017;31(1):5-16. doi:10.1055/s-0037-1598188

57. Ozgen A, Ariyurek M. Normative measurements of orbital structures using CT. *American Journal of Roentgenology*. 1998;170(4):1093-1096. doi:10.2214/ajr.170.4.9530066

58. Park NR, Moon JH, Lee JK. Hertel exophthalmometer versus computed tomography scan in proptosis estimation in thyroid-associated orbitopathy. *Clinical Ophthalmology*. 2019;13:1461-1467. doi:10.2147/OPTH.S216838

59. Bau V, Zierz S. Update on chronic progressive external ophthalmoplegia. *Strabismus*. 2005;13(3):133-142. doi:10.1080/09273970500216432

60. Engle EC, Goumnerov BC, McKeown CA, et al. Oculomotor nerve and muscle abnormalities in congenital fibrosis of the extraocular muscles. *Ann Neurol*. 1997;41(3):314-325. doi:10.1002/ana.410410306

61. Bosley TM, Oystreck DT, Robertson RL, Al Awad A, Abu-Amero K, Engle EC. Neurological features of congenital fibrosis of the extraocular muscles type 2 with mutations in PHOX2A. *Brain*. 2006;129(9):2363-2374. doi:10.1093/brain/awl161

62. Marenco M, Macchi I, Macchi I, Galassi E, Massaro-Giordano M, Lambiase A. Clinical presentation and management of congenital ptosis. *Clinical Ophthalmology*. 2017;11:453-463. doi:10.2147/OPTH.S111118

63. Watanabe K, Hagura R, Akanuma Y, et al. Characteristics of cranial nerve palsies in diabetic patients. *Diabetes Res Clin Pract*. 1990;10(1):19-27. doi:10.1016/0168-8227(90)90077-7

64. Lacey B, Chang W, Rootman J. Nonthyroid causes of extraocular muscle disease. *Surv Ophthalmol*. 1999;44(3):187-213. doi:10.1016/S0039-6257(99)00101-0

65. Nagy E V., Toth J, Kaldi I, et al. Graves' ophthalmopathy: Eye muscle involvement in patients with diplopia. *Eur J Endocrinol*. 2000;142(6):591-597. doi:10.1530/eje.0.1420591

9

66. Fraser CL, Skalicky SE, Gurbaxani A, McCluskey P. Ocular myositis. *Curr Allergy Asthma Rep*. 2013;13(3):315-321. doi:10.1007/s11882-012-0319-7

67. Goto H, Takahira M, Azumi A. Diagnostic criteria for IgG4-related ophthalmic disease. *Jpn J Ophthalmol*. 2015;59(1). doi:10.1007/s10384-014-0352-2

68. Montagnese F, Wenninger S, Schoser B. "Orbiting around" the orbital myositis: clinical features, differential diagnosis and therapy. *J Neurol*. 2016;263(4):631-640. doi:10.1007/s00415-015-7926-x

69. Gladstone JP, Dodick DW. Painful ophthalmoplegia: Overview with a focus on Tolosa-Hunt syndrome. *Curr Pain Headache Rep*. 2004;8(4):321-329. doi:10.1007/s11916-004-0016-x

70. Nishikawa N, Kawaguchi Y, Konno A, Kitani Y, Takei H, Yanagi Y. Primary isolated amyloidosis in the extraocular muscle as a rare cause of ophthalmoplegia: A case report and literature review. *Am J Ophthalmol Case Rep*. 2021;22:101052. doi:10.1016/j.ajoc.2021.101052

71. Jenkins PO, Soper C, Mackinnon AD, O'Sullivan E, Nitkunan A. Systemic lupus erythematosus presenting as orbital myositis. *Neuro-Ophthalmology*. 2014;38(5):264-267. doi:10.3109/01658107.2014.923915

72. Chan AJ, Rai AS, Lake S. Orbital myositis in systemic lupus erythematosus: A case report and literature review. *Eur J Rheumatol*. 2020;7(3):135-137. doi:10.5152/eurjrheum.2020.19217

73. Kim JS, Scawn RL, Lee BW, Lin JH, Korn BS, Kikkawa DO. Masquerading Orbital Sarcoidosis with Isolated Extraocular Muscle Involvement. *Open Ophthalmol J*. 2016;10(1):140. doi:10.2174/1874364101610010140

74. Pimentel R, Lago P, Pedroto I. Recurrent orbital myositis as an extra-intestinal manifestation of Crohn's disease. *J Crohns Colitis*. 2012;6(9):958-959. doi:10.1016/j.crohns.2012.05.018

75. Ramalho J, Castillo M. Imaging of orbital myositis in Crohn's disease. *Clin Imaging*. 2008;32(3):227-229. doi:10.1016/j.clinimag.2007.09.012

76. Bourikas LA, Roussomoustakaki M, Papadaki E, et al. A case of orbital myositis preceding the intestinal symptoms of Crohn's disease. *J Crohns Colitis*. 2010;4(3):349-350. doi:10.1016/j.crohns.2010.05.005

77. McNab AA. Orbital myositis: A comprehensive review and reclassification. *Ophthalmic Plast Reconstr Surg*. Published online 2020:109-117. doi:10.1097/IOP.0000000000001429

78. Nair AG, Patil-Chhablani P, Venkatramani D V., Gandhi RA. Ocular myasthenia gravis: A review. *Indian J Ophthalmol*. 2014;62(10):985-991. doi:10.4103/0301-4738.145987

79. Jeannet PY, Bassez G, Eymard B, et al. *Clinical and Histologic Findings in Autosomal Centronuclear Myopathy*. Vol 62.; 2004. doi:10.1212/01.WNL.0000124388.67003.56

80. Thornton CA. Myotonic dystrophy. *Neurol Clin*. 2014;32(3):705-719. doi:10.1016/j.ncl.2014.04.011

81. Choi SH, Yang HK, Hwang JM, Park KS. Ocular Findings of Myotonic Dystrophy Type 1 in the Korean Population. *Graefe's Archive for Clinical and Experimental Ophthalmology*. 2016;254(6):1189-1193. doi:10.1007/s00417-016-3266-5

82. Thiriez C, Vignal C, Papeix C, Yaici S, Vidailhet M, Roze E. Ophthalmoplegia as the presenting muscle-related manifestation of myotonic dystrophy. *Rev Neurol (Paris)*. 2010;166(5):538-541. doi:10.1016/j.neurol.2009.12.004

83. Van Der Beek NAME, De Vries JM, Hagemans MLC, et al. Clinical features and predictors for disease natural progression in adults with Pompe disease: A nationwide prospective observational study. *Orphanet J Rare Dis*. 2012;7(1):88. doi:10.1186/1750-1172-7-88

84. Fischer MD, Budak MT, Bakay M, et al. Definition of the unique human extraocular muscle allotype by expression profiling. *Physiol Genomics*. 2005;22:283-291. doi:10.1152/physiolgenomics.00158.2004

85. Burke G, Cossins J, Maxwell S, et al. Rapsyn mutations in hereditary myasthenia: Distinct early- and late-onset phenotypes. *Neurology*. 2003;61(6):826-828. doi:10.1212/01.WNL.0000085865.55513.AE

86. Finsterer J. Congenital myasthenic syndromes. *Orphanet J Rare Dis*. 2019;14(1):1-22. doi:10.1186/s13023-019-1025-5

87. Ferreira TA, Saraiva P, Genders SW, Buchem M v., Luyten GPM, Beenakker JW. CT and MR imaging of orbital inflammation. *Neuroradiology*. 2018;60(12):1253-1266. doi:10.1007/s00234-018-2103-4

88. Lakerveld M, van der Gijp A. Orbital Muscle Enlargement: What if It's Not Graves' Disease? *Curr Radiol Rep*. 2022;10(2):9-19. doi:10.1007/s40134-022-00392-y

89. Tiegs-Heiden CA, Eckel LJ, Hunt CH, et al. Immunoglobulin G4-related disease of the orbit: Imaging features in 27 patients. *American Journal of Neuroradiology*. 2014;35(7):1393-1397. doi:10.3174/ajnr.A3865

90. Garau LM, Guerrieri D, De Cristofaro F, Bruscolini A, Panzironi G. Extraocular muscle sampled volume in Graves' orbitopathy using 3-T fast spin-echo MRI with iterative decomposition of water and fat sequences. *Acta Radiol Open*. 2018;7(6):205846011878089. doi:10.1177/2058460118780892

91. Lennerstrand G, Tian S, Isberg B, et al. Magnetic resonance imaging and ultrasound measurements of extraocular muscles in thyroid-associated ophthalmopathy at different stages of the disease. *Acta Ophthalmol Scand*. 2007;85(2):192-201. doi:10.1111/j.1600-0420.2006.00807.x

92. Culver EL, Salmon JF, Frith P, Travis SPL. Recurrent posterior scleritis and orbital myositis as extra-intestinal manifestations of Crohn's disease: Case report and systematic literature review. *J Crohns Colitis*. 2008;2(4):337-342. doi:10.1016/j.crohns.2008.06.002

93. Pitceathly RDS, Morrow JM, Sinclair CDJ, et al. Extra-ocular muscle MRI in genetically-defined mitochondrial disease. *Eur Radiol*. 2016;26(1):130-137. doi:10.1007/s00330-015-3801-5

94. Lessell S, Coppeto J, Samet S. Ophthalmoplegia in myotonic dystrophy. *Am J Ophthalmol*. 1971;71(6):1231-1235. doi:10.1016/0002-9394(71)90968-8

95. Demer JL, Clark RA, Engle EC. Magnetic resonance imaging evidence for widespread orbital dysinnervation in congenital fibrosis of extraocular muscles due to mutations in KIF21A. *Invest Ophthalmol Vis Sci*. 2005;46(2):530-539. doi:10.1167/iovs.04-1125

96. Razek AAKA, Maher H, Kasem MA, Helmy E. Imaging of congenital cranial dysinnervation disorders: What radiologist wants to know? *Clin Imaging*. 2021;71:106-116. doi:10.1016/j.clinimag.2020.10.055

97. Chan JW, Orrison WW. Ocular myasthenia: A rare presentation with MuSK antibody and bilateral extraocular muscle atrophy [6]. *British Journal of Ophthalmology*. 2007;91(6):842-843. doi:10.1136/bjo.2006.108498

9

98. Ricciardi D, Todisco V, Tedeschi G, Cirillo G. Anti-MuSK ocular myasthenia with extrinsic ocular muscle atrophy: a new clinical phenotype? *Neurological Sciences*. 2020;41(1):221-223. doi:10.1007/s10072-019-04038-4

99. Keene KR, van Vught L, van de Velde NM, et al. The feasibility of quantitative MRI of extra-ocular muscles in myasthenia gravis and Graves' orbitopathy. *NMR Biomed*. 2021;34(1):e4407. doi:10.1002/nbm.4407

100. Pakdaman MN. Orbital inflammatory disease: Pictorial review and differential diagnosis. *World J Radiol*. 2014;6(4):106. doi:10.4329/wjr.v6.i4.106

101. Ding ZX, Lip G, Chong V. Idiopathic orbital pseudotumour. *Clin Radiol*. 2011;66(9):886-892. doi:10.1016/j.crad.2011.03.018

102. Tortora F, Cirillo M, Ferrara M, et al. *Disease Activity in Graves' Ophthalmopathy: Diagnosis with Orbital MR Imaging and Correlation with Clinical Score*. Vol 26.; 2013. doi:10.1177/197140091302600509

103. Mombaerts I, Rose GE, Garrity JA. Orbital inflammation: Biopsy first. *Surv Ophthalmol*. 2016;61(5):664-669. doi:10.1016/j.survophthal.2016.03.002

104. Lueangaram S, Tritanon O, Siriyotha S, et al. Radiological characteristics of extraocular muscles in myasthenia gravis patients with ocular manifestations: A case-control study. *Clinical Ophthalmology*. 2021;15:2279-2285. doi:10.2147/OPTH.S280508

105. Kirsch E, Hammer B, von Arx G. Graves' orbitopathy: Current imaging procedures. *Swiss Med Wkly*. 2009;139(43-44):618-623. doi:10.4414/smw.2009.12741

106. Dik WA, Virakul S, van Steensel L. Current perspectives on the role of orbital fibroblasts in the pathogenesis of Graves' ophthalmopathy. *Exp Eye Res*. 2016;142:83-91. doi:10.1016/j.exer.2015.02.007

107. Potgieser PW, de Win MMML, Wiersinga WM, Mourits MP. Natural Course of Mild Graves Orbitopathy: Increase of Orbital Fat But Decrease of Muscle Volume With Increased Muscle Fatty Degeneration During a 4-Year Follow-Up. *Ophthalmic Plast Reconstr Surg*. 2019;35(5):456-460. doi:10.1097/IOP.0000000000001319

108. Sogabe Y, Ohshima KI, Azumi A, et al. Location and frequency of lesions in patients with IgG4-related ophthalmic diseases. *Graefe's Archive for Clinical and Experimental Ophthalmology*. 2014;252(3):531-538. doi:10.1007/s00417-013-2548-4

109. Fischer D, Herasse M, Bitoun M, et al. Characterization of the muscle involvement in dynamin 2-related centronuclear myopathy. *Brain*. 2006;129(6):1463-1469. doi:10.1093/brain/awl071

110. De Meel RHP, Raadsheer WF, Van Zwet EW, Tannemaat MR, Verschuuren JJGM. Ocular Weakness in Myasthenia Gravis: Changes in Affected Muscles are a Distinct Clinical Feature. *J Neuromuscul Dis*. 2019;6(3):369-376. doi:10.3233/JND-190407

111. Almog Y, Ben-David M, Nemet AY. Inferior oblique muscle paresis as a sign of myasthenia gravis. In: *Journal of Clinical Neuroscience*. Vol 25. J Clin Neurosci; 2016:50-53. doi:10.1016/j.jocn.2015.08.026

112. Cleary M, Williams GJ, Metcalfe RA. The pattern of extra-ocular muscle involvement in ocular myasthenia. *Strabismus*. 2008;16(1):11-18. doi:10.1080/15569520701830992

113. Young JD, Leavitt JA. Lambert-Eaton myasthenic syndrome: Ocular signs and symptoms. *Journal of Neuro-Ophthalmology*. 2016;36(1):20-22. doi:10.1097/WNO.0000000000000258

114. Ryu WY, Kim YH, Yoon BA, Park HT, Bae JS, Kim JK. Pattern of extraocular muscle involvements in miller fisher syndrome. *Journal of Clinical Neurology (Korea)*. 2019;15(3):308-312. doi:10.3988/jcn.2019.15.3.308

115. Isen DR, Kline LB. Neuro-ophthalmic manifestations of wernicke encephalopathy. *Eye Brain*. 2020;12:49-60. doi:10.2147/EB.S234078

116. Yellin H. Unique intrafusal and extraocular muscle fibers exhibiting dual actomyosin ATPase activity. *Exp Neurol*. 1969;25(1):153-163. doi:10.1016/0014-4886(69)90078-8

117. Liu JX, Pedrosa Domellöf F. A novel type of multiterminal motor endplate in human extraocular muscles. *Invest Ophthalmol Vis Sci*. 2018;59(1):539-548. doi:10.1167/iovs.17-22554

118. Bishop KN, McClung JR, Goldberg SJ, Shall MS. Anatomic and physiological characteristics of the ferret lateral rectus muscle and abducens nucleus. *J Appl Physiol*. 2007;103(5):1706-1714. doi:10.1152/japplphysiol.00580.2007

119. Sekulic-Jablanovic M, Ullrich ND, Goldblum D, Palmowski-Wolfe A, Zorzato F, Treves S. Functional characterization of orbicularis oculi and extraocular muscles. *Journal of General Physiology*. 2016;147(5):395-406. doi:10.1085/jgp.201511542

120. Sekulic-Jablanovic M, Palmowski-Wolfe A, Zorzato F, Treves S. Characterization of excitation-contraction coupling components in human extraocular muscles. *Biochemical Journal*. 2015;466(1):29-36. doi:10.1042/BJ20140970

121. McLoon LK, Rowe J, Wirtschafter J, McCormick KM. Continuous myofiber remodeling in uninjured extraocular myofibers: Myonuclear turnover and evidence for apoptosis. *Muscle Nerve*. 2004;29(5):707-715. doi:10.1002/mus.20012

122. Kjellgren D, Thornell LE, Andersen J, Pedrosa-Domellöf F. Myosin heavy chain isoforms in human extraocular muscles. *Invest Ophthalmol Vis Sci*. 2003;44(4):1419-1425. doi:10.1167/iovs.02-0638

123. Kitamura K, Cho KH, Jang HS, Murakami G, Yamamoto M, Abe S ichi. Distance between intramuscular nerve and artery in the extraocular muscles: a preliminary immunohistochemical study using elderly human cadavers. *Surgical and Radiologic Anatomy*. 2017;39(1):3-9. doi:10.1007/s00276-016-1642-9

124. Morrow JM, Sinclair CDJ, Fischmann A, et al. MRI biomarker assessment of neuromuscular disease progression: A prospective observational cohort study. *Lancet Neurol*. 2016;15(1):65-77. doi:10.1016/S1474-4422(15)00242-2

125. Europa TA, Nel M, Heckmann JM. A review of the histopathological findings in myasthenia gravis: Clues to the pathogenesis of treatment-resistance in extraocular muscles. *Neuromuscular Disorders*. 2019;29(5):381-387. doi:10.1016/j.nmd.2019.03.009

126. Ferreira TA, Fonk LG, Jaarsma-Coes MG, van Haren GGR, Marinkovic M, Beenakker JWM. MRI of uveal melanoma. *Cancers (Basel)*. 2019;11(3). doi:10.3390/cancers11030377

127. Jaarsma-Coes MG, Marinkovic M, Astreinidou E, et al. Measuring eye deformation between planning and proton beam therapy position using magnetic resonance imaging. *Phys Imaging Radiat Oncol*. 2020;16:33-36. doi:10.1016/j.phro.2020.09.010

128. Chardon JW, Díaz-Manera J, Tasca G, et al. MYO-MRI diagnostic protocols in genetic myopathies. *Neuromuscular Disorders*. 2019;29(11):827-841. doi:10.1016/j.nmd.2019.08.011

9

129. Howard JF, Vu T, Mantegazza R, et al. MUS MGFA Abstracts: MRI OF THE EXTRA-OCULAR MUSCLES IN MYASTHENIA GRAVIS SHOW SMALL VOLUME AND FAT FRACTION INCREASES. *Muscle Nerve*. 2022;65:S1-S47. doi:10.1002/MUS.27540

130. von Haehling S, Morley JE, Coats AJS, Anker SD. Ethical guidelines for publishing in the journal of cachexia, sarcopenia and muscle: update 2017. *J Cachexia Sarcopenia Muscle*. 2017;8(6):1081-1083. doi:10.1002/jcsm.12261

131. Nadaj-Pakleza A, Richard P, Łusakowska A, et al. Oculopharyngeal muscular dystrophy: Phenotypic and genotypic characteristics of 9 Polish patients. *Neurol Neurochir Pol*. 2009;43(2):113-120.

132. Troost BT, Daroff RB. The ocular motor defects in progressive supranuclear palsy. *Ann Neurol*. 1977;2(5):397-403. doi:10.1002/ana.410020509

133. Straube A, Witt TN. *Oculo-Bulbar Myasthenic Symptoms as the Sole Sign of Tumour Involving or Compressing the Brain Stem*. Vol 237.; 1990. doi:10.1007/BF00315661

134. Liu Y, Wang M, Bian X, et al. Proposed modified diagnostic criteria for recurrent painful ophthalmoplegic neuropathy: Five case reports and literature review. *Cephalalgia*. 2020;40(14):1657-1670. doi:10.1177/0333102420944872

135. Martin TJ. Horner Syndrome: A Clinical Review. *ACS Chem Neurosci*. 2018;9(2):177-186. doi:10.1021/acschemneuro.7b00405

136. Jain R, Sawhney S, Koul RL, Chand P. Tolosa-Hunt syndrome: MRI appearances. *J Med Imaging Radiat Oncol*. 2008;52(5):447-451. doi:10.1111/j.1440-1673.2008.01988.x

137. Schoser B, Eymard B, Datt J, Mantegazza R. Lambert–Eaton myasthenic syndrome (LEMS): a rare autoimmune presynaptic disorder often associated with cancer. *J Neurol*. 2017;264(9):1854-1863. doi:10.1007/s00415-017-8541-9

138. Wirtz PW, Sotodeh M, Nijnuis M, et al. Difference in distribution of muscle weakness between myasthenia gravis and the Lambert-Eaton myasthenic syndrome. *J Neurol Neurosurg Psychiatry*. 2002;73(6):766-768. doi:10.1136/jnnp.73.6.766

139. Luigetti M, Sabatelli M. Cranial botulism. *Neuromuscular Disorders*. 2012;22(11):995-996. doi:10.1016/j.nmd.2012.05.009

140. Chatham-Stephens K, Fleck-Derderian S, Johnson SD, Sobel J, Rao AK, Meaney-Delman D. Clinical Features of Foodborne and Wound Botulism: A Systematic Review of the Literature, 1932-2015. *Clinical Infectious Diseases*. 2017;66(suppl_1):S11-S16. doi:10.1093/cid/cix811

141. Azam L, McIntosh JM. Alpha-conotoxins as pharmacological probes of nicotinic acetylcholine receptors. *Acta Pharmacol Sin*. 2009;30(6):771-783. doi:10.1038/aps.2009.47

142. Olsen TG, Heegaard S. Orbital lymphoma. *Surv Ophthalmol*. 2019;64(1):45-66. doi:10.1016/j.survophthal.2018.08.002

143. Claytor B, Li Y. Challenges in diagnosing coexisting ocular myasthenia gravis and thyroid eye disease. *Muscle Nerve*. 2021;63(5):631-639. doi:10.1002/mus.27118

144. Melcescu E, Horton WB, Kim D, et al. Graves Orbitopathy: Update on Diagnosis and Therapy. *South Med J*. 2014;107(1):34-43. doi:10.1097/SMJ.0000000000000038

145. Marinò M, Ionni I, Lanzolla G, et al. Orbital diseases mimicking graves' orbitopathy: a long-standing challenge in differential diagnosis. *J Endocrinol Invest*. 2020;43(4):401-411. doi:10.1007/s40618-019-01141-3

146. Xian J, Zhang Z, Wang Z, et al. Value of MR imaging in the differentiation of benign and malignant orbital tumors in adults. *Eur Radiol*. 2010;20(7):1692-1702. doi:10.1007/s00330-009-1711-0

147. Fatima Z, Ichikawa T, Ishigame K, et al. Orbital masses: The usefulness of diffusion-weighted imaging in lesion categorization. *Clin Neuroradiol*. 2014;24(2):129-134. doi:10.1007/s00062-013-0234-x

148. El-Sayed Mojahed M, Thabet EM, El-Khateeb MG, Elsayed Morgan A. Ocular vestibular evoked myogenic potential in patients with myasthenia gravis: A prospective clinical study. *Auris Nasus Larynx*. 2018;45(3):407-411. doi:10.1016/j.anl.2017.06.001

149. Decock CE, De Baere EE, Bauters W, et al. Insights into levator muscle dysfunction in a cohort of patients with molecularly confirmed blepharophimosis-ptosis-epicanthus inversus syndrome using high-resolution imaging, anatomic examination, and histopathologic examination. *Archives of Ophthalmology*. 2011;129(12):1564-1569. doi:10.1001/archophthalmol.2011.348

150. Xia S, Li RL, Li YP, Qian XH, Chong V, Qi J. MRI findings in Duane's ocular retraction syndrome. *Clin Radiol*. 2014;69(5). doi:10.1016/j.crad.2013.12.010

151. Thacker NM, Velez FG, Demer JL, Rosenbaum AL. Superior oblique muscle involvement in thyroid ophthalmopathy. *Journal of AAPOS*. 2005;9(2):174-178. doi:10.1016/j.jaapos.2004.12.005

152. Kupersmith MJ, Latkany R, Homel P. Development of generalized disease at 2 years in patients with ocular myasthenia gravis. *Arch Neurol*. 2003;60(2):243-248. doi:10.1001/archneur.60.2.243

153. Padua L, Stalberg E, Lomonaco M, Evoli A, Batocchi A, Tonali P. SFEMG in ocular myasthenia gravis diagnosis. *Clinical Neurophysiology*. 2000;111(7):1203-1207. doi:10.1016/S1388-2457(00)00307-2

154. Venhovens J, Meulstee J, Verhagen WIM. Vestibular evoked myogenic potentials (VEMPs) in central neurological disorders. *Clinical Neurophysiology*. 2016;127(1):40-49. doi:10.1016/j.clinph.2014.12.021

155. Rosengren SM, Colebatch JG, Straumann D, Weber KP. Why do oVEMPs become larger when you look up? Explaining the effect of gaze elevation on the ocular vestibular evoked myogenic potential. *Clinical Neurophysiology*. 2013;124(4):785-791. doi:10.1016/j.clinph.2012.10.012

156. Wirth MA, Valko Y, Rosengren SM, et al. Repetitive ocular vestibular evoked myogenic potential stimulation for the diagnosis of myasthenia gravis: Optimization of stimulation parameters. *Clinical Neurophysiology*. 2019;130(7):1125-1134. doi:10.1016/j.clinph.2019.03.033

157. Oh SJ. Distinguishing features of the repetitive nerve stimulation test between lambert-eaton myasthenic syndrome and myasthenia gravis, 50-year reappraisal. *J Clin Neuromuscul Dis*. 2017;19(2):66-75. doi:10.1097/CND.0000000000000190

158. Reijntjes RH, Potters W V., Kerkhof FI, et al. Deriving reference values for nerve conduction studies from existing data using mixture model clustering. *Clinical Neurophysiology*. 2021;132(8):1820-1829. doi:10.1016/j.clinph.2021.04.013

159. de Meel RHP, Tannemaat MR, Verschuuren JJGM. Heterogeneity and shifts in distribution of muscle weakness in myasthenia gravis. *Neuromuscular Disorders*. 2019;29(9):664-670. doi:10.1016/j.nmd.2019.07.006

9

160. Fortin E, Cestari DM, Weinberg DH. Ocular myasthenia gravis: An update on diagnosis and treatment. *Curr Opin Ophthalmol*. 2018;29(6):477-484. doi:10.1097/ICU.0000000000000526

161. Grob D, Brunner N, Namba T, Pagala M. Lifetime course of myasthenia gravis. *Muscle Nerve*. 2008;37(2):141-149. doi:10.1002/mus.20950

162. Smith S V., Lee AG. Update on Ocular Myasthenia Gravis. *Neurol Clin*. 2017;35(1):115-123. doi:10.1016/j.ncl.2016.08.008

163. Claytor B, Li Y. Challenges in diagnosing coexisting ocular myasthenia gravis and thyroid eye disease. *Muscle Nerve*. 2021;63(5):631-639. doi:10.1002/mus.27118

164. De Meel RHP, Raadsheer WF, Van Zwet EW, Tannemaat MR, Verschuuren JJGM. Ocular Weakness in Myasthenia Gravis: Changes in Affected Muscles are a Distinct Clinical Feature. *J Neuromuscul Dis*. 2019;6(3):369-376. doi:10.3233/JND-190407

165. Walsh FB. Myasthenia Gravis and Its Ocular Signs: A Review. *Trans Am Ophthalmol Soc*. 1943;41:556.

166. Jellema HM, Braaksma-Besselink Y, Limpens J, Von Arx G, Wiersinga WM, Mourits MP. Proposal of success criteria for strabismus surgery in patients with Graves' orbitopathy based on a systematic literature review. *Acta Ophthalmol*. 2015;93(7):601-609. doi:10.1111/aos.12717

167. Dysli M, Fierz FC, Rappoport D, et al. Divergence bias in Hess compared to Harms screen strabismus testing. *Strabismus*. 2021;29(1):1-9. doi:10.1080/09273972.2020.1871382

168. Coll GE, Demer JL. The edrophonium-Hess screen test in the diagnosis of ocular myasthenia gravis. *Am J Ophthalmol*. 1992;114(4):489-493. doi:10.1016/S0002-9394(14)71863-X

169. Melcescu E, Horton WB, Kim D, et al. Graves Orbitopathy: Update on Diagnosis and Therapy. *South Med J*. 2014;107(1):34-43. doi:10.1097/SMJ.0000000000000038

170. McClelland C, Manousakis G, Lee MS. Progressive External Ophthalmoplegia. *Curr Neurol Neurosci Rep*. 2016;16(6):1-10. doi:10.1007/s11910-016-0652-7

171. Fischmann A. Oculopharyngeal muscular dystrophy. *Neuromuscular Imaging*. Published online January 1, 2013:305-311. doi:10.1007/978-1-4614-6552-2_24

172. Pineles SL, Rosenbaum AL, Demer JL. Changes in binocular alignment after surgery for concomitant and pattern intermittent exotropia. *Strabismus*. 2008;16(2):57-63. doi:10.1080/09273970802020292

173. Ben Simon GJ, Syed AM, Lee S, et al. Strabismus after Deep Lateral Wall Orbital Decompression in Thyroid-Related Orbitopathy Patients Using Automated Hess Screen. *Ophthalmology*. 2006;113(6):1050-1055. doi:10.1016/j.ophtha.2006.02.015

174. Flanders M. Restrictive strabismus: Diagnosis and management. *American Orthoptic Journal*. 2014;64(1):54-63. doi:10.3368/aoj.64.1.54

175. Aylward GW, McCarry B, Kousoulides L, Lee JP, Fells P. A scoring method for hess charts. *Eye (Basingstoke)*. 1992;6(6):659-661. doi:10.1038/eye.1992.141

176. Cogan DG, Yee RD, Gittinger J. Rapid eye movements in myasthenia gravis. I. Clinical observations. *Arch Ophthalmol*. 1976;94(7):1083-1085. doi:10.1001/ARCHOPHT.1976.03910040003001

177. Benatar M. A systematic review of diagnostic studies in myasthenia gravis. *Neuromuscular Disorders*. 2006;16(7):459-467. doi:10.1016/j.nmd.2006.05.006

178. O'hare M, Doughty C. Update on ocular myasthenia gravis. *Semin Neurol*. 2019;39(6):749-760. doi:10.1055/s-0039-1700527

179. de Meel RHP, Keene KR, Wirth MA, et al. Repetitive ocular vestibular evoked myogenic potentials in myasthenia gravis. *Neurology*. 2020;94(16):E1693-E1701. doi:10.1212/WNL.0000000000009306

180. Valko Y, Rosengren SM, Jung HH, Straumann D, Landau K, Weber KP. Ocular vestibular evoked myogenic potentials as a test for myasthenia gravis. *Neurology*. 2016;86(7):660-668. doi:10.1212/WNL.0000000000002383

181. Kocak GS, Tütüncü M, Adatepe NU, et al. A novel diagnostic method for myasthenia gravis. *Muscle Nerve*. 2021;64(3):328-335. doi:10.1002/mus.27353

182. Cleary M, Williams GJ, Metcalfe RA. The pattern of extra-ocular muscle involvement in ocular myasthenia. *Strabismus*. 2008;16(1):11-18. doi:10.1080/15569520701830992

183. Oosterhuis HJGH. The ocular signs and symptoms of myasthenia gravis. *Documenta Ophthalmologica*. 1982;52(2):363-378. doi:10.1007/BF01675867

184. Almog Y, Ben-David M, Nemet AY. Inferior oblique muscle paresis as a sign of myasthenia gravis. *Journal of Clinical Neuroscience*. 2016;25:50-53. doi:10.1016/j.jocn.2015.08.026

185. Akan O, Baysal-Kirac L. Ophthalmologic manifestations in myasthenia gravis: presentation and prognosis. *Acta Neurol Belg*. 2021;121(5):1131-1140. doi:10.1007/s13760-020-01556-3

186. McClelland C, Manousakis G, Lee MS. Progressive External Ophthalmoplegia. *Curr Neurol Neurosci Rep*. 2016;16(6). doi:10.1007/s11910-016-0652-7

187. Renard D, Ferraro A, Lorenzini MC, et al. Orthoptic and video-oculographic analyses in oculopharyngeal muscular dystrophy. *Muscle Nerve*. 2015;52(4):554-558. doi:10.1002/mus.24600

188. Shechtman D, Shallo-Hoffmann J, Rumsey J, Riordan-Eva P, Hardigan P. Maximum angle of ocular duction during visual fixation as a function of age. *Strabismus*. 2005;13(1):21-26. doi:10.1080/09273970590901810

189. Hering E. *The Theory of Binocular Vision. New York: Plenum Press;*; 1977.

190. Melson AT, McClelland CM, Lee MS. Ocular myasthenia gravis: Updates on an elusive target. *Curr Opin Neurol*. 2020;33(1):55-61. doi:10.1097/WCO.0000000000000775

191. Howard JF, Bril V, Vu T, et al. Safety, efficacy, and tolerability of efgartigimod in patients with generalised myasthenia gravis (ADAPT): a multicentre, randomised, placebo-controlled, phase 3 trial. *Lancet Neurol*. 2021;20(7):526-536. doi:10.1016/S1474-4422(21)00159-9

192. Europa TA, Nel M, Heckmann JM. A review of the histopathological findings in myasthenia gravis: Clues to the pathogenesis of treatment-resistance in extraocular muscles. *Neuromuscular Disorders*. 2019;29(5):381-387. doi:10.1016/j.nmd.2019.03.009

193. Fortin E, Cestari DM, Weinberg DH. Ocular myasthenia gravis: An update on diagnosis and treatment. *Curr Opin Ophthalmol*. 2018;29(6):477-484. doi:10.1097/ICU.0000000000000526

194. De Meel RHP, Raadsheer WF, Van Zwet EW, Tannemaat MR, Verschuuren JJGM. Ocular Weakness in Myasthenia Gravis: Changes in Affected Muscles are a Distinct Clinical Feature. *J Neuromuscul Dis*. 2019;6(3):369-376. doi:10.3233/JND-190407

9

195. Weber KP, Rappoport D, Dysli M, et al. Strabismus Measurements with Novel Video Goggles. *Ophthalmology*. 2017;124:1849-1856. doi:10.1016/j.ophtha.2017.06.020

196. Wary C, Azzabou N, Giraudeau C, et al. Quantitative NMRI and NMRS identify augmented disease progression after loss of ambulation in forearms of boys with Duchenne muscular dystrophy. *NMR Biomed*. 2015;28(9):1150-1162. doi:10.1002/nbm.3352

197. Willcocks RJ, Arpan IA, Forbes SC, et al. Longitudinal measurements of MRI-T2 in boys with Duchenne muscular dystrophy: Effects of age and disease progression. *Neuromuscular Disorders*. 2014;24(5):393-401. doi:10.1016/j.nmd.2013.12.012

198. Klupp E, Weidlich D, Schlaeger S, et al. B1-insensitive T2 mapping of healthy thigh muscles using a T2-prepared 3D TSE sequence. *PLoS One*. 2017;12(2):e0171337. doi:10.1371/journal.pone.0171337

199. Janiczek RL, Gambarota G, Sinclair CDJ, et al. Simultaneous T2 and lipid quantitation using IDEAL-CPMG. *Magn Reson Med*. 2011;66(5):1293-1302. doi:10.1002/mrm.22916

200. Forbes SC, Walter GA, Rooney WD, et al. Skeletal muscles of ambulant children with Duchenne muscular dystrophy: Validation of multicenter study of evaluation with MR imaging and MR spectroscopy. *Radiology*. 2013;269(1):198-207. doi:10.1148/radiol.13121948

201. Poon CS, Henkelman RM. Practical T2 quantitation for clinical applications. *Journal of Magnetic Resonance Imaging*. 1992;2(5):541-553. doi:10.1002/jmri.1880020512

202. Ben-Eliezer N, Sodickson DK, Block KT. Rapid and accurate T2 mapping from multi-spin-echo data using bloch-simulation-based reconstruction. *Magn Reson Med*. 2015;73(2):809-817. doi:10.1002/mrm.25156

203. Carlier PG. Global T2 versus water T2 in NMR imaging of fatty infiltrated muscles: Different methodology, different information and different implications. *Neuromuscular Disorders*. 2014;24(5):390-392. doi:10.1016/j.nmd.2014.02.009

204. Delfaut EM, Beltran J, Johnson G, Rousseau J, Marchandise X, Cotten A. Fat suppression in MR imaging: Techniques and pitfalls. *Radiographics*. 1999;19(2):373-382. doi:10.1148/radiographics.19.2.g99mr03373

205. Wokke BH, Van Den Bergen JC, Hooijmans MT, Verschuuren JJ, Niks EH, Kan HE. T2 relaxation times are increased in Skeletal muscle of DMD but not BMD patients. *Muscle Nerve*. 2016;53(1):38-43. doi:10.1002/mus.24679

206. Dula AN, Gochberg DF, Does MD. Optimal echo spacing for multi-echo imaging measurements of Bi-exponential T2 relaxation. *Journal of Magnetic Resonance*. 2009;196(2):149-156. doi:10.1016/j.jmr.2008.11.002

207. Azzabou N, De Sousa PL, Caldas E, Carlier PG. Validation of a generic approach to muscle water T2 determination at 3T in fat-infiltrated skeletal muscle. *Journal of Magnetic Resonance Imaging*. 2015;41(3):645-653. doi:10.1002/jmri.24613

208. Mankodi A, Azzabou N, Bulea T, et al. Skeletal muscle water T2 as a biomarker of disease status and exercise effects in patients with Duchenne muscular dystrophy. *Neuromuscular Disorders*. 2017;27(8):705-714. doi:10.1016/j.nmd.2017.04.008

209. McPhee KC, Wilman AH. Transverse relaxation and flip angle mapping: Evaluation of simultaneous and independent methods using multiple spin echoes. *Magn Reson Med*. 2017;77(5):2057-2065. doi:10.1002/mrm.26285

210. Lebel RM, Wilman AH. Transverse relaxometry with stimulated echo compensation. *Magn Reson Med*. 2010;64(4):1005-1014. doi:10.1002/mrm.22487

211. Weigel M. Extended phase graphs: Dephasing, RF pulses, and echoes - Pure and simple. *Journal of Magnetic Resonance Imaging*. 2015;41(2):266-295. doi:10.1002/jmri.24619

212. Kan HE, Scheenen TWJ, Wohlgemuth M, et al. Quantitative MR imaging of individual muscle involvement in facioscapulohumeral muscular dystrophy. *Neuromuscular Disorders*. 2009;19(5):357-362. doi:10.1016/j.nmd.2009.02.009

213. Yao L, Gai N. Fat-corrected T2 measurement as a marker of active muscle disease in inflammatory myopathy. *American Journal of Roentgenology*. 2012;198(5):W475-W481. doi:10.2214/AJR.11.7113

214. Stokes AM, Feng Y, Mitropoulos T, Warren WS. Enhanced refocusing of fat signals using optimized multipulse echo sequences. *Magn Reson Med*. 2013;69(4):1044-1055. doi:10.1002/mrm.24340

215. Froeling M, Hughes E, Schlaffke L, Kan HE, Hollingsworth KG. The relation between fat calibration in multi-echo spin-echo water T2 mapping and STEAM fat T2 relaxation measurements. In: *Proceedings of the 27th Annual Meeting of ISMRM, Montréal, Canada*. ; 2019:1273.

216. Ren J, Dimitrov I, Sherry AD, Malloy CR. Composition of adipose tissue and marrow fat in humans by 1H NMR at 7 Tesla. *J Lipid Res*. 2008;49(9):2055-2062. doi:10.1194/jlr.D800010-JLR200

217. Hooijmans MT, Baligand C, Froeling M, et al. Multi-parametric {MR} shows increased T2 heterogeneity in fat infiltrated muscles in Becker Muscular Dystrophy. In: *Proc. Joint Annual Meeting ISMRM-ESMRMB, Paris, France*. ; 2018:816.

218. Otto LAM, Froeling M, Van Den Berg LH, Hendrikse J, van der Pol WL. Muscle MRI in a cross-sectional cohort of patients with Spinal Muscular Atrophy types 2-3. In: *Journal of Neuromuscular Diseases*. Vol 6. ; 2019:S54-S55.

219. Hooijmans MT, Niks EH, Burakiewicz J, et al. Non-uniform muscle fat replacement along the proximodistal axis in Duchenne muscular dystrophy. *Neuromuscular Disorders*. 2017;27(5):458-464. doi:10.1016/j.nmd.2017.02.009

220. Naarding K, Veeger T, Sardjoe Mishre A, et al. P.305MRI brachialis contractile cross-sectional area is correlated strongest to elbow flexion in non-ambulant Duchenne muscular dystrophy patients. In: *Neuromuscular Disorders*. Vol 29. ; 2019:S156. doi:10.1016/j.nmd.2019.06.419

221. Thomas LW. the Chemical Composition of Adipose Tissue of Man and Mice. *Q J Exp Physiol Cogn Med Sci*. 1962;47(2):179-188. doi:10.1113/expphysiol.1962.sp001589

222. Schlaeger S, Weidlich D, Klupp E, et al. Decreased water T2 in fatty infiltrated skeletal muscles of patients with neuromuscular diseases. *NMR Biomed*. 2019;32(8):e4111. doi:10.1002/nbm.4111

223. Arnold WD, Kassar D, Kissel JT. Spinal muscular atrophy: Diagnosis and management in a new therapeutic era. *Muscle Nerve*. 2015;51(2):157-167. doi:10.1002/mus.24497

224. Desguerre I, Mayer M, Leturcq F, Barbet JP, Gherardi RK, Christov C. Endomysial fibrosis in duchenne muscular dystrophy: A marker of poor outcome associated with macrophage alternative activation. *J Neuropathol Exp Neurol*. 2009;68(7):762-773. doi:10.1097/NEN.0b013e3181aa31c2

9

225. Saab G, Thompson RT, Marsh GD. Multicomponent T2 relaxation of in vivo skeletal muscle. *Magn Reson Med*. 1999;42(1):150-157. doi:10.1002/(SICI)1522-2594(199907)42:1<150::AID-MRM20>3.0.CO;2-5

226. Querleux B, Cornillon C, Jolivet O, Bittoun J. Anatomy and physiology of subcutaneous adipose tissue by in vivo magnetic resonance imaging and spectroscoy: Relationships with sex and presence of cellulite. *Skin Research and Technology*. 2002;8(2):118-124. doi:10.1034/j.1600-0846.2002.00331.x

227. Beekman R, Kuks JBM, Oosterhuis HJGH. Myasthenia gravis: Diagnosis and follow-up of 100 consecutive patients. *J Neurol*. 1997;244(2):112-118. doi:10.1007/s004150050059

228. Mazzoli M, Ariatti A, Valzania F, et al. Factors affecting outcome in ocular myasthenia gravis. *International Journal of Neuroscience*. 2018;128(1):15-24. doi:10.1080/00207454.2017.1344237

229. J. Smith T. TSHR as a therapeutic target in Graves' disease. *Expert Opin Ther Targets*. 2017;21(4):427-432. doi:10.1080/14728222.2017.1288215

230. Kung FP, Hung HC, Ou HY, Wu TJ. Graves' ophthalmopathy. *Journal of Internal Medicine of Taiwan*. 2012;23(1):9-20. doi:10.5005/jp/books/10258_7

231. De Abreu MR, Chung CB, Biswal S, Haghighi P, Hesselink J, Resnick D. Erdheim-Chester Disease: MR Imaging, Anatomic, and Histopathologic Correlation of Orbital Involvement. *American Journal of Neuroradiology*. 2004;25(4):627-630.

232. Das T, Roos JCP, Patterson AJ, Graves MJ, Murthy R. T2-relaxation mapping and fat fraction assessment to objectively quantify clinical activity in thyroid eye disease: an initial feasibility study. *Eye (Basingstoke)*. 2019;33(2):235-243. doi:10.1038/s41433-018-0304-z

233. Han E, Gold G, Stainsby J, Beaulieu J, Brittain J. *In-Vivo T1 and T2 Measurements of Muskoloskeletal Tussie at 3T and 1.5T*. Vol 166.; 2003.

234. Yushkevich PA, Piven J, Hazlett HC, et al. User-guided 3D active contour segmentation of anatomical structures: Significantly improved efficiency and reliability. *Neuroimage*. 2006;31(3):1116-1128. doi:10.1016/j.neuroimage.2006.01.015

235. Keene KR, Beenakker JWM, Hooijmans MT, et al. T2 relaxation-time mapping in healthy and diseased skeletal muscle using extended phase graph algorithms. *Magn Reson Med*. 2020;84(5):2656-2670. doi:10.1002/mrm.28290

236. Mourits MP, Prummel MF, Wiersinga WM, Koornneef L. Clinical activity score as a guide in the management of patients with Graves' ophthalmopathy. *Clin Endocrinol (Oxf)*. 1997;47(1):9-14. doi:10.1046/j.1365-2265.1997.2331047.x

237. Kiefer LS, Fabian J, Lorbeer R, et al. Inter- and intra-observer variability of an anatomical landmark-based, manual segmentation method by MRI for the assessment of skeletal muscle fat content and area in subjects from the general population. *British Journal of Radiology*. 2018;91(1089). doi:10.1259/bjr.20180019

238. Hiba B, Richard N, Hébert LJ, et al. Quantitative assessment of skeletal muscle degeneration in patients with myotonic dystrophy type 1 using MRI. *Journal of Magnetic Resonance Imaging*. 2012;35(3):678-685. doi:10.1002/jmri.22849

239. Hernando D, Sharma SD, Aliyari Ghasabeh M, et al. Multisite, multivendor validation of the accuracy and reproducibility of proton-density fat-fraction quantification at 1.5T and 3T using a fat–water phantom. *Magn Reson Med*. 2017;77(4):1516-1524. doi:10.1002/mrm.26228

240. Morrow JM, Sinclair CDJ, Fischmann A, et al. Reproducibility, and age, body-weight and gender dependency of candidate skeletal muscle MRI outcome measures in healthy volunteers. *Eur Radiol*. 2014;24(7):1610-1620. doi:10.1007/s00330-014-3145-6

241. Schlaffke L, Rehmann R, Rohm M, et al. Multi-center evaluation of stability and reproducibility of quantitative MRI measures in healthy calf muscles. *NMR Biomed*. 2019;32(9):e4119. doi:10.1002/nbm.4119

242. Hu HH, Kan HE. Quantitative proton MR techniques for measuring fat. *NMR Biomed*. 2013;26(12):1609-1629. doi:10.1002/nbm.3025

243. Liu CY, McKenzie CA, Yu H, Brittain JH, Reeder SB. Fat quantification with IDEAL gradient echo imaging: Correction of bias from T1 and noise. *Magn Reson Med*. 2007;58(2):354-364. doi:10.1002/mrm.21301

244. Forbes SC, Arora H, Willcocks RJ, et al. Upper and lower extremities in Duchenne muscular dystrophy evaluated with quantitative MRI and proton MR spectroscopy in a multicenter cohort. *Radiology*. 2020;295(3):616-625. doi:10.1148/radiol.2020192210

245. Higashiyama T, Iwasa M, Ohji M. Quantitative Analysis of Inflammation in Orbital Fat of Thyroid-associated Ophthalmopathy Using MRI Signal Intensity. *Sci Rep*. 2017;7(1). doi:10.1038/s41598-017-17257-6

246. Cros D, Harnden P, Pellissier JF, Serratrice G. Muscle hypertrophy in Duchenne muscular dystrophy - A pathological and morphometric study. *J Neurol*. 1989;236(1):43-47. doi:10.1007/BF00314217

247. Rautenbach RM, Pillay K, Murray ADN, Heckmann JM. Extraocular muscle findings in myasthenia gravis associated treatment-resistant ophthalmoplegia. *Journal of Neuro-Ophthalmology*. 2017;37(4):414-417. doi:10.1097/WNO.0000000000000534

248. Moon SY, Lee SS, Hong YH. Muscle atrophy in muscle-specific tyrosine kinase (MuSK)-related myasthenia gravis. *Journal of Clinical Neuroscience*. 2011;18(9):1274-1275. doi:10.1016/j.jocn.2011.01.010

249. Paz ML, Barrantes FJ. Autoimmune Attack of the Neuromuscular Junction in Myasthenia Gravis: Nicotinic Acetylcholine Receptors and Other Targets. *ACS Chem Neurosci*. 2019;10(5):2186-2194. doi:10.1021/acschemneuro.9b00041

250. Walters J. Muscle hypertrophy and pseudohypertrophy. *Pract Neurol*. 2017;17(5):369-379. doi:10.1136/practneurol-2017-001695

251. Tian S, Nishida Y, Isberg B, Lennerstrand G. MRI measurements of normal extraocular muscles and other orbital structures. *Graefe's Archive for Clinical and Experimental Ophthalmology*. 2000;238(5):393-404. doi:10.1007/s004170050370

252. Wong SH. Advocating Patient-Centred Research in Ocular Myasthenia Gravis (OMG): A Call for an OMG Research Consortium. *Frontiers in Ophthalmology*. 2022;0:35. doi:10.3389/FOPHT.2022.912805

253. Keene KR, de Nie JM, Brink MJ, et al. Diagnosing myasthenia gravis using orthoptic measurements: assessing extraocular muscle fatiguability. *J Neurol Neurosurg Psychiatry*. 2022;0:jnnp-2022-329859. doi:10.1136/JNNP-2022-329859

254. Nehrke K, Versluis MJ, Webb A, Börnert P. Volumetric B1 (+) mapping of the brain at 7T using DREAM. *Magn Reson Med*. 2014;71(1):246-256. doi:10.1002/MRM.24667

255. Bruenech JR, Kjellevold Haugen IB. How does the structure of extraocular muscles and their nerves affect their function? In: *Eye (Basingstoke)*. Vol 29. Nature Publishing Group; 2015:177-183. doi:10.1038/eye.2014.269

9

256. Spencer RF, Porter JD. Structural organization of the extraocular muscles. *Rev Oculomot Res*. 1988;2:33-79. Accessed February 15, 2021. https://pubmed.ncbi.nlm.nih.gov/3153651/

257. Haładaj R. Comparison of lateral and medial rectus muscle in human: an anatomical study with particular emphasis on morphology, intramuscular innervation pattern variations and discussion on clinical significance. *Surgical and Radiologic Anatomy*. 2020;42(5):607-616. doi:10.1007/s00276-019-02400-x

258. Ironside R. Progressive Exophthalmoplegia with Muscular Atrophy, Myasthenia, and Thyrotoxicosis. *J R Soc Med*. 1951;44(8):690-691. doi:10.1177/003591575104400812

259. Kornegay JN, Childers MK, Bogan DJ, et al. The Paradox of Muscle Hypertrophy in Muscular Dystrophy. *Phys Med Rehabil Clin N Am*. 2012;23(1):149-172. doi:10.1016/j.pmr.2011.11.014

260. Krampitz DE, Wolfe GI, Fleckenstein JL, Barohn RJ. Charcot-Marie-Tooth disease type 1A presenting as calf hypertrophy and muscle cramps. *Neurology*. 1998;51(5):1508-1509. doi:10.1212/WNL.51.5.1508

261. Jaarsma-Coes MG, Ferreira TA, van Houdt PJ, van der Heide UA, Luyten GPM, Beenakker JWM. Eye-specific quantitative dynamic contrast-enhanced MRI analysis for patients with intraocular masses. *MAGMA*. 2022;35(2):311-323. doi:10.1007/S10334-021-00961-W

262. Finlayson S, Morrow JM, Rodriguez Cruz PM, et al. Muscle magnetic resonance imaging in congenital myasthenic syndromes. *Muscle Nerve*. 2016;54(2):211-219. doi:10.1002/mus.25035

263. Demer JL. The orbital pulley system: A revolution in concepts of orbital anatomy. *Ann N Y Acad Sci*. 2002;956(1):17-32. doi:10.1111/j.1749-6632.2002.tb02805.x

264. Spencer RF, Porter JD. Biological organization of the extraocular muscles. *Prog Brain Res*. 2006;151:43-80. doi:10.1016/S0079-6123(05)51002-1

265. Kirchner J, Watson T, Lappe M. Real-Time MRI Reveals Unique Insight into the Full Kinematics of Eye Movements. *eNeuro*. 2022;9(1). doi:10.1523/ENEURO.0357-21.2021

266. Heskamp L, Miller AR, Birkbeck MG, et al. In vivo 3D imaging of human motor units in upper and lower limb muscles. *Clinical Neurophysiology*. Published online June 20, 2022. doi:10.1016/j.clinph.2022.05.018

267. Birkbeck MG, Heskamp L, Schofield IS, Blamire AM, Whittaker RG. Non-invasive imaging of single human motor units. *Clinical Neurophysiology*. 2020;131(6):1399-1406. doi:10.1016/j.clinph.2020.02.004

268. Heskamp L, Birkbeck MG, Whittaker RG, Schofield IS, Blamire AM. The muscle twitch profile assessed with motor unit magnetic resonance imaging. *NMR Biomed*. 2021;34(3). doi:10.1002/nbm.4466

9

10
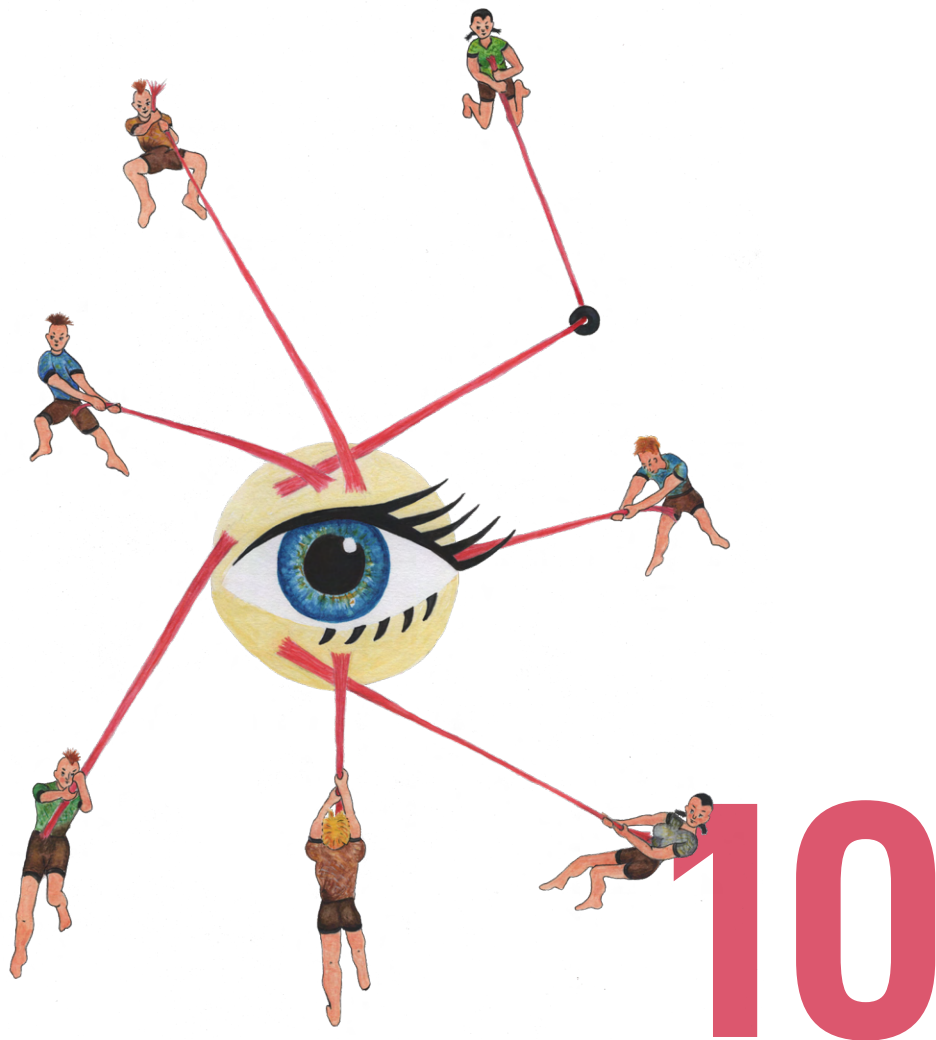
Nederlandse samenvatting
List of publications
Curriculum Vitae
Acknowledgements

Nederlandse samenvatting

Myasthenia gravis (MG) is een spierziekte waarbij patiënten last hebben van wisselende en vermoeibare spierzwakte. Oogspierzwakte en bulbaire zwakte komt het meest voor, waarbij oculaire klachten zoals dubbelzien (diplopie) en hangende oogleden (ptosis) vaak op de voorgrond staan. In de gegeneraliseerde vorm van de ziekte kunnen alle skeletspieren betrokken zijn waaronder de nekspieren, de armspieren, de beenspieren en de ademhalingsspieren. MG is een auto-immuunziekte en wordt veroorzaakt door antistoffen die aan eiwitten binden in de neuromusculaire overgang (synaps). Hierdoor is de zenuw minder goed in staat om de spier aan te zetten om samen te trekken en ontstaat spierzwakte. De nicotinerge acetylcholinereceptor, MuSK, VGCC, agrine en LRP4 zijn bekende eiwitten waar antistoffen tegen gevormd kunnen worden. In sommige gevallen worden deze antistoffen niet gevonden in het bloed en is de ziekte moeilijker vast te stellen; dit noemen we seronegatieve MG. Met medicatie is de spierzwakte van de meeste patiënten goed onder controle te krijgen, maar MG is momenteel niet te genezen. Er bestaat medicatie die de spierzwakte direct kan verbeteren en medicatie die (een deel van) het immuunsysteem onderdrukt om de ziekte op de langere termijn te onderdrukken.

Oculaire MG is een subtype van MG waarbij gedurende de hele ziekte alleen de oogspieren betrokken zijn en geen andere skeletspieren. Tien procent van de MG-patiënten heeft oculaire MG. Er zijn drie belangrijke medische uitdagingen in de behandeling van oculaire MG. Ten eerste is de helft van de oculaire MG-patiënten seronegatief en is bij hen de ziekte moeilijker objectief vast te stellen. Elektrofysiologische testen kunnen helpen bij de diagnose, maar ondanks deze testen blijft een deel van de diagnoses niet objectief bevestigd, omdat je de oogspieren niet direct kan meten. Ten tweede reageert de oogspierzwakte bij een deel van deze patiënten niet goed op behandeling waardoor zij zwakte van de oogspieren blijven houden. Tot slot worden oculaire MG-patiënten vaak uitgesloten van klinische studies naar de ontwikkeling van nieuwe medicatie, deels omdat de ernst van de oogspierzwakte moeilijk objectief te meten is.

Het doel van dit proefschrift was om nieuwe methoden te ontwikkelen die helpen de klinische zorg voor oculaire MG-patiënten te verbeteren. In dit proefschrift hebben we de oogspieren onderzocht met spierelektrofysiologie, orthoptische metingen en kwantitatieve MRI. De subdoelen van dit proefschrift zijn:

1. Om nieuwe methoden te ontwikkelen die bijdragen aan de objectieve bevestiging van de diagnose van oculaire seronegatieve MG.
2. Om de oorzaak van therapieresistente oogspierverlamming in MG te begrijpen.

3. Om methoden te ontwikkelen, die de oogspierfunctie kunnen meten, en deze te gebruiken als uitkomstmaat in klinische studies.

In **hoofdstuk 2** van dit proefschrift beschrijven we in een review aandoeningen waarbij de oogspieren betrokken zijn met oogspierverlamming, dubbelzien en/of hangende oogleden tot gevolg. Deze aandoeningen zijn uitgesplitst in ziekten met pathologie in de hersenen, de zenuw, de neuromusculaire overgang en de oogspier. Verschillende aanwijzingen in het patroon van symptomen, beeldvorming en welke oogspieren betrokken zijn kunnen helpen bij het stellen van de diagnose. Deze patronen wijzen vaak in de richting van een specifieke pathologische locatie of ziekte. Bij deze symptomatische patronen hebben we gekeken naar de aanwezigheid van ptosis, oogspierverlamming, diplopie, pijn, uitpuilende ogen, nystagmus, extra-orbitale symptomen, symmetrie en fluctuaties. Beeldvorming van de orbita kan daarbij helpen in de diagnose, bijvoorbeeld als er ontsteking, vervetting, zwelling of atrofie is van de oogspieren.

Hoofdstuk 3 beschrijft een studie naar de reproduceerbaarheid van een elektrofysiologische test, de RoVEMP (repetititive ocular vestibular evoked myogenic potentials) test. Bij de RoVEMP test wordt herhaaldelijk door een trilling op het hoofd, via het evenwichtsorgaan, een reflex opgewekt in een specifieke oogspier. Door deze reflex meerdere keren achter elkaar op te wekken en te registreren kan je de 'vermoeibaarheid' van deze spier meten. Het signaal van de spier wordt steeds zwakker bij meer trillingen. Deze test hebben wij twee keer gedaan bij deelnemers en hieruit bleek de reproduceerbaarheid van de uitslag van de test niet hoog te zijn. Hierdoor is deze test minder geschikt voor de diagnose van individuele patiënten.

In hoofdstuk 4 hebben we de kracht van de oogspieren en de afwijkingen tussen de ogen onderzocht met orthoptische tests. Dit hebben we gedaan in gezonde vrijwilligers, MG-patiënten, maar ook in patiënten met andere oogspieraandoeningen, zoals CPEO (chronisch progressieve externe oftalmoplegie; een mitochondriële spierziekte), OPMD (oculofaryngeale spierdystrofie; een dystrofische spierziekte) en Graves orbitopathie (een schildklierziekte waarbij de oogspieren soms ontstoken raken). We hebben ducties gemeten met een synoptofoor en de afwijking tussen de ogen in meerdere richten met een Hess-scherm. Aan het Hess-schermonderzoek hebben we vermoeibaarheidsmetingen toegevoegd door alle deelnemers een minuut in alle richtingen te laten kijken. Bij MG-patiënten zien we dat dit moeilijk vol te houden is en de afwijking in die minuut groter wordt door de vermoeibaarheid van de oogspieren. Dit zagen we bijna niet in de andere aandoeningen en niet in gezonde vrijwilligers. Hierdoor is deze test geschikt voor de diagnose van MG en ook interessant als een uitkomstmaat voor de ernst van oogspierzwakte voor klinische studies.

10

Hoofdstuk 5 en 6 beschrijven twee studies waarbij we nieuwe MRI-methoden hebben ontwikkeld. **In hoofdstuk 5** hebben we een methode verbeterd om de T2 van spier te meten. De T2 is de tijd dat de protonen in een weefsel weer uit fase raken na een elektromagnetische puls en de T2 verschilt tussen verschillende weefsels en weefseleigenschappen. De T2 van spier zou een goeie marker kunnen zijn van ziekteactiviteit, bijvoorbeeld omdat de T2 gevoelig is voor ontsteking van spieren. Deze T2 is moeilijk te bepalen omdat er bij spierziekten vaak vet aanwezig is, en vet heeft een hoge T2. Ook zijn er methodologische uitdagingen, zoals hoe je de T2 van vet bepaald en hoe je corrigeert voor de inhomogeniteit van het elektromagnetische veld (B1) en het profiel van de fliphoeken over de gemeten doorsnede. In dit werk hebben we een methode ontwikkelt waarbij de T2 van vet wordt bepaald op het onderhuidse vet, uitgaande van een klein deel water die ook aanwezig is in de vetcellen. Ook wordt er in deze methode gecorrigeerd voor de beschreven technische problemen door het fliphoekprofiel in de berekeningen mee te nemen. Deze methode zorgt dat je betrouwbaardere metingen kan doen en beter vergelijkbare metingen krijgt tussen verschillende centra en scanners. **In hoofdstuk 6** hebben we onderzocht of het haalbaar is om kwantitatieve MRI te doen van de oogspieren. Bij kwantitatieve MRI voer je metingen uit van spieren, waarbij je de volumes, vetfracties en T2 bepaald van een specifieke spier. Dit wordt al veel gedaan in skeletspieren, maar dit is bij de oogspieren uitdagender, omdat de oogspieren klein en beweeglijk zijn. We hebben aangetoond dat het haalbaar is om kwantitatieve MRI van de oogspieren te doen met een 7-Tesla-MRI-scanner. Deze scanner heeft een sterker magnetisch veld, waardoor we de kleine oogspieren in een hogere resolutie kunnen onderzoeken. Ook hebben we de patiënten middels een beamerscherm gecontroleerd laten knipperen met de ogen, zodat de ogen zoveel mogelijk stil stonden als de MRI-scanner aan het meten was. We zagen in deze pilotstudie dat MG-patiënten een kleine toename in volume en vetfractie hadden ten opzichte van de gezonde controles.

In hoofdstuk 7 wordt een studie beschreven waarbij we kwantitatieve MRI van de oogspieren hebben gedaan bij een grotere groep MG-patiënten, neuromusculaire controles en gezonde controles. We hebben recente MG-patiënten, chronische MG-patiënten en seronegatieve MG-patiënten in de studie geïncludeerd. We vonden weinig vervetting en geen atrofie van de oogspieren in MG. Alleen in de chronische MG-patiënten zagen we een significante vervetting en volumetoename in de meeste oogspieren. Ook in patiënten die blijvende oogspierverlamming hadden, zagen we geen atrofie van de oogspieren. Dit suggereert dat in de meeste MG-patiënten met refractaire oogspierzwakte er geen macroscopische anatomische afwijkingen zijn. Dat de oogspieren soms zelfs iets toenemen in volume, roept pathofysiologische vragen op. Dit kan komen omdat er een milde ontstekingsreactie in de oogspieren is of omdat de oogspieren de zwakte compenseren met een toename in spiervolume. Het meten van de water-T2 van de oogspieren zou meer informatie kunnen

geven over de aanwezigheid van ontsteking. Helaas was de variatie van onze T2 metingen te hoog om hier een conclusie aan te verbinden. Diagnostisch is orbitale MRI niet bruikbaar om gezonde controles van MG-patiënten te onderscheiden, want met name in de seronegatieve groep waren er geen oogspierveranderingen aanwezig die kunnen helpen met de diagnose. Wel is MRI nuttig mochten er andere oogspieraandoeningen, zoals CPEO, OPMD en Graves orbitopathie, in de differentiaal diagnose staan.

Concluderend hebben we in deze studie met drie verschillende methoden onderzoek gedaan naar de functie en structuur van de oogspieren in MG om de diagnostiek en zorg voor oculaire MG-patiënten verbeteren. We hebben verschillende stappen gemaakt op het gebied van diagnostiek, het begrip van refractaire oculaire klachten en in de ontwikkeling van objectieve metingen van oogspierzwakte in MG. Ten eerste is het met MRI mogelijk om onderscheid te maken tussen MG en een aantal andere oogspieraandoeningen, maar MG patiënten onderscheiden van gezonde deelnemers is niet mogelijk met deze techniek. De orthoptische test met het Hess-scherm, met de uitbreiding om vermoeibaarheid van de oogspieren te meten, bleek een bruikbare test om MG aan te tonen met een hoge sensitiviteit en specificiteit. Ten derde hebben we met MRI gezien dat de oogspieren niet atrofisch worden bij behandelde MG, zelfs niet bij patiënten die oogspierverlamming houden. Met het Hess-scherm hebben we geleerd dat bij MG-patiënten met dubbelzien de asymmetrie en vermoeibaarheid van de oogspieren meer op de voorgrond staat dan individuele oogspierverlamming. Namelijk als de ogen los onderzocht worden, kunnen deze vaak wel in alle richtingen bewegen. Dit betekent dat er ook een probleem is met hoe het brein de ogen aanstuurt in MG, bijvoorbeeld door een onvermogen om aan te passen aan de ontstane zwakte. Wellicht zou deze aansturing nog te trainen kunnen zijn. Tot slot zijn de orthoptische testen in staat om oogspierzwakte en -vermoeibaarheid in MG te kwantificeren, wat deze testen veelbelovend maakt als uitkomstmaten in klinische studies met MG-patiënten.

In de toekomst kan prospectief diagnostisch onderzoek naar de orthoptische testen nuttig zijn. De orthoptische testen zouden sensitiever en specifieker kunnen zijn en andere testen overbodig kunnen maken, en de combinatie van testen zou de gezamenlijke diagnostische opbrengst kunnen verhogen. Door te concentreren op de unieke vermoeibaarheid en fluctuaties van de spierzwakte in MG kunnen nieuwe diagnostische testen bedacht worden. Verder, om beter te begrijpen of er sprake is van macroscopische ontsteking, atrofie en vervetting in de spieren van MG-patiënten zou het waardevol zijn om kwantitatieve MRI van de skeletspieren te doen. Aangezien macroscopische afwijkingen aan de oogspieren in refractaire oculaire MG-patiënten ontbreken, zou het interessant zijn om met histologie van oogspierbiopten (in proefdieren of bijvoorbeeld post-mortem) te kijken of er wel microscopische schade is. Het is mogelijk dat er meer schade is aan de neuromusculaire

10

overgang dan in het spierweefsel in engere zin. Deze zeer lokale schade zou kunnen verklaren waarom deze niet zichtbaar is op MRI-beelden. Het vergelijken van histologie van oogspieren van goed te behandelen patiënten en moeilijk te behandelen patiënten zou ons veel kunnen leren over refractaire oogklachten. Tot slot zou het informatief kunnen zijn om oculaire MG-patiënten niet te excluderen uit studies naar de ontwikkeling van nieuwe medicijnen. Orthoptische testen kunnen bijdragen aan het kwantificeren van oogspierzwakte en zo kan ook bepaald worden of een medicijn werkt in deze doelgroep.

List of publications

Keene KR, van Vught L, van de Velde NM, Ciggaar IA, Notting IC, Genders SW, et al. The feasibility of quantitative MRI of extra-ocular muscles in myasthenia gravis and Graves' orbitopathy. NMR Biomed 2021;34:e4407. *doi: 10.1002/nbm.4407.*

Keene KR, Beenakker JWM, Hooijmans MT, Naarding KJ, Niks EH, Otto LAM, et al. T2 relaxation-time mapping in healthy and diseased skeletal muscle using extended phase graph algorithms. Magn Reson Med 2020;84:2656–70. *doi: 10.1002/mrm.28290*.

de Meel RHP*, **Keene KR*,** Wirth MA, Weber KP, Badrising UA, Verschuuren JJ, et al. Repetitive ocular vestibular evoked myogenic potentials in myasthenia gravis. Neurology 2020;94:E1693– 701. *doi: 10.1212/WNL.0000000000009306.* *Equal contribution.

Keene KR, Bongers J, de Meel RHP, Venhovens J, Verschuuren JJGM, Tannemaat MR. Test-Retest Reliability of Repetitive Ocular Vestibular Evoked Myogenic Potentials in Myasthenia Gravis Patients and Healthy Control Subjects. J Clin Neurophysiol. 2022 Jul 2. *doi: 10.1097/ WNP.0000000000000956*.

Keene KR, Kan HE, Meeren S van der, et al. Clinical and imaging clues to the diagnosis and follow-up of ptosis and ophthalmoparesis. J Cachexia Sarcopenia Muscle. Published online September 29, 2022. *doi: 10.1002/JCSM.13089.*

Keene KR, de Nie JM, Brink MJ, et al. Diagnosing myasthenia gravis using orthoptic measurements: assessing extraocular muscle fatiguability. Journal of Neurology, Neurosurgery & Psychiatry Published Online First: 19 October 2022. *doi: 10.1136/jnnp-2022-329859*.

Keene, KR, Notting, IC, Verschuuren, JJ, Voermans, N, De Keizer, RO, Beenakker, JM, Tannemaat, MR, & Kan, HE (2023). Eye Muscle MRI in Myasthenia Gravis and Other Neuromuscular Disorders. Journal of Neuromuscular Diseases, 1–15. *https://doi.org/10.3233/ jnd-230023.*

Vergoossen DLE, Ruiter AM, **Keene KR**, Niks EH, Tannemaat MR, Strijbos E, Lipka AF, van der Zijde ECJ, van Tol MJD, Bakker JA, Wevers BA, Westerberg E, Borges LS, Tong OC, Richman DP, Illa I, Punga AR, Evoli A, van der Maarel SM, … Huijbers MG. . Enrichment of serum IgG4 in MuSK myasthenia gravis patients. 2022. Journal of Neuroimmunology, 373, 577978. *doi: 10.1016/J.JNEUROIM.2022.577978.*

10

Veeger TTJ, van de Velde NM**, Keene KR**, Niks EH, Hooijmans MT, Webb AG, et al. Baseline fat fraction is a strong predictor of disease progression in Becker muscular dystrophy. NMR Biomed 2022;35:e4691. *doi: 10.1002/nbm.4691.*

Naarding KJ, **Keene KR**, Sardjoe Mishre ASD, Veeger TTJ, van de Velde NM, Prins AJ, et al. Preserved thenar muscles in non-ambulant Duchenne muscular dystrophy patients. J Cachexia Sarcopenia Muscle 2021;12:694–703. *doi: 10.1002/jcsm.12711.*

van de Velde NM, Hooijmans MT, Sardjoe Mishre ASD, **Keene KR**, Koeks Z, Veeger TTJ, et al. Selection Approach to Identify the Optimal Biomarker Using Quantitative Muscle MRI and Functional Assessments in Becker Muscular Dystrophy. Neurology 2021;97:e513–22. *https://doi.org/10.1212/WNL.0000000000012233.*

Santini F, Wasserthal J, Agosti A, et al. Deep Anatomical Federated Network (Dafne): an open client/server framework for the continuous collaborative improvement of deep-learning-based medical image segmentation. Published online 2023. *http://dx.doi.org/10.48550/arXiv.2302.06352.*

Howard JF, Bril V, Vu T, Karam C, Peric S, Margania T, et al. Safety, efficacy, and tolerability of efgartigimod in patients with generalised myasthenia gravis (ADAPT): a multicentre, randomised, placebo-controlled, phase 3 trial. Lancet Neurol 2021;20:526–36. doi: *10.1016/S1474-4422(21)00159-9.*

Talebian Yazdi M, **Keene KR**, Hiemstra PS, Van Der Burg SH. Recent progress in peptide vaccination in cancer with a focus on non-small-cell lung cancer. Expert Rev Vaccines 2014;13:87–116. *doi: 10.1586/14760584.2014.862499.*

Rodríguez JM, Barca CC, Puddu PE, Gialelis J, Chondros P, Karadimas D, **Keene KR**, et al. Archetype-based solution to tele-monitor patients with chronic diseases. IFMBE Proc 2014;41:1278–81. *doi: 10.1007/978-3-319-00846-2_316.*

Curriculum Vitae

Kevin Keene was born on the 22th of February 1992 in Delft, the Netherlands. In 2010 he completed gymnasium secondary school at Marnix College in Ede and moved to Leiden to study medicine. In 2018 he graduated and got his master in medicine and his master in biomedical sciences at the Leiden University Medical Center (LUMC). During his clinical internships he focused on neurology. His biomedical research internships were in the department of human genetics on whole genome sequencing and in the department of clinical neurophysiology studying diagnostic in myasthenia gravis.

After obtaining his bachelor's degree in medicine and pre-master biomedical sciences in 2013, he joined the full-time board of the rowing association Asopos de Vliet as treasurer for a year. After this he kept volunteering for Asopos de Vliet and became a member of merit in 2021. Next to medicine and biomedical research, Kevin always had an interest in computer technology and worked at a medical informatics company MEDrecord during his bachelor's degree and worked at Nictiz for half a year in 2018.

Kevin started as a PhD student at the LUMC in 2018 at the department of neurology, radiology and ophthalmology studying ocular symptoms in myasthenia gravis, under the supervision of prof. dr. Jan Verschuuren, dr. Martijn Tannemaat, dr. Hermien Kan and dr. Jan-Willem Beenakker. In his PhD he collaborated in Duchenne and Becker research in the LUMC and in Pompe research with the Erasmus University Medical Center.

Currently he is working as a resident in neurology at the Haga Hospital in The Hague.

10

Acknowledgements

First and foremost I would like to start with thanking everybody who helped me with the creation of this thesis. Without all your help this work would not have been possible. I am thankful for the intensive support of Martijn, Hermien, Jan-Willem and Jan. Thanks Martijn for all the support during both my internship and my PhD trajectory. You have always inspired me with your neuromuscular and electrophysiological knowledge, ability to put things into perspective and ability to think of new study ideas. Thanks Hermien for your honesty, expertise in muscle physiology and pathophysiology and extremely thorough comments on all the papers and writings during my PhD. Thanks Jan-Willem for everything you learned me about quantitative MRI, the help and persistence in explaining the (mis)behavior of our T2 models and the thorough review of all the methodology of our studies. Thanks Jan for all the inspiring discussions and insights into explaining all our study findings in a pathophysiological and clinical context. It has always amazed me how your knowledge stretches widely over both preclinical and clinical research fields. Also special thanks to Erik and Nathalie for being part of the support committee.

I can look back to interesting discussions during scientific meetings of the C.J. Gorter MRI center, the myasthenia gravis research group, the MR-EYE research group and the Duchenne muscular dystrophy research group. Many thanks for all the insights, knowledge and feedback. It was very inspiring to be able to participate in three departments: the neurology department, the radiology department and the ophthalmology department.

Also many thanks to everybody for the research collaborations and the opportunity to learn about other research field and other diseases. Thanks to you I learned a lot about Duchenne and Becker muscular dystrophy, about Pompe disease, manu other neuromuscular diseases, many neurodegenerative disease, eye disease and even about brown fat. Furthermore, I am also grateful for all the conferences I was allowed to go to. The ISMRM in Montreal, the many ISMRM Benelux editions, the ESMRMB in Rotterdam, the MYO-MRI conference in Berlin, the conference of the MGFA in Miami, the NOG conferences in Groningen and all the digital conferences during the covid pandemic.

I am also grateful for the fun moments and laughs I had with all colleagues. Unfortunately, I cannot name everybody here specifically for they stretch over three big departments in the hospital. In special I want to thank all my direct office mates from the old and new Oven for all the mental support and laughs: Francesca, Aashley, Lena, Bart and Martijn. The same goes for the my hypothetical other office the *Spierballenkamer*. It is a shame I never actually made it there, however still thanks I was always welcome Karin, Nienke, Esther, Linda, Annabel, Robert and Mink.

10